THE UNIVERSITY OF HULL

PREPARATION OF ANISOTROPIC MICROPARTICLES AND THEIR BEHAVIOUR AT LIQUID INTERFACES

being a Thesis submitted for the Degree of doctor of philosophy

in the University of Hull

by

Richard Forrest B. Sc. (Hons)

(September 2012)

ACKNOWLEDGMENTS

I would like to thank my supervisor Dr Tommy Horozov for giving me an opportunity to pursue this interesting project.

I would like to thank all members of the Surfactant & Colloid group at the University of Hull for their support and patience throughout my thesis.

I would also like to thank my industrial sponsors at Unilever for their financial support and their stimulating discussions on my project.

I greatly appreciate the support of Mr Tony Sinclair for SEM images and metal coatings, Mr Ian Dobson for his assistance with FTIR- Spectroscopy and Dr Howard Snelling for optical profilometry images.

PRESENTATIONS

Some of the findings obtained from this project have been presented at the following conferences:

Oral presentations:

1. "*Particle Fabrication Using Photolithography*" International Workshop on Emulsion Templating for Macroporous Polymers, Imperial College London, UK, May 2009.

2. "*Monolayers of Non- spherical Particles at Water- Fluid Interfaces*" University of Hull Research Colloquia, Department of Chemistry, University of Hull, UK, July 2011.

3. "*Monolayers of Non- spherical Particles at Water- Fluid Interfaces*", Unilever, Vlaardingen, Netherlands, July 2011.

Poster presentations:

1. "*Non- spherical Particles at Water- Fluid Interfaces*" 25th ECIS Conference, Prague, June 2010.

2. "*Non- spherical Particles at liquid Interfaces*" UK Colloids Conference, London, July 2011.

3. "*Particle Fabrication Using Photolithography*" UK Polymer Colloids Forum, University of Hull, UK, September 2009.

4. "*Non- spherical Particles at Water- Fluid Interfaces*" University of Hull Research Colloquia, Department of Chemistry, University of Hull, UK, July 2010.

ABSTRACT

Monolayers of solid particles at the liquid- fluid interface are of considerable interest in both academia and industry. Their behaviour during compression and expansion experiments in a Langmuir trough has important implications on particle stabilisation of foams and emulsions. This has been known for some time with regards to spherical particles. In this investigation, we have studied the role of non-spherical particles at the liquid- fluid interface. Particles have been fabricated using the technique of photolithography. The technique was modified in order to be able to apply it under normal laboratory conditions, thus making it more accessible for the fabrication of non- spherical particles of any size or shape. Flat plate- like particles with well controlled shape and size with disc, oval and rectangular geometry have been fabricated. Monolayers composed of such particles at both the air- water and oil- water interfaces exhibit important differences between each other and spherical particles. The geometry of the monolayers at the interface has been characterised, and preferential ordering of rectangular particles in domains consisting of side to side contacts has been discovered. A strong capillary attraction has been observed between the particles owing to the roughness and shape of the particles. It was found that during compression at the liquid- fluid interface, the surface pressure increases more slowly than that observed for spherical particles and this has been attributed to the tendency of the particles to undergo reorientation, tilting and flipping, the latter always occurred around the long axes of the particles. The thickness of the particles has significant implications on the stability of the monolayer; in addition the tendency for the particles to flip increases as the thickness of the particles is reduced. The non- spherical particles investigated here have been demonstrated to offer great potential as stabilisers of emulsion drops. The technique of photolithography has been utilised for the fabrication of Janus particles consisting of one face coated with metals, polyelectrolytes, silanes and colloidal particles.

CONTENTS

Chapter 1 Introduction 1

1. 1. Motivation and aims of thesis 1

1. 2. Liquid interfaces and interfacial tension 3

1. 3. Solid wetting and contact angles 3

1. 3. 1. Basic definitions 3

1. 3. 2. Solid particle attachment to a liquid interface 4

1. 4. Interactions between solid particles at the liquid interface 7

1. 5. Interactions between non- spherical and Janus particles at the liquid interface 11

1. 5. 1. Interactions between non- spherical particles at liquid interfaces 11

1. 5. 2. Interactions between Janus particles at liquid interfaces 17

1. 6. Investigation of particle monolayers using a Langmuir trough 20

1. 7. Methods for the fabrication of non- spherical particles 24

1. 7. 1. Mechanical stretching 24

1. 7. 2. Templating 25

1. 7. 3. Droplet microfluidics 26

1. 8. Methods for the fabrication of surface- anisotropic (Janus) particles 27

1. 9. The fabrication of anisotropic particles by photolithography 29

1. 9. 1. The Application of photolithography for the fabrication of non- spherical particles 31

1. 9. Outline of thesis 33

Chapter 2 Experimental 35

2. 1. Materials 35

2. 1. 1. Substrates 35

2. 1. 2. Photoresist and ancillaries 35

2. 1. 3. Photomasks 37

2. 1. 4. Chemicals and materials 37

2. 1. 5. Instruments 40

2. 2. Methods 42

2. 2. 1. Cleaning procedures 42

2. 2. 2. Silane, metal and polyelectrolyte application 43
2. 2. 3. Measurements of contact angles on solid surfaces using drop shape analysis 45
2. 2. 4. Photolithographic procedure for the fabrication of non-spherical particles 46
2. 2. 5. Partial modification of one surface of patterned photoresist 49
2. 2. 6. Spreading of solid particles at the liquid interface 51
2. 2. 7. Characterisation of the orientation and position of the particles at the liquid interface 52

Chapter 3 Fabrication of non- spherical particles using photolithography 54

3. 1. Introduction 54
3. 2. Experiments with low cost negative and positive photoresists 56
3. 2. 1. The effect of substrate wettability 57
3. 2. 2. The effect of the photoresist concentration on the thickness of the spin coated films 59
3. 2. 3. Pattern formation on photoresist films using photomasks 60
3. 3. Experiments with high performance photoresists 63
3. 3. 1. Initial test of the photoresist performance 64
3. 3. 2. Preparation of microparticle arrays on square substrates with small area 66
3. 3. 3. Preparation of microparticle arrays of negative photoresist on large silicon substrates 71
3. 4. Methods for releasing the fabricated photoresist microparticles from the substrate 78
3. 5. Characterisation of the photoresist microparticles 82
3. 5. 1. Particle shape and size 82
3. 5. 2. Particle wettability 85
3. 5. 3. Stability of photoresist particles in the presence of organic solvents 87
3. 6. Summary of the main findings 90
3. 7. Conclusions 93

Chapter 4 Behaviour of plate- like microparticles at liquid interfaces 94

4. 1. Introduction 94

4. 2. Monolayers of plate- like microparticles at the air- water and oil-water interfaces 95

4. 2. 1. Particle configuration at the liquid interface 95

4. 2. 2. Effect of particle shape on the monolayer structure 96

4. 2. 3. Implications for particle- stabilised foams and emulsions 102

4. 3. Behaviour of particle monolayers during compression and expansion in a Langmuir trough 106

4. 3. 1. Effect of spreading solvent on the surface pressure of the air-water interface 106

4. 3. 2. Effect of plate- like microparticle shape during compression in a Langmuir trough 110

4. 3. 3. Comparison of plate- like and spherical microparticle behaviour in Langmuir trough experiments 141

4. 4. Summary of the main findings 146

4. 5. Conclusions 147

Chapter 5 The fabrication of Janus plate- like microparticles 150

5. 1. Introduction 150

5. 2. Preparation of Janus microplates with homogeneous faces 153

5. 2. 1. Asymmetric functionalisation by chemical grafting 153

5. 2. 2. Asymmetric functionalisation by polyelectrolyte adsorption 154

5. 2. 3. Magnetic Janus plate- like microparticles 157

5. 3. Preparation of Janus microplates with one patterned face 160

5. 3. 1. Partial masking of negative photoresist microparticle arrays with positive photoresist patterns 162

5. 3. 2. Procedures for removal of positive photoresist patterns from partially masked negative photoresist microparticle arrays 167

5. 3. 3. Preparation of Janus microplates patterned with grafted amine groups by APTES treatment 173

5. 3. 4. Preparation of patterned Janus plate- like particles by metal deposition 179

5. 4. Summary of the main findings 189

5. 5. Conclusions 190

Chapter 6 Summary of main findings, conclusions and future work 191

6. 1. Main findings and conclusions 191

6. 2. Future work 196

References 198

CHAPTER 1

INTRODUCTION

1. 1. Motivation and aims of the thesis

The behavior of solid particles at the liquid- fluid interface is of paramount importance for understanding the stability of emulsions and foams and investigating particle interactions, aggregation and structure formation. [1- 9] The ability to tailor particle shape and properties in a convenient manner and to modify their physical or chemical properties is an ongoing challenge; moreover complex particle interactions at liquid interfaces has motivated many experimental and theoretical investigations. It is well established that particles like surfactants can absorb and modify the properties of an interface. Surfactants adsorb at the interface due to the hydrophilic-lipophilic balance (HLB) governed by the nature of the chains and headgroups and can lower the interfacial tension to permit the formation of emulsion droplets. In the case of solid particles, the interfacial adsorption is governed by the particle wettability quantified by the contact angle which the particles make at the liquid interface. Their presence essentially eliminates an area of the high energy liquid surface and therefore lowers the interfacial energy of the system. Unlike surfactants however, which readily desorb from the interface to establish equilibrium with the unabsorbed surfactant in the bulk, solid particles of intermediate wettability, i. e., contact angles as measured through the aqueous phase close to 90 °, are essentially irreversibly attached at the interface. Since the pioneering work of Ramsden and Pickering, the ability of particles to stabilise the interface between two immiscible fluids has been recognised. [10, 11] Since then, investigations have been carried out in order to understand the role played by particles in the stabilisation of emulsions and foams both with and without the presence of surfactant. More recently, the use of non- spherical particles has also been investigated at liquid interfaces. Their presence at the interface has been shown to be very advantageous in terms of the strength of attachment and the structures formed. New technologies and innovations have stimulated much research into the fabrication and study of non- spherical particles, e. g., microfluidics and photolithography. Their shape and aspect ratio can be tailored in such a way as to enable the rheological properties of the interface to be

controlled and have been shown to enhance the stability of emulsions and foams in a controlled way. [12-14] In addition, since the work of de Gennes, the fabrication and investigation of Janus particles has become a popular area of research and affords a means of introducing even more complex features to spherical and non- spherical particles. [15] Their presence at the interface, like particles with shape anisotropy, has been shown to enhance the strength of particle adsorption.

The nature of the interactions between the particles at the interface is still not fully understood, especially for the case of non- spherical and Janus particles. Recently, microparticles with rodlike and ellipsoidal shape at liquid interfaces have been investigated, but little is known for the behaviour of plate- like microparticles at air-water or oil- water interfaces. The aims of this thesis are to develop protocols for fabricating homogeneous and Janus plate- like microparticles with a range of different shapes and aspect ratios, and investigate the behavior of such particles at the air- water and oil- water interface. We utilise the technique of photolithography for the fabrication of the non- spherical particles because it offers the advantage of being able to tailor the shape, aspect ratio and thickness of the particles in a predetermined way, and the shape of the structures achieved using this method are not restricted. Since photolithography is a two dimensional technique and only half of the particle surface is exposed after fabrication on a solid substrate, the technique is also very advantageous for the selective modification of one half of the particle surface and therefore is a convenient method for the generation of Janus particles. The modification of one face of the particles by chemical or physical means offers the possibility of studying even more complex interfacial behavior. It is envisaged that much more work could be done in this area with relevance to a large range of investigations both in industry and academia where previously the more readily available homogeneous spherical particles were used.

In this first chapter, some principles of surface phenomena relevant for the investigation of particle adsorption and interactions at liquid interfaces will be described. Fabrication of anisotropic particles with surface functionality and their interactions at liquid interfaces will be discussed with references to other work published on the subject.

1. 2. Liquid interfaces and interfacial tension

An interface is defined as the boundary between two phases, e. g., solid- gas, solid-liquid, or a liquid in contact with gas or another liquid. Interfacial tension, also called specific surface energy, is the isothermal reversible work of creating unit area of interface. The interfacial tension can be considered to result from the extent of unsaturation of bonds when molecules are removed from the bulk and forced to reside at the surface. Molecules in the bulk are balanced by interaction forces of equal magnitude occurring in all directions: in contrast molecules residing at the surface experience an imbalance of forces due to a reduction in the number of like neighbouring molecules. The term tension then refers to the tendency of the surface to contract inwards normal to the surface, hence it could be considered as a force acting parallel to the surface and at a right angle to a line of unit length anywhere in the surface plane. [16] When liquid- fluid interfaces are considered, the tension is referred to as the interfacial tension, and in terms of solid surfaces, surface energy is usually used. The term surface tension is usually used for liquid-gas interfaces. The interfacial tension has units of N m^{-1} or J m^{-2} and is commonly denoted by the symbol γ.

1. 3. Solid wetting and contact angles

1. 3. 1. Basic definitions

For a droplet of liquid on a solid surface, the contact angle arises as a result of the balance of forces at the line of contact between the liquid and the solid resulting from the solid/ vapour (SV), solid/ liquid (SL) and liquid/ vapour (LV) interfacial tensions as shown in Fig. 1. 1. [17] These forces are balanced according to Young's equation

$$\gamma_{SV} = \gamma_{SL} + \gamma_{LV} \cos\theta \qquad (1.\ 1)$$

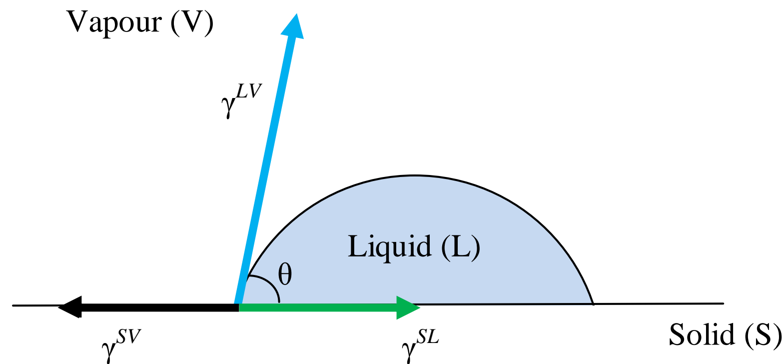

Fig. 1. 1. A droplet of liquid (L) resting on the surface of a solid (S) in a gas (V).

The application of Young's equation requires a smooth and chemically uniform surface that in practice is seldom encountered. Surfaces are often rough and chemically heterogeneous meaning that the energy of the surface will vary at different locations. If a liquid then advances along such a surface, an advancing contact angle is encountered which is larger than the receding contact angle resulting from the recession of the liquid along the surface, giving rise to contact angle hysteresis with the true contact angle occurring between these boundaries. [109]

1. 3. 2. Solid particle attachment to a liquid interface

When attached to a liquid interface, small solid particles adjust their position to minimise the surface free energy, thus forming a finite contact angle measured between the tangents to the particle and liquid surfaces at any point in the three phase contact line (Fig. 1. 2). It is conventional to measure the contact angle through the water phase and this convention is used throughout the thesis. The particle contact angle is linked to the respective surface energies via equation (1. 1). The contact angle that a particle makes at the interface depends on the particle wettability: hydrophilic (water- liking particles) such as silica reside preferentially in the water phase giving contact angles < 90 °, whereas hydrophobic particles such as silica treated with cationic surfactant or silane give contact angles > 90 °.

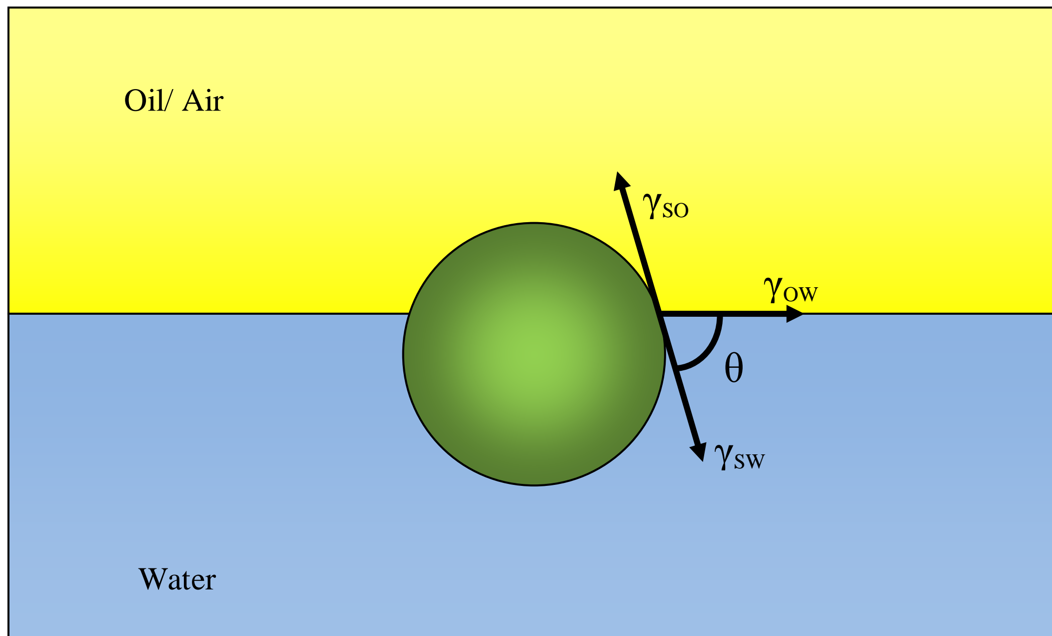

Fig. 1. 2. Schematic representation of a solid particle attached to the air/ oil-water interface showing the contact angle measured through the water.

The energy of detachment of a spherical particle from the interface into one of the bulk phases is related to the contact angle which the particle makes at the interface, the surface or interfacial tension of the liquid- fluid interface and the size of the particle as given by

$$\Delta E = \pi R^2 \gamma_{aw} (1 \pm \cos\theta)^2 \tag{1.2}$$

where ΔE is the detachment energy (the difference in the surface free energies between the particle in the bulk and at the interface), R is the radius of the particle, γ_{aw} is the surface tension of water and θ is the contact angle as measured into the aqueous phase. [80] The sign within the brackets is positive for particle detachment into the vapour or oil phase and negative for detachment into the aqueous phase. The equation shows that the energy required to remove a particle from the interface is greatest when the particle contact angle is 90 °. For particles with R larger than 5 nm and contact angles close to 90 °, the detachment energy can be several orders of magnitude larger than kT, meaning that particles of intermediate wettability are essentially irreversibly attached to the interface.

The detachment energy of a non-spherical particle depends on the particle configuration at the liquid interface. This is illustrated in Fig. 1. 3 in the case of a cylindrical particle with a contact angle of 90 °. The free energy of particle detachment into water or oil in this case is given by the equation

$$\Delta E = \gamma_{ow} A_c \tag{1. 3}$$

where A_c is the area occupied by the particle at the liquid interface. Therefore the detachment energy of a cylindrical particle with diameter d when its axis of symmetry is perpendicular to the liquid interface (Fig. 1. 3 a) is

$$\Delta E_a = \gamma_{ow} \frac{\pi d^2}{4} \tag{1. 4a}$$

When the particle axis of symmetry is parallel to the liquid interface (Fig. 1. 3 b) the detachment energy is given by

$$\Delta E_b = \gamma_{ow} hd \tag{1. 4b}$$

where h is the cylinder height. The comparison of ΔE_a with ΔE_b leads to

$$\frac{\Delta E_a}{\Delta E_b} = \frac{\pi}{4} \frac{d}{h} \tag{1. 5}$$

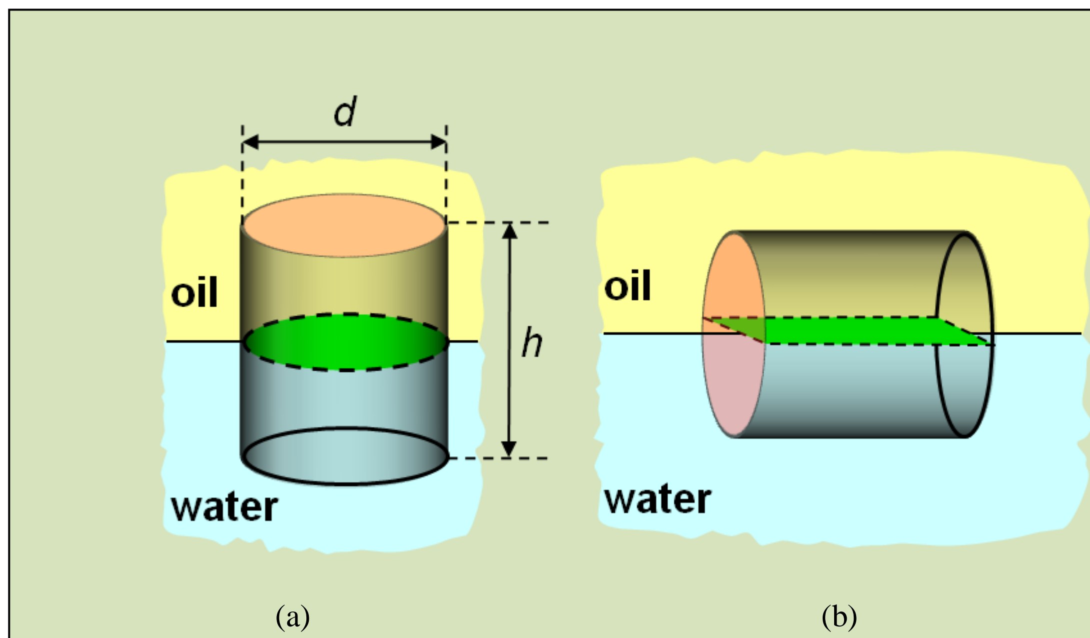

Fig. 1. 3. Schematic of the two possible configurations of a cylindrical particle with contact angles of 90 ° at the oil- water interface.

The preferred lowest energy configuration of the particle at the liquid interface corresponds to the largest detachment energy, and according to equation 1. 5 depends on the particle proportions. Short cylindrical particles (discs) with $h < \pi d/4$ should prefer to sit at the liquid interface in the configuration shown in Fig. 1. 3a (the axis of symmetry perpendicular to the liquid interface) while longer cylindrical particles (rods) with $h > \pi d/4$ should prefer to orient their axis of symmetry parallel to the liquid interface (Fig. 1. 3 b). This analysis could be extended to other particle shapes. It has been shown that the preferred configuration of prolate ellipsoids with long axis *a* and short axis *b* is that with the long axis, *a*, parallel to the liquid interface. [93]

Binks and Horozov [18] compared the detachment energies of spherical, rodlike and disc- like particles with the same volume. They came to the conclusion that for particles with equal volume and different shape, the free energy of particle detachment decreases in the order disc > rod > sphere. [18] Therefore non- spherical particles can attach to the interface with greater strength than spherical particles.

1. 4. Interactions between solid spherical particles at the liquid interface

Interactions among particles trapped at the liquid interface exhibit many of the characteristics of those in the bulk suspension which are well described by classical DLVO theory. However, there are several significant differences. In addition to the screened electrostatic repulsion through the aqueous phase, strong long range repulsion may occur through the non-polar phase (air or oil) due to charges at the particle- water interface [74] or some residual charges at the particle- oil (air) interface as suggested recently. [77, 78] This makes the interfacial particles much less prone to aggregation in comparison to those in the bulk when electrolyte has been added to the aqueous phase. [77, 78] To explain the observed long range repulsion between polystyrene spherical latex particles at the air- water surface, Pieranski has suggested that the partial immersion of spheres in the water sub- phase should result in an asymmetric double layer charge distribution around the particle- water surface. The resulting dipoles, being close to the surface, interact with each other through the air, thus leading to unscreened long range repulsion between the particles. [74] More recently, Aveyard *et al.* observed very strong long range repulsion between polystyrene microspheres at the octane- water interface. [77, 78] The interparticle

repulsion was been found to be quite insensitive to the presence of salt in the aqueous phase suggesting that the repulsion is mediated through the non- polar oil phase. They have proposed that the repulsion is due to the presence of residual charges originating from ionised sulphate groups stabilised by the presence of hydration water on the surface of the particle in contact with the oil. It has also been found that the repulsion between the same polystyrene microspheres is much weaker at the air- water interface, and is attributed to the lower particle contact angle (~ 30 °) in comparison to that at the octane- water interface (> 90 °). This suggests that enhanced repulsion between the particles at the oil- water interface may be tuned by variations in the particle wettability. Evidence of this has been provided by Horozov *et al.* from investigations of silane modified silica particles at the octane-water interface. They have observed a very strong repulsion between particles with a contact angle of 150 ° at the oil- water interface due to charges at the particle surface in the oil, resulting in a well ordered hexagonal array of particles at the interface. Particles with a lower contact angle (immersed more into the aqueous phase) formed more disordered monolayers due to aggregation of the particles. Furthermore, for the most hydrophobic particles, the monolayer order was found to be quite insensitive to the addition of electrolyte to the water sub- phase indicating that such particles are well immersed into the oil and stabilised by electrostatic interactions through the oil. [80, 81]

Similar to particles in a bulk liquid, attractive van der Waals interactions operate between interfacial particles, but they are influenced by the presence of both fluid phases. [31, 78] More importantly, the distortions of the liquid interface around the particles leads to strong capillary interactions which have no analog in the bulk. Distortions of the liquid interface may originate from the particle weight [84] electrostatic stresses caused by the electric field around charged particles [85] or chemical or topographical heterergeneity (roughness) on the particle surface. [87] These interactions are always attractive between similar particles. In an early work by White *et al.* the attraction between floating particles on a liquid was attributed to the deformation of the interface caused by the particle weight (Fig. 1. 4 a). They reported that the excess energy caused by the deformation can be reduced when the two particles approach one another and occupy the same depression. Such capillary

forces due to the effect of gravity are known as the flotation type. They are very long ranged and decay logarithmically with the interparticle separation. [84]

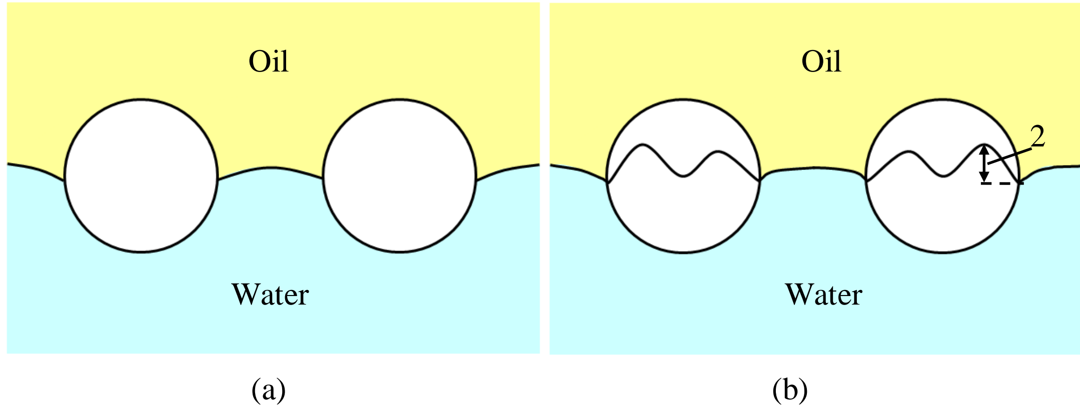

Fig. 1. 4. Deformations of the water- oil (air) interface around floating particles due to particle weight (a) and chemical or topographical heterogeneity (roughness) on the particle surface (b). Capillary attraction occurs when the deformations around neighbouring particles overlap.

The weight of small latex particles (R < 5 μm) is insufficient to cause significant deformations of the liquid interface. The capillary attraction between such particles is comparable to kT and is therefore negligible. However, capillary interactions between spherical particles could arise due to undulations of the three phase contact line caused by chemical heterogeneity and/ or roughness of the particle surface (Fig. 1. 4 b). [87] The latter are responsible for contact angle hysteresis due to pinning of the three phase contact line which creates deformations (depressions and elevations) at the liquid interface near the particle. It has been shown that the deformations of the liquid interface around adjacent particles can correlate and the particles adjust their mutual orientation (by rotating in the plane of the liquid interface) to minimise their potential energy. The capillary interaction can be considered to be a result of interactions between capillary multipoles, with the main contribution coming from capillary quadrupoles (Fig. 1. 5). [87, 110]

The pair potential of capillary attraction due to capillary quadrupoles in their most favorable mutual orientation (Fig. 1. 5 a) corresponding to the minimum potential energy is given by [87]

$$U_{cap} = -\frac{12\pi\gamma\delta^2 R_c^4}{L^4} \tag{1. 6}$$

where γ is the interfacial tension of the liquid interface, $R_c = R\sin\theta$ is the radius of the three phase contact line projection on the plane of the liquid interface, and δ is the amplitude of the three-phase contact line undulations (Fig. 1. 4 b).

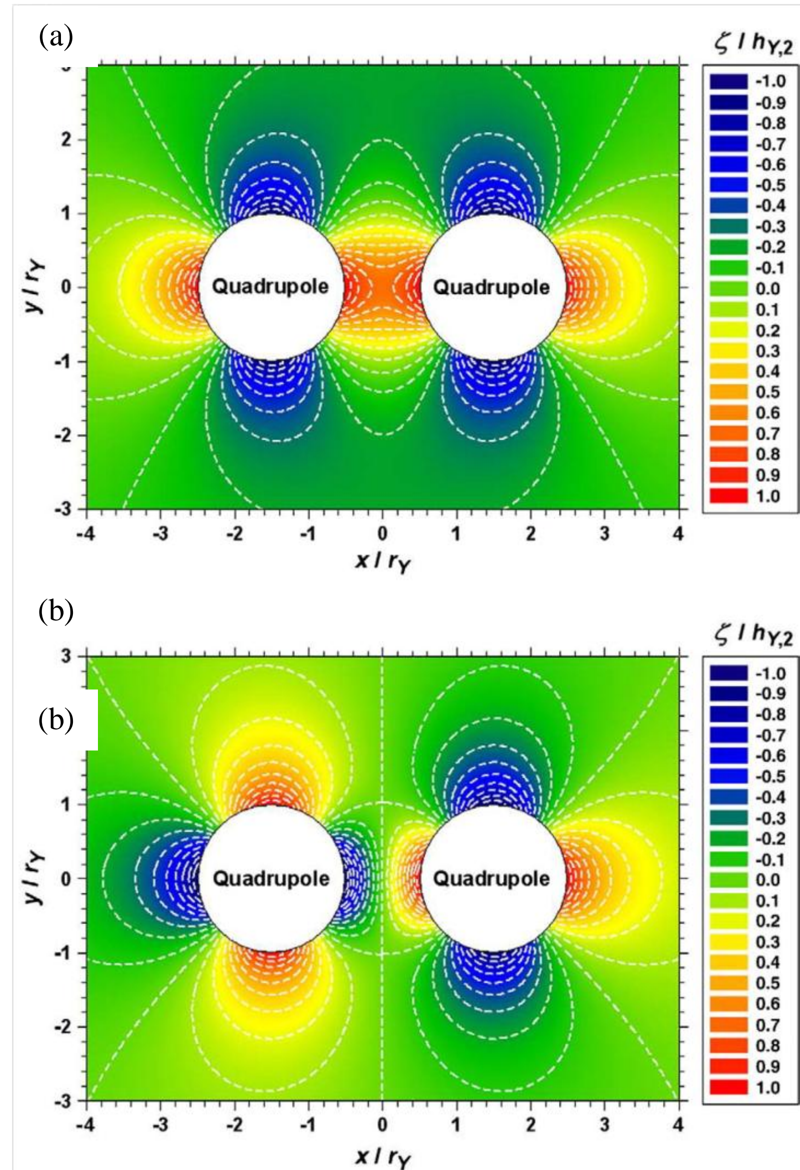

Fig. 1. 5. Contour-plot diagram of the meniscus shape z = ζ (x, y) around two similar capillary quadrupoles with radius r_Y, separated at a center- to- center distance L = $3r_Y$. (a) The most advantageous (overlapping elevations or depressions) and (b) the most disadvantageous (overlapping depressions with elevations) orientation of the two quadrupoles with respect to their interaction energy. The orientation in (a) leads to attraction, while that in (b) to repulsion. Reproduced from ref. 110.

Recently, Park *et al.* have provided evidence for such capillary interactions between polystyrene latex spheres with diameters of 3. 1 ± 0. 2 μm at the interface between water and decane in the presence of NaCl using optical tweezers. The dominant force between the particles was found to be a dipole- dipole repulsion. However, the attraction between the particles was found to be longer range than that expected for van der Waals forces and this was attributed to the presence of capillary forces originating from distortion of the interface due to chemical or topographical heterogeneity. The excess distortion of the water surface created this way is minimised when two particles adopt an optimum orientation and distance (Fig. 1. 5 a). [86] This effect was reported before by Stamou *et al.* for colloidal particles at an air- water interface. They noted that a distortion of the fluid contact line, δ, by as little as 50 nm around the particle surface resulted in an interaction energy of ~ 104 *kT* for particle diameters of 1 μm and an interparticle distances of 2 μm. This capillary attraction decays as the inverse 4th power of the distance between the particles (see eq. 1. 6). At a longer range, repulsive electrostatic interactions dominate with an inverse 3rd power distance dependence. [87] Other groups have observed a long range attraction between particles floating on a liquid surface in the form of a secondary minimum in the interaction potential. [2, 88- 90]

1. 5. Interactions between non- spherical and Janus particles at the liquid interface

1. 5. 1. Interactions between non- spherical particles at liquid interfaces

The interactions between spherical particles considered above operate also between non- spherical particles with one very significant difference: the particle shape itself can cause large deformations of the liquid interface. This is because Young's equation must be satisfied everywhere on the three phase contact line requiring deformations (elevations or depressions) of the liquid interface. An example of an ellipsoid at the liquid interface is shown in Fig. 1. 6. For non- spherical particles with axial symmetry, e. g., prolate ellipsoids or rods; the deformations generate capillary quadrupoles (Fig. 1. 6); therefore the capillary interactions are dominant and dictate the structure of such non- spherical particle monolayers at liquid interfaces.

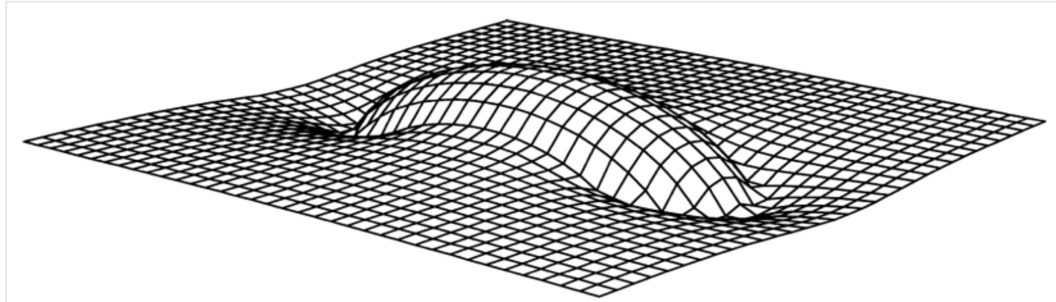

Fig. 1. 6. Possible interfacial profile around a prolate ellipsoidal particle with contact angle 45 ° and aspect ratio $a/b = 4$ oriented with its long axis, a, parallel to the liquid interface. Reproduced from ref. 96.

In a paper published by Vermant *et al.* the self assembly of PS latex ellipsoidal particles at the air- water and oil- water interface resulting from the particle charge and wetting properties was investigated. For uncharged particles at the oil- water interface, open networks of linear chains in a predominantly tip to tip configuration was observed with some of the particles arranged side by side or in flower like arrangements. A lateral capillary interaction energy of ~ 104 kT was attributed to the tip to tip and side to side arrangement. Densification of the monolayer occurred over time, and the monolayer became more heterogeneous. At a higher concentration of particles, the side to side configuration was the preferred orientation. This was attributed to the fact that the total energy of the interface was reduced when the particles interacted over more of their perimeter. For charged ellipsoids at the oil- water interface, the particles were separated to a greater extent for a comparable coverage as observed for the uncharged particles. Some particles were arranged into triangular and quadrilateral groups in addition to the presence of individual particles. Linear aggregates were observed at a higher surface coverage and no long range order was observed in the initial structure. It was found that the particles aggregated even without the addition of salt (Fig. 1. 7), under conditions where spherical particles normally aggregate, and this was due to the dominance of capillary forces over electrostatic repulsion. For charged particles at the air- water interface, where the contact angles of the particles at the interface and its surface tension is changed, a denser structure was observed in contrast to the particles at the oil- water interface due to a decrease in stabilisation. The monolayer consisted predominately of particles arranged into a triangular backbone with tip to tip contacts with some

particles stacked side by side and did not change appearance after several days. In this work, it was assumed that electrical dipoles exist at the oil- water interface and therefore in this case, a strong repulsion would be expected for particles in the side to side configuration and a tip to tip configuration would therefore be expected, as observed. For particles at the air- water interface, electrostatic interactions are expected to be weaker; however the capillary interaction will be altered and therefore there may be a balance of forces at play. In this case side to side contacts would be predicted. [91] In summary, this work has demonstrated that the structure of the monolayer formed from non- spherical particles depends on particle shape, surface chemistry and wetting properties, and that shape induced capillary interactions cause particle aggregation in the absence of added electrolyte and therefore dominates over electrostatic repulsion. [92]

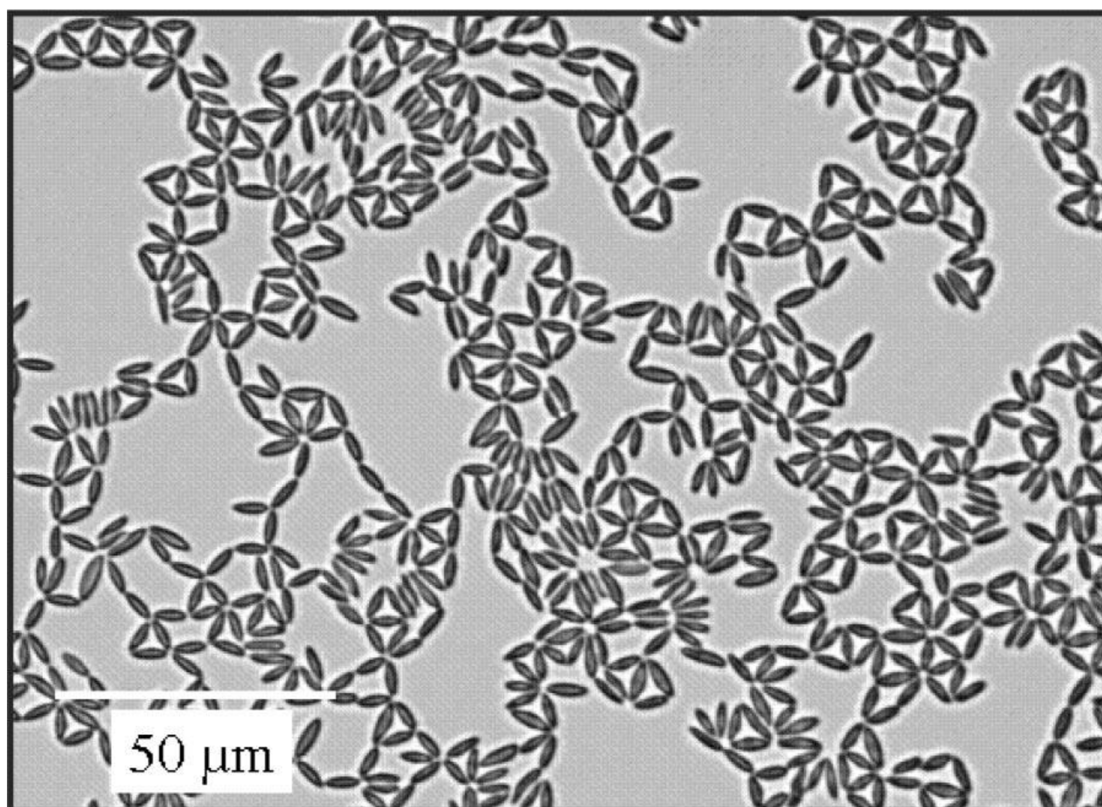

Fig. 1. 7. A monolayer of charged ellipsoidal PS particles at a decane- water interface. Unlike spherical particles with the same composition, the ellipsoidal particles aggregated at the oil- water interface even without the addition of salt. Reproduced from ref. 92.

In a work carried out by Loudet *et al.* the capillary interaction between ellipsoidal particles at the oil- water interface was also investigated. The particles with a long axis between 1. 5- 14 μm were spread at the oil (decane, 70. 5 vol. % and undecane, 29. 5 vol. %) water interface in a glass container. The attraction between the particles was observed to be at a distance of several times the ellipsoid long axis and the particles were found to stick irreversibly upon contact. They observed that PS ellipsoids aligned preferentially in a tip to tip arrangement as in ref. 92, whereas silica coated ellipsoids aligned preferentially in a side to side arrangement. These differences were attributed to the different wetting properties of the particles. The preferential organisation of the particles minimised the interfacial distortions and the overall interfacial energy. The structures were not influenced by slight variations in the particle aspect ratio due to polydispersity. They also observed that groups of ellipsoids could freely rotate around one another without coming apart. This is because the interaction energies are much larger than kT. These interactions could not be attributed to van der Waals forces of attraction as these are much smaller than kT at a distance of more than 1 μm. [94] In contrast, spherical particles interact with an energy comparable to kT, and can approach one another very closely without making contact. The enhanced particle contacts observed for ellipsoids were attributed to complex interfacial distortions and consequently strong capillary interactions. They have determined, using a particle tracking technique, that the ellipsoids could feel one another at distances of tens of microns. They also determined that the interfacial deformation around the particles have quadrupolar symmetry and interact with a power law dependence of r^{-4} (where r is the centre to centre distance between two particles). This has been determined directly using interferometry and optical trapping. [95] The interface mediated interactions arising from ellipsoidal particles trapped at the interface were explored further by the same research group. [96] They found that static interfacial deformations (the particles experience forces in the direction parallel to the interface normal, e. g., if the particles are pushed into the lower phase) result when the particle contact angle is different from 90 °, and lead to orientation dependant capillary interactions between the particles. Gravity mediated capillary forces have been neglected for these particles (< 10 μm). [96] In a work published by the group of Stebe, the alignment of non- spherical particles at a non-planar air- water interface characterised by optical microscopy was reported. The particles were fabricated by photolithography using SU- 8 2000 photoresist which

therefore became the composition of the particles. The zeta potential of the photoresist particles at a pH of 5. 8 was found to be < 25 mV and therefore the particles are only weakly charged. The interfacial shape was determined by fabricating grooves into a glass block before adding the water. It was found that after spreading cylindrical particles at the air- water interface, the particles aligned in a direction determined by the curvature of the interface. The cylinders aligned in opposite directions depending on whether the interface was concave or convex as shown in Fig. 1. 8.

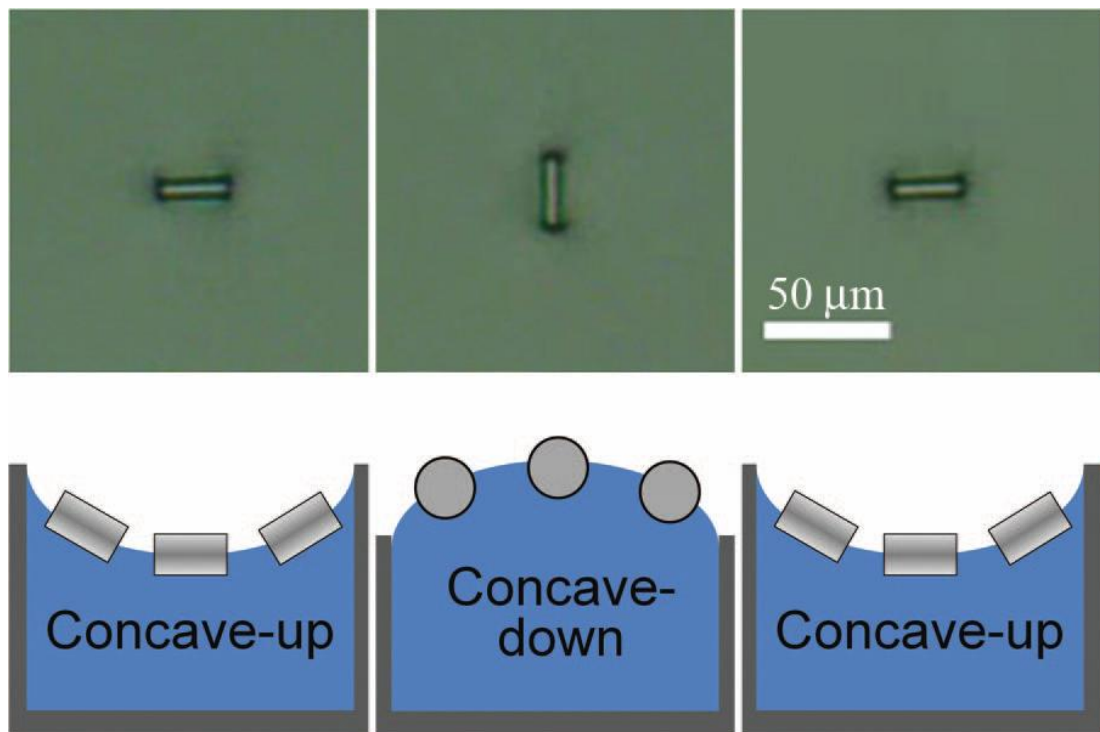

Fig. 1. 8. Cylindrical particles at the air- water interface with different curvatures. The particles composed of SU- 8 2000 photoresist with a zeta potential of < 25 mV, adjusted their orientation depending on the curvature of the interface and the orientation was found to be reversible. Reproduced from ref. 97.

The preferred alignment of the cylinders was determined by a capillary interaction that is induced in order to minimise the excess area of quadrupolar deflection resulting from the presence of the particles at the interface. They have used these findings to corroborate the preferential tip to tip chaining of ellipsoids on a planar interface as reported by Loudet *et al.* [95] In the present case it was found that a high excess area of interface existed at the tip of the cylinders resulting in the tip to tip chaining. [97] Following on from this investigation, the group of Stebe has

investigated the effect of complex interfacial curvature on cylindrical particle migration and rotation. The interfacial shape was distorted by the presence of SU- 8 photoresist microposts positioned perpendicularly to the interface such that the contact line of the water is pinned at the top edges of the SU- 8 posts, and the curvature of the interface decreased with distance from the posts. The presence of cylindrical photoresist particles with aspect ratios between 2. 0 and 3. 0 were then investigated at the hexadecane- water interface. The particles distorted the oil- water interface in order to satisfy the wetting requirements of the particles. The deformation of the interface around a particle was described as an elongated quadrupolar structure. Once a particle had attached to the interface, it rotated so as to align its quadrupolar axes along the principle axes of the interface and the particle then accelerated towards the SU- 8 micropost. The gravitational potential energy of the particles and the Laplace pressure gradients due to the curvature of the interface were described as negligible in this study. The migration of the particles in this case was attributed to the interfacial energy. The particles were found to migrate uphill of the interfacial deformation created by the micropost. For particles located within the vicinity of square shaped microposts, the particles adopted both tip to tip and side to side configurations with the particles being confined only to the corners of the microposts due to repulsive capillary forces created by the curvature gradients. The overall tendency of the particles is to migrate towards regions of the interface with high curvature. [98] In another work by Stebe and co workers, a pair potential for elongated particle cylinders approximated as two elliptical quadrupoles (which was shown to be the dominant deformation mode around the cylinders) was derived. This was observed experimentally as a capillary rise at the flat ends, and a downward slope along the curved sides of the particles with the extent of the deformation depending on the aspect ratio and wetting properties of the particles. They also investigated the behavior of the photoresist cylinders in isolation, in pairs and in dense assemblies. The derived anisotropic potential predicts torques, which promote preferential alignment during approach and assembly of the particles with a strong dependence on the particle aspect ratio. The orientation of the particles after adsorption at the interface was found to depend on the orientation of the particles when they initially contacted the interface; once there the particles were trapped in metastable states due to the surface tension induced energy barrier to reorientation. For this reason, particles were found to be orientated with their major axes

perpendicular with the interface or parallel with the interface. For particles interacting at the interface, it was found that at very large distances the particles attracted each other, but rotation of the particles was negligible as the torque force decayed faster than the attractive force. When the particles were separated by 10 particle radii, the ability of the particles to rotate became much more pronounced and the particles were able to align in an end to end configuration (where the interface deformation was larger). Additional particles were then able to join the existing dimers in an end to end manner to form linear chains. In densely packed monolayers as demonstrated by a particle laden water drop on hexadecane, the particles were observed to produce linear chains that were aligned together with side to side contacts as shown in Fig. 1. 9. [99]

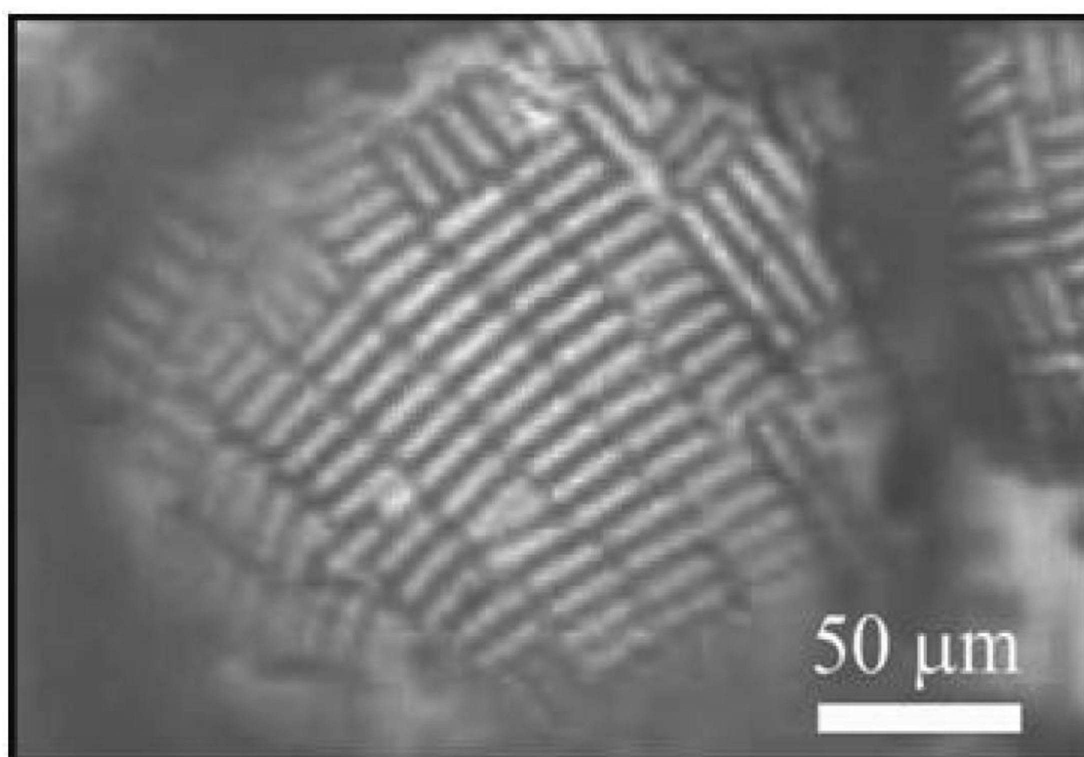

Fig. 1. 9. A lattice of photoresist cylinders trapped on the surface of a water droplet in hexadecane. Reproduced from ref. 99.

1. 5. 2. Interactions between Janus particles at liquid interfaces

Binks and Fletcher, in a theoretical work have investigated the adsorption of both a homogeneous particle and a Janus particle at an oil- water interface. The Janus particles were described as amphiphilic; that is the particles are composed of polar and apolar regions. It was found that the effect of introducing amphiphilicity on a

particle with a contact angle of 90 ° produced a maximum of a threefold increase in the surface activity and in contrast to homogeneous particles, a Janus particle can remain strongly attached to the interface even when the average contact angle approaches 0 or 180 °. [100] In a paper by Krausch and co workers [102], the theoretical predictions of Binks and Fletcher [100] have been confirmed experimentally. Janus particles with diameters of ~ 14 nm were prepared consisting of Au and Fe_3O_4 according to the methods of Yu *et al.* [101] The amphiphilicity of the particles was enhanced by attaching dodecanethiol or octadecanethiol to the gold surface. They have investigated the interfacial activity of both homogeneous (unmodified) particles and Janus particles at the interface between hexane and water. For unmodified Fe_3O_4 and Au particles, the interfacial tension was found to be 34. 5 mN/ m and 33. 0 mN/ m respectively. For the pure hexane- water interface before adsorption of the particles, the interfacial tension was found to be ~ 48. 5 mN/ m. For the Janus particles modified with DDT, the interfacial tension was reduced to 22. 5 mN/ m and when ODT was used, the interfacial tension was reduced further to 18. 0 mN/ m due to the greater hydrophobicity of the surface of the particles. [102] In a paper published by Isenbügel *et al.* [103] the technique of partially embedding silica particles followed by silane treatment was investigated in order to determine if the interparticle interactions differed to unmodified particles. They studied the assembly behavior of the particles in water induced by evaporation. In the silane treated silica particle case, extensive aggregation and the formation of highly ordered structures was observed. Lee and co workers have investigated the assembly of spherical PS modified Janus particles at the oil- water interface. The assembly was found to be strongly dependant on the difference between the surface wettability of the hemispheres. Capillary interactions were induced due to the presence of intrinsic heterogeneity at the boundary between the two hemispheres. They also demonstrated that long range repulsion exists between two Janus particles consisting of two negatively charged hemispheres. Gold coated Janus particles were prepared from a monolayer of PS particles on a glass substrate. [70-72] The metals, chromium followed by gold were coated on the exposed hemisphere by thermal evaporation. The gold surfaces were further modified with a series of silanes to alter the wettability of the surface. In contrast to untreated polystyrene particles that form a regular hexagonal lattice at the oil- water interface due to electrostatic dipolar repulsion, the gold coated Janus particles immediately assembled together into two

dimensional aggregates which was attributed to the strong capillary interaction between the particles as shown in Fig. 1. 10.

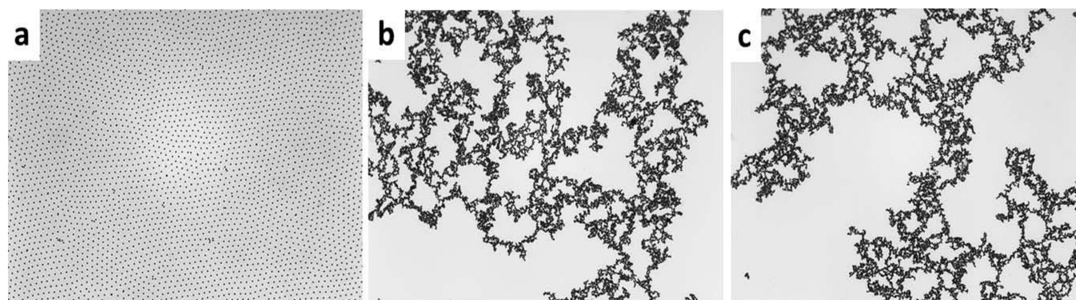

Fig. 1. 10. Structures at the oil- water interface for monolayers of spherical unmodified PS (a), Au- PS Janus particles (b) and DDT (1- Dodecanethiol)- Au- PS Janus particles (c) at the oil- water interface. Scale bar shows 100 μm. Reproduced from ref. 104.

For the silane treated gold surfaces, the hydrophobic hemisphere was found to be immersed into the oil phase, with the boundary between the two hemispheres orientated parallel with the interface. When the gold surface was not hydrophobised, some particles were orientated with their gold hemispheres immersed into the aqueous phase. They also found that in cases where the boundary between the hemispheres was tilted at the interface, the contacting particles did not necessarily have their gold surfaces facing each other as might be expected, indicating that the chemistry of the surfaces is not the only driving force for assembly. They have demonstrated the presence of a quadruploar capillary interaction between the Janus particles due to the overlap of the undulated interface deformation. [104] In a theoretical work, Lee and Park have investigated the equilibrium orientations of non-spherical Janus particles at a liquid- fluid interface. They have investigated both ellipsoidal and dumbbell shaped Janus particles at the oil- water interface. In order to establish the equilibrium orientation of the particles, they have considered the minimisation of the attachment energy of the Janus particles as a function of their orientation at the interface. The equilibrium orientation of the particle was found to depend on its size, aspect ratio and surface properties. When the difference between the wettability of the two faces is large or the aspect ratio is close to 1, the particles prefer to orientate perpendicularly to the interface for both the dumbbell and ellipsoidal particles, whereas if the difference between the wettability of the two faces is small or the aspect ratio is large, the particles prefer to tilt at the interface. Ellipsoidal particles were found to adopt a metastable state under certain conditions

due to the presence of a secondary energy minimum. In contrast, dumbbell shaped particles adopt a single orientation at the interface and therefore are more likely to adopt a uniform orientation. [108]

1. 6. Investigation of particle monolayers using a Langmuir trough

The Langmuir trough is used to investigate the surface phenomena of surface active material at a liquid interface as the monolayer undergoes compression and expansion. Originally, the trough was a simple set up consisting of metal trays rendered hydrophobic by the use of wax such as that used by Irving Langmuir (Langmuir's film balance). [19] The films of material on the surface of the water were kept confined by means of a floated length of waxed silk which divided the surface into two compartments; one of the compartments was filled with oil of known surface pressure. Modern troughs are often made of Polytetrafluoroehtylene (PTFE) with PTFE or Delrin barriers driven on motorised linear guides which allow the surface coating (a monolayer) on the water phase to be compressed or expanded at a certain rate controlled by computer software. Changes in surface tension, or surface pressure, can be monitored by recording surface pressure vs. surface area isotherms as the density of the monolayer changes. The surface pressure is given by

$$\Pi = \gamma_o - \gamma \qquad (1.\ 7)$$

Where γ_o is the surface tension of the pure water phase and γ is the surface tension of the water after addition of particles to the interface.

The surface tension is recorded by means of a Wilhelmy plate which is immersed into the sub- phase (typically water). The forces acting on the plate are surface tension and gravity acting downwards and buoyancy acting upward. The effect of gravity and buoyancy is eliminated by ensuring that the recorded pressure is zeroed and the plate is kept at a constant level before making measurements. The measured force is then given by:

$$F = 2(w + t)\gamma \cos\theta \qquad (1.\ 8\ a)$$

Where *w* and *t* are the width and thickness of the plate. The contact angle that the water makes with the plate (θ) is reduced to zero by means of a plate made of filter paper. Therefore

$$F = 2(w + t)\gamma \quad (1.\ 8\ b)$$

In most cases, it is necessary to spread the material of interest at the interface with the aid of a suitable spreading solvent. The solvent must be volatile, e. g., chloroform or ethanol in order to ensure its removal by evaporation. All materials, solvents and the trough itself must be free from contamination before commencing experiments. Monolayers undergo phase transitions during compression in the trough; such transitions can be identified by noticeable changes in the shape of the isotherm. As an example, lipid monolayers are described as liquid- expanded (fluid-like) at large areas, liquid- condensed (crystalline liquid, often found to occur in combination with the liquid- expanded phase), crystalline (solid- like) and at sufficiently small areas of the trough, the monolayer will collapse into the bulk with a corresponding sharp decrease in surface pressure. [20] Monolayers that occupy a small area per molecule are often described as incompressible, whereas monolayers occupying large areas per molecule are described as compressible. [16] More recently the technique has been applied to study the behavior of solid particles at both the air-water and oil- water interface. Such monolayers can act as model systems for the study of particles at the surface of droplets as in emulsions and as a means of studying particle interactions in two dimensional systems, [21-26] and particle aggregation studies. [27-31] A typical isotherm for a particle monolayer is shown in Fig. 1. 11. The surface pressure shows no change (K1) until the monolayer is close packed (K2); further compression results in a rapid rise in pressure until the particles are ejected from the interface or the monolayer starts to buckle. This is labeled K3 in the isotherm and is often referred to as the collapse pressure. A two dimensional lattice composed of the monolayer material can be formed, which can later be transferred to a solid substrate. [7, 32- 38] Some troughs, as in the type used in this work, are small enough to be transferred to a microscope stage to allow simultaneous observation of the monolayer during compression and expansion.

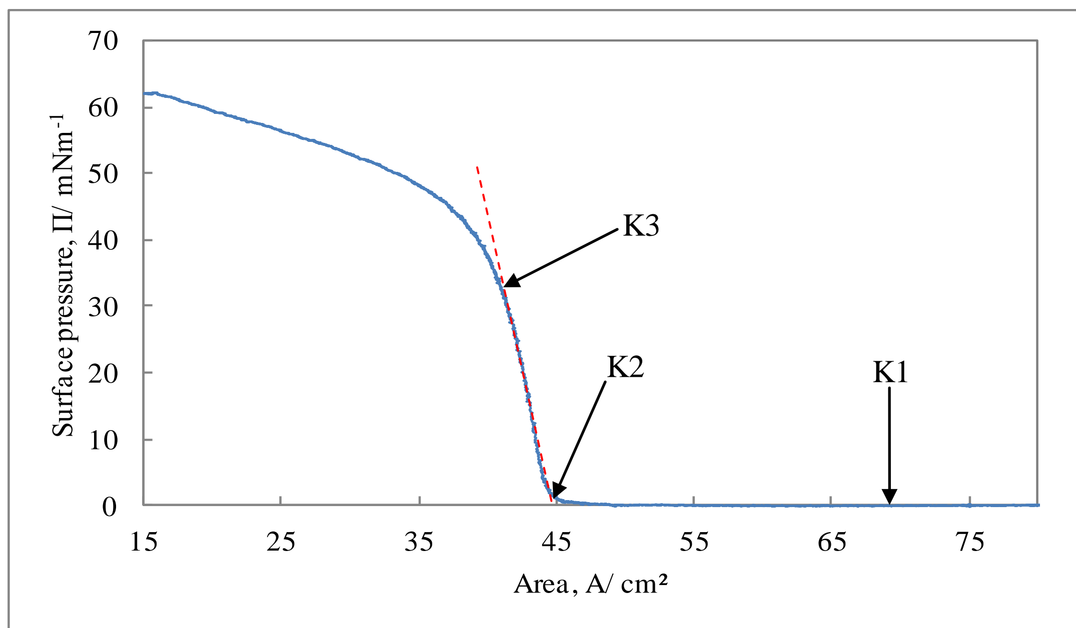

Fig. 1. 11. Surface pressure vs. area isotherm for a solid particle monolayer undergoing compression in a Langmuir trough. Different regions of the isotherm are labeled K1, K2 and K3.

Experiments performed in a Langmuir trough have revealed some interesting behavior of colloidal monolayers confined between two compressing barriers. In a work investigating the behavior of monolayers of charged polystyrene latex particles with diameters ranging from 0. 21- 2. 60 μm during compression and expansion in a Langmuir trough, Aveyard *et al.* found that addition of 0. 1M NaCl to the aqueous phase reduced the interparticle separation by screening the interparticle repulsion. However for particles at the oil- water interface, the interparticle repulsion was found to be quite insensitive to the presence of the salt. This was proposed to be due to the presence of residual charges on the surface of the particle in contact with the oil resulting from the presence of hydration water trapped in surface undulations and localised around the hydrophilic sulphate groups. Monolayers of particles at the air-water interface resulted in the formation of large interconnected networks at a sufficiently high salt concentration and during compression the formation of hexagonally ordered rafts of particles consisting of close packed particles were observed. Upon reexpansion of the monolayer, the rafts broke apart and the particles within the rafts remained close packed. In contrast, the monolayers at the oil- water interface were well ordered in a hexagonal array at low surface pressures with interparticle separations of several particle diameters: beyond the collapse pressure,

the monolayer underwent buckling and the hexagonal ordering was recovered upon expansion. These observations support the presence of long range repulsion at the oil- water interface. [77] In another paper, the group of Aveyard noted that the buckling of the monolayer occurred when the surface pressure was equal to the surface tension of the bare oil- water interface. This is perhaps not surprising as the very low surface tension is not sufficient to prevent distortion of the fluid interface. They also noted that particles were not ejected from the interface during monolayer collapse. [78]

Further experiments using a Langmuir trough have revealed that the cohesiveness and stability of a monolayer subjected to a lateral compression is also dependant on the wettability of the particles. In a work published by Hórvölgyi *et al.* glass beads with diameters of 75 ± 5 μm were silanised to various extents using trimethylsilyl *N*, *N*-dimethylcarbamate and spread at the air- water interface using a Langmuir trough. After spreading of the particles, aggregation occurred. For both the hydrophilic and hydrophobic particles, close packed hexagonal ordering of the particles occurred during compression of the monolayer. For particles with contact angles of ~ 90 °, no particle ejection was observed into the bulk water sub- phase during collapse of the monolayer, in contrast to those particles with a lower degree of hydrophobicity. Particle ejection was inferred from the shift of the isotherms to smaller areas during repeated compressions. The whitish appearance of the undulations of the monolayer at the collapse pressure was attributed to the transfer of monolayer material into air. The hydrophobic particles tended to form a more cohesive monolayer than the less hydrophobic particles where electrostatic and hydration forces were more prevalent. [82] In another paper, it was proposed that a surface pressure gradient in the monolayer exists which is attributable to the amount of spread particles and the cohesiveness of the monolayer. The more hydrophobic particles are strongly attracted to each other by dispersion forces and the extent of rupture of these particle contacts during compression depends on the position of the particles with respect to the moving barriers. [83]

Non- spherical particle monolayers are less studied by Langmuir trough experiments. In a work by Vermant *et al.* compression and expansion isotherms for ellipsoidal particles at the air- water interface in a Langmuir trough were obtained. They demonstrated that the surface pressure of the monolayer during compression

exhibited a more gradual rise than that observed for spherical particles due to a different structural rearrangement of the monolayer. During compression, some of the particles flipped with their major axes perpendicular to the interface. In this way, some of the compressional stress is relieved. Therefore the presence of compressible aggregates formed after spreading and the occurrence of "flippers" resulted in a more gradual increase in pressure during compression. At the smallest areas of the trough, buckling of the monolayer occurred with some of the particles ejected from the interface. Flipping was found to originate in the denser regions of the monolayer and the presence of voids in the monolayer after compression suggested that the compressive stress was not distributed uniformly. During expansion of the monolayer, a very abrupt decrease in pressure was observed and the monolayer became more heterogeneous.

1. 7. Methods for the fabrication of non- spherical microparticles

1. 7. 1. Mechanical stretching

In papers by Keville *et al.* and Ho *et al.* PMMA (Poly(methyl methacrylate) and polystyrene particles were synthesised. The spherical particles were then embedded in a matrix of PDMS (Polydimethylsiloxane) or PVA (Polyvinyl alcohol) which was subsequently cross linked. At a temperature above the glass transition, the elastic films produced were stretched under unaxial extension by clamping the film into a metal frame producing prolate particles with aspect ratios of up to 8 (the aspect ratio could be controlled by stretching the film to a predetermined extent). After cooling below the glass transition temperature, the ellipsoidal particles were liberated from the matrix by dissolution of the film. [39, 40] The technique has been applied by other researchers to fabricate ellipsoidal particles with a specific aspect ratio. [41- 48] These investigations involved the fabrication of non- spherical particles in two dimensions. Paunov and co workers have established a 3D procedure for the fabrication of ellipsoidal particles. In this technique, an oil in water emulsion template was used, where the oil was polymerisable. The emulsion was then mixed with an aqueous phase containing a gelling agent. After setting, the gelled continuous phase was subjected to stretching or compression which caused deformation of the oil droplets. The deformed droplets were then solidified using UV curing and the gelled

continuous phase was heated above its melting temperature to liberate the non-spherical particles. [49]

1. 7. 2. Templating

Microstructured particles have been synthesised by Velev *et al.* by growing colloidal crystals in aqueous droplets suspended in fluorinated oil. The method allows control of particle size and shape through ellipsoids to toroids by varying the droplet composition. In this method, close packed colloidal crystals were templated into porous particles. Suspended droplets were used as the templates within which the colloidal particles were gradually concentrated by drying to form 3D crystals. Interplay of droplet size, gravitational force and interfacial tensions allows control of the shape of the suspended template droplets. Variation of latex concentration and addition of varying concentrations of surfactants during the drying process, produced examples of shape control during assembly. [50] In a paper published by Lee *et al.* peanut shaped colloidal particles were fabricated. In this method, core hematite particles were first produced using a sol- gel method. The particles were then coated with rhodamine isothiocyanate modified silica. Hollow silica shells were produced by dissolving the hematite core with HCl. During preparation of the hematite particles, dimer particles were produced and after dissolution of the core, the peanut shaped silica shell was released. The non- spherical silica particles produced in this way had a thickness of 65 nm and dimensions of 2. 84 x 1. 36 µm. [51] Variations of the technique can be found in refs 52- 54. Mejia *et al.* have established a technique of fabricating disc shaped particles based on an emulsion drop templating technique. First, α- eicosene- wax emulsions were prepared by electrospraying the melted α-eicosene in an SDS solutions. During cooling, the alkene undergoes surface freezing and a crystalline monolayer was created around the wax droplets which acted as a nuclei. The emulsion droplets crystallised from the surface towards the centre and the curvature and shape of the discotic particles obtained was controlled by the packing density of the SDS surfactant. A high degree of packing of the surfactant was required to fabricate flat disc shaped particles. [55]

1. 7. 3. Droplet microfluidics

Non- spherical particles have been fabricated using droplet microfluidics by Hwang *et al*. Using a T- junction microfluidic device in combination with a UV light reflector, emulsion droplets prepared from poly (ethylene glycol) diacrylate mixed with magnetic iron oxide particles and light mineral oil were driven through the PDMS microfluidic channels using air pressure and were polymerised with UV light with a wavelength of 355 nm. By controlling the dimensions of the channels, disc and cylindrical shaped particles with controlled sizes could be fabricated. These non- spherical particles could then be manipulated with a magnetic field. In the presence of a magnetic field, the particles acquire dipole moments and long ranged dipolar interactions between the particles resulted in chain- like or columnar structures along the direction of the applied field as shown in Fig. 1. 12. [56]

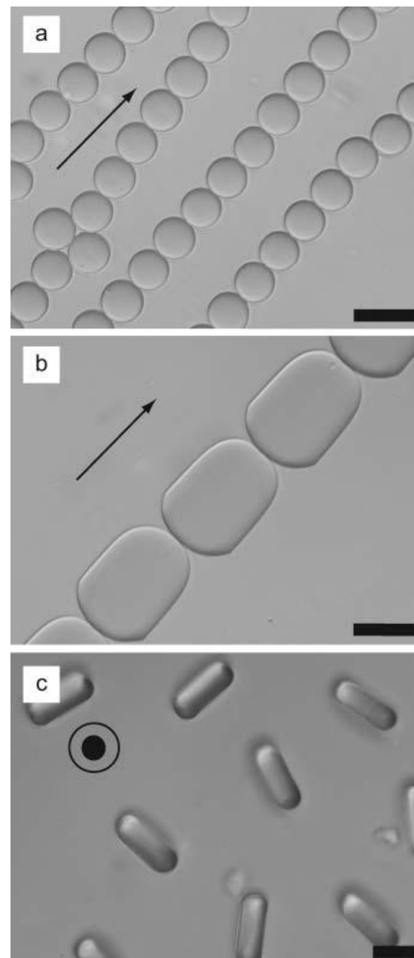

Fig. 1. 12. Microscopy images of spherical and non- spherical particles in response to a magnetic field along the direction of the arrows shown in the figure. The magnetic field was applied in plane (a and b) and out of plane of the interface (c). Scale bars show 25 μm. Reproduced from ref. 56.

1. 8. Methods for the fabrication of surface - anisotropic (Janus) particles

Liu *et al*. have developed a method for the fabrication of polymeric Janus particles. In this technique, a combination of LB (Langmuir- Blodgett) deposition of PS/ BPMA (polystyrene/ benzophenone methacrylate) and spin coating was first applied to deposit a monolayer of particles on a solid substrate. First the PS particles were dispersed in methanol and spread onto a water surface. The monolayer was then transferred onto a quartz substrate previously spin coated with a layer of glucose to facilitate binding and later release of the particles, i. e., a sacrificial layer. The monolayer was then spin coated again to achieve a closer packed array and was then dried in an oven to adhere the particles to the substrate. A photografting technique using UV light was then applied to attach PAM [poly- (acrylamide)] or chitosan to the surface. The chitosan surface was then modified to allow the binding of a layer of gold nanoparticles to one hemisphere of the particles. [57] Magneto responsive Janus particles have been fabricated by Kim *et al*. In this technique, silica particles were mixed with iron oxide particles and dispersed in ethanol containing a photosensitive resin. After removing the ethanol, the photocurable suspension was driven though a channel of a microfluidic device and was mixed with a surfactant solution from another channel. The monodisperse emulsion droplets collected were solidified by application of UV light. When a magnetic field was applied to the droplets, the iron oxide particles migrated towards the field leaving the silica particles anchored to the interface; the Janus particles were obtained after the photocurable resin was solidified. [58] In a work by Zhang *et al*. magnetic Janus particles were fabricated in a single- step synthetic approach. An Fe_3O_4 particle suspension was treated with hexadecyltrimethylammonium bromide (CTAB) and further modified with tetraethyl- orthosilicate (TEOS) to provide a source of silica. The silica was found to grow on one half of the particle surface and a rather interesting tail- like appendage on the iron particle surface was observed. The aspect ratio of the formed particles could be tailored by varying the amount of Fe_3O_4 or TEOS. Straight chains of the modified particles were found to align towards a magnetic field as shown in Fig. 1. 13. [59]

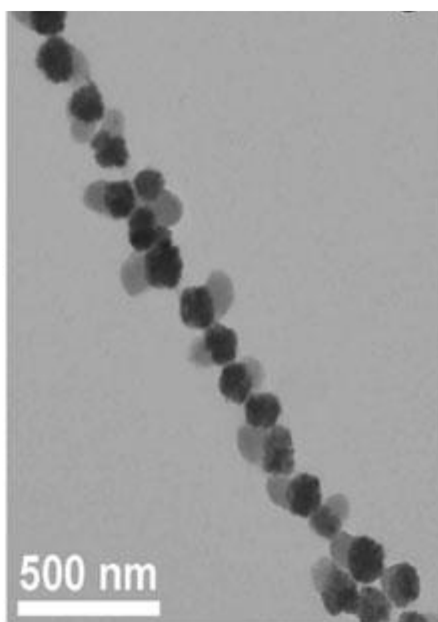

Fig. 1. 13. A straight chain of magnetic Fe_3O_4 particles with silica particle attachments (shown by a lighter tone) to one half of the surface of each sphere aligned in a magnetic field. Reproduced from ref. 59.

The group of Anderson *et al.* have fabricated Janus particles composed of a combination of organic and inorganic components. Silica particles with diameters of 3 μm were cast onto a spin coated film of polystyrene which acted as a sacrificial layer. After heating, the particles became partially embedded in the PS film. The particles were then coated with acrylonitrile, ferrocene or pyridine by plasma deposition to modify one half of the particle surface. In order to release the particles, the PS sacrificial layer was dissolved in toluene. [60] Synytska *et al.* have prepared Janus particles by silanisation of the surface of silica particles. The silica particles were first mixed with wax and water at elevated temperatures. With the particles partially embedded in the wax, the exposed surface of the particle was treated with aminopropyl- trimethoxysilane (APS) and after liberating the particles from the wax, the other surface was treated with octadecyl- trichlorosilane. The surface active nature of the obtained particles was utilised to allow the surface of textiles to be rendered hydrophobic; thus imparting water- repellent properties to the textiles. [61] In a similar way, the group of Granick have investigated the application of various silanes to partially embedded silica particles by chemical vapour deposition in a nitrogen atmosphere. They found that the particles fabricated in this way could self assemble in water by forming chains with the oppositely charged particles linked

together. [62, 63] Ye *et al.* have prepared bimetallic particles composed of silica particles with different metals on the opposite hemispheres. In this approach, a suspension of silica particles was applied to the surface of a hydrophilic glass substrate to give a close packed monolayer. E- beam vacuum evaporation was then employed to apply a metal on one half of the particle surface, then after removing the monolayer with an adhesive support, the opposite surface was coated with another metal. The metals used were silver, nickel, cobalt, aluminium, platinum and gold (an adhesive layer of titanium was used prior to applying the gold). [64] McConnell *et al.* have developed a method to create self assembled patchy gold on amine modified silica particles. Silica particles with diameters of 230 nm were attached to a styrene-acrylic acid copolymer film and partially sunk into the film. Gold nanoparticles with diameters of 15 nm were then electrostatically assembled onto the exposed silica particle surface. Upon thermal annealing, gold hemispherical caps were formed on one surface of the silica spheres. By controlling the wetting properties of the silica, it was found to be possible to form a patchy gold surface. [65] Fujimoto *et al.* have investigated a different approach for the fabrication of Janus particles. In this approach, the particles were fabricated on the solid- liquid or liquid- air interface. Human immunoglobulin G (IgG) was first adsorped onto a polystyrene surface and a dispersion of spherical particles composed of methacrylic acid, p- Nitrophenyl acrylate and methylenebisacyrlamide was obtained after polymerisation. The spheres were then allowed to react with the IgG and the exposed surface of the spheres was then hydrolysed using NaOH before detaching the particles from the polystyrene to render the partial modification of the particles. [66]

1. 9. The fabrication of anisotropic particles by photolithography

Photolithography is routinely used in microelectronics for patterning solid surfaces and in the fabrication of microfluidic devices via wet etching of glass blocks. The technique utilises a UV sensitive polymer known as a photoresist which consists of a resin, a photoactive compound and a solvent. During exposure the photoresist is changed chemically and/ or physically to render exposed areas either soluble or insoluble in a basic developer solution. In the case of a positive acting, or positive photoresist, the polymer is degraded in exposed regions and becomes soluble in developer, whereas in the case of a negative acting, or negative photoresist, crosslinking of the polymer occurs and the exposed regions become insoluble in

developer. A subsequent development step will therefore differentiate between exposed and unexposed areas of the photoresist. A typical composition of a positive photoresist is a resin such as polymerised phenol and formaldehyde otherwise known as Novolac, a volatile solvent and a photoactive compound such as diazonapthoquinone (DNQ). The mechanism of its action is as follows: upon exposure to UV, the precursor Novolac is converted into a ketene with the elimination of nitrogen, a process known as the Wolff rearrangement. The presence of water then converts the ketene into a carboxylic acid that is soluble in a basic solution as shown below in Fig. 1. 14.

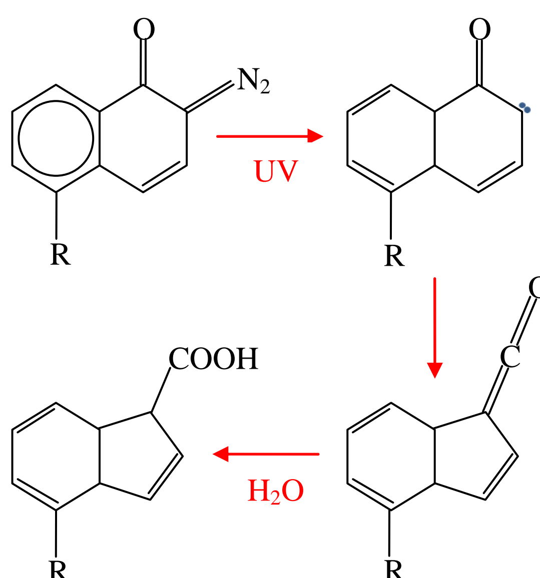

Fig. 1. 14. Reaction mechanism for the formation of a base soluble carboxylic acid from the DNQ photoactive group.

For the negative photoresist, a commonly used system involves the use of mixtures of cyclised polyisoprene and photoactive diazides. Upon irradiation with UV, the diazide forms a bisnitrene which then crosslinks the polyisoprene by reacting with its double bonds to produce an insoluble matrix. [67] A pattern can be generated following development in a basic solution if the photoresist is exposed through selected regions using a suitable photomask.

1. 9. 1. The application of photolithography for the fabrication of non- spherical particles

A variation of the photolithographic technique can be employed in which the crosslinked photoresist pattern is preserved which allows the fabrication of non-spherical particles composed of the chemically and thermally stable polymer to be realised. The first step is the design of a suitable photomask containing an image of the desired particle shape and size. Several important steps are involved in the photolithographic process and the key stages of photolithography for the fabrication of non- spherical particles are summarised schematically in Fig. 1. 15. First the photoresist is spin coated onto a solid substrate (wafer) that is typically silicon or glass in order to produce a thin film of uniform thickness. The thickness of the film and therefore the particles fabricated can be controlled by adjusting the spin speed and spinning time. For the negative photoresist used in this work, a sacrificial layer consisting of a resin that is not sensitive to UV is spin coated onto the substrate before spin coating the photoresist in order to enable the patterned photoresist particles to be removed from the substrate at a later stage by dissolution of the sacrificial layer. The alternative approach of etching the wafer was not performed in this work as the technique is subtractive, i. e., the substrates cannot be reused. The sacrificial layer is baked to remove solvent before applying the photoresist. Pre-baking of the spin coated photoresist film is then carried out in order to reduce the remaining solvent content left over after spin coating. This step has important implications for the exposure and development stages. The dry photoresist is then exposed to UV for a certain period of time; exposure times too short or too long result in size variations in the patterns generated. In the case of the negative photoresist, a further baking step is performed after exposure in order to complete the crosslinking process. In order to develop the pattern, the substrate is placed in developer solution consisting of a base such as NaOH, or more commonly, TMAH (tetramethylammonium hydroxide) until the remaining soluble photoresist is dissolved. In order to enhance the chemical stability of the photoresist (negative only), it is sometimes necessary to hard bake the photoresist at the last stage. In order to reproduce accurately the size, shape and thickness of the pattern, each of these stages need to be carefully optimised.

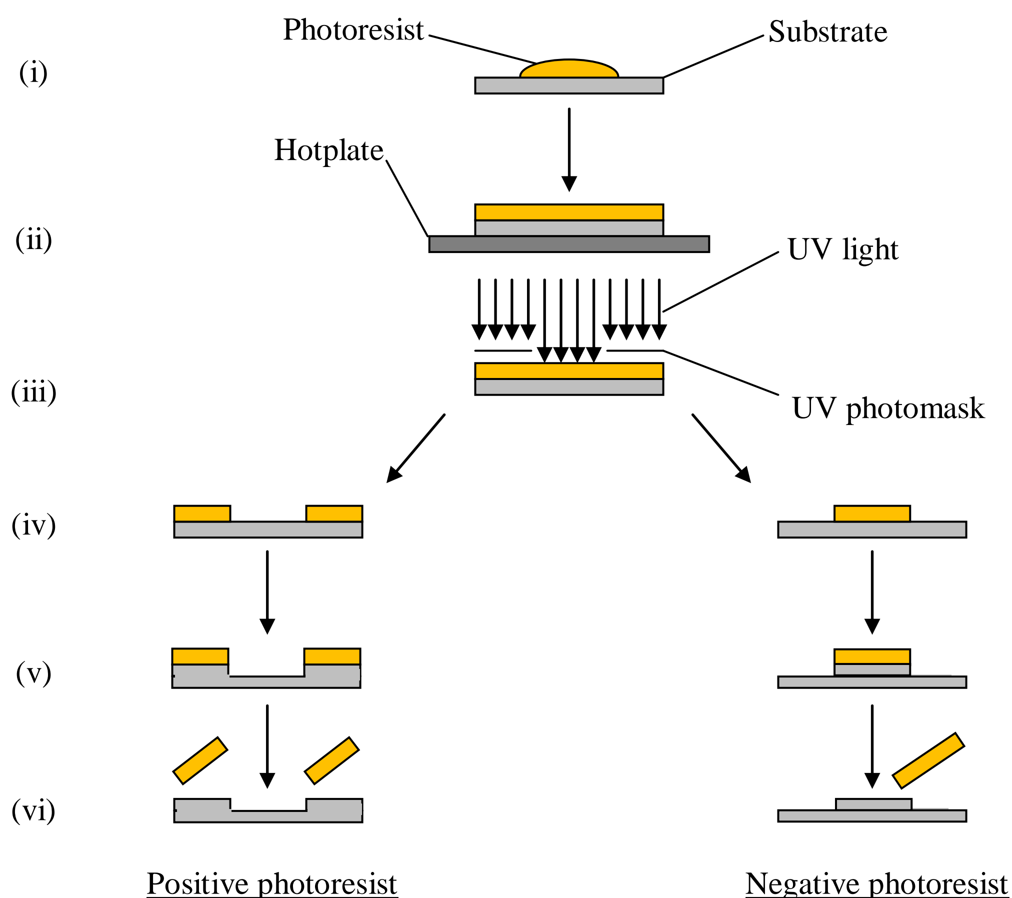

Fig. 1. 15. Schematic representation of the photolithographic process: (i) formation of a thin photoresist film on the substrate by spin coating; (ii) pre-baking to remove residual solvent from the spin coated film; (iii) exposure of the photoresist film with UV light through a suitable photomask; (iv) development of the photoresist film to remove soluble regions; (v) etching of the substrate; (vi) removal of the photoresist from the etched substrate.

Recently, photolithography was used for the preparation of solid microdisks. The group of Stroock at Cornell University, USA has demonstrated the preparation of solid microdisc particles from the negative photoresist SU- 8. [68, 69] Particles with homogeneous surfaces (both microdisc faces having the same chemistry); various geometries (circular, triangular etc) and low diameter- to- thickness aspect ratios (1: 1 and 3: 1) have been fabricated. They have observed various structures of aggregated particles in aqueous suspensions (incl. columnar aggregates) by tuning the particle interactions, adding electrolytes (electrostatic repulsion), adsorbing appropriate surfactants (steric repulsion) and adding dextran (attractive depletion).

More recently, Hernandez and Mason have prepared microscale polymer particle dispersions representing all 26 letters of the alphabet and investigated various shape-dependant assemblies of crosses, square donuts, triangular and pentagonal prisms driven by depletion attraction. In addition, hybrid bilayer Janus particles were fabricated by a double exposure using square, cross and triangle shaped masks. In a similar way to the group of Stroock *et al.*, [68, 69] the photolithographic process involved the application of a sacrificial layer onto a silicon substrate by spin coating. Then a layer of an epoxy based (SU- 8) negative photoresist was spin coated onto the sacrificial layer followed by exposure using a high- throughput automated stepper exposure system and development. The particles were then liberated from the solid substrate by dissolution of the sacrificial layer. [70, 71] Brown *et al.* have fabricated a range of particles of different shapes and sizes from a positive photoresist film with a thickness of ~ 1. 3 μm. The particles studied ranged from discoid, crosses, rectangles and diamonds. After evaporating metals onto the surface of 5 μm diameter discoidal particles, the discs became curved as a result of the stresses induced by the evaporation of the metals with radius of curvature of 4- 5 μm. The resulting discs consisted of a hydrophobic and a hydrophilic face and were found to distort a planar air- water interface and give rise to anisotropic capillary forces between the particles resulting in the formation of particle chains. [72]

1. 10. Outline of the thesis

The overall aims of this thesis are to fabricate non- spherical particles with a range of aspect ratios and Janus particles with different surface functionalities and then investigate the effect of shape and surface properties on the particle interactions at liquid interfaces. The materials and methods used in our investigation are summarised in Chapter 2. In Chapter 3, the technique of photolithography is investigated for the fabrication of micron- size discoid particles with well defined geometry, thickness and known surface properties (wettability). The interactions between the anisotropic particles fabricated by the procedures developed in Chapter 3 were investigated at both the air- water and oil- water interface using a Langmuir trough and microscopy and the results are described in Chapter 4. In Chapter 5 of the thesis, protocols for the fabrication of Janus particles are investigated by applying a range of surface modifications to one surface of the discoidal particles. A

summary of the main findings, conclusions and suggestions for future work is given in Chapter 6, followed by the list of references.

CHAPTER 2

EXPERIMENTAL

2. 1. Materials

2. 1. 1. Substrates

Reclaim grade silicon substrates with diameters of 150 mm and an approximate thickness of 0. 6 mm were purchased from Pi-Kem Ltd, UK. In other experiments, Menzel plain microscope glass slides purchased from Fisher chemicals, UK with a thickness 1 mm were cut into 25 × 25 mm squares before use.

2. 1. 2. Photoresist and ancillaries

All particles produced in this work were fabricated from photoresist (Table. 2. 1). Negative photoresist, developer and thinner, part of the negative photoresist kit (Cat. No: 654892), were purchased from Sigma Aldrich, UK. PRP positive photoresist spray and PDN photoresist developer containing NaOH were purchased from Electrolube, UK. AZ5214 E image reversal photoresist, AZ nLOF 2070 negative photoresist and AZ 726 MIF (metal ion free) developer containing 2. 38 % TMAH (Tetramethylammonium hydroxide) were purchased from Microchemicals, GmbH. LOR 5A (lift-off resist), used as a sacrificial layer, 1162 remover containing N-methyl- 2- pyrrolidone (referred to hereafter as NMP), SU- 8 2002 negative photoresist and MF 319 developer containing 2. 2 % TMAH and surfactant < 1 % were purchased from Chestech Ltd, UK. Propylene glycol monomethyl ether acetate (PGMEA), 99 % was used to develop the SU- 8 photoresist and was purchased from Sigma Aldrich Ltd, UK.

Table. 2. 1. Composition of the photoresists used.

Photoresist	Ingredients	Amounts/ %
Aldrich negative photoresist	O- Xylene	> 75
	Methyl glycol acetate	0. 5- 10
Positive photoresist spray	Dimethyl ether	30- 60
	Acetone	30- 60
	1- methoxy- 2- propanol	5- 10
	2- methoxy- 1- methylethyl acetate	5- 10
	Butyl acetate	1- 5
	Napthalene	< 0. 5
AZ 5214	1- methoxy- 2- propanol acetate	73
	Cresol Novolak resin	≥ 22
	Diazonapthoquinonesulfonic esters	≥ 3
	Phenolic compounds	≥ 1
AZ nLOF 2070	1- methoxy- 2- propanol acetate	< 65
	Modified melamine formaldehyde resin	< 5
	Phenolic compounds	< 2
	Cresol Novolak resin	28
	Benzeneacetonitrile derivative	≥ 2
SU- 8 2002	Cyclopentanone	23- 78
	Mixed Triarylsulfonium/ Hexafluoroantimonate Salt	1- 5
	Propylene carbonate	1- 5
	Epoxy resin	25- 75
LOR 5A	Cyclopentanone	65- 90
	Propylene glycol monomethyl ether	10- 15
	Polyaliphatic imide copolymer	1- 20
	Proprietary dye	0. 1- 2
	Proprietary surfactant	< 1

2. 1. 3. Photomasks

Emulsion film darkfield and clearfield photomasks were purchased from JD Phototools Ltd, UK. The patterns produced from these photomasks depends on which type of photomask (darkfield or clearfield) and photoresist (negative or positive) is used as shown schematically in Fig. 2. 1. A range of different photomask designs were employed for the fabrication of particles with different shapes. All designs were generated using CorelDraw X3 software.

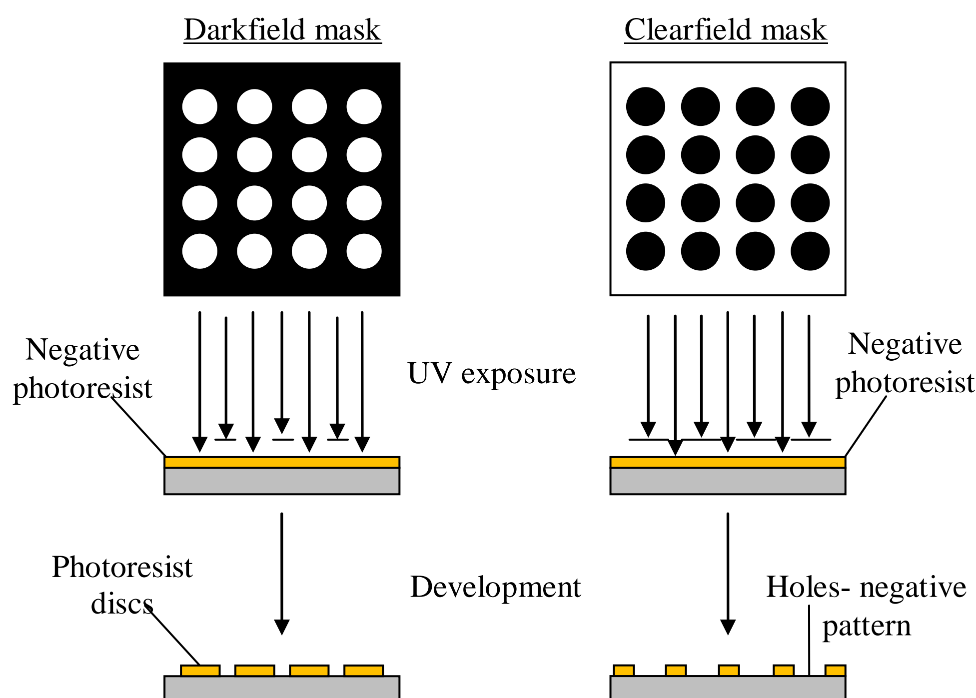

Fig. 2. 1. Schematic representation depicting pattern formation on a negative photoresist through a darkfield and a clearfield photomask. When a negative photoresist is used, the exposed areas become insoluble in a basic developer and the darkfield photomask shown will result in the formation of disc shaped particles. The opposite is the case when a positive photoresist is used, in this case, the clearfield photomask may be used to generate the same pattern.

2. 1. 4. Chemicals and materials

2. 1. 4. 1. Chemicals

Hydrogen peroxide, 33 %, sulphuric acid and nitric acid, analytical grade were purchased from Fisher chemicals Ltd, UK. Sodium hydroxide, potassium hydroxide

pellets, ≥ 98 % and sodium dichromate ≥ 99. 5 % were purchased from Sigma-Aldrich Ltd, UK. Sodium chloride > 99 % was purchased from BDH laboratories. Silica particles with diameters of 1 μm were purchased from Fibre Optic Centre, Inc. Sulphate latex particles with a 3 μm diameter were purchased from Invitrogen Ltd, UK as an 8 wt. vol. % aqueous dispersion. Chromium etch number 1 was purchased from Micropur Ltd, UK. Cotton (lint-free) pads, purchased from Rock Supplies Ltd, UK, were used to clean the Langmuir trough and photomasks.

2. 1. 4. 2. Organic solvents

The organic solvents used in this work, including purity, manufacturer and application are tabulated in Table. 2. 2.

Table. 2. 2. Organic solvents used in this thesis.

Solvent	Purity	Supplier	Application
Acetone	≥ 99. 8 %	Fisher scientific	Cleaning glassware or silicon substrates
Propan- 2- ol (IPA)	≥ 99. 8 %	Fisher scientific	Cleaning glassware or silicon substrates and as a spreading solvent
Absolute ethanol	≥ 99. 8 %	Fisher scientific	Cleaning of the Langmuir trough and a solvent for silanes and dyes
Chloroform	≥ 99. 8 %	Fisher scientific	Cleaning of the Langmuir trough and glassware
Methanol	≥ 99. 8 %	Fisher scientific	Spreading solvent
Hexane	≥ 99. 8 %	Fisher scientific	Removing residual silanes

2. 1. 4. 3. Oils

Decane ≥ 99 % and tetradecane, 99 % were purchased from Sigma- Aldrich Ltd, UK. Before use, the oils were purified by passing through basic alumina powder three times to remove polar impurities.

2. 1. 4. 4. Silanes

Dichlorodimethylsilane (DCDMS), 99. 5 % was purchased from Fluka Ltd, UK and Hexamethyldisilane (HMDS), 98. 0 % was purchased from Lancaster Synthesis Ltd, UK. (3- Aminopropyl) triethoxysilane (APTES), 99 % was purchased from Sigma-Aldrich Ltd, UK.

2. 1. 4. 5. Dyes

Rhodamine 6G, 99 % and Fluorescein 5(6)-isothiocyanate (FITC) were purchased from Sigma-Aldrich Ltd, UK.

2. 1. 4. 6. Polyelectrolytes

Polyallylamine hydrochloride (PAH) and 30 wt % sodium- 4- styrene sulfonate (PSS) were purchased from Sigma- Aldrich Ltd, UK.

2. 1. 4. 7. Metals

Nickel wire with 0. 25 mm thickness was purchased from Fisher chemicals Ltd, UK. Gold wire with a thickness of 0. 2 mm was purchased from Agar Scientific Ltd, UK. Chromium was provided by Mr. Tony Sinclair, a technician from the University of Hull.

2. 1. 4. 8. Water

The deionised water used in these experiments was from a Milli-Q Reagent Water System. The water was purified by reverse osmosis through a Millipore system with a 0. 22 μm membrane filter. The resistivity of the water was at least 18 MΩ/ cm and the surface tension of the water as determined by drop shape analysis was 72. 6 ± 0. 2 mN/ m.

2. 1. 5. Instruments

2. 1. 5. 1. Photolithography

Spin coating was carried out using a SCS P6700 spin coater (Cookson electronic Equipment) with a Busch vacuum pump. For pre- baking and post exposure baking; a precision vacuum hotplate with a PID temperature controller (model 1000-1) purchased from Electronic Microsystems Ltd, UK or a Stuart CC162 hotplate with a temperature controller was used. For UV exposure; an RS 559-934 UV curing unit with 4 $\times$ 40 W tubes, timer and peak UV output at 350 nm purchased from RS Components Ltd, UK was used. A Grant ultrasonic bath was used for sonication. Oven baking took place in a convection oven (Advantage-Lab). An auto bench centrifuge (Baird and Tatlock, Mark 14) was used for centrifugation pf the particle suspensions.

2. 1. 5. 2. Analysis

An optical microscope (Nikon, Optiphot-2) with a Qicam Fast 1394 camera and Image Pro Plus 5. 1 software was used to obtain images. Low magnification images were taken by a digital camera (Finepix 55700, Fujifilm). A Zeiss evo 60 0. 2- 30 kv scanning electron microscope was used for SEM images. Fluorescent microscopy images were obtained from an Olympus BX51 microscope with an Olympus DP70 camera and image pro- plus software. A Veeco NT1100 optical profiler was used to measure the photoresist thickness. Contact angles were measured by drop shape analysis using a DSA 10 instrument (Kruss) with DSA imaging software. A syringe pump (New Era Pump Systems Inc) was used to pump or withdraw water from the water drop during contact angle measurements. A Thermo Nicolet Nexus Fourier transform infrared (FTIR) spectrometer with a MCT detector was used for infrared analysis.

2. 1. 5. 3. Gel trapping technique

For the gel- trapping technique, C 18- silica chromatographic columns were provided from Phenomenex, UK, and Gellan gum was obtained from CPKelco Ltd, UK.

2. 1. 5. 4. Experiments on particle monolayers at the fluid interface

A miniature Teflon Langmuir trough, model 601 M, was supplied by KSV- Nima Technology, UK. The trough consisted of a stainless steel lining and barriers working over an area of 15 cm^2 to 80 cm^2. The trough was fitted with a PS4 pressure sensor with an attached filter paper Wilhelmy plate. Nima software was used to record the isotherms. A 100 μl Hamilton gas- tight glass syringe was used to spread the particles at the interface. The set up and dimensions of the trough are summarised in Fig. 2. 2.

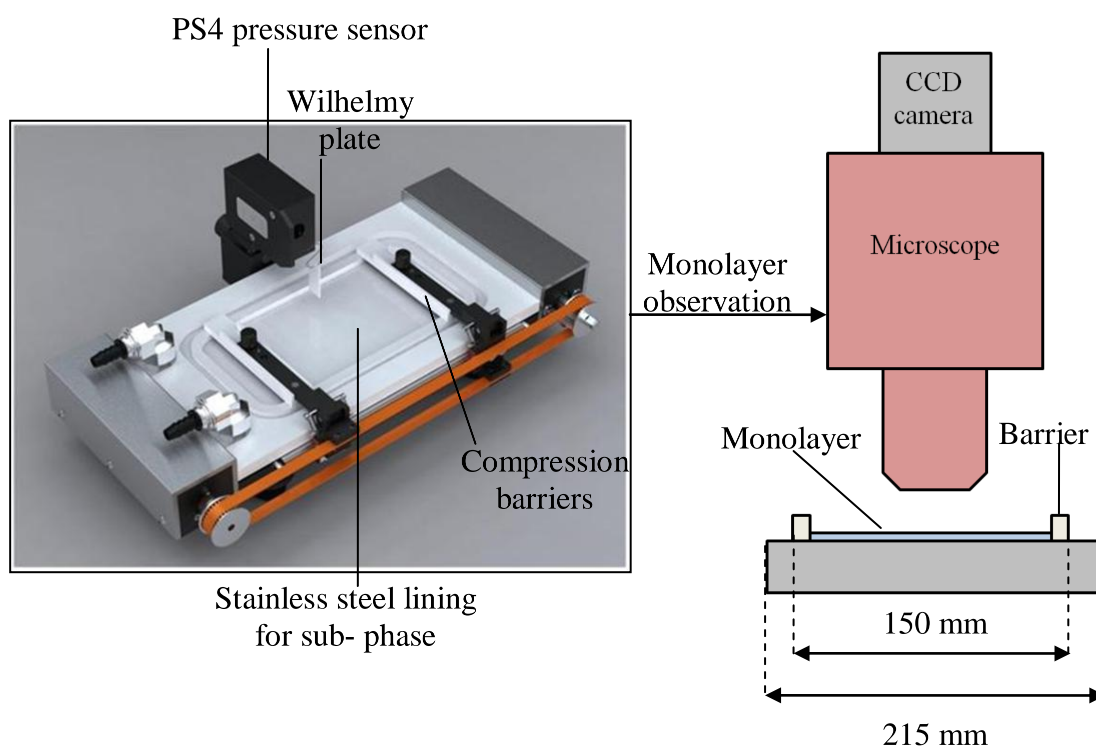

Fig. 2. 2. Experimental set up of the Langmuir trough for the observation and investigation of monolayers at the liquid- fluid interface.

2. 2. Methods

2. 2. 1. Cleaning procedures

2. 2. 1. 1. Glassware

Pyrex glassware was cleaned in sulfochromic acid (prepared from 40 g of sodium dichromate and 40 ml of water with 1 L of H_2SO_4) for 15- 30 min if the solution was freshly prepared; otherwise the glassware was immersed in the acid overnight. The acid was replaced when discolouration of the acid occurred. Alternatively, the glassware was immersed in a KOH/ EtOH solution (prepared from 290 g of KOH in 2 L EtOH) overnight. In each case the glassware was rinsed thoroughly with tap water followed by deionised water before placing in an oven at 120- 180 °C for 30 min to dry.

2. 2. 1. 2. Glass and silicon substrates

Glass slides were cut into pieces with approximate dimensions of 25 x 25 mm and were sonicated in acetone followed by propan-2-ol and finally deionised water. The slides were sonicated using an ultrasonic bath at ~ 21 °C for 5 min, 3 times for each solvent (using fresh solvent each time). The slides were blow dried with nitrogen and finally baked in an oven at a minimum temperature of 120 ºC for 30 min. The same procedure was applied for the silicon substrates (cut or uncut) if photoresist was not previously applied, otherwise excess photoresist was removed by sonicating in NMP at 65 °C for 30 min in an ultrasonic bath and repeating using deionised water before blow drying with nitrogen. The substrate was then immersed in Piranha solution prepared from 3 parts H_2SO_4 and 1 part H_2O_2 at 90- 110 °C for 15 min before rinsing thoroughly with tap water followed by deionised water, blow drying with nitrogen and drying in an oven at 180 °C for 30 min. The Piranha solution was reused for a period of no more than 24 hrs after preparation. The Piranha solution was prepared and used in a fume cupboard at all times.

2. 2. 1. 3. Photomasks

The photomasks were cleaned using a lint- free cotton pad dampened with IPA or hexane. The pads were replaced frequently to prevent scratching of the photomasks by embedded particles. The photomask was then blown gently with nitrogen.

2. 2. 1. 4. Hamilton syringes

Syringes were sonicated in EtOH in a 50 ml measuring cylinder for 10 min followed by $CHCl_3$ for 10 min and finally with EtOH for a further 10 min in an ultrasonic bath at ~ 21 °C. The syringe was then flushed several times with fresh deionised water.

2. 2. 1. 5. Langmuir trough

Before use, the Langmuir trough and barriers were wiped 3 times with lint- free cotton pads soaked in fresh EtOH each time and the procedure was repeated using $CHCl_3$. The trough was then filled and emptied 3 times with fresh deionised water each time. The trough was then filled again and the cleanliness of the water was verified by ensuring that the surface pressure did not change by more than 0. 2 mN/ m during compression of the water surface to the smallest area of the trough. In some cases it was necessary to remove the steel lining and fill the PTFE trough with fresh sulfochromic acid for 30 min.

2. 2. 2. Silane, metal and polyelectrolyte application

2. 2. 2. 1. Silanisation of glass slides with DCDMS

Glass slides were silanised by vapour deposition as shown in Fig. 2. 3. After cutting, cleaning and drying the glass, the slides were placed in Teflon holders and placed inside a glass jar with a volume of ~ 690 cm^3. The jar could be sealed with a screw on cap consisting of sealable holes that allow the jar to be purged with nitrogen. The slides were placed within the jar as soon as possible after removing from the oven before flushing the jar for 5 min with nitrogen. DCDMS liquid with a volume of 300 μl was introduced at the bottom of the jar through a micropipette and after sealing the jar, the slides were left for not less than 24 hrs. DCDMS was used in a fume cupboard at all times. After removing from the jar, the slides were sonicated in hexane for 10 min at room temperature in an ultrasonic bath to remove excess

DCDMS before drying at room temperature with nitrogen. A similar set up was applied for the hydrophobisation of large 150 mm diameter silicon substrates using DCDMS or HMDS in a larger container.

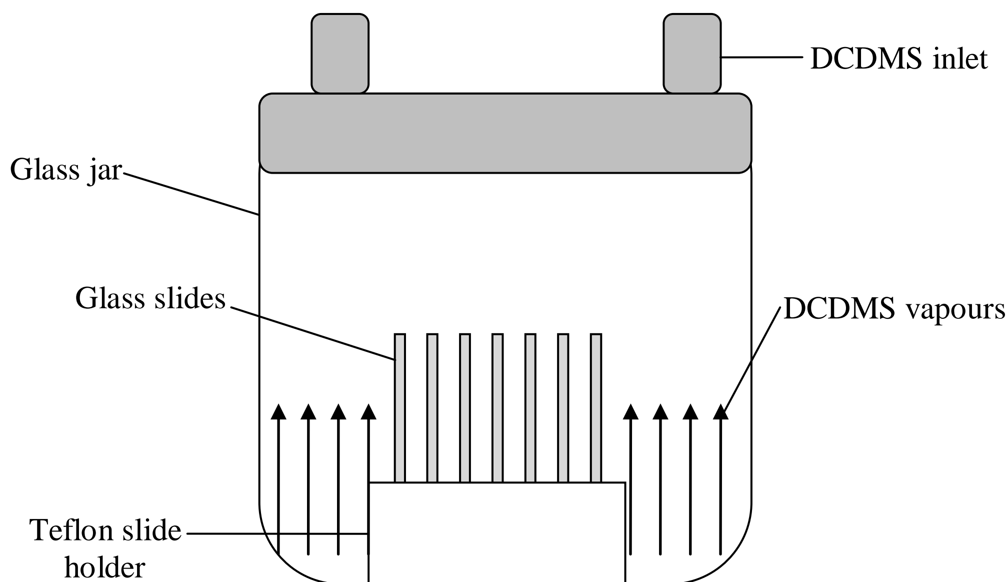

Fig. 2. 3. Experimental set up for the vapor deposition of DCDMS onto glass slides.

2. 2. 2. 2. Application of APTES and fluorescent dyes

Patterned photoresist attached to the silicon substrate via a sacrificial layer was immersed in a 10 vol. % solution of APTES in deionised water or absolute EtOH for 3- 3. 5 hrs in a fume cupboard. After removing from the APTES, the substrate was rinsed thoroughly with deionised water and then placed in a 1 mM aqueous solution of rhodamine 6G for ~ 10 min. The substrate was finally rinsed thoroughly again with deionised water. For fluorescein treated particles, fluorescein isothiocyanate (FITC) was prepared by dissolving the FITC in absolute EtOH to give a 5. 5 mM solution and then transferring the solution in a glass container to a refrigerator at 5 °C. The patterned photoresist on the substrate was then added to the solution before sealing the container and leaving refrigerated for ~ 17 hrs.

2. 2. 2. 3. Application of polyelectrolytes and colloidal particles to solid surfaces

PAH was applied to the surface of glass, silicon or patterned photoresist by immersing the substrate in PAH solution consisting of 20 mg of PAH in 20 g of 0. 5 M NaCl solution for 20 min without shaking or stirring. Before this, the substrate

was rinsed in ethanol followed by deionised water. In some cases a second treatment with PSS was applied after PAH treatment. Before application of the PSS, excess PAH was removed by rinsing three times with 1 mM NaCl. After applying the last layer of polyelectrolyte, the surface was rinsed with 1 mM NaCl three times before placing in a silica or iron oxide suspension consisting of 1 mg of powder in 1 ml of deionised water for 20 min. The suspension was sonicated in an ultrasonic bath for 10 min at 21 °C immediately before use. After removing the coated substrate from the suspension, the substrate was immersed in fresh deionised water for 10 min. In each case, no shaking or stirring of the liquids was performed. The surface was then allowed to dry at room temperature.

2. 2. 2. 4. Application of metals onto the photoresist surface

An Edwards E12E vacuum evaporator was used to apply a layer of metal onto the patterned photoresist surface. One coating of metal gave a thickness of ~ 10 nm. For thicker layers, multiple evaporations were carried out. The metals were normally evaporated at an angle of 0 °, i. e., directly above the sample. In order to evaporate at an angle, the sample was reorientated with respect to the source. Chromium and nickel could be applied directly to the photoresist. In the case of gold, it was necessary to apply an adhesion layer of titanium to the photoresist beforehand.

2. 2. 3. Measurements of contact angles on solid surfaces by drop shape analysis

To determine the wettabilty of glass, silane treated glass or photoresist in air or oil; contact angles of sessile water drops on the treated surface were measured using drop shape analysis. The experimental set up is shown in Fig. 2. 4. A 1 ml glass syringe (Hamilton) was cleaned with ethanol before filling with deionised water and then attaching to the syringe pump. The syringe was connected via plastic tubing to a needle and water was passed through the tube and needle two times before fixing the needle above the sample stage of the DSA instrument. Approximately 0. 4 ml of water remained in the syringe. The pump rate was selected at 2. 4 μl per min. The DSA software was instructed to measure the contact angle every 2 s for approximately 7 min. The method used to acquire the contact angle was tangent method 2. The software was also instructed to acquire the drop base diameter and measurement time. All acquired data was then transferred to an Excel spreadsheet

for processing. Advancing contact angles were acquired by pumping water into the drop or withdrawing water from the drop when the receding contact angle was required. Before acquiring measurements, the groove running along the perimeter of the enclosed sample container was filled with deionised water in order to reduce evaporation from the drop. The sample was then placed on the stage and the syringe, lamp, camera magnification and focus were adjusted until the drop was clearly visible on the monitor and a contact angle could be successfully recorded. Both advancing and receding contact angles were acquired for two or three drops at different locations on each surface at a temperature of 21 ± 1 °C.

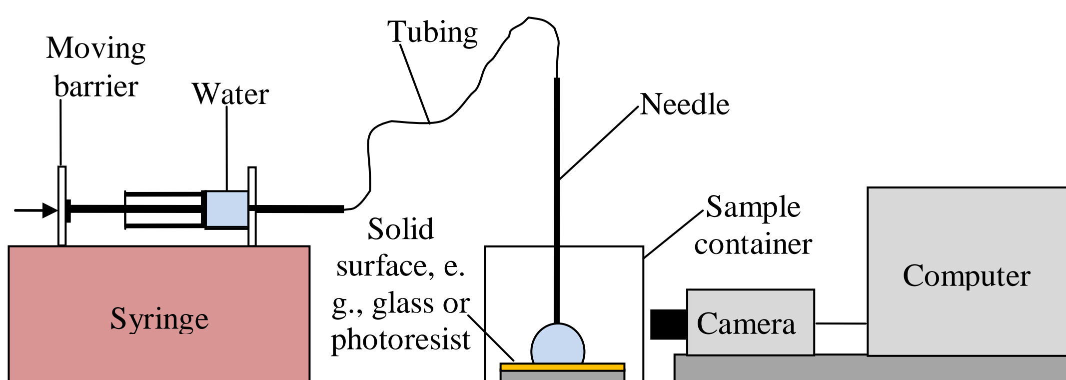

Fig. 2. 4. Experimental set up to measure advancing and receding contact angles of a sessile water drop on a solid surface.

2. 2. 4. Photolithographic procedure for the fabrication of non- spherical particles

2. 2. 4. 1. Photoresist preparation

The photoresist was prepared into clean and dry 10 ml Pyrex beakers several hours before use and kept sealed and refrigerated in the dark until ready to use. The photoresist was allowed to attain room temperature before spin coating. The photoresist was dispensed into the beakers through a sintered glass filter disc with a pore size of 1 μm attached to a clean and dry 5 ml Hamilton gas- tight syringe.

2. 2. 4. 2. Photoresist application

The negative photoresist from Aldrich was dispensed with a volume of ~ 500 μl onto the centre of a small glass substrate using a micropipette and then spin coated at 500 r. p. m. for 5 s at an acceleration of 100 r. p. m/ s. In some cases the photoresist was diluted 50 % by volume using photoresist thinner (part of the photoresist kit).

The positive photoresist spray was applied by sweeping left to right and back for around 2 s at a distance of ~ 30 cm and an angle of ~ 45 °. After exposure, each slide was developed for up to 1 min. For experiments with the AZ and SU- 8 photoresists, the LOR sacrificial layer was first dispensed onto the centre of the substrate and spin coated at 3000 r. p. m for 40 s at an acceleration of 1000 r. p. m/ s and then baked at 160 °C for 15 min on a hotplate or 180 °C for 30 min in a convection oven; then the photoresist was spin coated at 500 r. p. m for 5 s at an acceleration of 100 r. p. m/ s followed by 4000 r. p. m for 40 s at an acceleration of 300 r. p. m/ s. Both the LOR and photoresist were dispensed by pouring ~ 5 ml directly from the 10 ml Pyrex beakers (or 500 μl from a micropipette for the small substrates) onto the centre of the substrate at a distance of ~ 5 mm.

2. 2. 4. 3. Baking and post exposure baking of the photoresist

For the negative photoresist from Aldrich and the positive photoresist spray, baking was achieved by placing the spin coated slides onto the centre of the Stuart hotplate, switching on the power, and heating up to 82 ºC for approximately 12 min and then baking for 20 min. For all other experiments the precision vacuum hotplate was used. AZ 5214 image reversal resist and AZ nLOF 2070 were baked at 110 °C for 60 s. The latter was baked again at the same temperature and time after exposure. In each case, no heat up ramp was applied. The SU- 8 photoresist was baked at 65 °C for 90 s followed by 95 °C for 180 s (pre- bake) and 65 °C for 90 s followed by 95 °C for 120 s (post exposure- bake). The photoresist was allowed to rest and cool for ~ 15 min before exposure was carried out.

2. 2. 4. 4. Photoresist exposure

For the negative photoresist from Aldrich and the positive photoresist spray, a UV lamp was placed face down to cover the photomask and spin coated slides and then switched on for 4- 16 s. The exposure wavelength used was 365 nm (often referred to as i-line). When the UV curing unit was used (AZ and SU- 8 photoresist), before exposure, the unit was switched on for 5 min to allow the maximum UV intensity to be reached. The photomask was placed emulsion side facing away from the surface of the unit's glass surface and then the photoresist surface was placed over the photomask in direct contact with the emulsion side before closing the lid and

commencing exposure. The AZ photoresist was exposed for typically 8- 12 s (AZ nLOF 2070) or 8- 15 s (AZ 5214) and the SU- 8 photoresist was exposed for 15 s.

2. 2. 4. 5. Photoresist development

The negative photoresist from Aldrich was developed by immersing the coated substrate in a 50 ml beaker containing 10 ml developer (part of the photoresist kit) with the photoresist film on the upper side, followed by rinsing in propan-2-ol. Each developed pattern was then blow dried with nitrogen. In some cases, sonication in an ultrasonic bath at room temperature was applied during development. AZ nLOF 2070 photoresist was developed in AZ- 726 or MF- 319 developer for 120 s when the developer was undiluted. Diluted developer required a longer development time. AZ 5214 was developed for 60 s in undiluted developer. In each case the developed photoresist was rinsed with deionised water for ~ 60 s. SU- 8 photoresist was developed for 60 s in PGMEA developer followed by rinsing in IPA for ~ 60 s or until the presence of a white film (indicative of underdevelopment) disappeared. The developed photoresist was dried with nitrogen at room temperature.

2. 2. 4. 6. Hard- baking

AZ nLOF 2070 photoresist was hard- baked for 30 min at 145 °C in order to ensure stability of the photoresist during further processing. It was not necessary to hard-bake SU 8 photoresist after development.

2. 2. 4. 7. Release of patterned photoresist particles

For AZ nLOF 2070, the developed and hard- baked photoresist was released by dissolution of the underlying sacrificial layer of LOR using NMP at room temperature or at 65 °C with the aid of sonication in an ultrasonic bath. In the case of SU- 8, the patterned photoresist was released by dissolution of the sacrificial layer in 0. 2 M NaOH. The particle suspensions were then filtered through a 40- 100 μm pore size sintered glass filter into a Buchner flask with the aid of a vacuum pump. The suspensions were then centrifuged 3 times using fresh NMP or NaOH each time at 2700 r. p. m for 30 min.

2. 2. 5. Partial modification of one surface of patterned photoresist

In order to apply silanes, metals or polyelectrolytes to predesignated portions of the patterned photoresist surface, a masking procedure was developed by application of the AZ 5214 image reversal photoresist (processed as a positive photoresist) followed by further patterning. To achieve this the AZ 5214 photoresist was spin coated on the patterned negative photoresist surface at 500 r. p. m for 5 s at an acceleration of 100 r. p. m/ s and 3000 r. p. m for 40 s at an acceleration of 300 r. p. m/ s. After baking, a clearfield photomask was aligned over the negative photoresist pattern which was found to be transparent through the top surface of positive photoresist. The experimental set up is shown schematically in Fig. 2. 5. The coated substrate was attached by sticky tape to a flexible polycarbonate backing sheet between two silicon supports of the same thickness as the substrate. Then the photomask was placed over the substrate and the whole set up was transferred to an X, Y stage. The photomask was then attached to another stage that allowed the photomask to be moved in the X or Y position. Alignment of the photomask with the negative photoresist pattern was achieved by observing the photomask through the eye piece of a 5 x objective lens with variable magnification during adjustment. After alignment, the photomask was secured in place using masking tape before exposing the positive photoresist. The photoresist pattern either consisted of positive photoresist lines or rectangles; the latter was achieved by two exposures through two photomasks consisting of lines with the second mask orientated at 90 ° with respect to the first. After development of the positive photoresist, the surface of the patterned photoresist was modified. The positive photoresist was removed at a later stage by immersion in IPA or acetone.

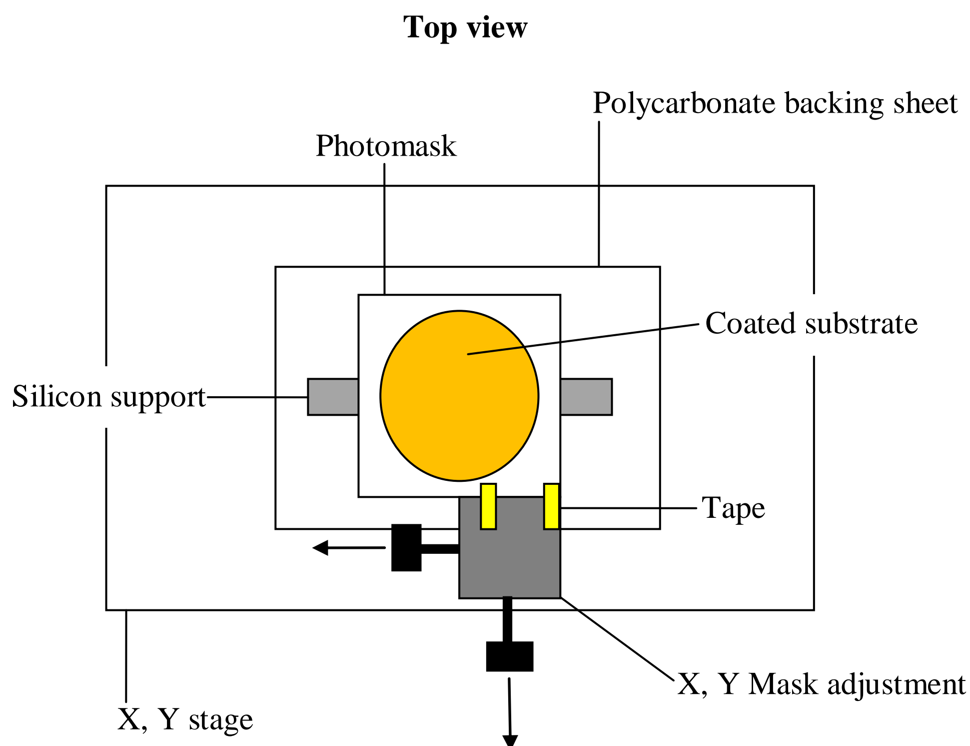

Fig. 2. 5. Schematic of the photomask alignment configuration. The photomask is placed on top of the substrate containing the patterned photoresist and secured to a second stage which allowed the photomask to be adjusted in the X and Y position by means of adjustable screws. The stage could also be rotated manually. Silicon supports are placed on each side of the substrate to prevent photomask deformation after securing the photomask. After aligning, the photomask was secured directly to the polycarbonate backing sheet using masking tape. The entire set up was performed on a microscope stage to allow simultaneous observation of the photomask and photoresist pattern.

2. 2. 6. Spreading of solid particles at the liquid interface

2. 2. 6. 1. Spreading of particles at an air- water or oil- water interface in a glass Petri dish

For latex or AZ photoresist particles (modified or unmodified), methanol was added to the particle suspension in water to make a spreading suspension containing 50 wt. vol. % methanol. For SU- 8 photoresist, methanol or IPA in water was used as a spreading solvent. Before producing the monolayer, the surface of the water was cleaned by aspirating with the aid of vacuum through a Pasteur pipette. In this way a volume of water was removed and the process was continued until the surface of the

water appeared to be flat. A few drops of the spreading suspension were then applied to the surface of the sub- phase at different locations on the surface. The glass dish with a 25 mm diameter was mounted beneath a microscope objective lens in order to view the monolayer and acquire images. After each sample of suspension was dispensed on the surface of the water, images of the particles were captured from the microscope in transmitted and/ or reflected light.

2. 2. 6. 2. Spreading of particles at an air- water interface in a Langmuir trough

The particle suspension was applied to the sub- phase as described in Sec. 2. 2. 6. 1. It was found that the methanol alone from 200 μl of suspension decreased the surface tension of the water by ~ 0. 7 mN/ m. The Wilhelmy plate was immersed ~ 2 mm into the water and was orientated parallel to the trough barriers. Before compression of the monolayers, the monolayer was allowed to equilibrate for at least 15 min. Compression and expansion of the monolayer was performed at a barrier speed of 2 or 3 cm^2/ min. In some experiments, the trough was mounted onto the stage of a microscope in order to record images of the monolayer during compression and expansion. For experiments at the oil- water interface, the oil was layered over the water by filling the adjacent area outside the trough area until the water was covered by several millimeters of oil. The particles were then applied by immersing the needle into the oil until the droplet made contact with the water surface and detached.

2. 2. 7. Characterisation of the orientation and position of the particles at the liquid interface

2. 2. 7. 1. The gel- trapping technique

In order to view the particles at the interface laterally and therefore to be able to determine the depth of immersion of the particles into the water at the oil- water and air- water interface, the gel- trapping technique was applied according to the method of Paunov. [111] A 0. 5 wt. vol. % solution of gellan in Milli-Q water was prepared by heating to 90 ºC and stirring before filtration 3 times through a C- 18 column for the removal of surface-active impurities. Filtration was carried out at ~ 50 ºC to prevent premature gelling of the gellan solution. This was achieved using an arrangement of hot air dryers applied to the column. Finally, the filtered gellan was heated to evaporate

excess water, bringing the concentration of the solution up to 2 wt. vol. %. A small amount of this solution was then placed in a small Petri dish and a drop of the spreading suspension containing the photoresist particles was applied to the surface. Once the gellan solution had set (at room temperature), a layer of PDMS was poured over the top, and once again allowed to set. Once set, the PDMS mould containing the replicated monolayer was peeled off the surface and imaged by SEM.

2. 2. 7. 2. Orientation and number density of disc, oval and rectangular shaped particles at the liquid interface

Images of the monolayer at the air- water and oil- water interface were captured at different areas of the trough during compression and expansion. A macro was designed that enabled the orientation of the particles with respect to a reference plane to be determined. Approximately 500 particles were analysed from each image and plots of orientation vs. trough area were obtained. The number density of particles at different areas of the trough was obtained my manually counting particles from the microscopy images as the poor contrast of the transparent particles at the interface did not permit an automated technique by the software to be applied. The number of particles in a given image was corrected for the actual area of the trough from which the image was obtained and then the number of particles per cubic centimetre was determined.

CHAPTER 3

FABRICATION OF NON- SPHERICAL MICROPARTICLES USING PHOTOLITHOGRAPHY

3. 1. Introduction

Photolithography is an advanced technology used in microelectronics and other industries for patterning solid surfaces, usually with sub-micrometer resolution. This requires very high quality photomasks and expensive specialist equipment, e. g., a clean room, mask aligners, etc. Recently, photolithography was used for the fabrication of non-spherical microparticles such as cylinders[97-99] and plates[68, 69]. The possibility for precise control of particle geometry is a serious advantage of the photolithographic technique, but the special requirements in terms of the equipment and a very clean environment limit its application. Here we investigate the capabilities of photolithography for the fabrication of microparticles with well defined geometry under normal laboratory conditions. In all experiments, the photomasks were placed directly on the top of the photoresist layer (contact photolithography) thus eliminating the need for expensive equipment (a projection unit, mask aligners) used in projection photolithography: this approach however will require a clean and homogeneous surface. The aim of this investigation is to develop inexpensive but reliable protocols for the preparation of non- spherical photoresist microparticles which can be used for studying the particle behaviour at air- water and oil- water interfaces. A range of different systems including photoresists, photomasks and processing procedures are investigated in order to determine the optimum conditions for particle preparation and their release from the solid substrate. The fabricated particles are characterised using microscopy, surface profilometry and drop shape analysis on the photoresist surface.

The first thing to consider is the proper selection of the photoresist. There are a variety of positive and negative photoresists available on the market. Although the negative photoresist SU- 8 has been used for the fabrication of microparticles [68-70], it is not clear if SU- 8 is the most suitable photoresist for our purpose. The photoresist type is certainly important but it should be considered together with other factors

involved in the photolithographic process. Some of the most important aspects of the photolithographic process and their implications are outlined below.

- Photoresist application: photoresist is typically applied to a substrate by spin coating. It is necessary to carefully control the spin coating parameters such as spin speed, time and acceleration as these will determine the thickness and the uniformity of the photoresist films.

- Photoresist dispensed volume: in order to ensure complete coverage of the substrate with the photoresist required for patterning, it is important to ensure that the dispense volume is just sufficient to cover the entire substrate. The application of excess photoresist is not only wasteful but is also likely to wet the spinning chuck during spin coating causing failure of the spin coating process and consequently damage to the substrate. If an insufficient volume of photoresist is applied, the substrate will not be completely coated and the photomask may not be able to make uniform contact with the surface during exposure.

- Substrate wettability: photoresist is typically hydrophobic in nature; however this depends on the extent of dilution of the photoresist, and therefore usually requires a hydrophobic substrate for its application. A hydrophilic substrate such as untreated glass or silicon may cause the photoresist to dewet the substrate after spin coating. [114] Commercially available adhesion promoters are available and application of hydrophobic silanes is another option.

- Baking time and temperature: after spin coating, it is necessary to remove excess solvent by baking the photoresist; typically on a hot plate. For an insufficient baking temperature or time, the excess solvent causes sticking of the photomask to the photoresist during exposure and therefore the delicate features of the photomask can become irreversibly damaged. [115] In addition, the photoactive components of the photoresist can flow during exposure causing distortion of the pattern. An excess baking temperature or time results in premature crosslinking of negative photoresist and therefore patterning becomes impossible. [116, 117] The image reversal photoresist used in this work must be kept below ~ 115 °C during baking to prevent crosslinking in undesired regions when processed as a positive photoresist. A temperature > 115 °C causes the photoresist to act as a negative photoresist, i. e., crosslinking occurs in regions exposed to UV.

- Exposure time: the size and quality of the generated patterns strongly depends on the exposure time. If the exposure time is too short, the patterned features will be incomplete; on the other hand if the exposure time is too long, unexpected patterns are generated on the image. [118]

- Development time and concentration of developer: the time required for development is determined by the exposure dose, baking time and temperature, agitation during development, concentration of the developer and the geometry of the pattern; all of these factors need to be carefully optimised to obtain reproducible results. [119]

- Release of patterned photoresist from the substrate: in order to successfully release the fabricated particles from the substrate, it is necessary to select a suitable release medium and appropriate processing conditions of the sacrificial layer.

The photoresists used in this work are summarised in Table. 2. 1 of Chapter 2. They fall into two groups: (i) low cost photoresist and (ii) high performance photoresists for microelectronic applications. The positive photoresist spray (PRP, Electrolube) and the negative photoresits kit from Aldrich (Cat. No: 654892, referenced hereafter as “Aldrich negative photoresist”) belong to the first group and were chosen due to their low price and availability in the beginning of our investigation. From the second group, we have investigated the negative photoresists AZ nLOF 2070 and SU-8 2002, the image reversal photoresist AZ5214 E (acting as a positive or negative photoresist depending on the processing conditions) and LOR 5A (lift- off resist used as a sacrificial layer) all purchased from Chestech Ltd, UK.

3. 2. Experiments with low cost negative and positive photoresists

All experiments with the Aldrich negative photoresist and positive photoresist spray were performed using small glass substrates (25 $\times$ 25 mm squares cut from microscope slides). The ability of these photoresists for patterning with relatively large features was tested by using homemade photomasks on transparent plastic sheets printed by an inkjet printer.

3. 2. 1. The effect of substrate wettability

Good wetting of the substrate by the photoresist is an important requirement for the formation of stable photoresist films with a uniform thickness. Photoresist is typically hydrophobic in nature and would require hydrophobic substrates to be used. Clean glass is hydrophilic, but can be hydrophobised by treatment with, for example, dichlorodimethylesilane (DCDMS) vapours or other silanising agents. The dilution of photoresist with thinner (used to decrease the viscosity and therefore the thickness of the spin coated photoresist film) may also affect the wetting properties. To test the effect of substrate wettability on the quality of photoresist films, we hydrophobised glass substrate by treatment with DCDMS vapour as described in section 2. 2. 2 in chapter 2. Both hydrophobic and hydrophilic (non- treated substrates) were then investigated in the presence of diluted and non- diluted photoresist. Fig. 3. 1 shows the effect of substrate hydrophobicity on the contact angle of a sessile water drop on a DCDMS treated and non- treated glass slide in air. Static contact angles obtained by placing a water droplet on the substrate were measured on several substrates and averaged. Average contact angles of 107 ± 1 ° for the hydrophobic slides and < 10 ° for the hydrophilic slides were obtained.

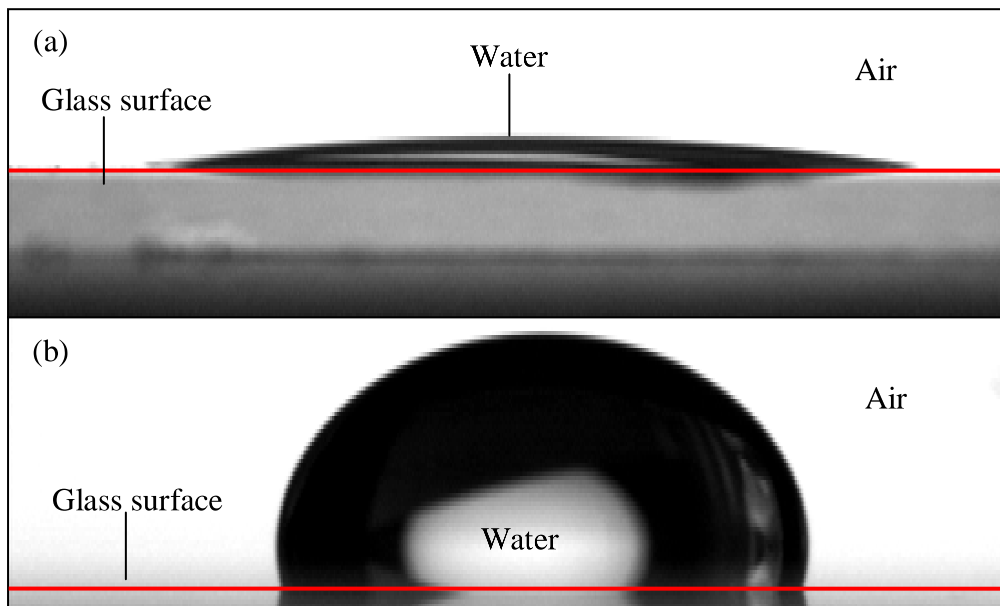

Fig. 3. 1. Typical images of a water drop on a glass slides in air before hydrophobisation (a) and after hydrophobisation (b) with DCDMS vapour. Average contact angles are (a) $\theta < 10$ ° and (b) $\theta = 107 \pm 1$ °.

Images of hydrophilic and hydrophobic substrates after coating with photoresist are shown in Fig. 3. 2. It is expected that because the photoresist is essentially organic (> 75 % Xylene), it should preferentially wet a hydrophobic surface. A spin coated film on a hydrophobised glass substrate is shown in Fig. 3. 2 c, which shows that the photoresist coating was homogeneous with very few defects. During baking at a temperature of 82 °C, recommended by the manufacturer, there was some blistering of the photoresist at the substrate corners which is believed to be due to the relatively rapid heating rate during baking; blistering was observed when the hot plate temperature reached ~ 50 ºC and was only observed with the undiluted photoresist. It was apparent that film thickening had occurred at some of the substrate edges due to the darker appearance of the photoresist in these regions, which was expected for the square substrates used here. When the photoresist was diluted, it was found that dewetting of the substrate readily occurred (Fig. 3. 2 c inset), indicating that the diluted photoresist was not able to effectively wet a hydrophobic substrate. Because the diluted photoresist was shown to be incompatible with a hydrophobic substrate; it was decided to investigate its wetting behaviour on a non- hydrophobised substrate. It can be seen that the non- treated hydrophilic glass substrates gave good quality films with both diluted and undiluted photoresist. Because both types of photoresist generated good quality films on hydrophilic substrates, untreated glass substrates were used in further experiments.

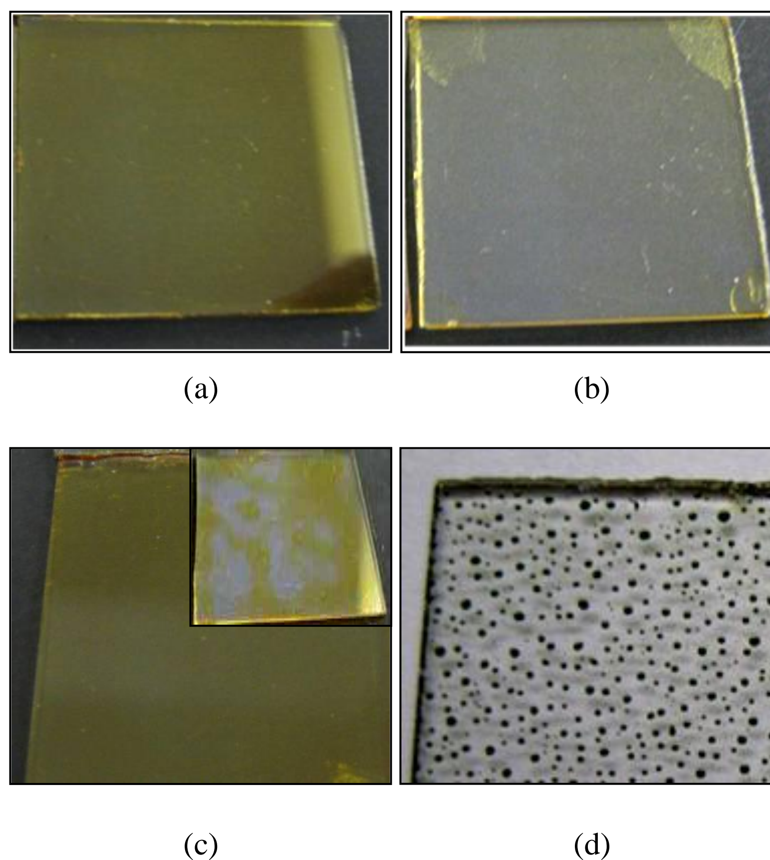

Fig. 3. 2. Images of low cost photoresist deposited on hydrophilic (a, b) and hydrophobic (c, d) glass substrates using undiluted Aldrich negative photoresist (a, c) and Aldrich negative photoresist diluted to 50% with thinner (b) and the inset in (c) and positive photoresist spray (d). The contact angles of water drops on hydrophobic glass substrates in air are: 107 ± 1 ° (c, d) and less than 10 ° (a, b) (see Fig. 3. 1).

3. 2. 2. The effect of the photoresist concentration on the thickness of the spin coated films

For the fabrication of thin, non- spherical particles, it is anticipated that the thickness of the photoresist, and therefore the particles, will be less than a few micrometers. It is known that the thickness of the spin coated films can be controlled by varying the viscosity of the photoresist via its concentration. Samples were prepared by spin coating glass substrates at 500 r. p. m. using undiluted and diluted Aldrich negative photoresist and the thickness of the obtained films was determined by optical profilometry and SEM imaging. Typical images are shown in Fig. 3. 3. The thickness of the film prepared with undiluted photoresist was ~ 15 μm. Much

thinner films (~ 1 μm) were obtained for the the photoresist diluted with thinner to 50 vol. %, thus confirming that the thickness of the photoresist film can be controlled by varying the photoresist concentration. The images in Fig. 3. 3 show that the photoresist films have rough surfaces and a non- uniform film thickness. It is believed that a non- uniform film thickness is due in part to the relatively low spin speed, but could also be due to the shape of the substrate used: it is known that photoresist films spin coated on square or rectangular substrates are thicker at the edges and corners. [146]

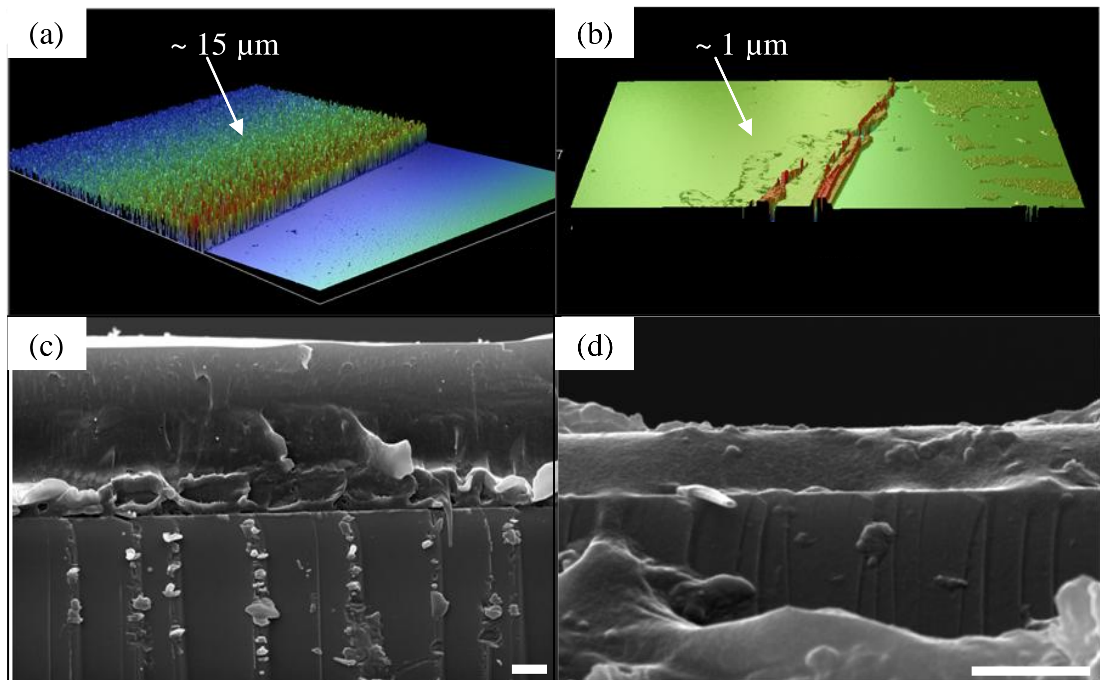

Fig. 3. 3. Optical profilometry images (a, b) and SEM images (c, d) obtained for an undiluted photoresist film (a, c respectively) and a diluted photoresist film with 50 vol. % thinner (b, d respectively) on a glass substrate. Scale bars show 2 μm.

3. 2. 3. Pattern formation on photoresist films using photomasks

The ability of these low cost photoresists for patterning was tested by masking half of the photoresist film with aluminium foil, or applying homemade photomasks printed on transparent plastic sheets by an inkjet printer (HP Deskjet 895Cxi) over the entire surface. The masked photoresist films were exposed to UV light using a UV curing unit, developed and the obtained patterns inspected using optical microscopy. First, the suitability of the printed photomasks was investigated. A black rectangle with dimensions of 5 × 5 cm was printed on a transparent plastic sheet using an inkjet printer, then its optical transmittance in the range 325- 445 nm

was measured using a UV- VIS spectrophotometer and compared to that of the non-printed transparent sheet. The results shown in Fig. 3. 4, show that at a wavelength of 365 nm (used throughout the experiments so far), the percentage of UV transmittance for the black ink coated sheets was only ~ 0. 2 %; however the percentage of UV transmittance for the non- printed transparent sheets was ~ 99. 9 %; therefore the black ink is essentially opaque to UV radiation whereas the unprinted sheet is transparent; hence, ink patterns printed on transparent plastic sheets using an inkjet printer could be used as simple photomasks for patterning the photoresist surface, for the relatively large features used here, which will help to establish protocols for pattern generation on photoresist films. Photomasks consisting of a series of alternating thick and thin lines of 1 mm and 0. 1 mm thickness with a spacing (pitch) of 3 mm (see Fig. 3. 5), and a series of spots with diameters of 0. 2 mm and a pitch of 0. 3 mm were produced for photoresist patterning. Each photomask was designed using CorelDraw X3 software.

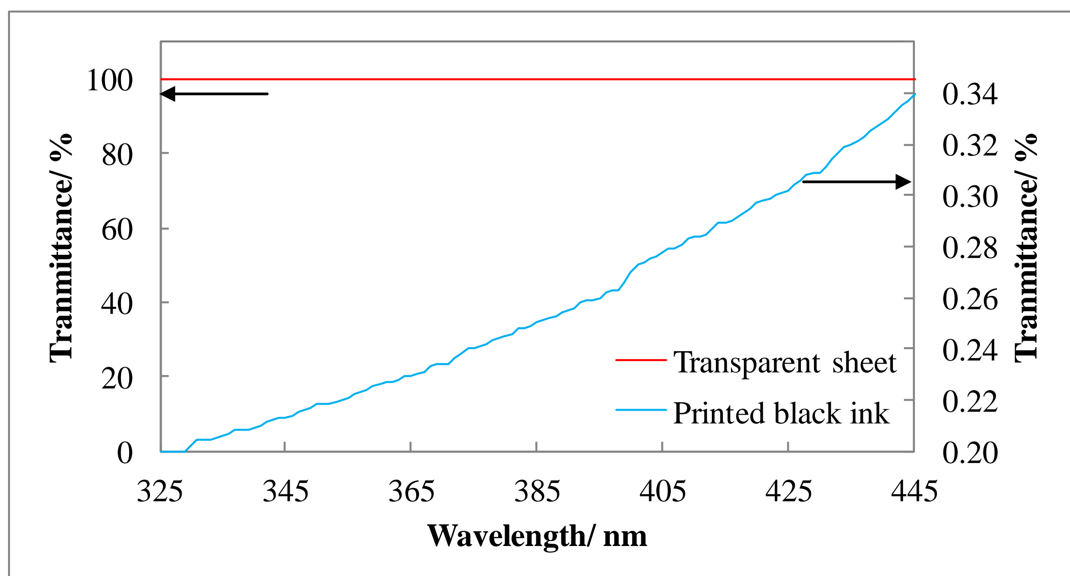

Fig. 3. 4. UV data showing the percentage of UV transmittance at different wavelengths on a transparent plastic sheet (red line) and after printing the sheet with black ink (blue line).

In a series of experiments, the time for UV exposure and development at different concentrations of developer were varied in order to determine the optimum conditions. It was found that the Aldrich negative photoresist performed best at 12-16 s exposure time followed by 45 s development in developer diluted to 50 vol. %.

The positive photoresist spray gave best results at an exposure time of ~ 240 s and 45 s development with undiluted developer.

Typical images of photoresist films exposed through photomasks of parallel lines followed by development at the optimum conditions are shown in Fig. 3. 5. Despite the precautions taken, the quality of the patterns generated were poor- even with the relatively large features used here (Fig. 3. 5). The edges of the patterns were uneven and jagged, and the contrast was poorly resolved, especially for the negative photoresist. The adhesion of the positive photoresist was very poor and only the thicker lines were preserved; an adhesion promoter, in this case DCDMS, caused the photoresist to dewet rapidly from the glass surface after application (see Fig. 3. 2 d).

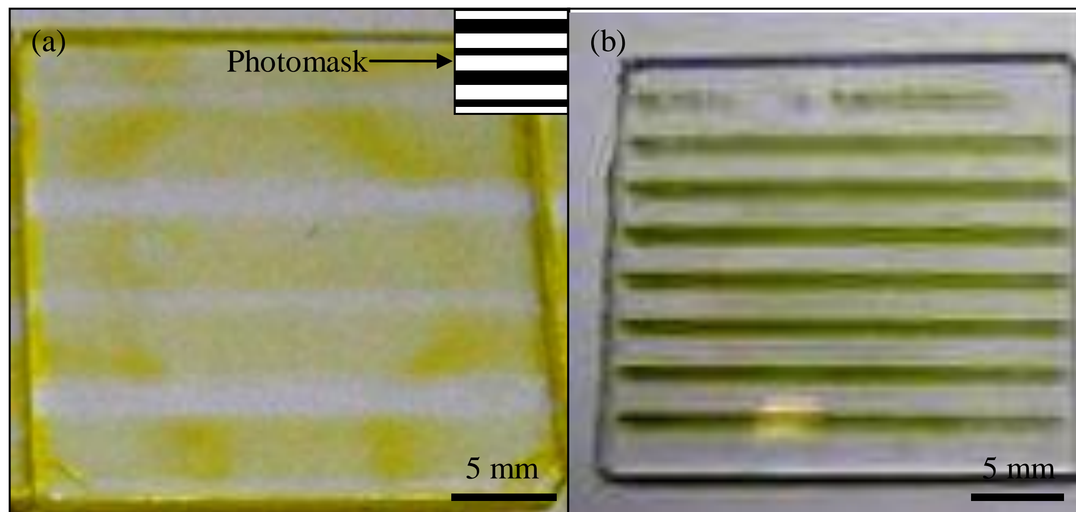

Fig. 3. 5. Typical images obtained by a digital camera of patterned photoresist films on glass substrates after development of Aldrich negative photoresist (a) and positive photoresist spray (b). The inset in (a) shows the design of the photomask used (the lines shown in black and white are UV opaque and UV transparent respectively).

Pattern formation on negative photoresist films using printed photomasks of periodic arrays of spots with 0. 2 mm diameter using both clearfield and darkfield photomasks (transparent photomasks with black spots and black photomasks with transparent spots respectively) gave even poorer results. The spots resulting from exposure through the darkfield photomask were found to be more oblong shaped than circular, and the holes resulting from exposure through the clearfield photomask were barely visible. The best resolved features were confined to the substrate edges and no features were observed towards the centre of the substrate; perhaps due to the

non- uniform thickness of the photoresist film (see Fig. 3. 3). As the photoresist is thicker at the edges of the substrate, the photomask would make direct contact at the substrate edges and would be elevated towards the centre of the substrate where the UV intensity would be reduced. Another possible cause could be due to the fact that the photomask was larger than the substrate by several millimetres and therefore may have become distorted during the contact exposure. The experiment was repeated after trimming down the photomask to a size slightly smaller than the substrate and after exposure and development, it was demonstrated that on this occasion the pattern was transferred to the entire substrate; however, like the previous experiment, the transferred pattern was poorly resolved and variations in the feature size were considerable. The poor quality of the patterns was at least partially due to the poor quality of the print on the transparent films used as photomasks. Microscopy images of the photomasks revealed that the coverage of the ink was not uniform and the features were somewhat distorted; however because the appearance of oblong features was fairly consistent in the transferred image (unlike the photomask), it is more likely that these unusual shapes are due to optical effects during exposure such as light scattering due to both non- uniform photomask contact and the presence of possible particulate contamination; [142, 143] light diffraction also becomes more important when longer exposure times are applied (typically, exposure times of 60-120 s are applied to other, more widely used photoresists).

In summary, the technique of transferring smaller features onto low cost negative and positive photoresist using homemade photomasks did not give satisfactory results. It was possible to generate larger features on the negative photoresist films, but the photoresist surface was uneven and the pattern boundaries and geometry were poorly resolved. The contrast of the patterns generated with the positive photoresist and the sharpness of the features was far greater than that observed with the negative photoresist; however the photoresist was much more sensitive to the development process and adhesion to the glass substrates was poor. The unsatisfactory results could also be attributed to the low quality of the homemade photomasks. One can conclude that the low cost photoresists investigated are unsuitable for the preparation of plate- like microparticles with dimensions < 10 μm.

3. 3. Experiments with high performance photoresists

Several high performance photoresists were investigated in this work. These were the negative photoresists AZ nLOF 2070 and SU-8 2002, and the image reversal photoresist AZ5214 E. Lift- off resist LOR 5A was also used in some experiments as a sacrificial layer to facilitate the removal of particles from the solid substrate. AZ5214 image reversal photoresist can be processed as either a positive or negative photoresist. Under normal processing conditions however, the photoresist acts in positive mode, i. e., the photoresist exposed to UV light becomes soluble in the developer, and when the baking temperature of the photoresist film is increased, a crosslinking agent within the photoresist is activated and subsequent exposure causes the photoresist to crosslink only in the exposed areas, thus acting as a negative photoresist. The use of an image- reversal photoresist permits the investigation of both a positive and a negative photoresist in a convenient way. AZ photoresist was chosen for this work due to its ability to produce good quality thin films (the film thickness is expected to be ~ 1. 5 μm under these processing conditions according to the manufacturer's data sheets). Films of 150 nm using AZ5214 have been produced by the manufacturer by diluting the photoresist with its own solvent. In this investigation, it was decided to produce films with a thickness of ~ 1.5 μm in order to facilitate the processing of the photoresist and analysis of the results.

3. 3. 1. Initial tests of the photoresist performance

Initial tests on the performance of the photoresists were conducted using a microfluidic- type photomask consisting of a continuous line pattern with varying width (Fig. 3. 6) generated by JD Phototools Ltd.

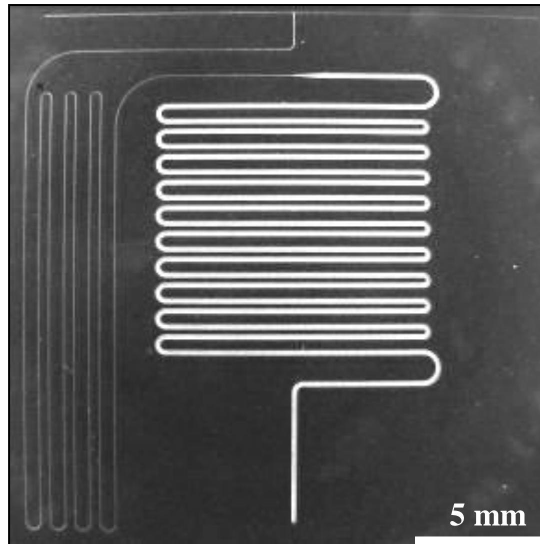

Fig. 3. 6. An image of a darkfield photomask with a thick line width of 200 μm and thin line width of 50 μm. Its use with a positive photoresist film will generate a channel etched in the photoresist after development.

Before commencing the experiments, the effectiveness of exposure and development was established for the new photoresist, similar to that used in Sec. 3.2, using a very simple masking procedure that covered a larger area of the photoresist surface. Several exposure times varied between 7 s and 27 s using the new photomask were investigated at a fixed development time of 60 s. As can be seen in Fig. 3. 7, exposure times ≥ 15 s gave the optimum results, whereas shorter exposure times resulted in only the partial removal of the exposed photoresist in developer.

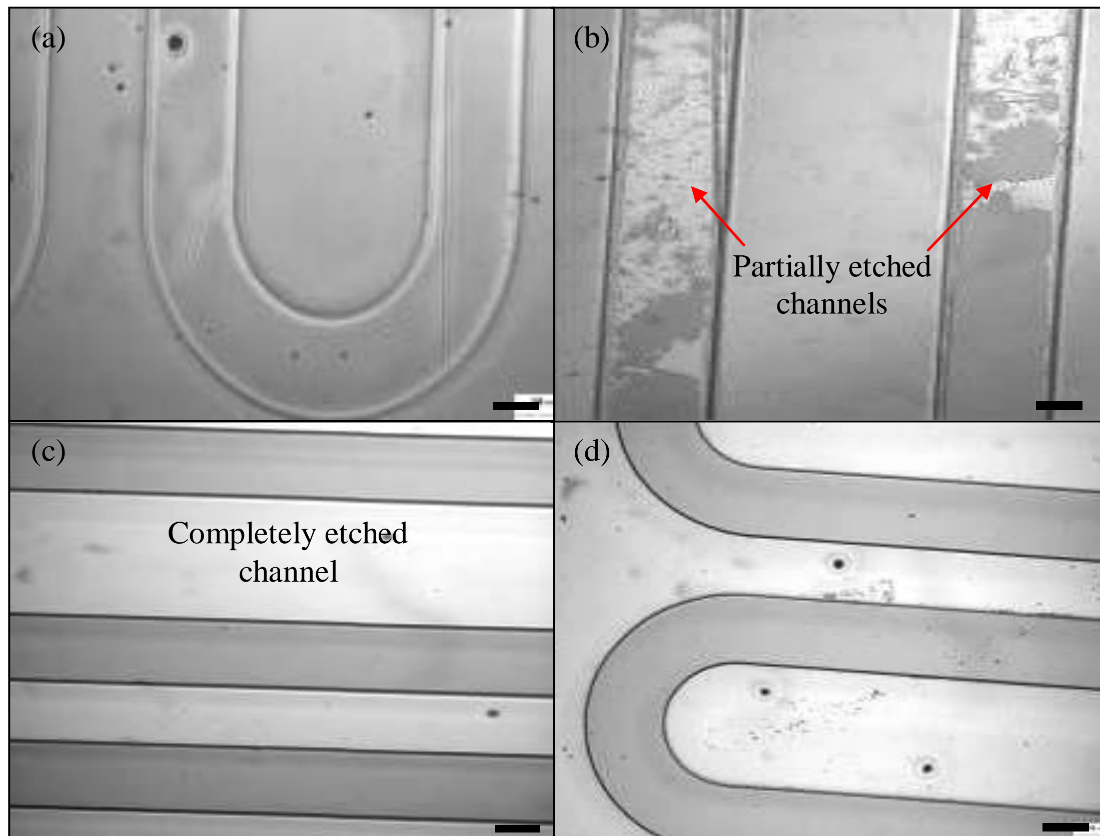

Fig. 3. 7. Optical microscopy images of 200 µm thick lines etched in a positive photoresist film (AZ5214) on a glass substrate after 60 s development following exposure times of: 7 s (a), 10 s (b), 15 s (c) and 23 s (d) using the photomask shown in Fig. 3. 6. The scale bars show 100 µm.

It was found that with the AZ photoresist, it was possible to apply multiple exposures to the photoresist surface to generate even more interesting patterns with smaller features, which may be a convenient method for the fabrication of particles with controlled shape. The photomask was reorientated 90 ° anti-clockwise after the first exposure and then a second exposure was carried out for the same exposure time. The effect of exposure time was again investigated as in the previous experiment. Fig. 3. 8 shows the results of a photoresist film exposed for 20 s following multiple exposures. It was demonstrated that rectangular and squared shaped particles could be generated using this procedure, and by applying three consecutive exposures (20 s each), interesting shapes such as rhombus and right angled triangles were observed (Fig. 3. 8).

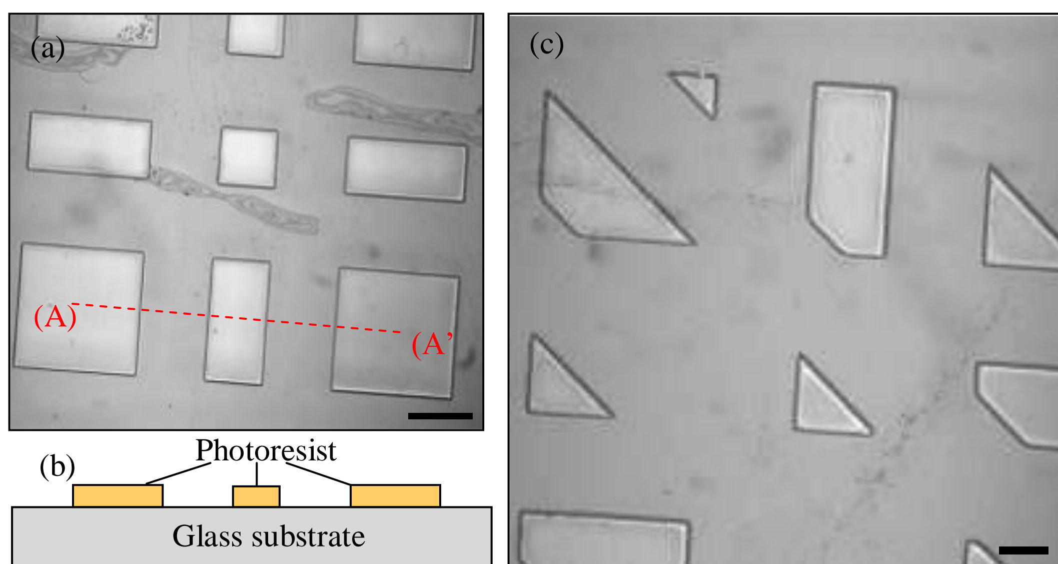

Fig. 3. 8. Optical microscopy images of a positive photoresist pattern (AZ5214) generated by exposing the photoresist surface twice by rotating the mask 90 ° for the second exposure (a). A sketch of the cross section along the line A- A' is shown in (b) and a photoresist pattern generated after 3 exposures by rotating the photomask 45 ° for each exposure is shown in (c). Scale bars show 100 µm.

From these results, it is demonstrated that the high quality positive photoresist AZ5214 is capable of resolving patterns effectively and maintains the integrity of the photomask image.

3. 3. 2. Preparation of microparticle arrays on square substrates

Our initial tests have shown that the transferred patterns with relatively large size and pitch were well resolved. The next step of our investigation was to determine if it is possible to resolve features with sizes of the order of tens of micrometers. This is a prerequisite for the fabrication of microparticles on a larger scale as the last step of our study. These experiments were performed using small area substrates with dimensions 25 × 25 mm cut from glass slides or silicon substrates. High quality photomasks (clearfield and darkfield) consisting of an array of squares with dimensions of 25 × 25 µm were used with a pitch of 8 µm. For the purpose of microparticle preparation, it is advantageous to keep the separation between particles in the array (the pitch) as small as possible in order to increase the yield. Typical images of the arrays obtained on glass substrates are shown in Figs. 3. 9- 3. 11. It was found that the squares that were fabricated using the clearfield photomask on the

positive photoresist after an exposure time of 10 s were connected together, suggesting that the exposure time was too short; the dimensions of the squares generated were ~ 5 µm larger than those on the photomask and in some cases, entire columns of squares had detached from the substrate surface after exposure for 15 s, with the squares connected by a thin layer of photoresist (Fig. 3. 9). It is expected that this issue of merging of the photoresist pattern was due to the small pitch on the photomask pattern.

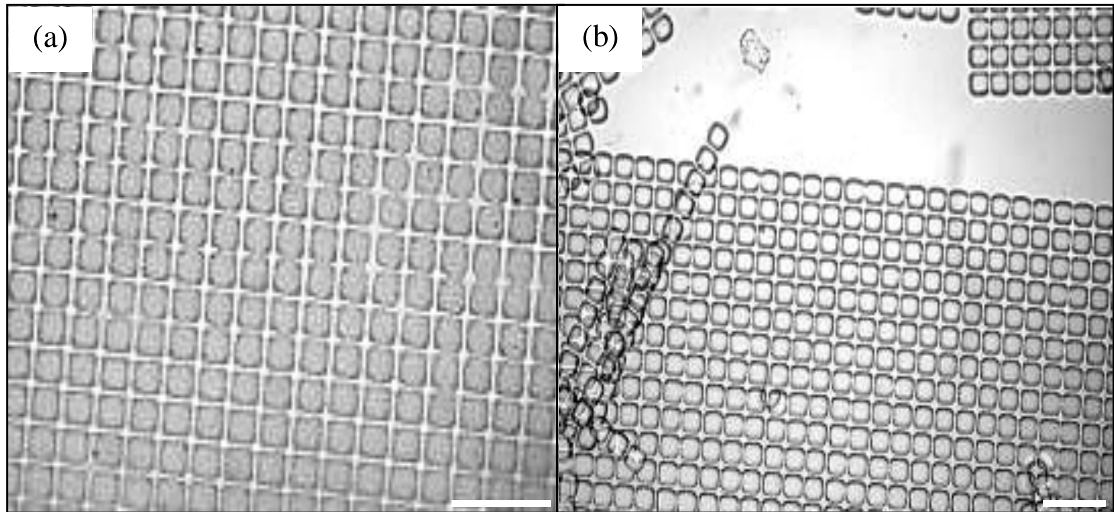

Fig. 3. 9. Optical microscopy images of a patterned positive photoresist film (AZ5214) exposed for 10 s (a) and 15 s (b) through a clearfield photomask consisting of UV opaque squares with dimensions of 25 x 25 µm. Scale bars show 100 µm.

In an effort to reduce the problem of particles merging; experiments with photomasks consisting of squares with a greater pitch were investigated. The photomask used in this case consisted of 25 × 25 µm squares with 20 µm pitch. The following observations were made. Exposure times > 15 s resulted in individual particles (not merged) lifting off the substrate during development (Fig. 3. 10). The particles remained intact on the substrate after a 7 s exposure time and the squares did not merge together. Promising results were therefore found for photoresist exposed for 7 s; although finer adjustment may be required for optimum exposure. The detachment of particles from the substrate with increasing exposure time may be due UV light diffraction during exposure, causing a part of the masked regions to be exposed and therefore developed and etched from the substrate; in support this, it was found that priming of the substrate with HMDS vapour did not improve the adhesion of the photoresist.

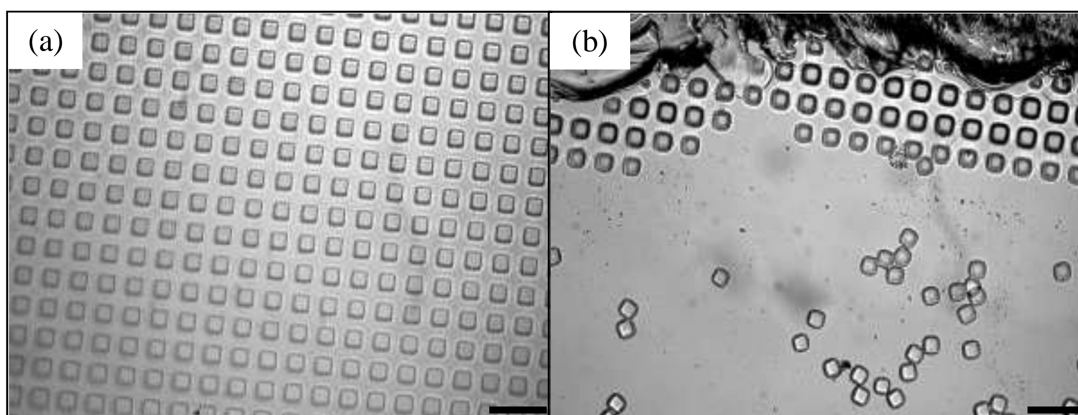

Fig. 3. 10. Optical microscopy images of patterned positive photoresist (AZ5214) exposed for 7 s (a) and 15 s (b) through a clearfield photomask consisting of an array of 25 x 25 µm squares with 20 µm pitch. Scale bars show 100 µm.

It was not possible to successfully fabricate the same pattern by processing the AZ image reversal photoresist as a negative photoresist due to the inability to resolve the pattern on the smaller scale used here. According to the manufacturer, a dedicated negative photoresist such as AZ nLOF 2070 is able to resolve features < 800 nm and also possesses enhanced chemical and thermal stability which would be desirable for our work.

To investigate the effect of substrate type, experiments with small squared substrates cut from a silicon substrate were made (previously glass was used). The motivation for using silicon substrates instead of glass stems from the availability of large silicon substrates routinely used and tailored for the photolithographic process. This will enable the fabrication of a larger number of particles. The quality of the surface is expected to be considerably greater and more homogeneous than that of the ordinary glass microscope slides used previously. Therefore, it was decided not to pursue investigations involving glass slides as, in addition to the points raised above, the optical properties of glass and silicon will be expected to affect the UV exposure process differently; for example because glass is optically transparent, UV light can penetrate the glass and cause exposure artefacts.

For the positive photoresist; various exposure times were applied to the photoresist at a fixed development time and developer concentration in accordance with the manufacturer's recommendation for silicon substrates. [127] In each case small square shaped silicon substrates with approximate dimensions of 25 x 25 mm were used. Images obtained from an optical microscope indicated that underexposure had

occurred when exposure times of 4, 8 and 12 s were applied. It was found that an exposure time of 15 s gave a particle size and shape corresponding to that on the photomask used (Fig. 3. 11) and further exposure after 15 s resulted in particle detachment from the substrate as a result of UV diffraction. [128]

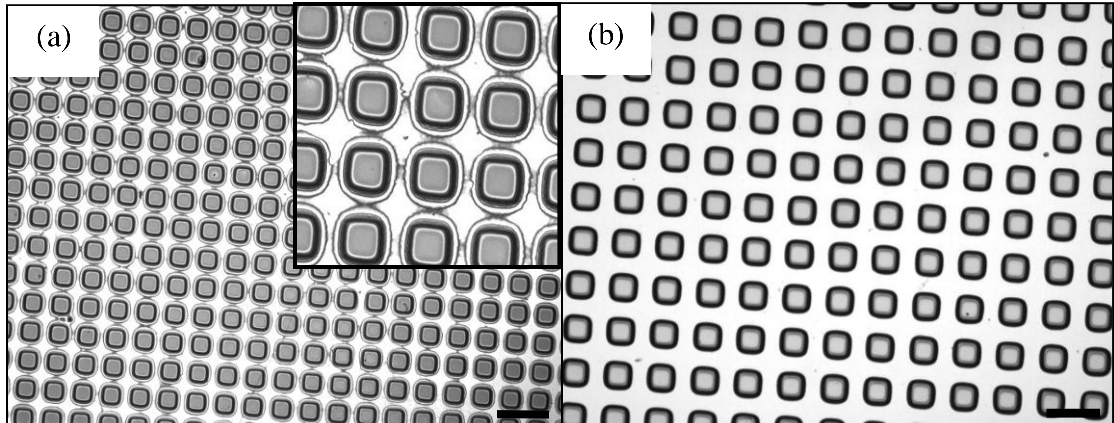

Fig. 3. 11. Optical microscopy images of positive photoresist (AZ5214) patterned onto silicon substrates through a clearfield photomask consisting of an array of 25 x 25 μm squares with 20 μm pitch after exposure for 12 s (a) and 15 s (b). Inset shows 4 x magnification. Scale bars show 50 μm.

The thickness of the photoresist film will determine the thickness of the plate- like microparticles generated by photolithography. For best results, the film should have an even thickness of less than a few micrometers. The photoresist patterns obtained on small substrates appeared to become progressively distorted (squares became more circular) approaching the edge of the square substrates. As mentioned before, it is expected that the film becomes thicker towards the edge of the substrate; especially for square or rectangular substrates. Variations in film thickness have been demonstrated to result in variations of the shape and size of the pattern. [128, 129] Using optical interferometry, changes in the thickness of the film can be determined by analysing the interference fringes obtained when the patterned photoresist surface is observed in monochromatic reflected light. From optical microscopy images, the interference fringes could be counted by identifying the fringes corresponding to the order of interference (m), e. g., 0, 1, 2 etc, and a knowledge of the wavelength of light used (λ) together with the refractive index (n_f) of the photoresist allows the thickness of the film (h) to be calculated by:

$$h = \frac{m\lambda}{2n_f} \tag{3. 1}$$

The wavelength of light in this case was 546 nm and the refractive index of the photoresist is 1. 63. Fig. 3. 12 shows a plot of film thickness vs. distance between the interference minima, and shows that the film becomes progressively thicker towards the edge of the substrate by as much as 2 x over a distance ~ 200 μm from the far edge; optical interferometry (Fig. 3. 12) and SEM images (Fig. 3. 13) both confirm this. The film thickness at the edge of the coated substrate was found to be 4 x greater than at the centre.

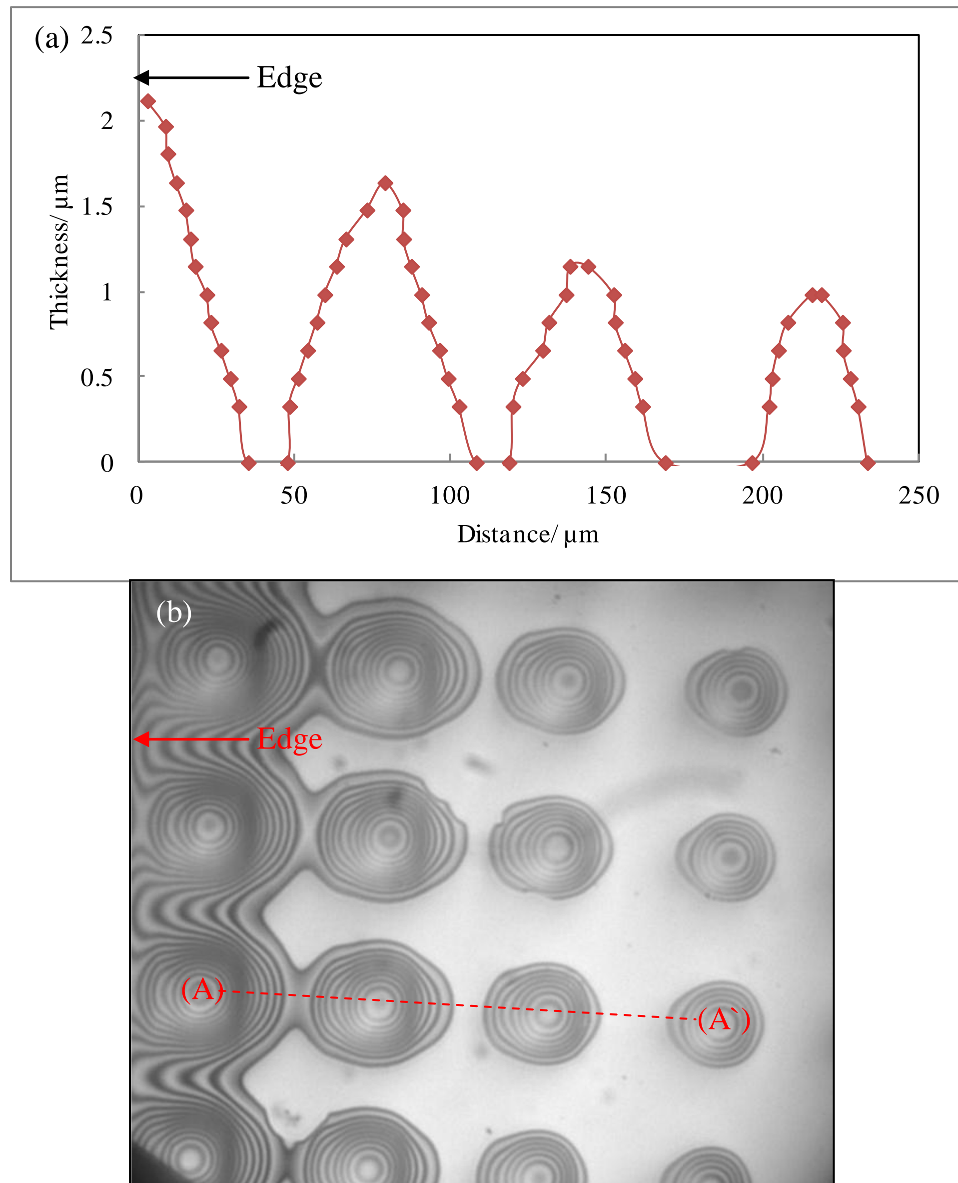

Fig. 3. 12. (a) A plot of photoresist film thickness vs. distance for the interference minima along the line A- A' shown in (b). Data was obtained from grey-scale analysis using Image Pro Plus 5. 1 software. (b) Optical microscopy image of the photoresist film at the edge of the substrate (using reflected light) from which the measurements were made.

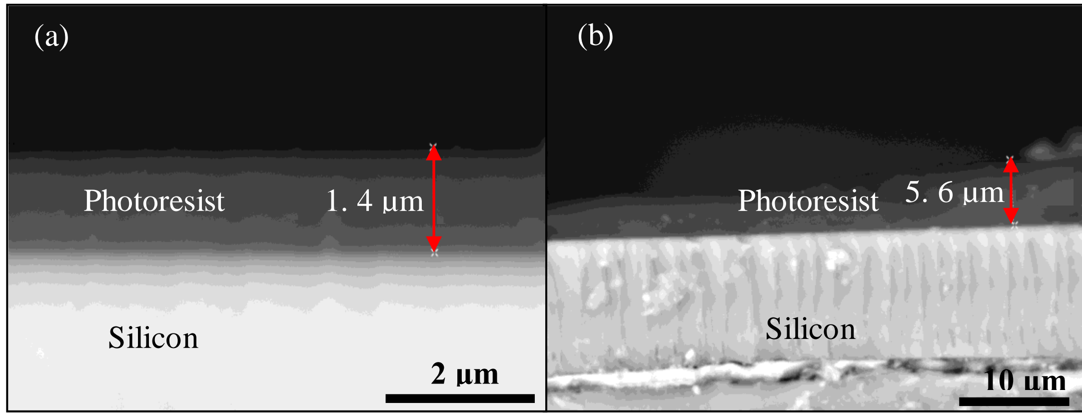

Fig. 3. 13. SEM images of the photoresist film centre (a) and the same film measured 300 µm from the edge (b).

3. 3. 3. Preparation of microparticle arrays of negative photoresist on large silicon substrates

We have investigated the application of photolithography using AZ nLOF 2070 and SU- 8 photoresist on large circular silicon substrates. This was motivated by the fact that the large substrates are less likely to cause the variation in the photoresist film thickness observed previously for square substrates, due to the presence of a bevelled edge on the large circular silicon substrate. In addition, the large substrates permit a higher yield of fabricated particles to be realised (it should be considered that photolithography is a 2D process and therefore the yields of particles produced are typically small). Negative photoresist was chosen for this investigation due to its greater chemical and thermal stability over that of the positive photoresist, which may be beneficial for further processing and modification of the surface. The composition of the resin that remains after photolithographic processing is the same as that for the positive photoresist when AZ photoresist is used; however the extent of crosslinking for the negative photoresist is greater than that of the positive photoresist. Experiments were performed both with and without the application of a sacrificial layer in order to allow any processing issues involving the sacrificial layer to be addressed at an early stage, for example the LOR sacrificial layer is sensitive to developer concentration and time. [130, 141, 144, 145] When the sacrificial layer was applied by spin coating, it was found to be crucial to prevent the formation of 'comets' on the spin coated films resulting from the presence of particles or bubbles, which had serious implications for the quality of the top surface of patterned photoresist, resulting in the presence of defects in the pattern. [127] In these

experiments, the LOR that was used as a sacrificial layer was filtered and left to stand for several hours before use in order to minimise defects. In addition, it was found that the quality of the spin coated film of LOR depended on how the substrate was treated before application. If the substrate was cleaned using Piranha solution, giving rise to a highly oxidised surface, triangular regions of uncoated film were observed after spin coating and it was necessary to increase the acceleration rate to prevent their formation. It was desirable to be able to develop both the photoresist and sacrificial layer, preferably in one step, in order to permit modification of the top surface of the photoresist for the preperation of Janus particles (Chapter 5 of this thesis). In the first experiment, the exposure time was investigated without application of a sacrificial layer in order to demonstrate if pattern formation with the desired features was possible. It was then decided to investigate the development time and developer concentration required for the fabrication of photoresist disc shaped particles on a sacrificial layer of LOR. A darkfield photomask consisting of UV transparent circles with 10 μm diameter and 10 μm pitch arranged in a hexagonal array was used. This type of photomask will generate solid disc shaped particles with a negative photoresist. The exposure times were varied between 11 s and 14 s and undiluted developer (AZ MIF 726) was used as the developer for a development time of 120 s. As shown in Fig. 3. 14 for a photoresist pattern generated without application of a sacrificial layer, an exposure time of 11 s gave the optimum results and a photoresist disc diameter of 10. 0 μm ± 0. 5 μm, demonstrating that it was possible to resolve features of 10 μm. The discs that were fabricated in this way were not always perfectly circular and monodisperse due to small variations of the uniformity of the pattern on the photomask and possibly exposure artefacts.

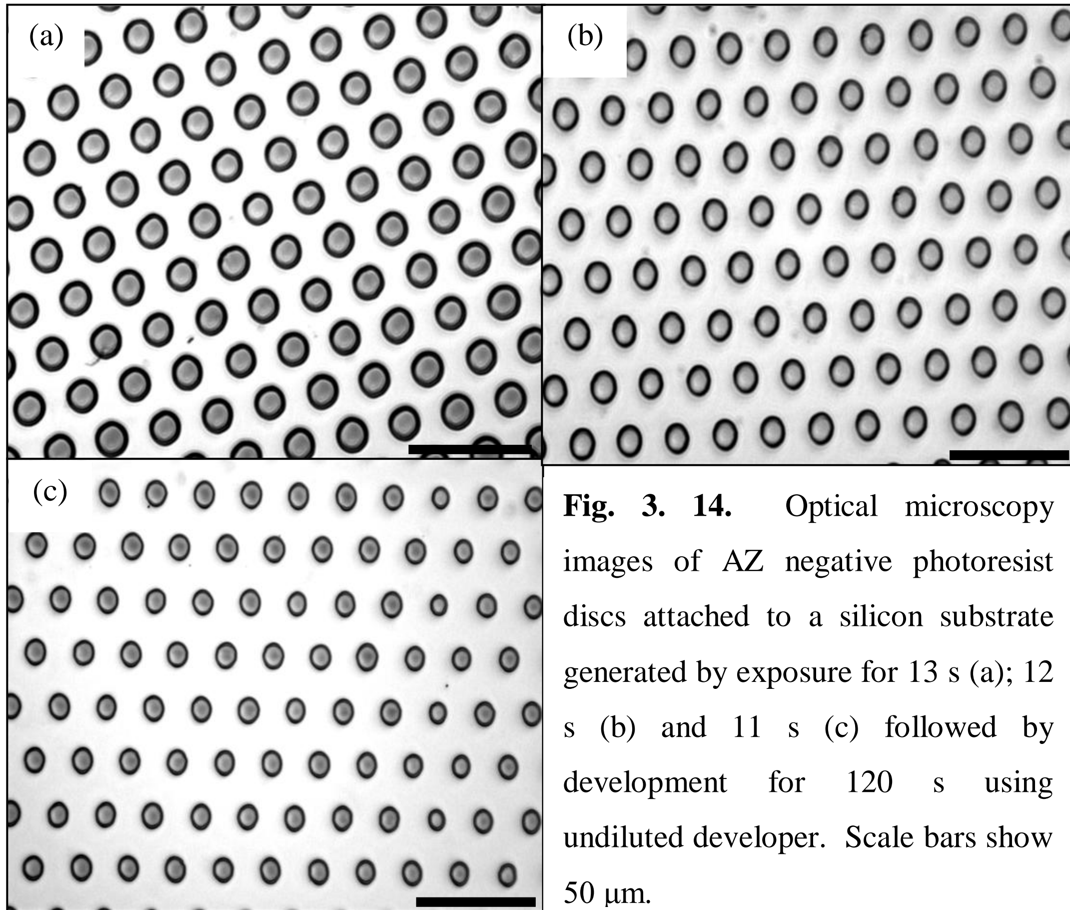

Fig. 3. 14. Optical microscopy images of AZ negative photoresist discs attached to a silicon substrate generated by exposure for 13 s (a); 12 s (b) and 11 s (c) followed by development for 120 s using undiluted developer. Scale bars show 50 µm.

Next, a sacrificial layer of LOR was applied to the substrate before applying the layer of photoresist in order to permit the simultaneous development of the photoresist and sacrificial layer using different concentrations of the developer. This method will permit modification of the top surface of the photoresist discs at a later stage and facilitate the release of the particles from the substrate by dissolution of the sacrificial layer using the photoresist developer or 1165 remover. It was found that when the developer was undiluted, the development process became very difficult to control and would result in rapid dissolution of the sacrificial layer and premature release of the photoresist particles in the developer. During development using diluted developer, the partially developed photoresist pattern was occasionally removed from the developer and observed using an optical microscope in order to follow the progress of the development process. The effect of developer dilution was investigated in the range 75 % developer (3: 1 dilution with water by volume) to 83. 3 % developer (5: 1 dilution with water by volume). Using 75 % developer, noticeable changes in the appearance of the sacrificial layer were observed, and although the disc were reduced in size with increasing development time, the final

size of the discs was ~ 12. 0 ± 0. 5 μm after 13 min. This suggests that the photoresist was not completely developed after this relatively long time and the presence of the sacrificial layer was still evident (Fig. 3. 15) indicating that the developer was too diluted.

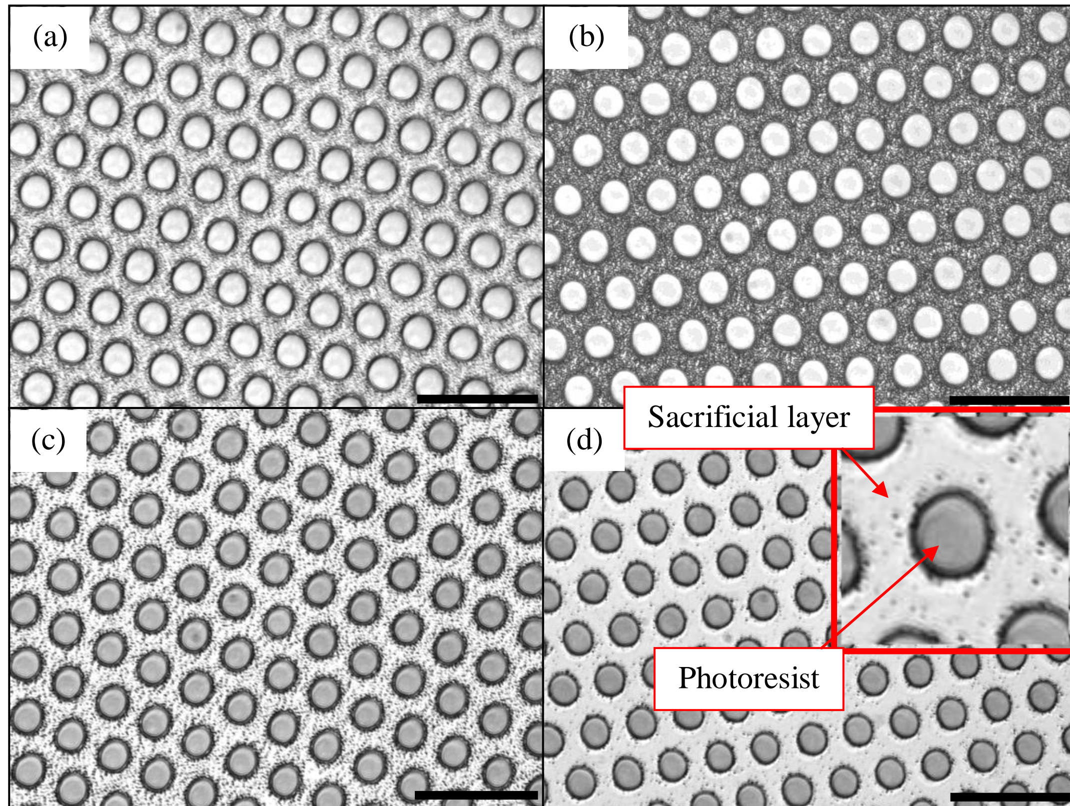

Fig. 3. 15. Optical microscopy images of AZ negative photoresist discs attached to a silicon substrate via a sacrificial layer of LOR 5A generated by exposure for 11 s and development (developer diluted to 3 parts developer to 1 part water) for 169 s (a), 228 s (b), 597 s (c) and 792 s (d). Inset shows 4 x magnification and scale bars show 50 μm.

Using 80 % developer it was found that the presence of the sacrificial layer could not be observed after a development time of ~ 5 min due to its complete dissolution, revealing the bare silicon surface (Fig. 3. 16). This was considered to be the complete development of the sacrificial layer. The final size of the discs after ~ 9. 5 min was 11. 7 ± 0. 5 μm, i. e., closer to that on the photomask used (10 μm).

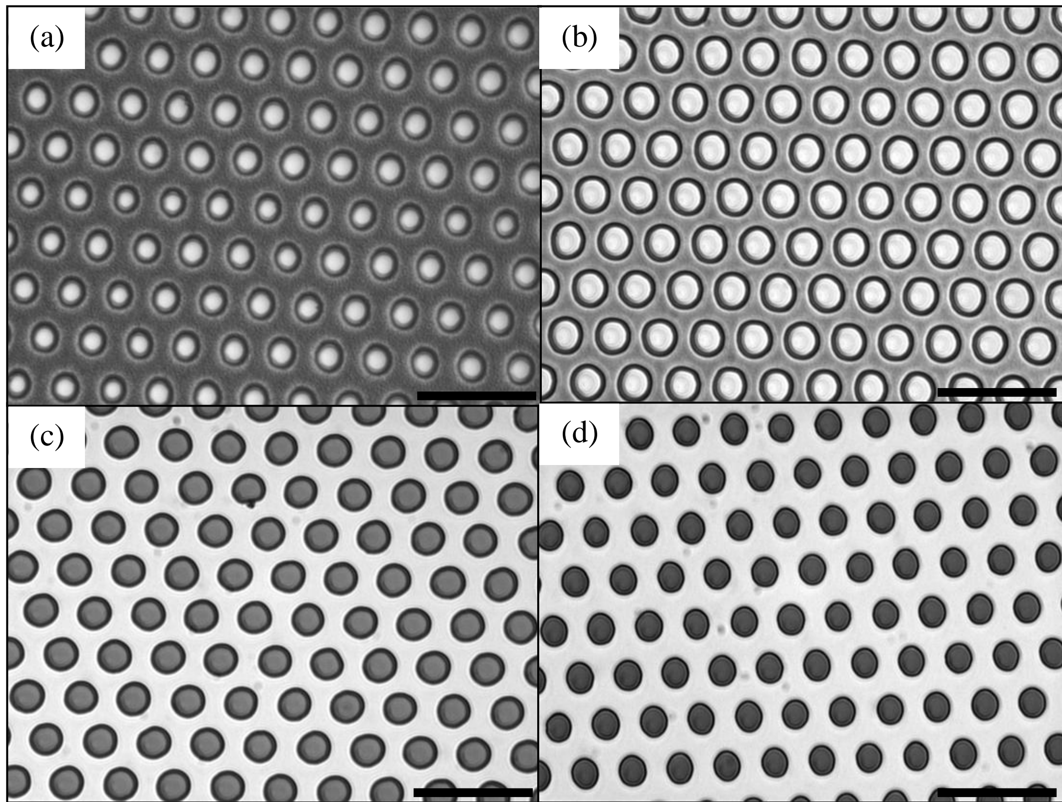

Fig. 3. 16. Optical microscopy images of AZ negative photoresist discs attached to a silicon substrate via a sacrificial layer of LOR 5A generated by exposure for 11 s and development (developer diluted to 4 parts developer to 1 part water) for 65 s (a), 129 s (b), 304 s (c) and 565 s (d). Scale bars show 50 µm.

At the higher developer concentration of 83. 3 %, it was evident that the photoresist discs were completely developed after ~ 4 min immersion in the developer as shown in Fig. 3. 17 d. The size of the discs after this time was 9. 5 ± 0. 5 µm (very close to those on the photomask). It appears therefore that the photoresist and sacrificial layer were completely developed after this time; therefore this concentration of developer was found to be optimum.

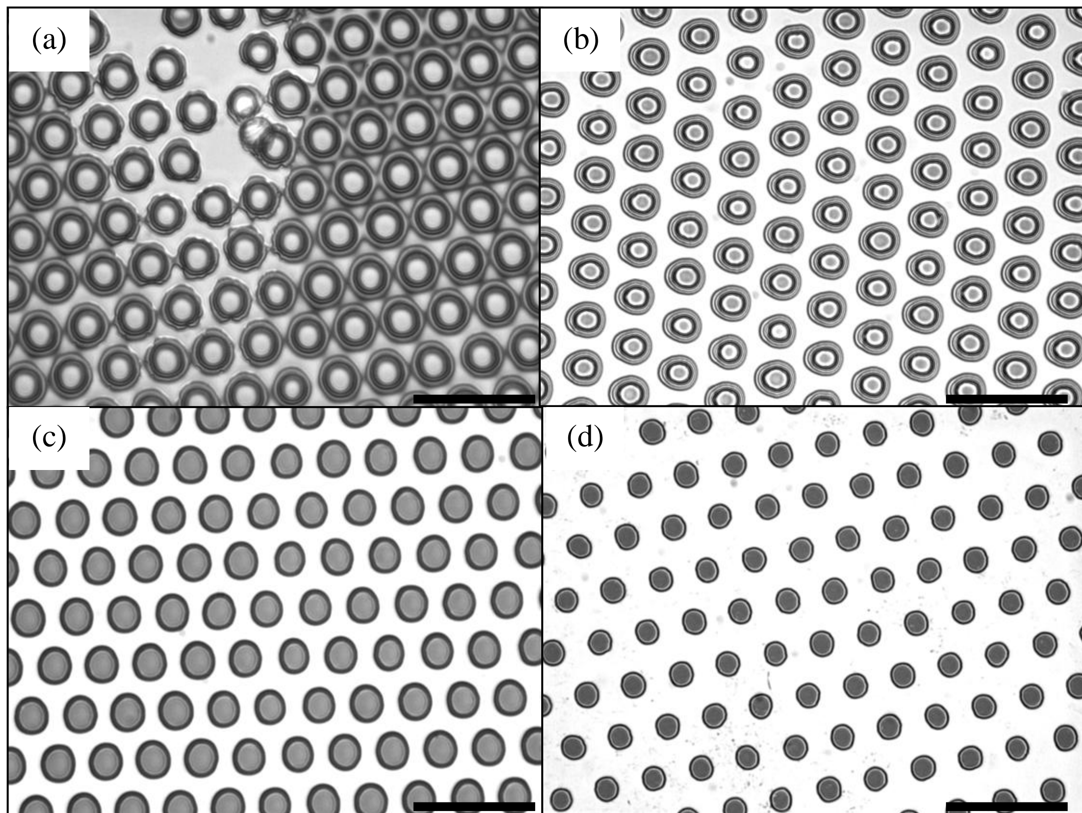

Fig. 3. 17. Optical microscopy images of negative photoresist discs attached to a silicon substrate (via a sacrificial layer of LOR 5A) generated by exposure for 11 s and development (developer diluted to 5 parts developer to 1 part water) for 64 s (a), 130 s (b), 212 s (c) and 240 s (d). Scale bars show 50 μm.

Having established suitable processing conditions for this photoresist, the fabrication of particles with different shapes was investigated. The use of a photomask with rectangular shaped features however generally resulted in photoresist with rounded shapes, hereafter called ovals or rounded rectangles (Fig. 3. 18). The photomasks consisting of 10 x 20 μm rectangles resulted in oval shaped photoresist patterns and the photomask consisting of 10 x 40 μm rectangles resulted in rounded rectangular shaped photoresist patterns. The photomask with 10 x 20 μm rectangles gave the poorest quality features on the photoresist with significant variations in the size and shape of the features (regardless of which type of photoresist was used) and may be due to the quality of the photomask on this occasion; however the photomask with 10 x 40 μm rectangles gave much better results. The conditions for the fabrication of the particles were kept the same as the disc shaped particles described in the previous section with only small variations. For example, some of the 10 x 40 μm rectangles tended to bridge together between their long axes and therefore it was necessary to

reduce the exposure time to amend this. The bridging was not completely eliminated; however it is anticipated that this will be resolved when the particles are released from the substrate. Some patterns were also generated using SU- 8 negative photoresist. Images of oval and rectangular AZ photoresist and disc shaped SU- 8 photoresist attached to a silicon substrate via a sacrificial layer of LOR are shown in Fig. 3. 18 and Fig. 3. 19 respectively.

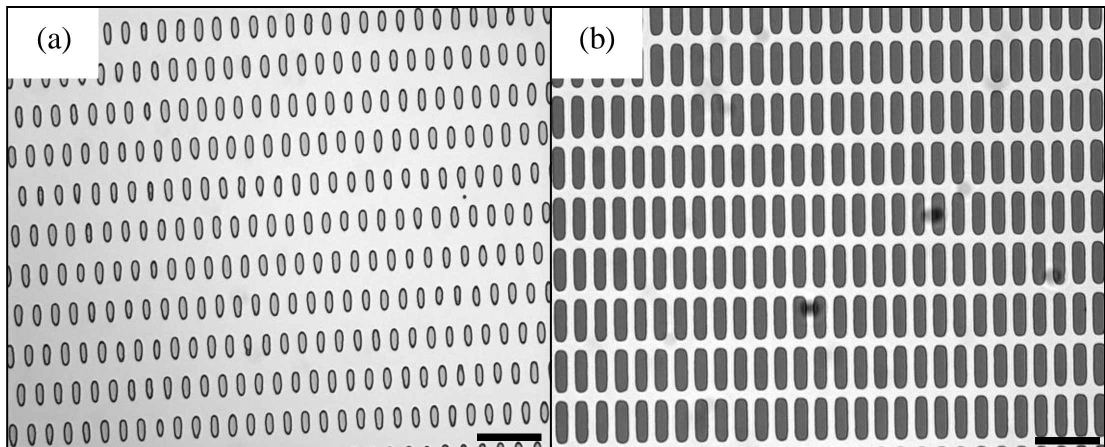

Fig. 3. 18. Optical microscopy images of AZ negative photoresist ovals (a) and rectangles (b) attached to a silicon substrate via a sacrificial layer of LOR 5A. Scale bars show 50 μm.

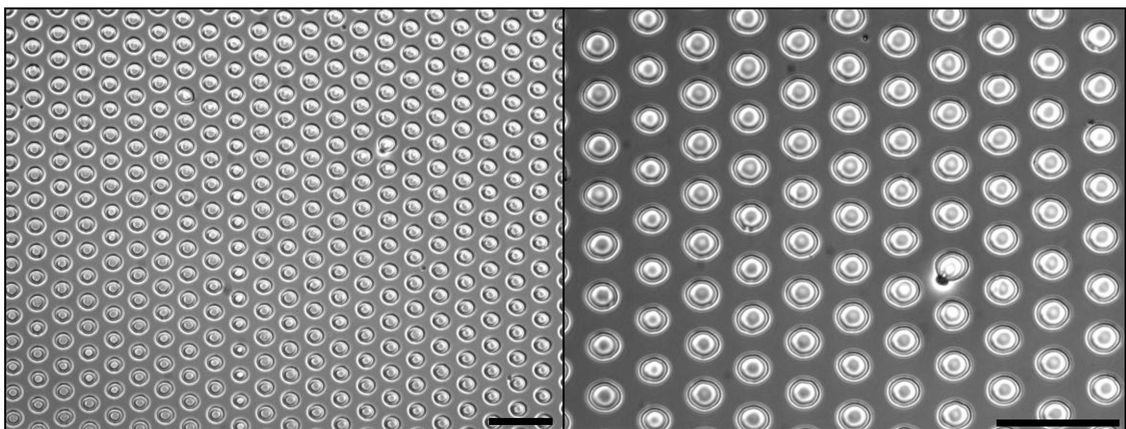

Fig. 3. 19. Optical microscopy images of SU- 8 negative photoresist discs attached to a silicon substrate via a sacrificial layer of LOR 5A. Scale bars show 50 μm.

3. 4. Methods for releasing the fabricated photoresist particles from the substrate

In order to generate anisotropic photoresist particles for the investigation of the effect of particle shape and aspect ratio on monolayers at the liquid- fluid interface, it is necessary to establish a suitable method for their release from the substrate and recovery from the suspension. In these experiments, protocols are established for the release of both positive and negative photoresist particles.

It was found previously that positive photoresist squares were effectively detached from the silicon substrate without the need for a sacrificial layer simply by controlling the exposure time: for an exposure time of > 15 s, the photoresist was released from the substrate during development (see Fig. 3. 10 b). Because it is known that the presence of the undiluted developer solution significantly affects the roughness of the photoresist surface (Sec. 3. 5. 2) and may ultimately etch away the photoresist, it was decided to dilute the developer solution immediately after the particles had detached from the substrate. It was found that an exposure time of 15 s on this occasion was sufficient to cause the particles to detach from the substrate after 60 s of development. After the particles were released and the developer solution diluted, the particles were recovered by centrifugation. Fig. 3. 20 shows some rectangular photoresist particles suspended in the diluted developer. Some of the photoresist particles appeared to be broken, which may be due to sonication of the suspension using ultrasound at 20 W for 60 s to effectively disperse the particles before and after centrifugation cycles. Some of the particles were observed to assemble into clusters which could be due to incomplete dispersion of the particles after centrifugation. Variations in the size and shape, i. e., rectangular or oval shape may be due partial etching of the photoresist in the developer solution. It may be the case that the photoresist in some areas of the substrate was more exposed to UV than in other areas of the substrate, thus giving rise to variations in the rate of etching in the developer. This approach therefore, although shown to be very effective for the release of the positive photoresist particles, resulted in variation of the size and shape of the particles. Particles prepared using this photoresist could not be released by dissolution of a sacrificial layer using NMP due to their instability in this solvent.

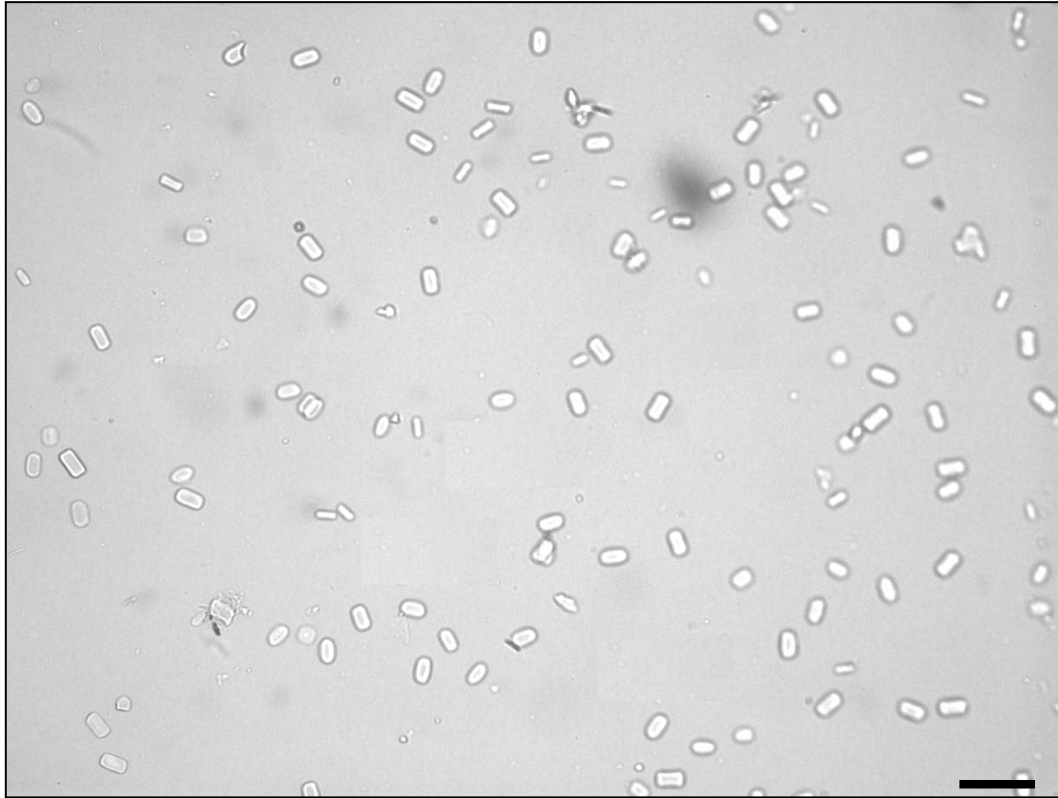

Fig. 3. 20. Optical microscopy image of positive photoresist rectangles suspended in diluted developer solution. Scale bar shows 50 μm.

For particles fabricated using the AZ negative photoresist, it was decided to determine if it was possible to release the particles directly from the substrate without application of a sacrificial layer. It was expected that partial crosslinking at the base of the photoresist during exposure (exposure begins at the top surface of the photoresist) would facilitate release of the particles from the substrate if the exposure time was short enough, as the UV would not be able to penetrate the entire depth of the photoresist completely; however it was found that the only way to effectively release the particles in NMP or developer was to apply sonication by sonicating the photoresist in NMP using an ultrasonic bath, indicating that the extent of crosslinking at the base of the photoresist film was appreciably large. Although the particles could be released by sonication, when the particles were observed in the suspension by microscopy, they were found to be broken into two or more fragments. One reason for the occurrence of the broken particles could be due to embrittlement of the photoresist, particularly during the final hard bake step (this is necessary to prevent dissolution of the photoresist in the NMP). [138] Breakage of the photoresist particles could then be induced by sonication of the photoresist in NMP as the particles are loosened from the substrate. Further experiments were performed

in the presence of a sacrificial layer as this would facilitate particle release and also enable the surface of the particles to be modified at a later stage before release. As indicated previously, the sacrificial layer could be developed isotropically leaving a pillar of the sacrificial layer directly beneath the photoresist particles (see Fig. 3.17 d). The photoresist particles were successfully released by dissolution of the sacrificial layer in NMP at ~ 65 °C. When it was apparent that the particles had been released from the substrate, sonication was applied in an ultrasonic bath to break up any bridging particles for 30 s. In many of the experiments, the suspended particles were filtered to remove columns of particles resulting from photomask defects; however this approach significantly reduced the yield of particles obtained. No filtration was applied when rectangular (10 x 40 μm) particles were used as photomask defects in this case were not significant. The particles that were released using this procedure were not damaged when the suspensions were sonicated for no more than 2 min in an ultrasonic bath. Images of disc and rectangular shaped photoresist particles suspended in NMP are shown in Fig. 3. 21. Occasionally, and especially for the rectangular particles, the suspended particles appeared to be bent perhaps as a result of the large dimensions of the particles relative to their thickness.

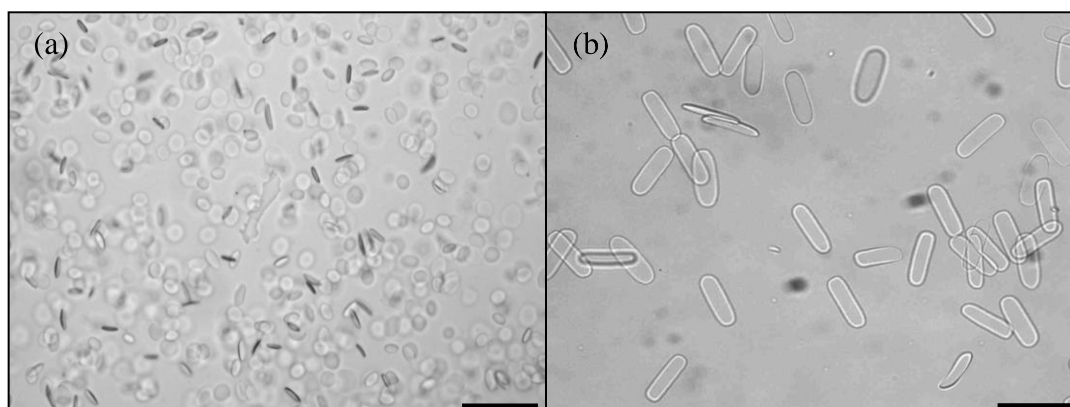

Fig. 3. 21. Optical microscopy images of AZ nLOF 2070 negative photoresist discs (a) and rectangles (b) suspended in NMP after dissolution of the sacrificial layer to liberate the particles from the silicon substrate. Scale bars show 50 μm.

After releasing the particles, washing of the particles by centrifugation was performed; however this was only effective when concentrated NMP solution was used, i. e., without dilution. Dilution of the NMP resulted in retention of the particles on the inner walls of the glass due to the lower refractive index of the solution with respect to the photoresist particles. It should be considered that the

photoresist is fairly hydrophobic (AZ photoresist has a refractive index is ~ 1. 6) and when the refractive index of the release medium is significantly different from this, van der Waals forces cause the particles to stick to the inner walls of the centrifuge tubes. The alternative approach of grafting surfactants to the surface of the photoresist particles was not performed in this study as this would affect the interactions between the particles at the fluid interface, covered in chapter 4 of this thesis.

Disc shaped SU- 8 photoresist particles could only be released intact when developer or NaOH solution was used (Fig. 3. 22). NMP caused the particles to break; possibly because certain stresses are imparted to the photoresist when immersed in NMP, and because the SU- 8 photoresist particles were very thin (~ 750 nm or approximately half of the thickness of the AZ photoresist), the particles were more susceptible to this; therefore for these experiments it was necessary to employ a basic solution to dissolve the sacrificial layer as this did not result in breakage of the particles.

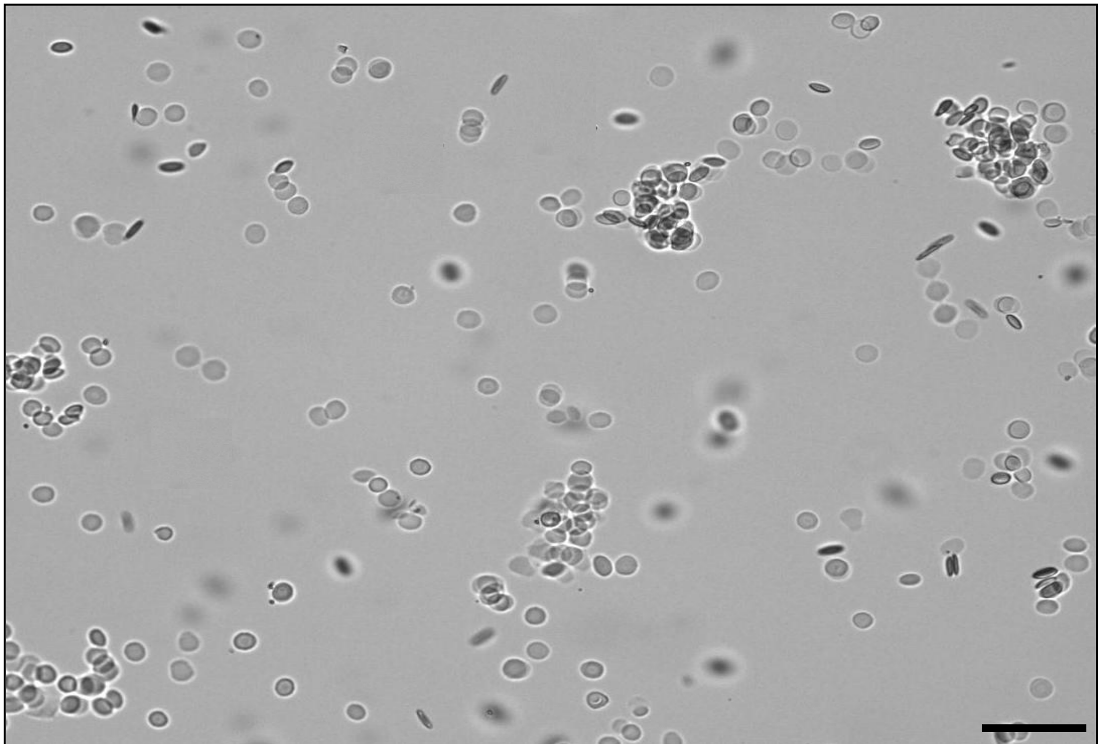

Fig. 3. 22. Optical microscopy image of SU- 8 2002 negative photoresist discs suspended in 0. 2 M NaOH after dissolution of the sacrificial layer to liberate the particles from the silicon substrate. Scale bar shows 50 μm.

3. 5. Characterisation of the photoresist microparticles

3. 5. 1. Particle shape and size

Images obtained by SEM revealed that the surface of the photoresist particles were somewhat rough. The presence of a thin layer of the LOR sacrificial layer was observed outside the periphery of the particles and therefore, suggests a slight underdevelopment of the sacrificial layer. The side walls of the photoresist structures were not perfectly vertical; instead a re- entrant profile was observed which is attributed to the exposure and development process, and may also be due to non- uniform photomask contact during exposure due to diffraction effects. [131- 135] As mentioned; if the exposure dose is not sufficient to completely penetrate the photoresist, the extent of crosslinking will diminish as the bottom of the photoresist is approached. This means that development will occur more rapidly where the extent of crosslinking is least, i. e., at the bottom of the photoresist and therefore may give rise to the re-entrant profile of the side- walls observed: it was mentioned briefly in a previous section that depending on the concentration of developer, the photoresist patterns lifted off the substrate prematurely and this can be understood as complete dissolution of the photoresist at its base. The thickness of the AZ photoresist determined by SEM was 1. 1 ± 0. 3 µm. SEM images of the AZ photoresist (Figs. 3. 23, 3. 24 and 3. 26) and SU- 8 photoresist patterns (Fig. 3. 25) are shown below. The appearance of the SU- 8 photoresist discs was somewhat more unusual, the photoresist was very rough at the periphery of the discs (significantly more than the AZ photoresist) and the thickness was found to be ~ 0. 75 µm- significantly thinner than expected. Under similar processing conditions, the group of Stroock reported a film thickness of ~ 1. 2 µm for the same photoresist; [68] in addition they applied an i- line filter designed to eliminate UV below a wavelength of 360 nm which is known to improve the quality of the photoresist patterns. [117, 136, 137] As no filter was applied in these experiments, the significant roughening of the SU- 8 edges is perhaps due to exposure at these shorter wavelengths. The UV curing unit used in these experiments generated a fairly broad range of UV wavelengths with a peak at 350 nm.

The geometrical characteristics of the AZ negative photoresist after fabrication using photolithography are shown in Fig. 3. 27 and Table. 3. 1.

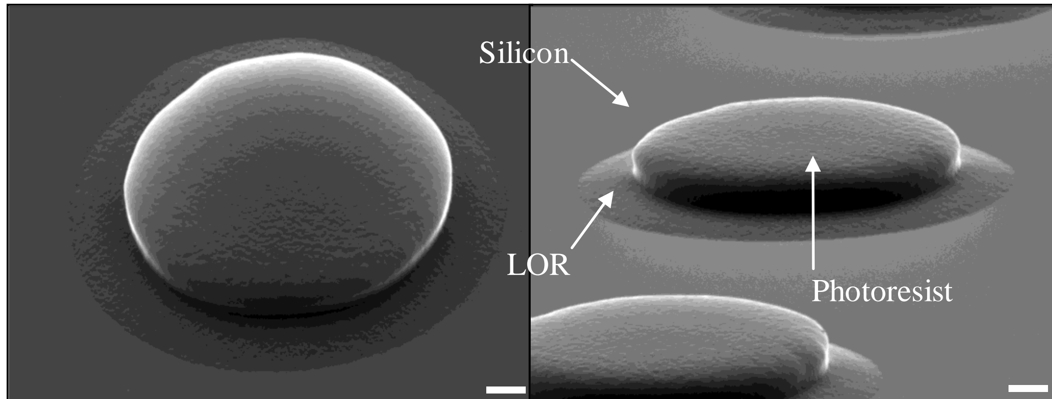

Fig. 3. 23. SEM images of AZ negative photoresist discs attached to a silicon substrate via a sacrificial layer of LOR 5A. Scale bars show 1 μm.

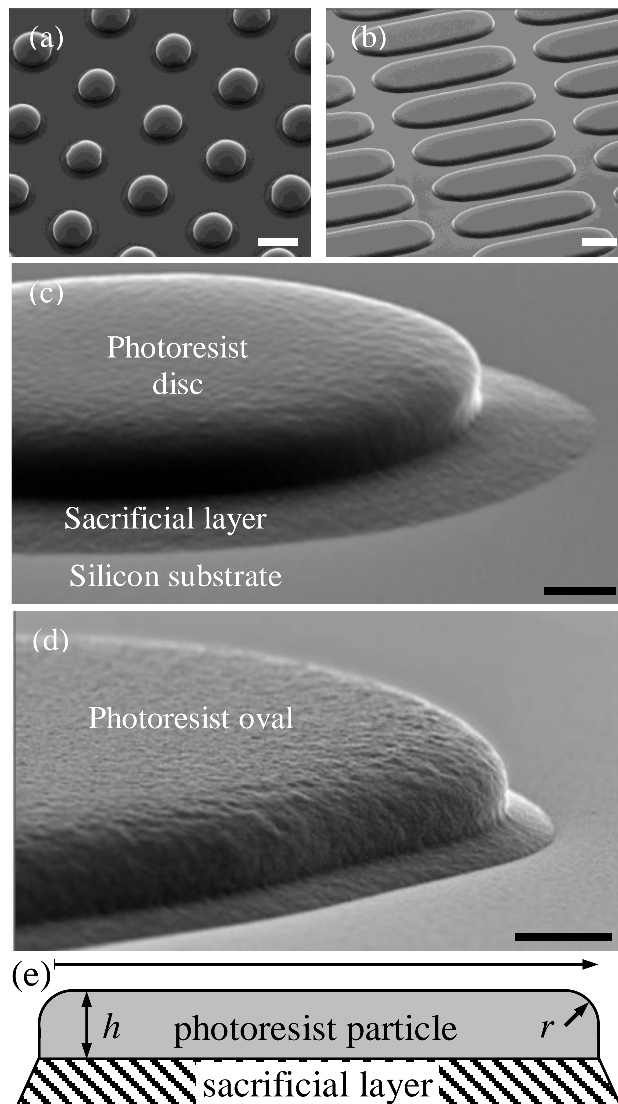

Fig. 3. 24. SEM images of photoresist discs (a, c), photoresist rectangles (b) and photoresist ovals (d) attached to a silicon substrate via a sacrificial layer of LOR 5A. The diagram below shows the cross sectional profile deduced from the images. The radius of the rounded edges was estimated to be $r = 0.069$ (e). Scale bars are (a, b) – 10 μm, (c, d) – 1 μm.

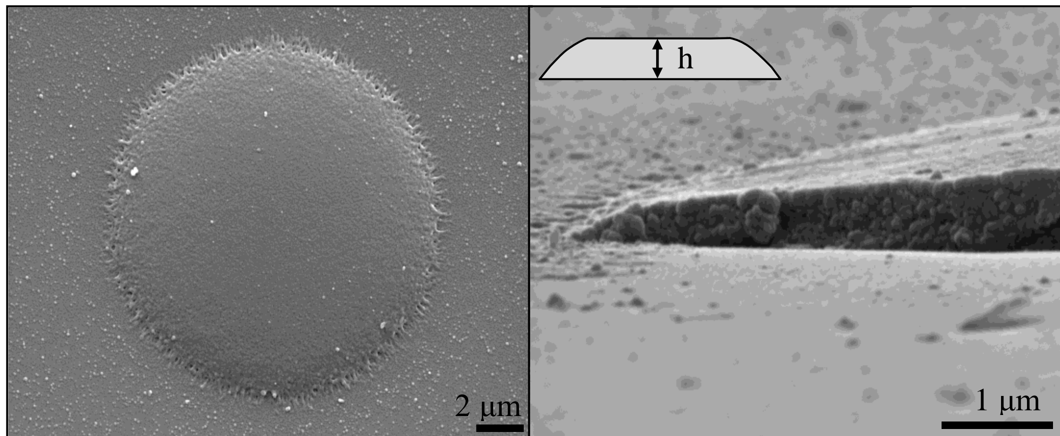

Fig. 3. 25. SEM images of SU- 8 negative photoresist discs attached to a silicon substrate via a sacrificial layer of LOR 5A. The image on the right shows part of a fragment of SU- 8 that was used to determine the thickness of the photoresist.

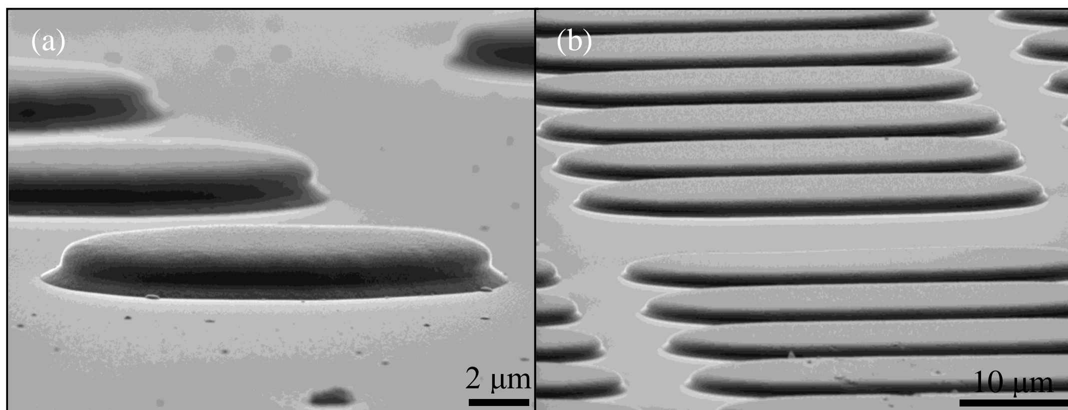

Fig. 3. 26. SEM images of AZ negative photoresist ovals (a) and rectangles (b) attached to a silicon substrate via a sacrificial layer of LOR 5A.

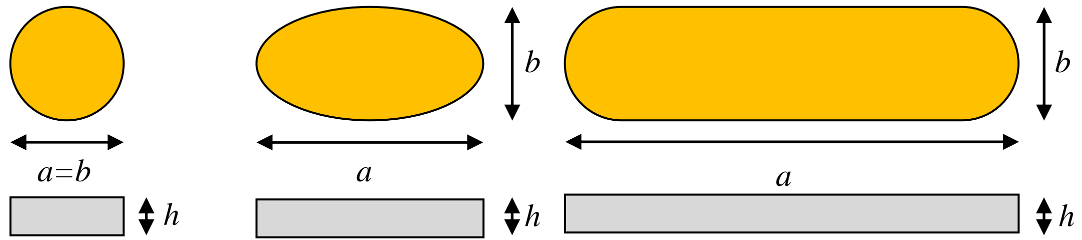

Fig. 3. 27. Schematic of the geometrical characteristics of the AZ negative photoresist particles after fabrication using photolithography: projected shape (top) and cross section (bottom).

Table. 3. 1. Geometrical characteristics of the photomasks and photoresist produced by photolithography using AZ and SU- 8 * negative photoresist.

Photomask			**Fabricated particles**			
Shape	Dimensions/ µm		Shape	Dimension/ µm		
	a	b		a	b	h
Circle	10 ± 0. 6	10 ± 0. 6	Disc	12 ± 2	12 ± 2	1. 1 ± 0. 1
	10 ± 0. 6	10 ± 0. 6	Disc *	10 ± 2	10 ± 2	0. 75 ± 0. 1
Rectangle	20 ± 0. 6	10 ± 0. 6	Oval	17 ± 2	8. 0 ± 2	1. 1 ± 0. 1
Rectangle	40 ± 0. 6	10 ± 0. 6	Rounded rectangle	40 ± 2	10 ± 2	1. 1 ± 0. 1

3. 5. 2. Particle wettability

Measuring the contact angle directly on the particle surface is difficult due to the small particle size. Assuming that the wetting properties of the particles are the same as those of the macroscopic photoresist film, we measured the contact angles of water drops on the surface of the photoresist surface. The photoresist was processed in the same way as for making particles, including exposure and development, with the exception that a photomask was not used to pattern the surface. Both advancing and receding contact angles were measured before and after development of the photoresist film. Typical plots of the contact angle evolution and drop base diameter during pumping water in or sucking water out of a drop on a photoresist film in air are shown in Fig. 3. 28 and their values are tabulated in Table. 3.2. During pumping the contact angle increases at a fixed three phase contact line (constant drop base

diameter) before reaching a plateau when the three phase contact line advances on the surface (the advancing contact angle). When liquid is withdrawn from the drop, the contact angle initially decreases at a fixed drop base diameter (pinned three phase contact line) and later reaches an almost constant lower value when the three phase contact line shrinks; hence the receding contact angle is established. A significantly greater hysteresis was observed between the advancing and receding contact angles after development and could be attributed to an increase of surface roughness due to the development process. Hysteresis caused by development of photoresist has been reported by the group of Stroock. [69] Such roughening following development may be due to partial degradation of uncrosslinked polymer, and its extent depends on the development time. [69, 139, 140]

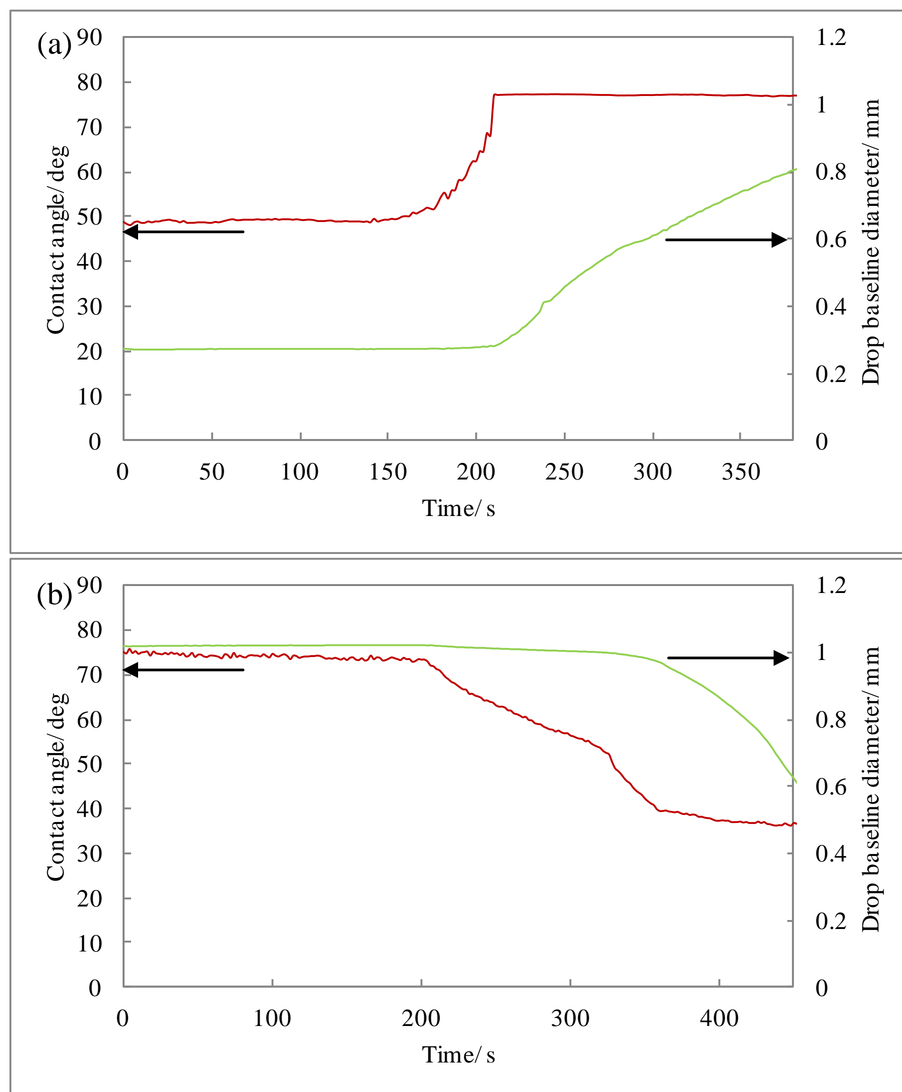

Fig. 3. 28. Evolution of the contact angle and drop base diameter of a water drop on a developed SU- 8 photoresist film in air during pumping in (a) and withdrawing water from the drop (b).

Table. 3. 2. Advancing, θ_A, and receding, θ_R, contact angles of water drops on different types of photoresist films in air obtained after development. θ_{av} is the arithmetic mean of advancing and receding angles, and $\Delta\theta$ is their difference (hysteresis). Each value was averaged from 3 sets of data.

Photoresist	**Photoresist type**	**Contact angle after development/ deg**			
		θ_A	θ_R	θ_{av}	$\Delta\theta$
AZ 5214	positive	84 ± 1	18 ± 1	51 ± 33	66 ± 2
AZ nLOF 2070	negative	83 ± 1	29 ± 1	56 ± 27	54 ± 1
SU- 8 2002	negative	81 ± 1	40 ± 1	61 ± 21	41 ± 2

3. 5. 3. Stability of photoresist particles in the presence of organic solvents

When investigating particle interactions at a water- fluid interface, it will be necessary to ensure that the particles are not affected by typical spreading solvents such as propan- 2- ol or methanol. The positive photoresist of the type used in these experiments, is of limited stability in the presence of organic solvents. [127] In addition to spreading solvents, chemical modification of the particle surfaces to make Janus particles will also be performed; therefore an indication of the photoresist particle stability is essential in order to maintain the particle integrity. The effect of immersing the positive photoresist in undiluted propan- 2- ol and methanol is shown in Fig. 3. 29. It can be seen that the positive photoresist was unstable in the presence of pure propan- 2- ol and damaged in pure methanol.

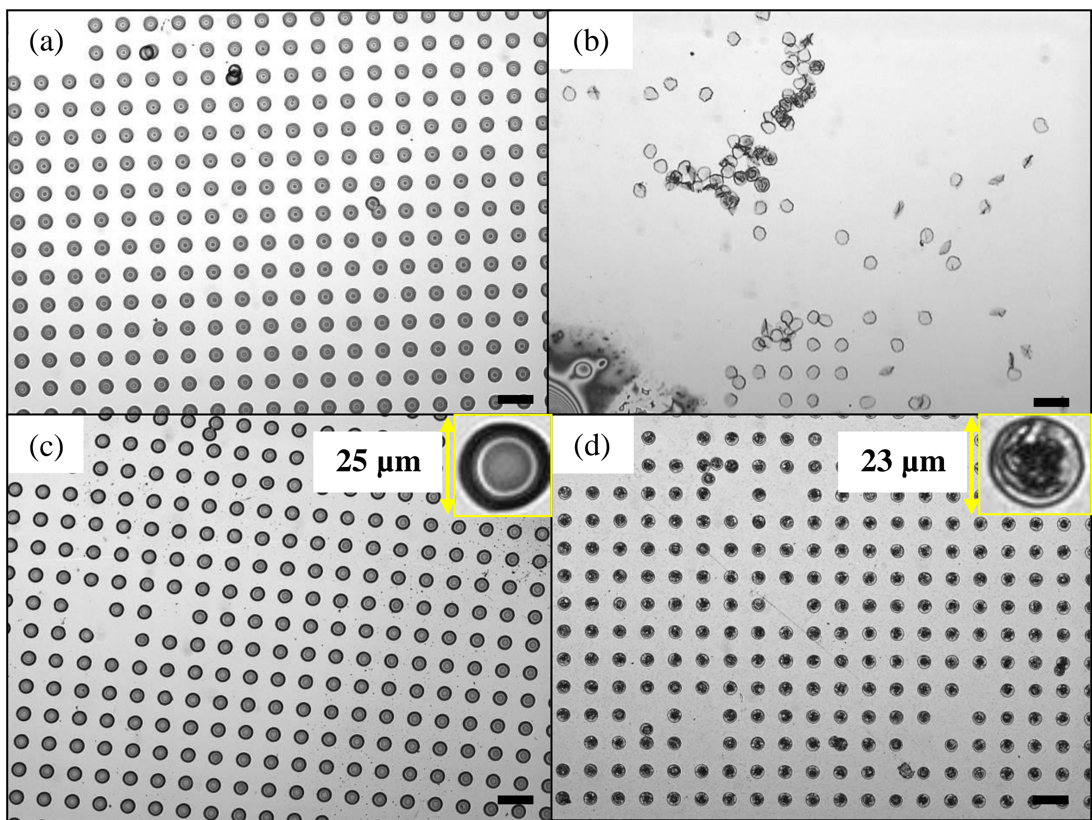

Fig. 3. 29. Optical microscopy images of positive photoresist discs on a silicon substrate generated after a 15 s exposure through a clearfield photomask consisting of 25 µm diameter circles with 20 µm pitch followed by development for 60 s. The images were acquired before (a) and after 45 min immersion in pure propan-2-ol (b), and before (c) and after 45 min immersion in pure methanol (d). Insets show higher magnifications. Scale bars show 50 µm.

Significant changes to the photoresist surface occurred even at large dilution ratios of a relatively mild solvent like methanol as judged by the clear difference between Fig. 3. 30 (c and d).

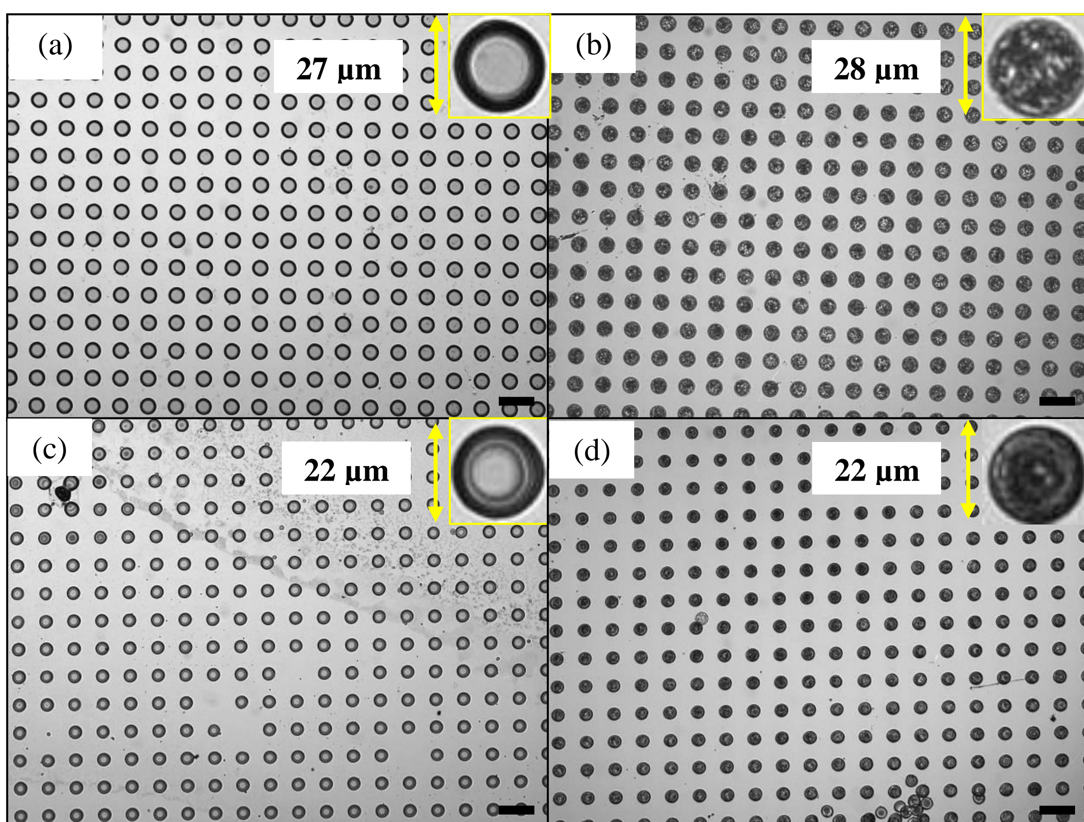

Fig. 3. 30. Optical microscope images of positive photoresist discs on a silicon substrate generated after a 15 s exposure through a clearfield photomask consisting of 25 µm diameter circles with 20 µm spacing on a UV transparent background followed by development for 60 s. The images were acquired before (a) and after 45 min immersion in 50 vol. % propan-2-ol in water (b), and before (c) and after 45 min immersion in 50 vol. % methanol in water (d). Insets show higher magnifications. Scale bars show 50 µm.

No visible evidence of photoresist instability was observed for the negative photoresist, even in the presence of pure propan- 2- ol (Fig. 3. 31), thus confirming that this crosslinking photoresist is more stable to organic solvents than the positive photoresist. [127] The larger than expected size of the photoresist features in Fig. 3.31 was due to over exposure of the photoresist on this occasion.

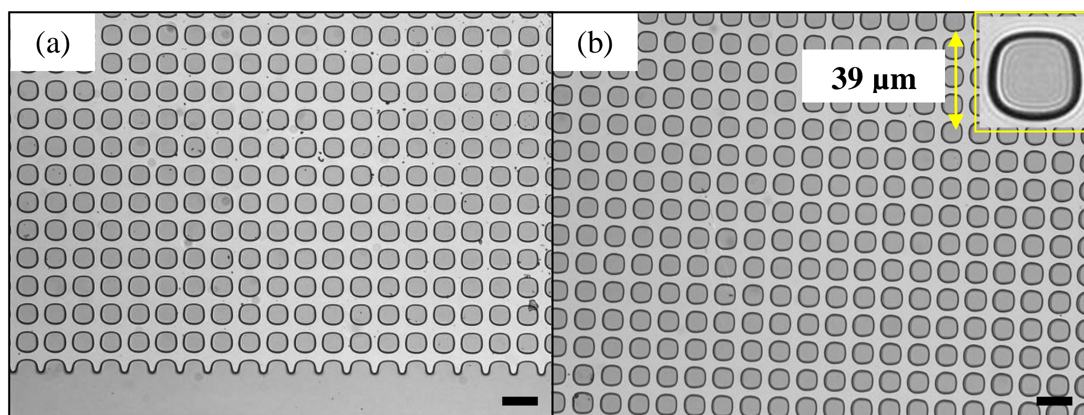

Fig. 3. 31. Optical microscope images of negative photoresist squares on a silicon substrate generated after a 15 s exposure through a clearfield photomask consisting of 25 × 25 μm transparent squares with 20 μm spacing on a UV opaque background followed by development for 120 s. The images were acquired before (a), and after immersion in pure propan-2-ol and after immersion for 45 min in pure propan-2-ol (b). Inset shows a higher magnification. Scale bars show 50 μm.

3. 6. Summary of the main findings

Various experimental factors in the photolithographic process for the fabrication of non- spherical particles with controlled shape and aspect ratio with different types of photoresist on glass and silicon substrates have been investigated. The main findings are summarised below.

- Photoresist dispense volume: for 150 mm diameter silicon substrates, the optimum volume for undiluted AZ and SU- 8 photoresist was found to be 5 ml.

- Substrate wettability: the wettability of the substrates has a significant effect on the integrity and quality of the photoresist films deposited by spin coating, and depends also on the type of photoresist used. AZ and SU- 8 photoresists preferentially wet hydrophobic substrates; however the application of a sacrificial layer of LOR (which is quite insensitive to substrate wettability) onto silicon substrates provided a surface with the right wetting conditions for the photoresist top layer.

- Substrate type: square or rectangular substrates resulted in uneven surfaces after photoresist application which gave rise to deformations in the photoresist pattern

and significant variations in the film thickness: this problem did not arise when large bevel edged circular silicon substrates were used.

- Photoresist concentration: the photoresist concentration has a strong effect on the thickness of the spin coated photoresist films. The dilution of the negative photoresist from Aldrich by 2 × with thinner caused a decrease of the film thickness by ~ 15 times.

- Photoresist application: the AZ and SU- 8 photoresist gave the best quality films after spin coating at 4000 r. p. m for 30- 40s at an acceleration of 300 r. p. m. / s.

- Baking time and temperature: the control of the conditions during the baking stage is crucial for the performance of the overall photolithographic process. For the negative photoresist, it was necessary to ensure that the temperature and time was well controlled in order to prevent thermal crosslinking of the photoresist.

- Exposure time: the size and quality of the generated patterns strongly depends on the exposure time: it is necessary to ensure that the exposure time is carefully controlled in order to give reproducible results.

- Development time and concentration: it was found to be necessary to control carefully the development time and concentration for both the top layer of photoresist and the bottom layer of the sacrificial layer. The optimum conditions for exposure and development for the AZ photoresists used in this work are tabulated in Table. 3. 3.

Table. 3. 3. Optimum exposure and development conditions for the AZ photoresists used in this work.

Photoresist	Exposure time / s	Developer	Developer concentration/ vol. %	Development time/ s
AZ 5214	< 15	AZ MIF 726	100	60
AZ nLOF 2070	8- 10	AZ MIF 726	100	120
	8- 10	AZ MIF 726	80	240
LOR 5A	N/ A	AZ MIF 726 or MF 319	100	< 60
		AZ MIF 726 or MF 319	80	< 120

- Photomask type: the quality of the patterns generated by photolithography depends crucially on the type and quality of the photomask used during exposure. Transparent sheets containing patterns generated by an inkjet printer gave poor quality images; whereas commercially available photomasks with superior quality gave sharper and better quality images on the photoresist.

- Release of patterned photoresist from the substrate: the release medium used to dissolve the sacrificial layer and liberate the top layer of photoresist has significant implications on the aspect ratio of the photoresist particles. SU- 8 photoresist discs with diameters of ~ 10 µm and a thickness of ~ 0. 75 µm are significantly damaged when NMP based removers are used. It was found that application of 0. 2 M NaOH was sufficient to dissolve the sacrificial layer without damaging the particles. For the thicker negative AZ photoresist particles, the NMP based remover gave the best results.

3. 7. Conclusions

The technique of photolithography for the fabrication of non- spherical particles composed of thermally and chemically stable photoresist with well defined shape and aspect ratio has been investigated. Protocols for the preparation of disc, oval and rounded rectangle shape particles under normal laboratory conditions, without the use of clean rooms and specialised equipment have been developed which permit the technique to be used for the fabrication of reasonably monodisperse particles with controlled aspect ratio and shape, and facilitates a convenient means of modification of one face of the particles before release from the substrate. The technique of photolithography under these conditions worked particularly well for AZ type photoresist consisting of a phenolic resin. Particles with this composition and geometry have not been reported in the literature by other researchers. SU- 8 photoresist could not be processed effectively under normal conditions resulting in particles with very rough surfaces and poor quality side walls and may benefit from an exposure instrument incorporating a filter to remove wavelengths below 350 nm.

CHAPTER 4
BEHAVIOUR OF PLATE- LIKE MICROPARTICLES AT LIQUID INTERFACES

4. 1. Introduction

In this chapter, non- spherical particles fabricated using the technique of photolithography as described in chapter 3 are investigated at the air- water and oil- water interface. The behaviour of plate- like particles composed of AZ negative photoresist with a range of different aspect ratios is investigated and compared to that of spherical PS- latex particles. Using SU- 8 photoresist, results will be presented for discoidal particles with a different composition and sub- micrometer thickness. Using the Gel Trapping technique and SEM analysis, the configuration of the particles at the interface is characterised. Results for emulsions and foams stabilised by the particles in the absence of surfactant are also presented and discussed.

The overall aims of these experiments are to establish how the shape and aspect ratio of thin colloidal particles, affects their behaviour at the liquid interface following spreading, compression and expansion in a Langmuir trough. The motivation of this work is to gain insights into particle interactions at interfaces and an understanding of how these particles could stabilise emulsions and foams. The use of a Langmuir trough enables changes in surface pressure to be monitored during the compression and expansion of the monolayers at different areas of the trough, and together with in situ microscopy analysis provides information on the behaviour of the particles at the interface. The use of particles with a range of aspect ratios in terms of length and width may exhibit a tendency to align in a particular direction during compression of the monolayers; in addition, the use of very thin particles will provide further insight into the investigation of monolayers of solid particles as such particles may be more flexible at the interface.

4. 2. Monolayers of plate- like microparticles at the air- water and oil- water interfaces

4. 2. 1. Particle configuration at the liquid interface

SEM analysis of the particles has shown that they have an interesting asymmetrical cross- sectional profile (see Fig. 3. 23- 3. 26) with one sharp edge (bottom) and one rounded edge (top). One should expect that plate- like particles with such a profile will adjust their position at the liquid interface so that the three phase contact line is located on the rounded edge in order to match the particle contact angle as illustrated in Fig. 4. 1 a. [18] To obtain information on the particle configuration at the air- water and oil- water interface, we used the gel trapping technique (GTT). [111] The GTT allows the position of the particles at the interface to be observed with a scanning electron microscope. The SEM images in Fig. 4. 1 show rather unexpected results: the photoresist discs lay flat at the fluid interface as expected due to this being the lower energy configuration, but are oriented with the bottom (sharp edge) or top (round edge) surface in the water with no apparent preference for either orientation. The three phase contact line is always located at the almost vertical side (the rim) of the particle but not at the round edge; therefore the apparent macroscopic contact angle of these discoidal particles at the liquid interface is ~ 90 ^{o} and differs from the average contact angle values of 56 ± 27 ^{o} and 99 ± 16 ^{o} measured at the air- water and decane- water interface using shape analysis of sessile drops, respectively. This discrepancy could be explained if we recall that the particle surface has significant roughness, evident from the SEM images (Fig. 3. 24) and large contact angle hysteresis. Therefore the three phase contact line is pinned at the side of the particle surface far from the edges, and the particles are trapped in a metastable configuration with higher energy than the equilibrium configuration shown in Fig. 4. 1a. As a result the three phase contact line is undulated and generates deformations of the liquid interface (Fig. 4. 1f). This should lead to capillary interactions between adjacent particles as discussed in Chapter 1. The pair potential of capillary attraction between two disc shape particles with diameter d can be calculated by eq. (1. 6), which in this case reads

$$U_{disc} = -\frac{12\pi\gamma\delta^2 R_c^4}{L^4} \qquad (4.\ 1)$$

where $R_c = d/2$ is the radius of the three phase contact line projection on the plane of the liquid interface. The amplitude of the three- phase contact line undulations,δ, was estimated from the surface roughness from the SEM images (Fig. 3. 24) to be in the range 30- 100 nm. Hence for two disc shape particles with diameter d = 10 μm separated at a centre- to- centre distance L = 20 μm (two particle diameters) at the air-water surface (γ = 72 mN/m) and δ = 30 nm, the pair potential of capillary attraction is $U_{disc} \sim 10^3$ kT; therefore significant attraction between these particles should be expected.

The random orientation of particle faces at the liquid interface (rounded edge in water or in air/ oil) could be attributed to the process of spreading the particles at the interface and the very large energy of particle detachment. Spreading is expected to be a turbulent process; particles are able to rotate freely and hit the liquid interface with either face; however once attached to the interface the particles are not able to rotate to assume a preferred orientation without application of an external force. The other option for the particle is to detach, reorient in the bulk and then attach again; this however would require significant energy input; indeed, the detachment energy of a disc shape particle with diameter d = 10 μm and contact angle 90 ^{o} from the air-water interface into water calculated by eq. (1. 4a) is ~ 10^9 kT- much greater than the thermal energy. This may also have implications for the orientation of Janus plate- like particles at the liquid interface considered in Chapter 5.

The analysis of many images like those in Fig. 4. 1b-e revealed that on average, the depth of the particle thickness immersed in water at the air- water interface was 52. 7 ± 0. 1 % of the total thickness, whereas at the decane- water interface, the depth of immersion of the particle into water was 36. 3 ± 0. 1 % of the total thickness, indicating that at the oil- water interface, the discs are more immersed into the oil whereas at the air- water interface, ~ 50 % of the thickness of the discs are in air.

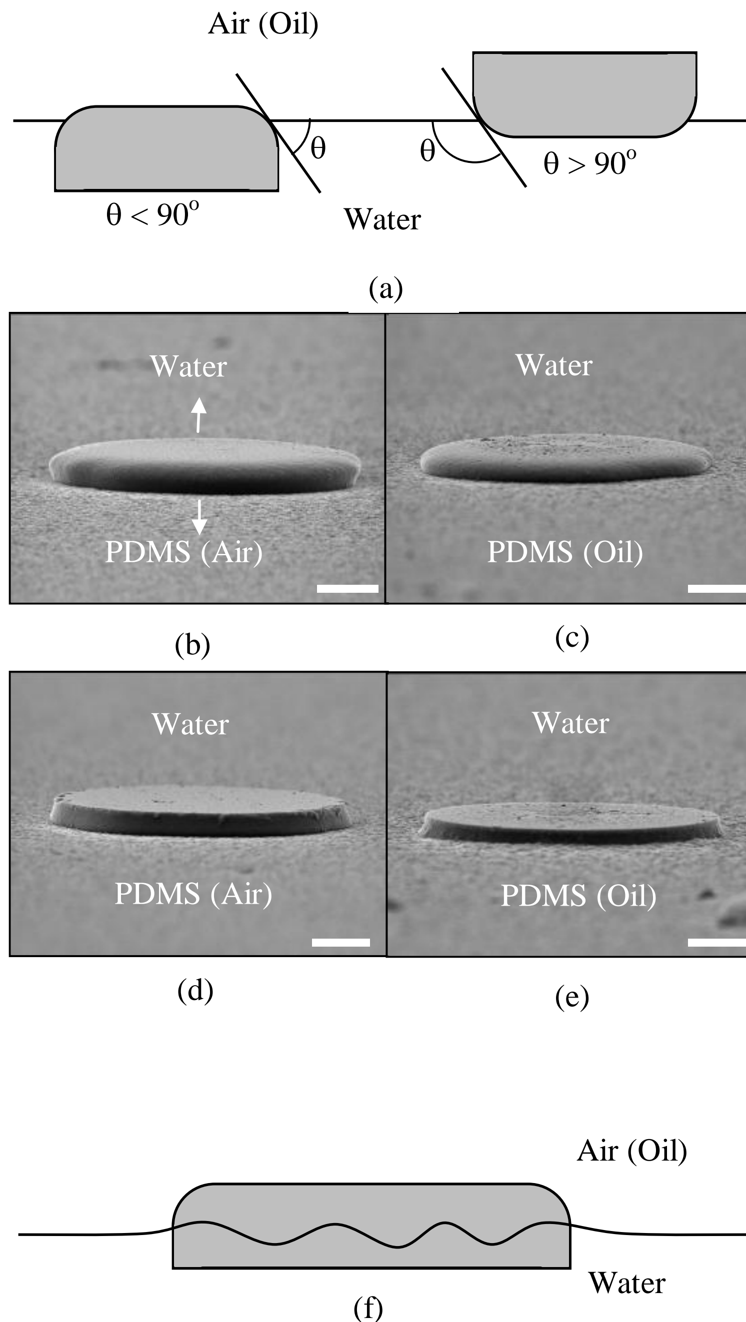

Fig. 4. 1. Expected configuration of plate- like particles at the liquid interface for particle contact angle < 90 ° (left) and > 90 ° (right) (a). (b- e) SEM images of disc shaped photoresist particles trapped at an air- water (b, d) and a decane-water interface (c, e) following application of the Gel trapping technique. The particles are shown embedded in a layer of PDMS that represents the air or oil phase. A diagram of a plate- like particle trapped at the liquid interface in a metastable configuration due to contact angle hysteresis caused by the roughness of the particle surface is shown in (f). The undulations of the three phase contact line cause deformations of the liquid interface leading to capillary interactions between adjacent particles. Scale bars in (b- e) show 2 μm.

4. 2. 2. Effect of particle shape on the monolayer structure

Optical microscopy images of photoresist particles with different shapes at the air- water interface (Fig. 4. 2) show that the plate- like particles lay flat on the surface of the water forming a large interconnected network of aggregated particles. During the initial stages of aggregation, the particles formed dimers, trimers, etc., before coming together to form larger aggregates within a few minutes. The rapid aggregation is not surprising due to the expected strong capillary attraction between particles. For the oval and rectangular shaped particles, domains existed in which the particles formed tip- to- tip or side- to- side contacts.

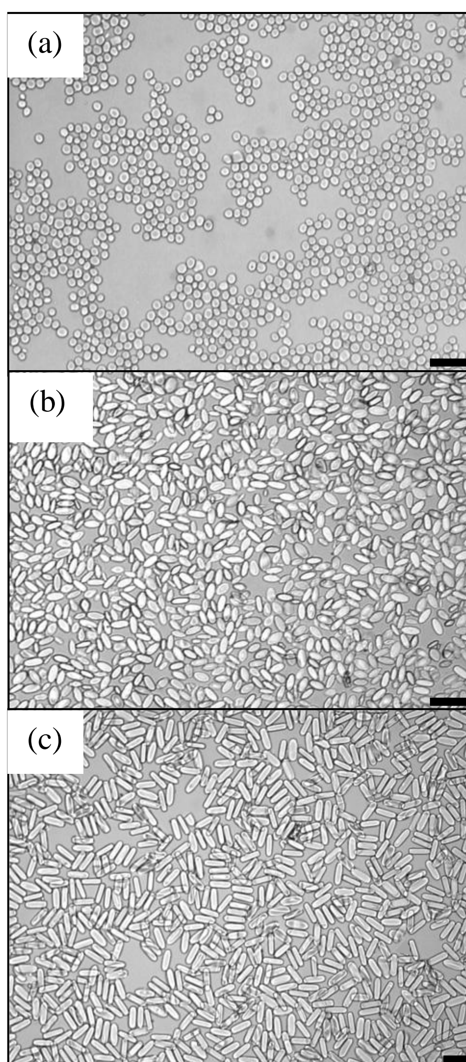

Fig. 4. 2. Optical microscopy images of photoresist discs (a), ovals (b) and rectangles (c) after spreading at the air- water interface. Scale bars show 50 μm.

Images like those shown in Fig. 4. 2 were analysed, and the number fraction of particles with oval and rectangular shape in tip- to- tip (T- T) and side- to- side (S- S) configuration was determined. The results are shown in Table. 4. 1 and Fig. 4. 3. These results show a clear tendency for the particles to adopt a particular configuration depending on the shape of the particles. The fraction of aggregated particles in a T- T configuration rapidly decreases with an increase of the aspect ratio, while that of the S- S configuration shows the opposite trend. Clearly, the S- S configuration is preferred by the non-spherical particles with the highest aspect ratio of 3. This tendency could be explained if the pair potential of capillary attraction between particles in T- T and S- S configuration is considered. Let us assume that the round end of the rectangular particles is part of a circle with radius equal to a half of the particle width, i. e., $b/2$, and the angle between long particle axes, a, is 180 ^{o} for the T- T or 0 ^{o} for the S- S configuration. Then the pair potential of the T- T configuration should be $U_{TT} = U_{disc}$ calculated by eq. (4. 1) with $R_c = b/2$. Assuming additivity in the pair potentials between different parts of the particles, the pair potential of capillary attraction in the S- S configuration, U_{SS}, can be expressed as

$$U_{SS} = u_{SS} l + 2u_{TT} \tag{4. 2}$$

where u_{SS} is the pair potential per unit length of the straight portions of the interacting particles, $l = a - b$ is the length of the straight portion and $2u_{TT}$ is the contribution from both hemicircular ends. It is reasonable to assume that $u_{TT} \approx U_{TT}/2$, hence

$$U_{SS} \approx u_{SS} l + U_{TT} \tag{4. 3}$$

Therefore the attractive pair potential between particles in the S- S configuration is larger than that in the T- T configuration and the difference between them increases with the increase of the aspect ratio because $l = b(a/b - 1)$. The S- S configuration has lower energy (stronger attraction) and would therefore be preferred to the T- T configuration.

Stars and crosses formed by tip to tip contacts were also observed with round rectangle shape particles but their occurrence was very rare. The fraction of particles with the S- S configuration remained approximately the same after spreading more

particles (Fig. 4. 4). Stacking between particles was also observed far from the aggregated network as shown in Fig. 4. 4 d. The three main types of configurations adopted by the rectangles are illustrated in Fig. 4. 4e. Here the depictions only represent a few examples and do not represent the monolayer as a whole; for example tip to tip contacts may occur between individual particles or stacks of particles. A capillary attraction has been attributed to tip to tip and side to side contacts for ellipsoidal particles by the group of Loudet. [95] In this case a stronger capillary attraction was observed for the tip to tip configuration. A stronger capillary attraction is observed where the interfacial curvature is high [98] but this can depend on the orientation adopted by the particles initially after spreading [99]; however in the present case further experiments will be required in order to determine how the curvature of the interface is affected by the particle shape.

Table. 4. 1. Number fraction of plate- like microparticles with different shapes in tip-to-tip (T-T) and side-to-side (S- S) configuration in a monolayer at the air-water interface (see Fig. 4. 2).

Particle shape	Aspect ratio, a/b	Number fraction, N/N_{tot}	
		T-T configuration	S-S configuration
discs	1. 0	1. 00	1. 00
ovals	2. 0 ± 0. 3	0. 32 ± 0. 06	0. 15 ± 0. 03
round rectangles	3. 0 ± 0. 3	0. 09 ± 0. 03	0. 27 ± 0. 03

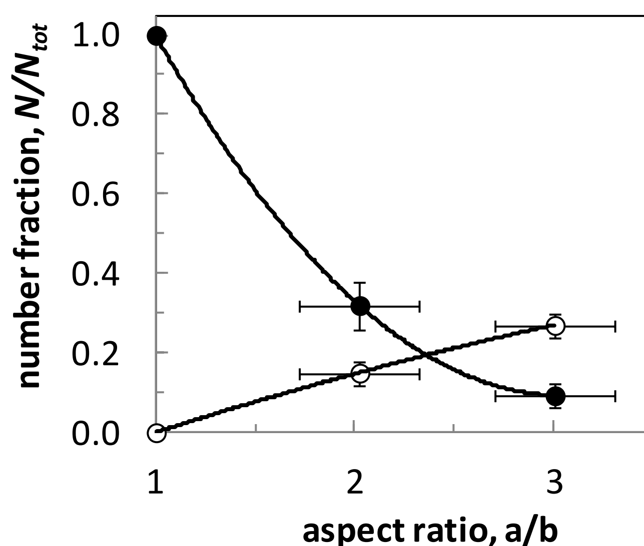

Fig. 4. 3. Number fraction of plate- like microparticles at the air- water interface in tip- to- tip (filled circles) and side- to- side (empty circles) configuration versus particle aspect ratio (see Table 4. 1).

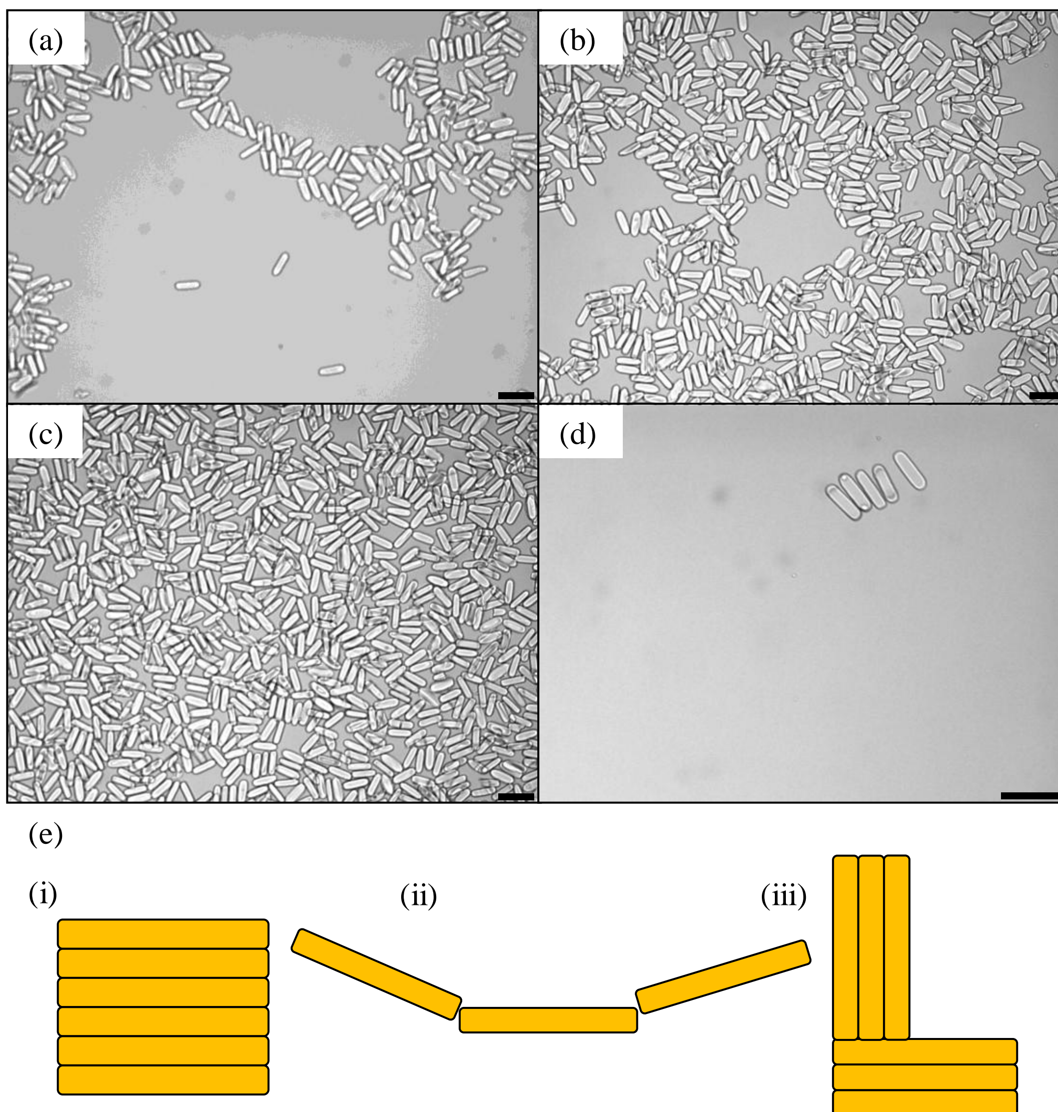

Fig. 4. 4. Optical microscopy images of flat rectangular particles after spreading at the air- water interface in a Langmuir trough. The different volumes of spreading suspension shown are 100 µl (a), 500 µl (b) and 800 µl (c). A stack of rectangles isolated from the aggregate network is shown in (d). A schematic representation of some of the configurations of the rectangles is shown in (e). Particles stacked side by side (i) were the most prevalent configuration; the occurrence of the other configurations (ii and iii), or similar, were few in comparison. Scale bars show 50 µm.

4. 2. 3. Implications for particle- stabilised foams and emulsions

Our results show that the plate- like particles studied, lay flat at the liquid interface and have an apparent macroscopic contact angle of ~ 90°. At the air- water interface, approximately half of their thickness is immersed in water and ~ 1/ 3 of their thickness is inside water when they are attached to the oil- water interface (Fig. 4. 1). As already discussed, this rather unexpected configuration of the particles at the liquid interface could be attributed to their rough surface and is expected to have important implications for their ability to stabilise foams or emulsions. It is known that if a solid particle with a contact angle of 90 ° is simultaneously attached to both surfaces of a liquid film in a foam (particle bridging); the film would break because its equilibrium thickness in this situation should be equal to zero. [154] Such particle bridging is very common at the early stages of foam or emulsion formation in the presence of solid particles when bubbles/ drops, sparsely populated with particles, collide with each other. Because the studied plate- like particles have a contact angle of ~ 90 °, they would be expected to easily break the films separating the colliding bubbles/ drops, thus enhancing their coalescence. The foam bubbles or emulsion drops could become stable only if they are almost completely covered by the particles. Hence one should expect that the particles studied here will not be effective in foam stabilisation at low concentrations.

In order to test the above hypothesis, we made foaming and emulsion experiments with photoresist discs dispersed in water at a concentration of ~ 2 wt. %. Foams were prepared by bubbling air through the particle suspension via a thin needle immersed in the suspension. The air was introduced into the suspension contained within a cuvette for a period of ~ 90 s by means of a syringe connected to the needle and operated by a syringe pump. The depth of suspension present in the cuvette was ~ 7 mm. In the absence of added electrolyte to the water, only a transient foam with a volume of ~ 3 × that of the suspension was generated (Fig. 4. 5). The foam survived for ~ 5 s after the termination of air flow; hence the particles were not able to stabilise the foam effectively, most probably due to their poor attachment to the bubbles. When 10 mM NaCl was added to the same suspension, no foaming was observed; only a single large bubble was generated from the introduced air. These observations suggest that the bubbles in the transient foam were mainly stabilised by the electrostatic repulsion between foam film surfaces rather than by the presence of

particles. It was found however that after the gas flow was stopped (where electrolyte was used in the foam), the bubble ruptured to leave a single film spanning the entire width of the cuvette as shown in Fig. 4. 5b. The film survived for more than several hours most probably stabilised by the dense particle layers on its surfaces.

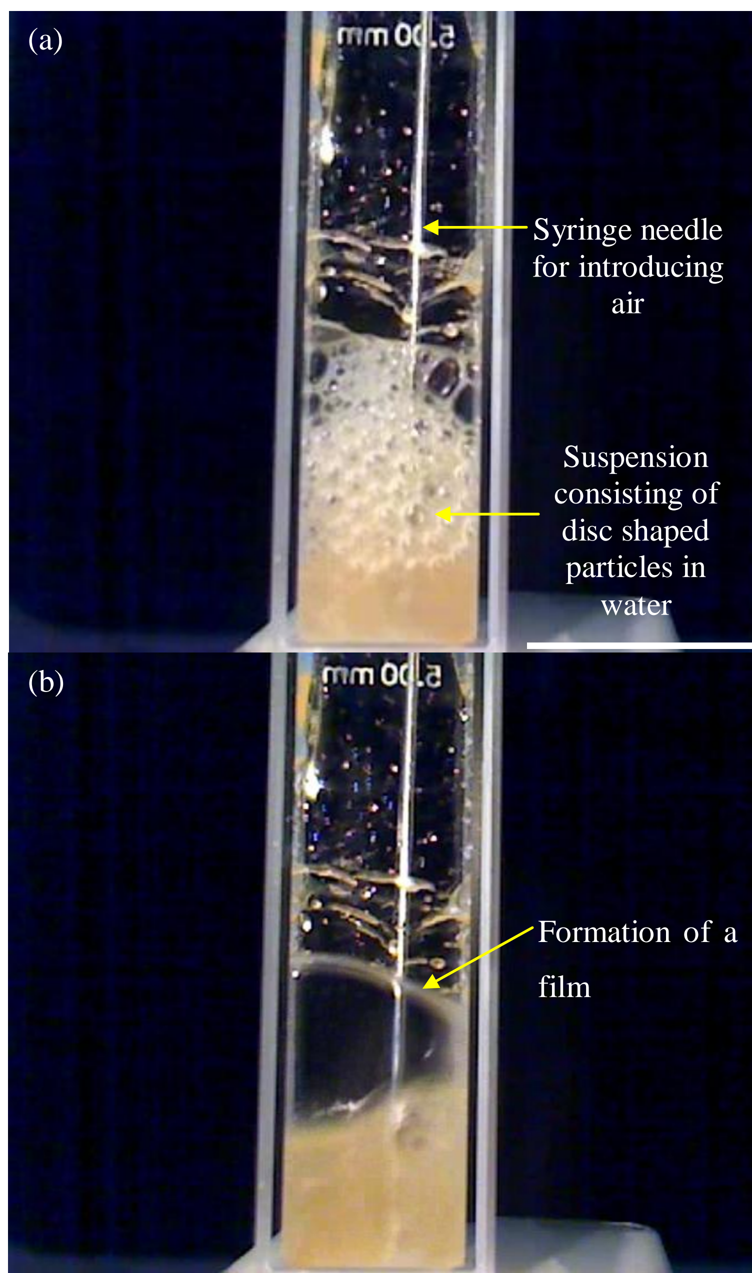

Fig. 4. 5. Images obtained by a digital camera of foams generated by pumping air into a suspension consisting of disc shaped particles in water (a) and after addition of 10 mM NaCl to the water (b). Scale bars show 1 cm.

In contrast to the poor foaming of the aqueous disc shaped particle suspension, it was found that emulsion drops formed from equal volumes of tetradecane and water suspension after simple hand shaking of the mixtures could be stabilised more effectively (Fig. 4. 6). The drop size varied from ~ 100- 400 μm in diameter and, judging from the sedimentation behaviour, these were water drops in tetradecane. The surface of the emulsion drops was almost completely covered with close packed monolayers or multilayers of particle discs. Non- spherical droplets were also observed (Fig. 4. 7). Most probably, the non-spherical drops were formed as result of partial coalescence between droplets partially covered by particles.

These results support our hypothesis that the disc shape particles studied should not be very efficient in foam stabilisation. For particle stabilised emulsions, stability could be achieved between droplets covered with dense monolayers or multilayers of plate- like particles.

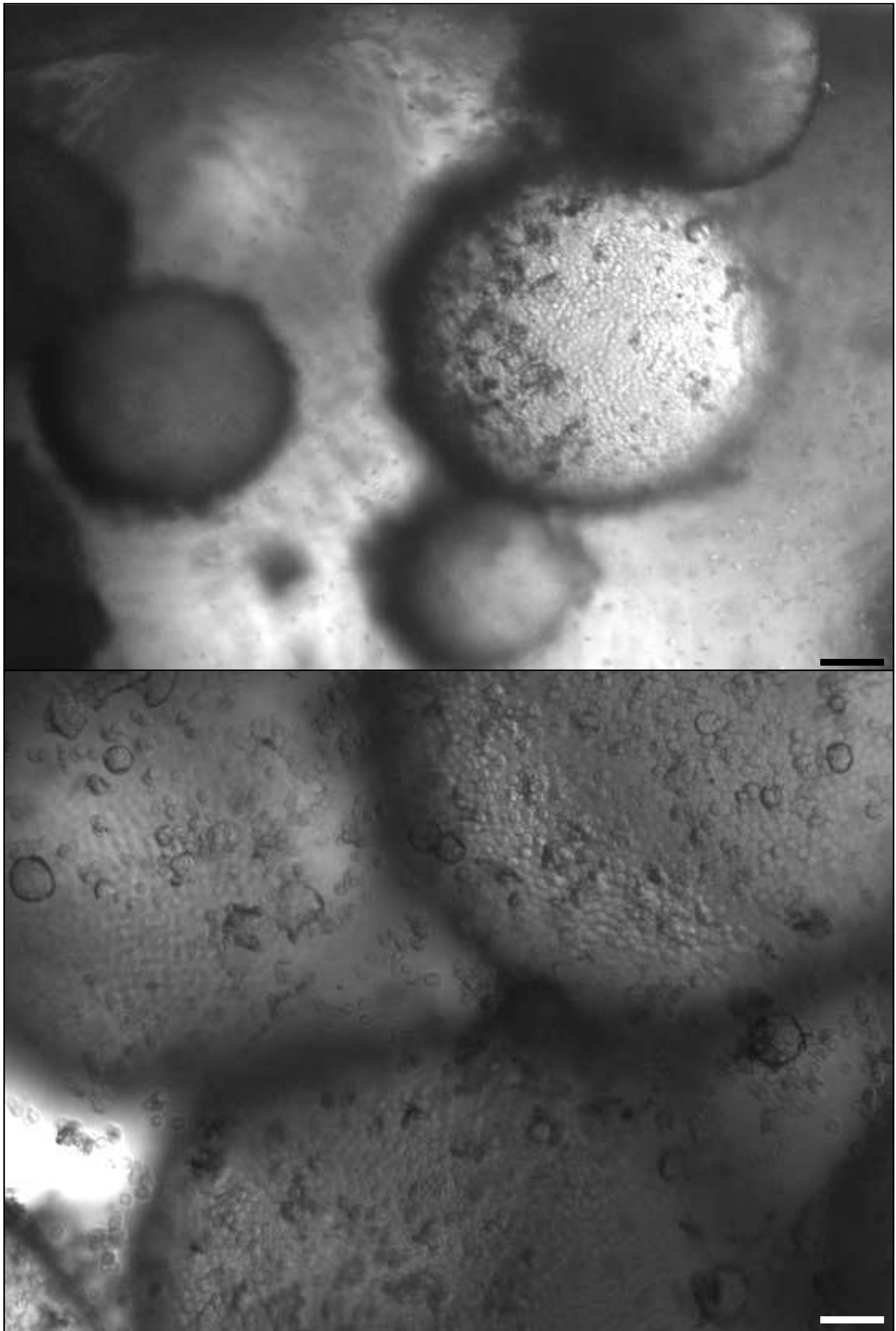

Fig. 4. 6. Water- in tetradecane emulsion drops stabilised by disc shaped AZ photoresist particles. Scale bars show 50 μm.

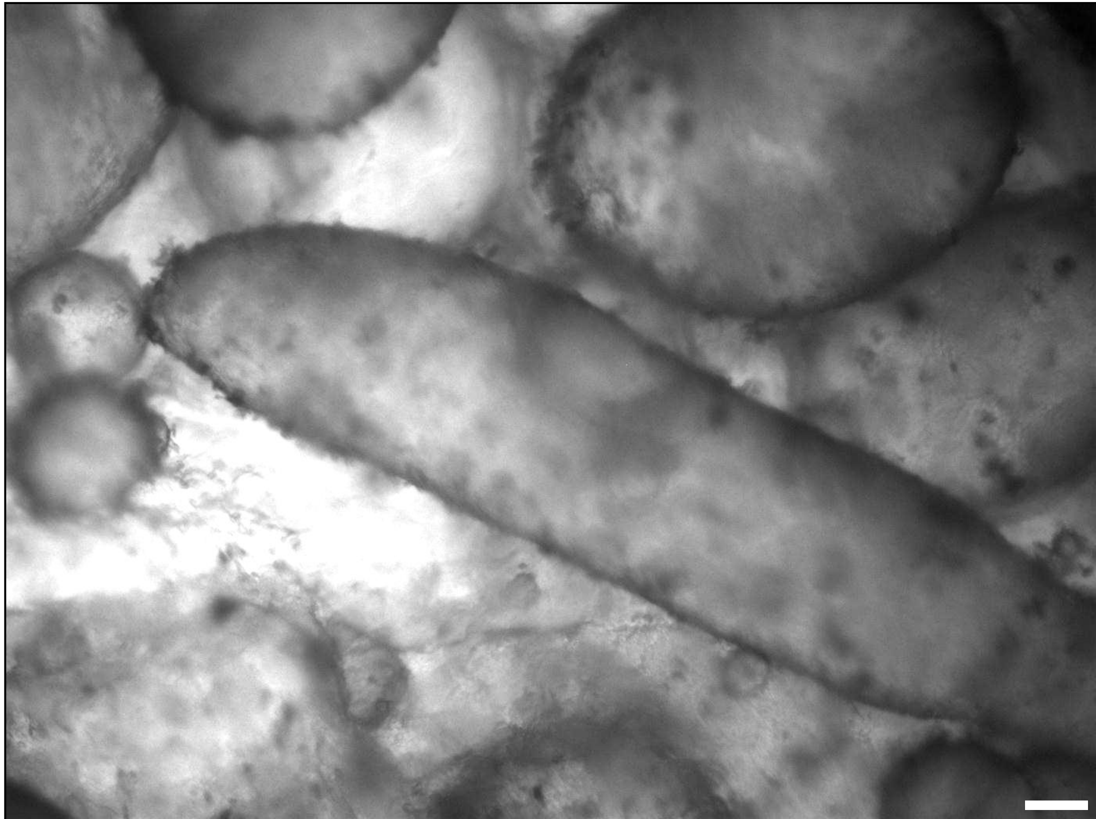

Fig. 4. 7. Water- in tetradecane emulsion drops stabilised by disc shaped AZ photoresist particles. Scale bar shows 50 μm.

4. 3. Behaviour of particle monolayers during compression and expansion in a Langmuir trough

4. 3. 1. Effect of spreading solvent on the surface pressure of the air- water interface

Plate- like particles of photoresist were spread at the interface using methanol or IPA as spreading solvents. IPA was not used for the AZ type photoresist as a precaution: the exceptional chemical stability of SU- 8 photoresist formed by the crosslinked epoxy resin is not expected to be affected by IPA. As will be discussed in the next section, significant losses of the discs into the sub- phase was observed during spreading SU- 8 particles at the air- water interface when methanol was used as the spreading solvent; therefore in order to determine if monolayer losses could be reduced by using a different spreading solvent, experiments were performed using IPA. IPA is slightly less soluble in water than methanol and therefore may be able to spread with the particles on the surface of the water more efficiently. In order to determine if the presence of the IPA had any significant effect on the surface

pressure, compression experiments were carried out in the absence of particles to monitor the changes in surface pressure attributable to the spreading solvent alone. In the case of methanol, the surface pressure changed by ~ 0. 7 mN/ m when the compression rate was 3 cm^2/ min, and was therefore it was felt not to be necessary to account for this change. The SU- 8 photoresist discs were liberated from the silicon substrate by dissolution of the sacrificial layer of LOR using NaOH. The particles were then suspended in 0. 2 M of NaOH and after centrifugation, the supernatant was removed until ~ 50 µl of the NaOH remained- it was not possible to remove the NaOH completely by multiple centrifugations using water as the discs could not sediment effectively when the pH was lowered. Therefore in order to reproduce the experimental conditions, 50 µl of 0. 5 M NaOH (extracted from the supernatant of the particle suspension after centrifugation) was added to 1000 µl of the spreading solvent consisting of 50 wt. % IPA and water without the presence of the particles, and the barriers were closed to an area of 15 cm^2 at 3 cm^2/ min. First, the effect of the volume of spreading solvent on surface pressure was investigated without compression as shown in Fig. 4. 8.

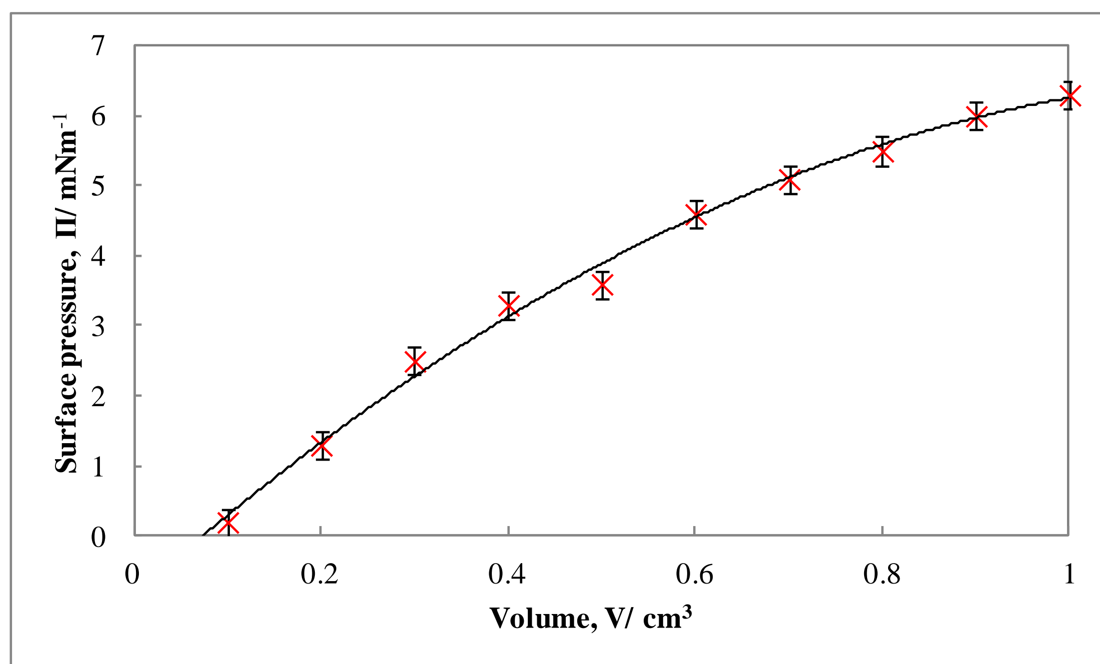

Fig. 4. 8. A plot of surface pressure vs. volume of spreading solvent (50 wt. % IPA in water) after spreading at the air- water interface.

For 1000 μl of the spreading solvent, the surface pressure reached a value of ~ 6. 2 mN/ m and fell to a value of ~ 0. 6 mN/ m after 15 min: before compression, the surface pressure was set to zero. It was found that the surface pressure depended significantly on the rate of compression. After applying 500 μl of the spreading solvent, the surface pressure after the barriers had been closed to an area of 19 cm^2 was ~ 2 mN/ m when the rate of compression was 50 cm^2/ min, and when the compression rate was reduced to 3 cm^2/ min, the surface pressure was only ~ 0. 7 mN/ m (Fig. 4. 9). Therefore under these conditions, the presence of the spreading solvent has little effect on the isotherm and therefore further corrections due to the presence of the spreading solvent were not deemed to be necessary. As shown in Fig. 4. 9 (c), when the volume of spreading solvent was 1000 μl, the surface pressure during compression at a rate of 3 cm^2/ min increased to ~ 1 mN/ m at an area of 15 cm^2.

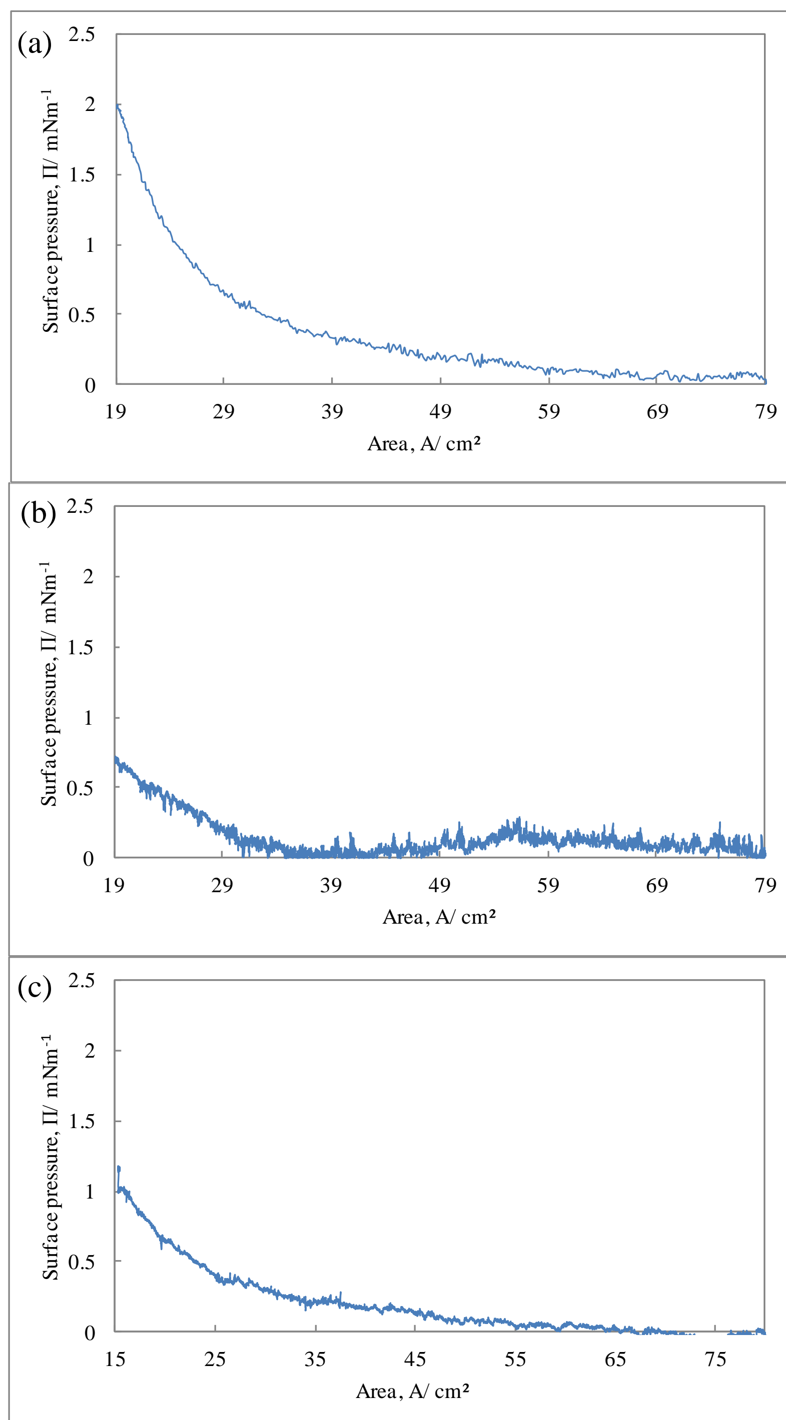

Fig. 4. 9. Surface pressure vs. area isotherms for a spreading solvent prepared from 50 wt. % IPA and water. The isotherm shown in (a) was produced by 500 μl of the spreading solvent at a compression rate of 50 cm²/ min. The isotherm shown in (b) was produced by 500 μl of the spreading solvent at a compression rate of 3 cm²/ min and in (c), a plot of surface pressure vs. area during compression of the water surface 15 min after addition of 1000 μl of the spreading solvent at a compression rate of 3 cm^2/ min.

4. 3. 2. Effect of plate- like microparticle shape during compression in a Langmuir trough

4. 3. 2. 1. Monolayers of AZ negative photoresist discs

The non- spherical particles used in this investigation were composed of photoresist resin consisting of polymerised phenol and formaldehyde commonly referred to as Novolac resin. The photoresist discs used consisted of two sizes and were used in separate experiments. All experiments were performed using ~ 10 μm diameter discs except where noted otherwise. In each case, the thickness of the particles was ~ 1. 1 μm. For each experiment, the discs were recovered from two 150 mm diameter silicon substrates by dissolution of the sacrificial layer using NMP and after extracting as much of the NMP as possible after centrifugation of the suspensions, the discs were prepared in a spreading solvent consisting of 50 wt. % methanol and water. Typically, a spreading suspension of 1000 μl contained ~ 50 μl of NMP. It was not possible to remove the NMP completely, for example by repeated centrifugation in water; however the presence of the NMP has not been shown to affect the surface pressure during compression.

An image of the photoresist discs 5 min after spreading at the air- water interface in a Langmuir trough is shown in Fig. 4. 10. During compression, jamming of the monolayer occurred at an area of ~ 45 cm^2 (K1 as shown in Fig. 4. 11) and further compression beyond this area resulted in the formation of creases in the monolayer occurring in lines running diagonally with respect to the compressing barriers (K2). The creases observed were actually regions were the discs had tilted and flipped at the interface (Fig. 4. 11 and 4. 12). At the second knee in the isotherm (K3), the creases became more vertical, and general tilting of the discs became more prevalent; in addition some of the discs were observed to overlap other discs (Fig. 4. 11 and Fig. 4. 12). Compression beyond the second knee in the isotherm revealed that the monolayer had undergone buckling with a peak to peak wavelength of ~ 360 μm and motion of the discs was still observed in the monolayer due to continual tilting of the discs. The formation of buckles in the monolayer coincided with regions that consisted of large numbers of flipped and tilted discs running vertically, the edges of the flipped discs were orientated parallel with the compressing barriers and flipped and tilted discs tended to occur in rows running in the same direction.

During the onset of buckling, some of the discs were observed to overlap other discs and ultimately, overlapped discs were ejected from the interface into the water. Dense regions of photoresist discs were observed to accumulate at the trough barriers with increasing density as the monolayer was compressed further beyond the second knee of the isotherm, where monolayer buckling had occurred. During expansion of the monolayer, discs that were initially tilted were observed to relax back into the plane of the interface. Further expansion resulted in the fragmentation of the monolayer into rafts of aggregated discs and a corresponding shift of the isotherm to smaller areas during repeated compression- expansion cycles (Fig. 4. 11).

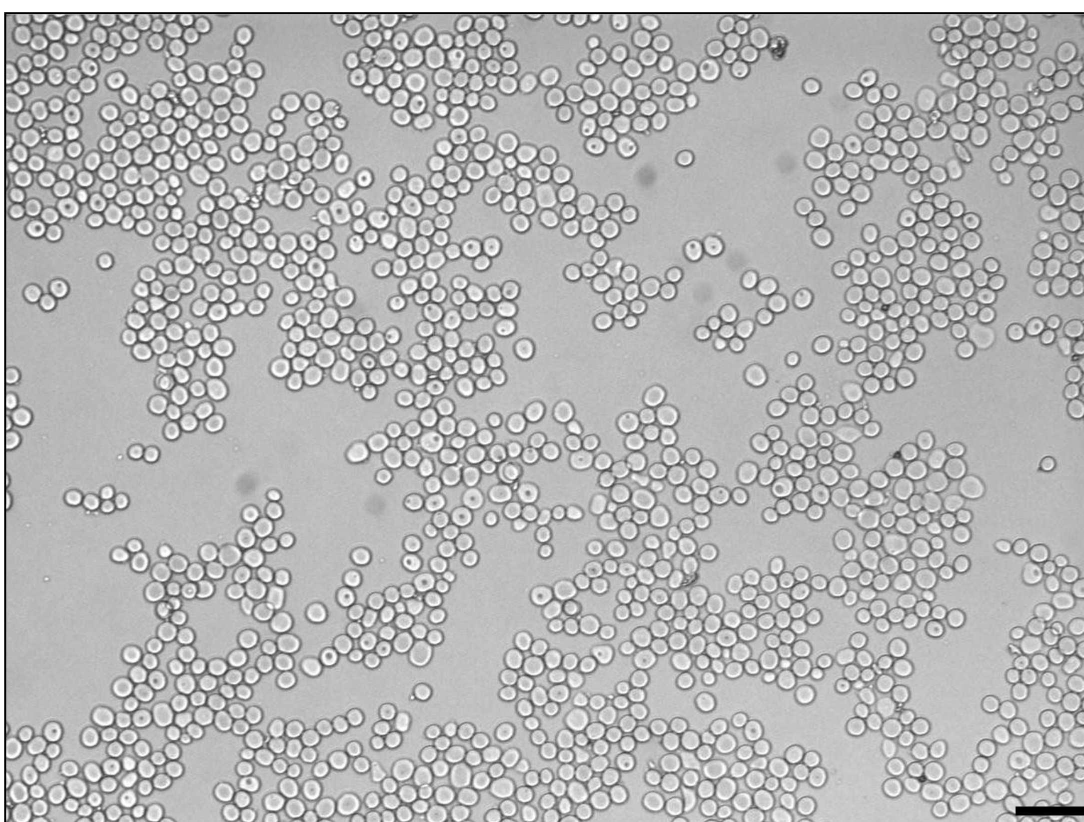

Fig. 4. 10. Optical microscopy image of photoresist discs at the air- water interface 5 min after spreading 1000 μl of a suspension prepared from 50 wt. % methanol and water. Scale bar shows 50 μm.

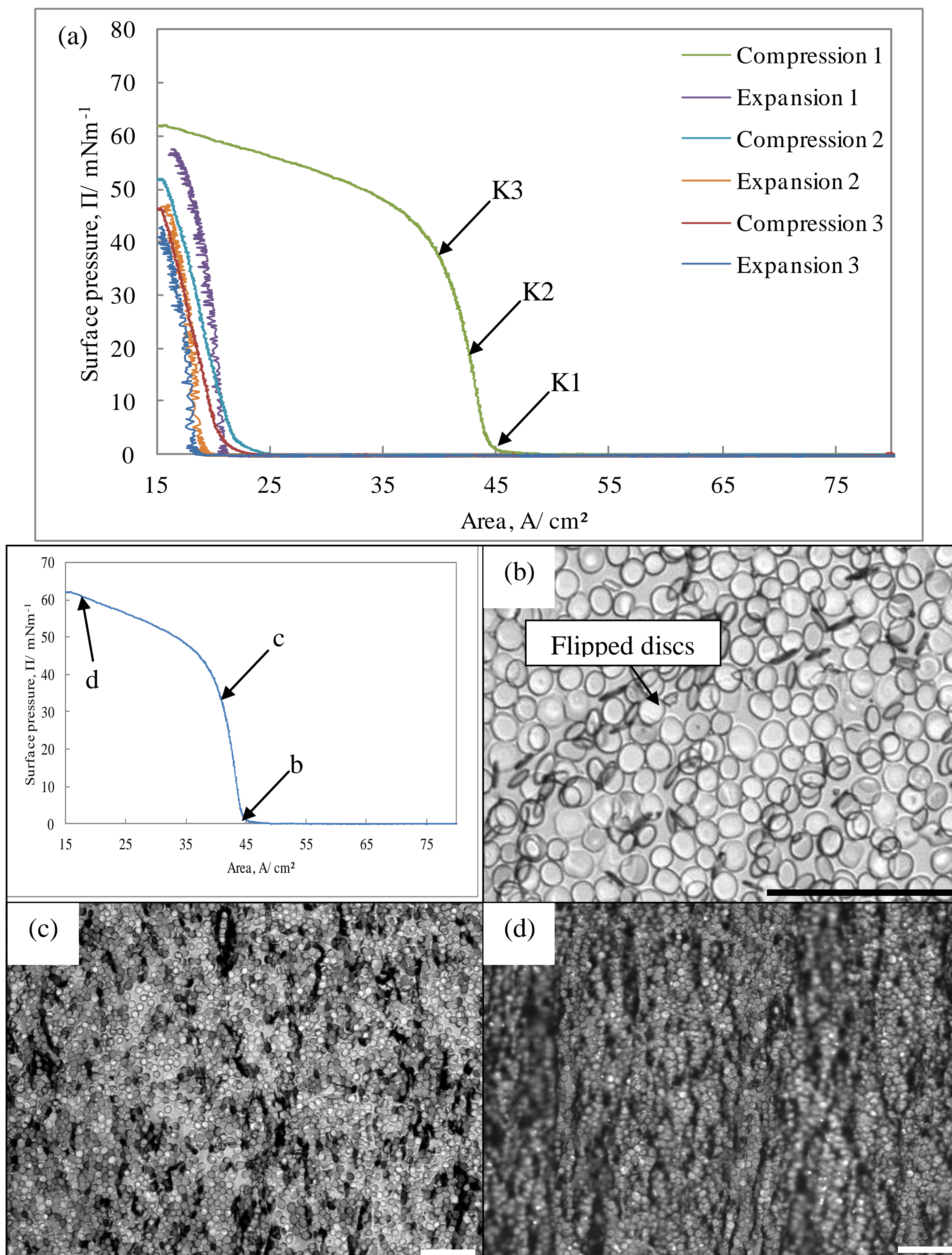

Fig. 4. 11. An isotherm resulting from repeated compression- expansion cycles of a monolayer of 10 µm diameter photoresist discs at an air- water interface during compression and expansion in a Langmuir trough (a) and optical microscopy images of a monolayer of photoresist discs at an air- water interface during compression in a Langmuir trough (b- d). The area corresponding to the images labeled b, c and d are shown on the isotherm in the top left with the corresponding labels. Scale bars show 50 µm.

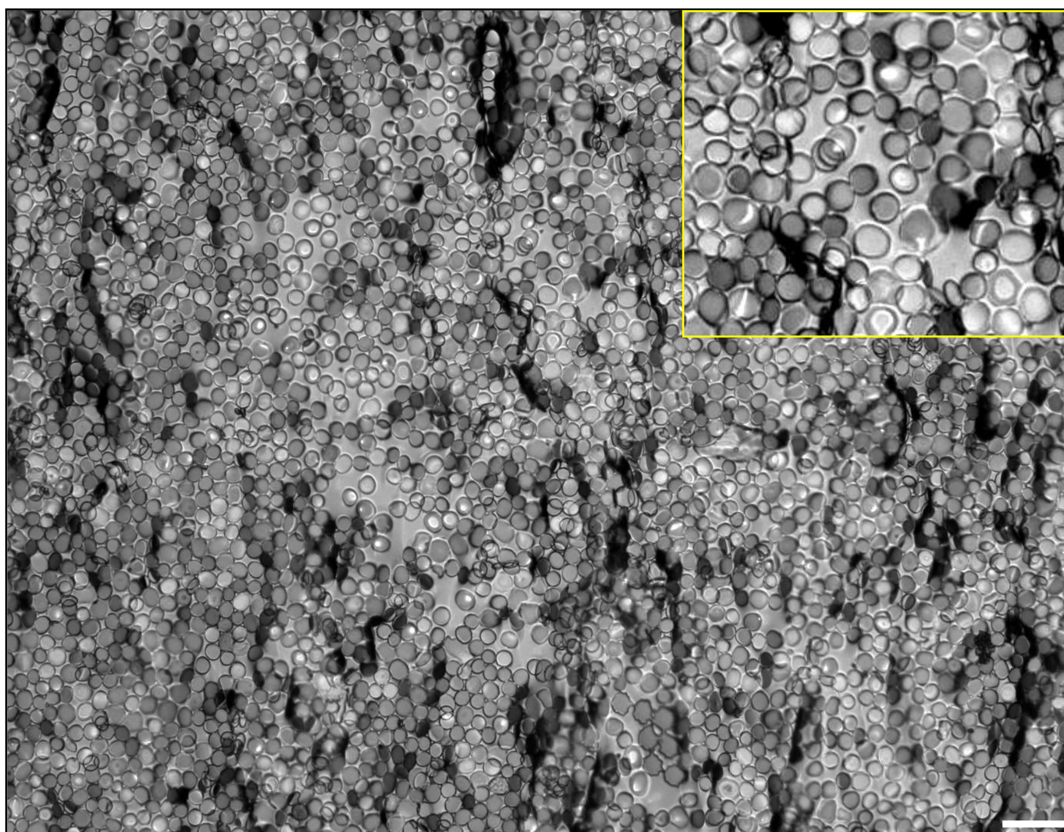

Fig. 4. 12. An optical microscopy image of photoresist discs at an air- water interface [reproduced from Fig. 4. 11 (c)] during compression in a Langmuir trough at the second knee of the isotherm (K2 in Fig. 4. 11). In addition to discs lying flat on the surface of the water, some discs were also tilted and flipped at the interface. Scale bar shows 50 μm. Inset shows a higher magnification.

Repeated experiments with photoresist discs with diameters of 10 μm were found to give consistent isotherms. In this experiment, results are presented for larger discs with diameters of ~ 15 μm. The larger size of the discs was due to over exposure of the photoresist during fabrication; the greater variation in the size and shape of the discs was also due to the over exposure. Although the behaviour of the discs during compression in the Langmuir trough is identical for both disc sizes, the larger, more polydisperse and irregularly shaped discs exhibited an even broader isotherm during compression (Fig. 4. 13). One possible explanation for the appearance of the isotherm could be due to the greater polydispersity and irregularity of the discs: the less symmetrical discs may assume various orientations during compression which allows the monolayers to alleviate the compression forces.

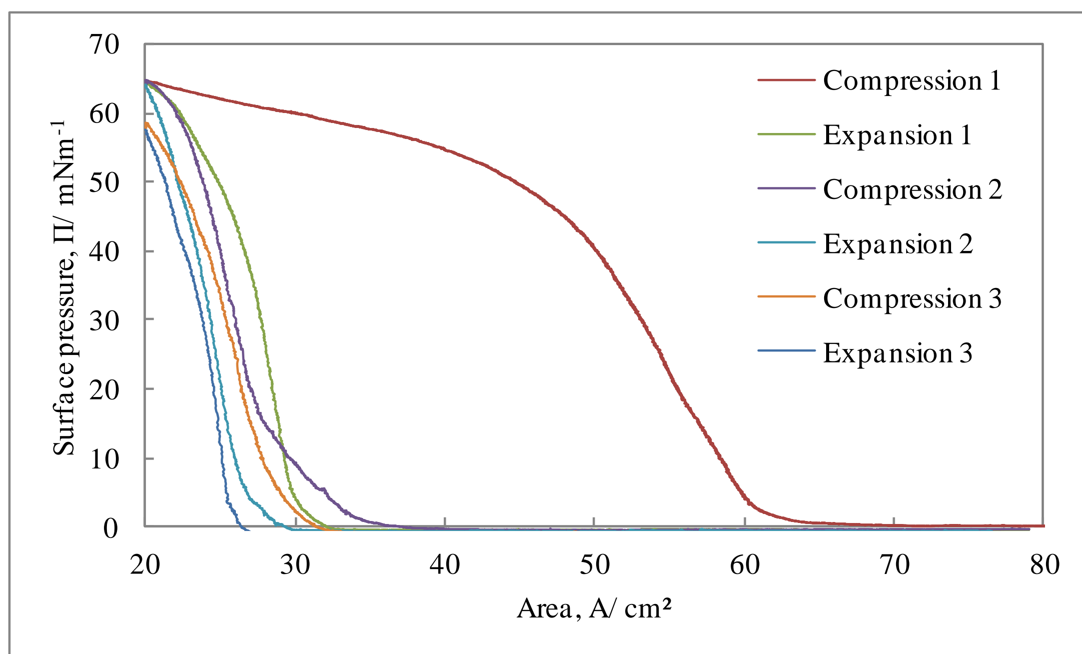

Fig. 4. 13. Isotherms resulting from repeated compression- expansion cycles of a monolayer of 15 µm diameter photoresist discs at an air- water interface during compression in a Langmuir trough. The discs were more varied in their size and shape than those shown in Fig. 4. 10 and gave a broader compression isotherm.

4. 3. 2. 2. Monolayers of SU- 8 negative photoresist discs

When spreading the thinner SU- 8 discs at the air- water interface (thickness ~ 0. 75 µm and diameter ~ 10 µm), it was found that with the same volume of the spreading solvent and concentration of particles in the suspension that was used previously with the AZ photoresist, it was not possible to induce jamming of the monolayer at the same area of the trough. One possible contribution to this effect may be due to losses of the SU- 8 particles after spreading, resulting from the greater density of the SU- 8 photoresist (1. 123 g/ cm^3); the density of the AZ negative photoresist used previously was 1. 071 g/ cm^3 (the value quoted was before dilution to a 1: 0. 4 ratio with its solvent as used in the experiments). In order to verify this, and to determine if it was possible to alleviate these losses by introducing more particles to the interface, the effect of particle concentration and spreading volume was investigated.

In order to calculate the area at which a close packed monolayer is expected, assuming hexagonal close packing, a theoretical yield of particles can first be calculated as follows:

The number of particles (N) per substrate can be calculated from

$$N = \frac{2A}{\sqrt{3}d^2} \tag{4. 4}$$

Where A is the area of the substrate and d is the particle centre to centre distance on the substrate, which in this case is 20 μm; therefore the number of particles per substrate is 5.1×10^7 and the close packed area from this number of particles is expected to be 44 cm^2 (assuming that no particles are lost during processing). If the particles are recovered from 4 substrates and transferred into 1 ml of spreading solvent, it is expected that a close packed monolayer at ~ 44 cm^2 can be prepared from 250 μl of the spreading suspension. Before spreading the particles at the interface, the suspension was shaken vigorously by hand in order to ensure that the particles were well dispersed. The appearance of the monolayer after the addition of different volumes of spreading suspension is shown in Fig. 4. 14. As shown in the microscopy images, some particles were observed beneath the monolayer after spreading and were therefore lost from the monolayer; these appear larger than the particles at the surface. The number density of the particles located at the interface was very small; even after addition of 500 μl of suspension (Fig. 4. 14).

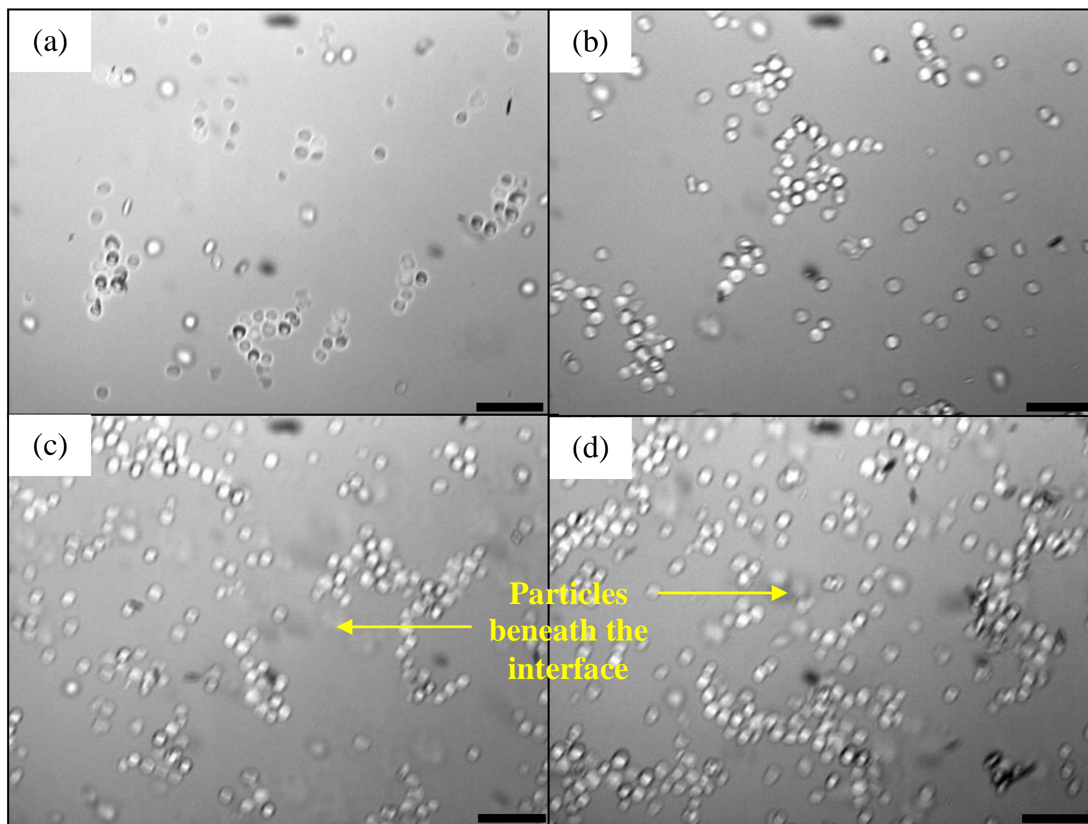

Fig. 4. 14. Optical microscopy images of SU- 8 2002 photoresist particle discs with a concentration of 2. 2 wt. %, after spreading at the air- water interface at an area of 80 cm^2. The different volumes of the spreading suspension shown are: (a) 50 µl, (b) 100 µl, (c) 250 µl and (d) 500 µl. Particles that appear to be out of focus are located within the bulk of the water sub- phase. Scale bars show 50 µm.

An isotherm was obtained after addition of 250 µl of the spreading suspension as shown in Fig. 4. 15. The pressure increase during compression at 3 cm^2/ min was almost linear with a slow increase in pressure indicative of an increasing number density of particles. The barriers were stopped at an area of 15. 4 cm^2 (the trough has a minimum area of 15 cm^2) when the surface pressure was 14. 1 mN/ m. After spreading 1000 µl of the suspension (4 x greater than that used previously), the monolayer appeared to be close packed after the barriers had closed to 15. 4 cm^2 (Fig. 4. 16) however, the isotherm did not indicate a rapid rise in pressure. It is possible however that the monolayer was close packed before the minimum area was reached, and further compression caused particle ejection from the interface due to overlapping of the discs; in addition tilting and flipping of the particles occurred which was found to be more extensive for these particles. The shape of the

isotherms for both 250 μl and 1000 μl of the spreading suspension indicated that no monolayer jamming event took place (Fig. 4. 15).

Observations of the monolayers and the isotherms indicates that for 250 μl and 1000 μl of 2. 2 wt. % of particles in the spreading suspension, there was an insufficient number of the particles at the interface to produce a close packed monolayer at the area expected. Possible reasons for the low concentration of particles at the interface may be:

i. Particles were lost during washing cycles by centrifugation due to sticking to the walls of the glass vessels. No evidence for this was found however, and and the supernatants present after centrifugation were clear.

ii. Monolayer leakage may have occurred. In this case, the monolayer may leak to the area outside the barriers during compression of the monolayer and would give rise to the slow rise in pressure observed.

The presence of particles in the bulk sub- phase after spreading however, suggests that fewer particles were present at the interface before compression, resulting in an insufficient number to produce a close packed monolayer during compression.

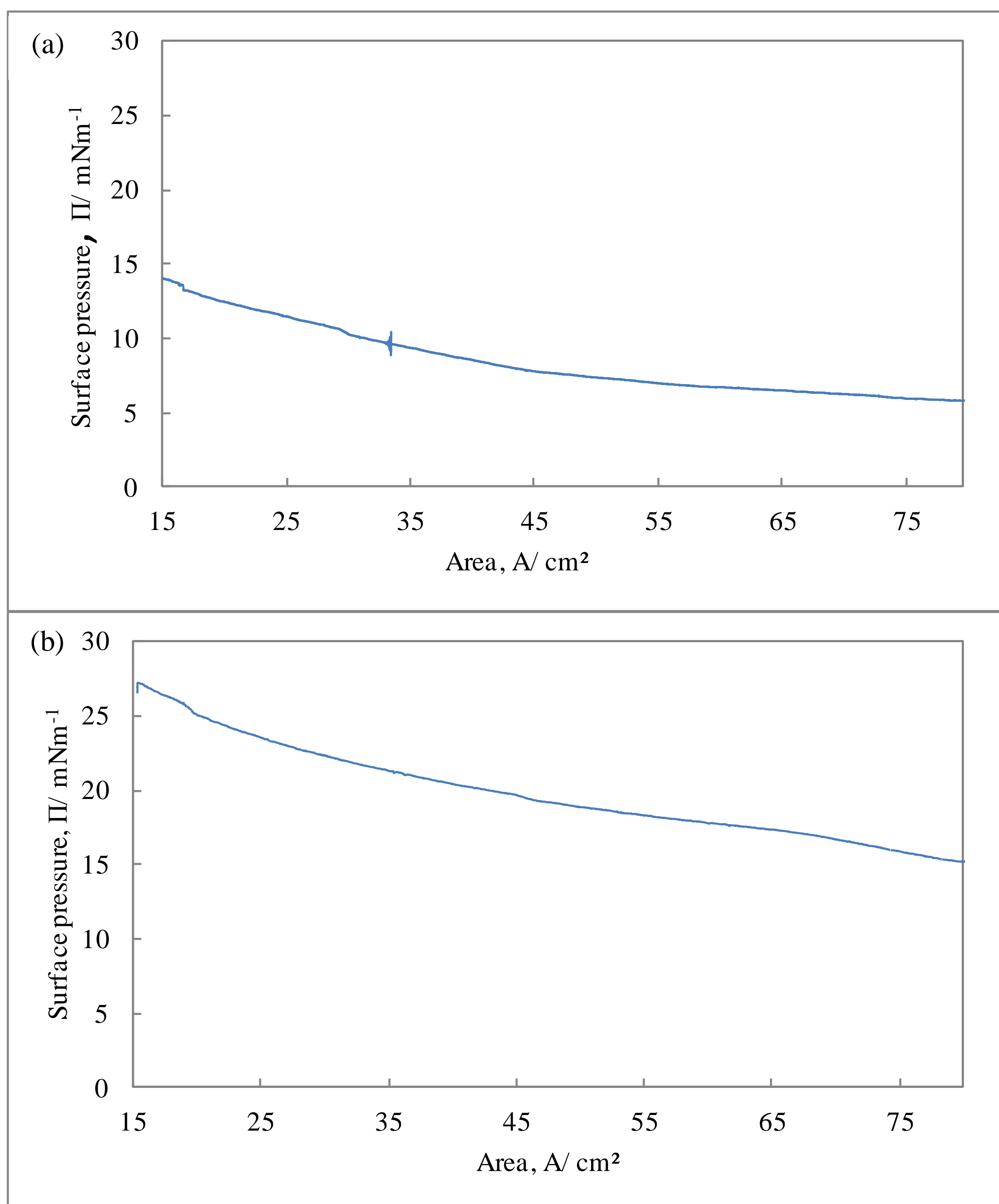

Fig. 4. 15. Pressure vs. area isotherms for SU- 8 discs at an air- water interface during compression of the monolayer to an area of 15. 4 cm^2, after spreading 250 μl (a) and 1000 μl (b) of a 2. 2 wt. % spreading suspension.

By increasing the concentration of the particles in the suspension, it will not be necessary to spread such a large amount of the particles and therefore the volume of spreading solvent required will be less. It is anticipated that this may help to keep the particles at the interface after spreading. In this experiment, the concentration of the particle suspension was increased from 2. 2 wt. % to 5. 4 wt. %. During the experiment, great care was taken to ensure that no water escaped the trough area during spreading of the particles or during compression. A total of 1000 μl of the spreading suspension was spread at the clean air- water interface. The monolayer occupied ~ 75 % of the trough at an area of 80 cm^2, and even before compression of the monolayer, many of the discs were found to be flipped at the interface (Fig. 4. 16). When observed by eye, the surface of the water within the barriers was grayish and homogeneous in appearance, and the area outside the barriers was clear indicating that no monolayer material had leaked outside the barriers after spreading. The compression isotherm was essentially linear during compression (see Fig. 4. 15) and the final surface pressure, at an area of 15. 4 cm^2 was 27. 3 mN/ m. Once again, no buckling of the monolayer occurred during the compression despite the apparent close packing of the monolayer at an area of ~ 43 cm^2. After compression, flipping and tilting of the discs was found to be extensive and there appears to be more than one layer of particles at the interface (Fig. 4. 16). No accumulation of the monolayer was present on the trough barriers; as in the case of the thicker AZ photoresist discs. When the monolayer was expanded at the same rate as the compression, it was found that the isotherm did not follow the same path as during compression, suggesting that some hysteresis was present. During expansion it became clear that a significant amount of monolayer material had been deposited on the bottom of the trough as observed by eye, and was found to occupy an area > 70 % of the total trough area. The observation of more than one layer of particles at the interface after compression may explain the loss of particles into the sub- phase: a particle that has been ejected by sliding beneath another particle has no chance of adsorbing at the interface as the interface is already completely occupied. Extensive flipping of the particles at small areas is perhaps also due to a particle overlapping another; in this case however the particle is not completely ejected from the interface.

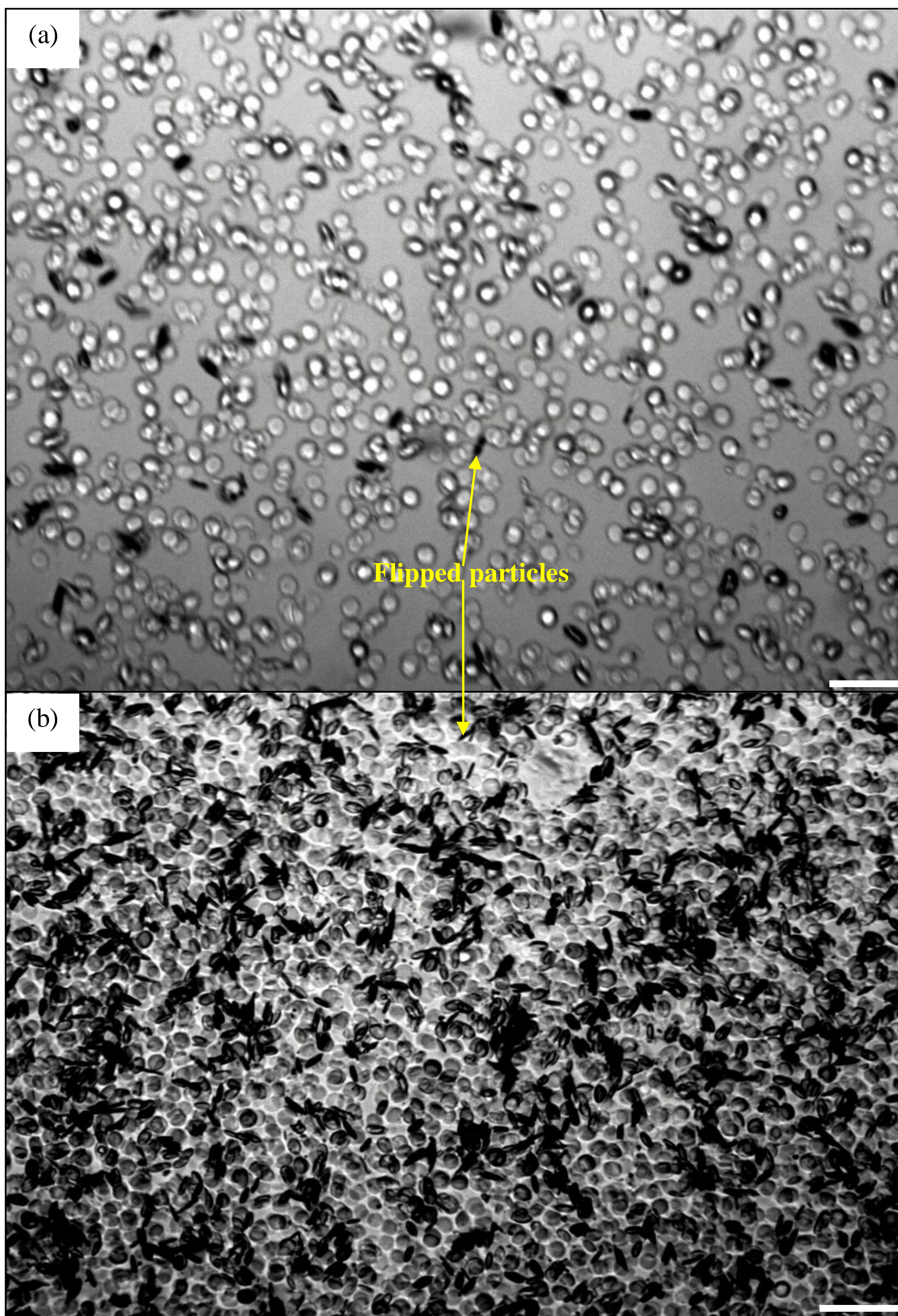

Fig. 4. 16. Optical microscopy images of SU- 8 photoresist discs from a concentration of spreading solvent of 5. 4 wt. % at the air- water interface during compression in a Langmuir trough at areas of 80. 0 cm² (a) and 15. 4 cm² (b). The spread volume was 1000 µl. Scale bars show 50 µm.

Because no jamming of the monolayer took place during compression and due to the appearance of monolayer material at the bottom of the trough, it was clear that insufficient particles were present at the interface during compression to permit jamming. As indicated previously, a significant number of particles were ejected from the interface after spreading and during compression. To quantify the ejection of particles from the interface and be able to attribute the shape of the isotherm with the response of the monolayer during compression, it was decided to count the particles present at the interface during various stages of compression by analysing images obtained from an optical microscope. An automated counting procedure could not be performed using Image Pro Plus software due to the poor contrast between the transparent particles and the interface. It was therefore decided to count the particles manually. The total number of particles (N_t) counted at a given area (A) was calculated by:

$$N_t = \frac{(N_s + N_f + N_o)A}{2.6 \times 10^{-3} cm^2} \quad (4.5)$$

Where N_s represent the number of particles that are located at the surface only and orientated parallel with the interface (referred to as surface particles in plane in the captions), N_o represents the number of particles that are located immediately beneath those at the surface (overlapped particles) and N_f represents the number of flipped or tilted particles. The value of 2.6×10^{-3} cm² is the area of the monolayer within which the particles were counted. It is noted that some particles could be observed in the bulk of the aqueous sub- phase after spreading and during compression which could not be counted. At a volume of 850 µl of spreading suspension, the total number of particles expected is 3.5×10^{8}. The total number of particles expected (N_t), and observed during compression of the monolayer normalized to those counted before compression is shown in Fig. 4. 17 and Fig. 4. 18 shows the total number density of particles (per cm²) incorporating each of the three orientations during compression of the monolayer, together with that calculated assuming no losses. It can be seen that the number of particles actually counted is significantly less than that calculated confirming that losses were occurring during compression.

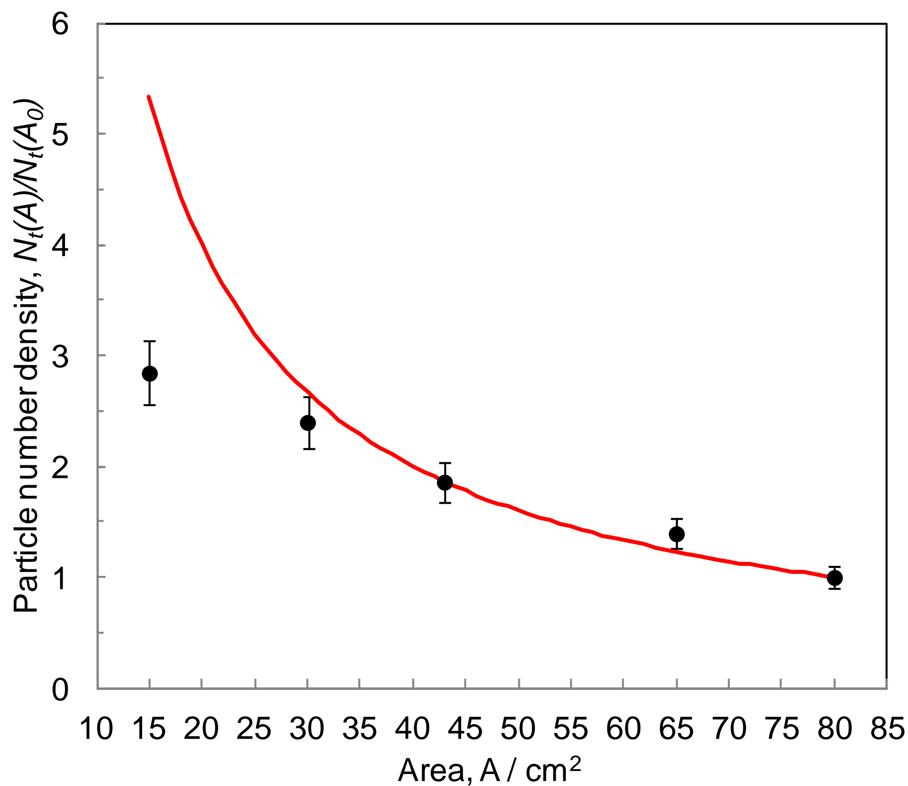

Fig. 4. 17. Measured (circles) and calculated (line) total number density of SU-8 disc shape particles at the air-water interface, N_t (A), normalised with that at the initial area A_0 = 80 cm^2 versus trough area, during compression of the particle monolayer in the Langmuir trough at a rate of 3 cm^2/min. The line corresponds to calculated density assuming N_t (A) = $N_t(A_0)$, i. e., no particle detachment during compression.

In Fig. 4. 18, it can be seen that during compression, the number of particles orientated parallel and located at the interface (N^s) increases from 2. 5 × 10^5 cm^{-2} to 4. 1 × 10^5 cm^{-2} and then decreases more slowly to a final value of 3. 2 × 10^5 cm^{-2}. In contrast, the number of flipped particles increases in an exponential trend from 1. 3 × 10^4 cm^{-2} to 3. 7 × 10^5 cm^{-2}. For the overlapped particles, a steady increase in number was observed which gave a final value of 3. 1 × 10^5 cm^2. Losses in the number of particles orientated parallel with the interface are consistent with a corresponding increase in the number of flipped particles. The decrease in the number of particles orientated parallel with the interface was 1. 4 ± 0. 4 × 10^7, and the increase in the number of flipped particles was 4. 7 ± 0. 4 × 10^6; therefore the loss of particles orientated parallel with the plane of the interface was due mainly to particle flipping. The decrease observed in the number of overlapped particles can only result from their loss into the bulk phase; therefore the flipping and overlapping of particles relieves some of the compressional stress, and the change in pressure during compression is essentially linear, consistent with a continual increase in surface pressure without a rapid rise in pressure indicative of particle jamming. It is frequently observed that flipped particles were present in stacks of two or more particles as shown in Fig. 4. 20, which may indicate that the cohesion or attractive forces between the faces of the discs is strong. The response of the individual particle orientations during expansion of the monolayer at the same rate as compression is shown in Fig. 4. 19, which includes the total number of particles counted, i. e., the sum of the three orientations for both compression and expansion. The shape of the plots for both compression and expansion were found to be similar for the three orientations. This indicates a relaxation of flipped particles back into the plane of the interface; the total number of particles counted during compression and expansion practically coincide (Fig. 4. 19) indicating that the number of particles is unchanged for both processes. In the case of the first layer of overlapped particles, this suggests that they may re- adsorp to the interface. Because the discs were so thin and their surface was so rough with large protrusions present at the perimeter of the discs (as observed from SEM images on the dry particles), there was a tendency for small fragments of the photoresist with sizes < 2 μm to detach from the discs and become suspended with the discs giving rise to a mixture of discs and small fragments of photoresist at the interface. The discs prepared in this way were

therefore not suitable for this type of investigation, and further experiments were not performed using SU- 8.

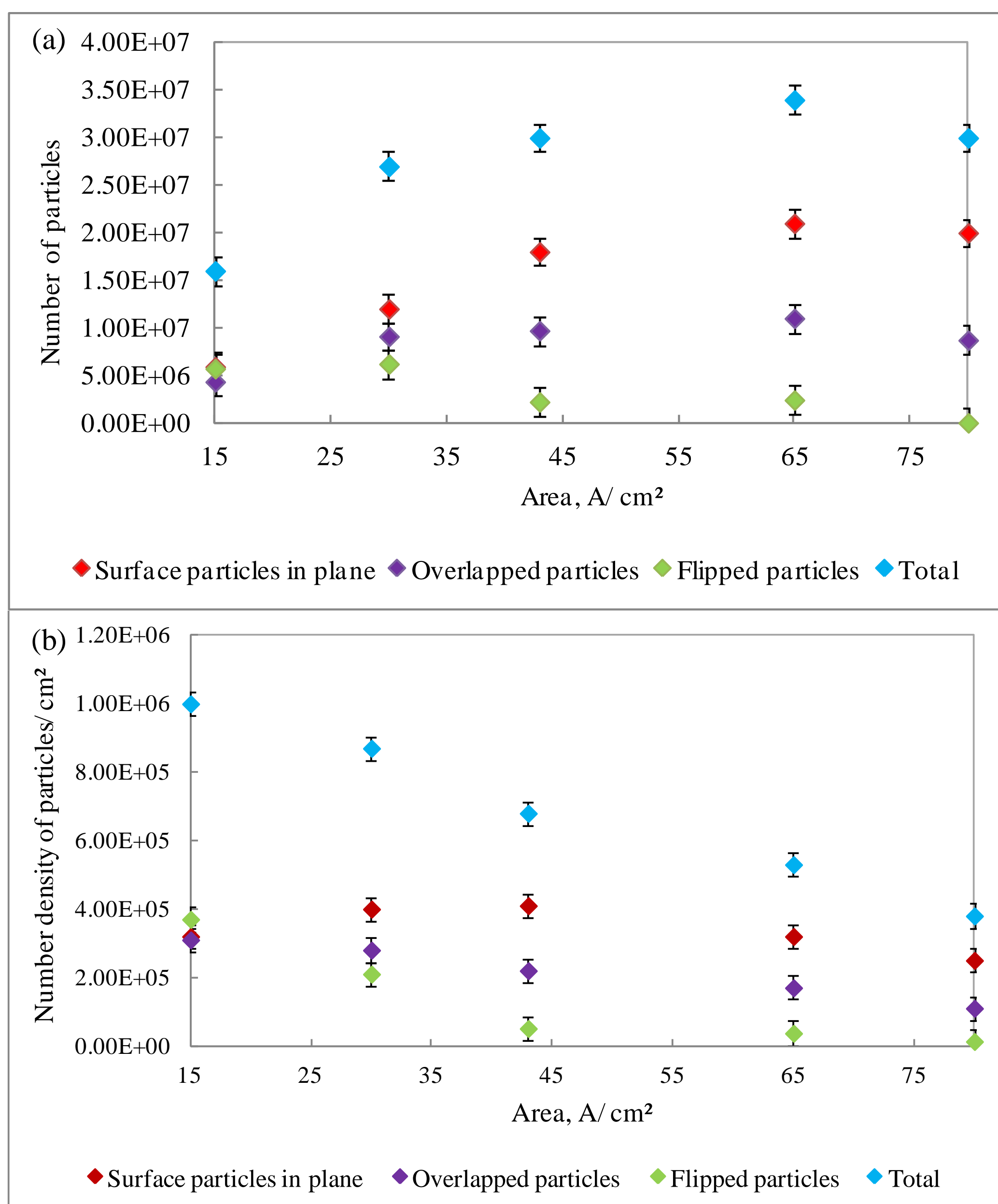

Fig. 4. 18. Plots of the number of SU- 8 discs counted for each orientation of the particles at an air- water interface during compression. The orientations shown are: i), surface particles orientated parallel with the interface at the surface only (ii), overlapped particles orientated parallel with the interface and located beneath the surface particles and (iii), flipped particles orientated at angles approaching 90 ° with respect to the interface. The number of particles counted over the whole of the available trough area is shown in (a) and particle numbers per cm^2 (number density) are shown in (b).

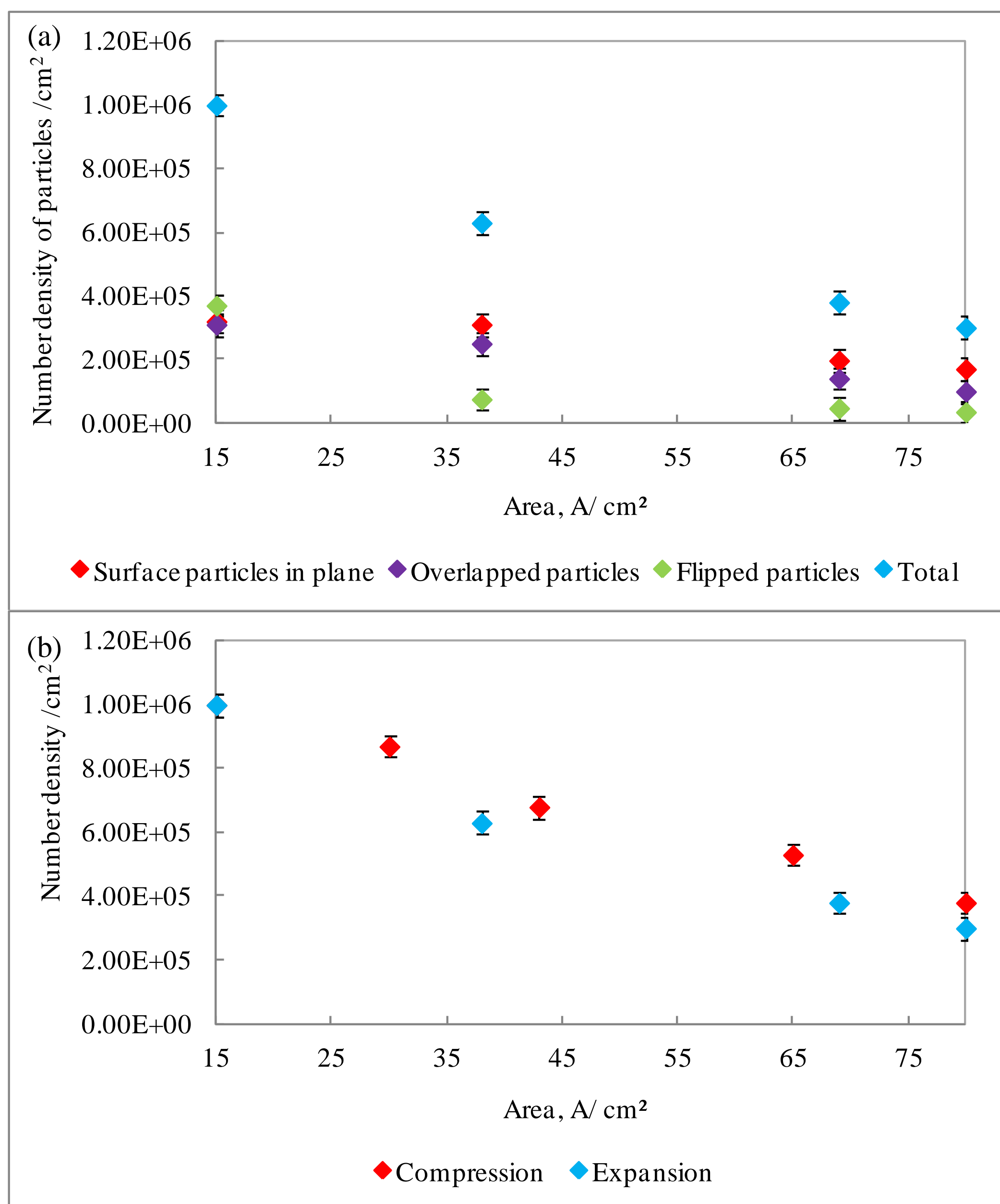

Fig. 4. 19. Plot of the number density of SU- 8 discs counted for each orientation of the particles at the air- water interface during expansion of the monolayer (a). Plot showing the total number density of SU- 8 discs counted composed of the sum of the three orientations (total number) of the particles at the air- water interface during compression and expansion of the monolayer (b).

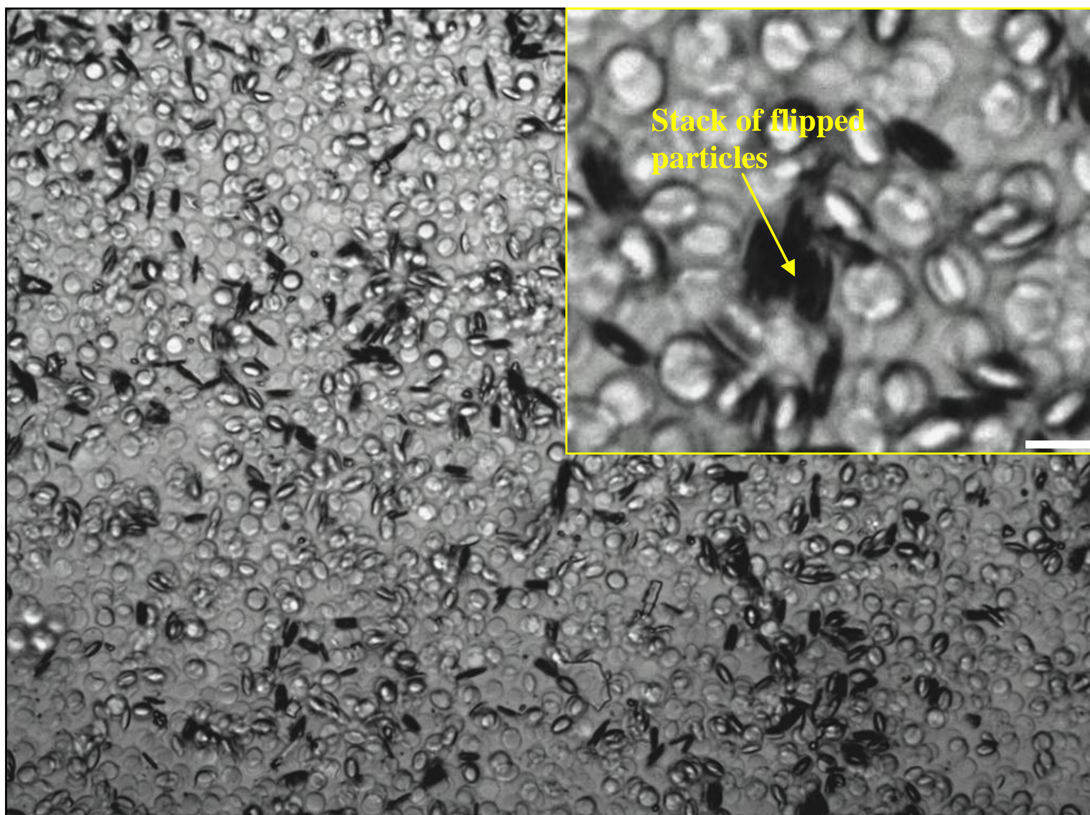

Fig. 4. 20. A monolayer of SU- 8 discs at the air- water interface. The image shows the monolayer at an area of 30 cm^2 during compression. The black ellipsoidal shaped particles are flipped particles. It is often observed that the flipped particles exist in stacks of two or more particles. The scale bar shows 10 µm.

Overall there appears to be a steady loss of particles from the interface during compression of the monolayer due to the tendency of the discs to overlap each other, and there may be more than one layer of overlapped particles (Figs. 4. 16 and 4. 20). At the same time, there is a continual increase in the number of flipped particles. After compression and expansion of the monolayer, the appearance of a dense deposit of particles at the bottom of the trough was clearly visible with the naked eye covering an area of ~ 80 cm^2. These particles cannot possibly result from the ejection of overlapped particles that were counted during compression as their number it too small to account for what appears to be more than one layer of particles deposited at the bottom of the trough. As mentioned, there may have been more than one layer of overlapped particles that were perhaps lost onto the bulk phase during compression. In addition it was noticed that some particle were dispersed in the bulk phase after spreading the suspension at the interface; however it was not possible to quantify these particles. It is therefore expected that the number

of particles observed at the bottom of the trough results from both particle losses after spreading and to losses during compression due to overlapping of particles; however if we consider that the carpet of particles observed at the bottom of the trough covered almost all of the trough area with a thick layer of particles, then it seems likely that the majority of the particles were deposited on the bottom of the trough before compression. If the number of particles present at the interface before compression is subtracted from the number of particles expected in the spreading suspension (3.5×10^8), the number of particles deposited at the bottom of the trough is expected to be ~ 3.2×10^8; therefore massive losses were observed for the SU- 8 photoresist discs after spreading and during compression of the monolayer. It was found that losses during spreading of the suspension could be minimised by spreading from a syringe with a smaller diameter; however the diameter of the needle is limited by the tendency of the discs to clog the needle. Addition of NaCl to the sub- phase before spreading also reduced the losses to a small extent. Despite the measure taken however, there was still an insufficient number of particles at the interface to observe a jamming event and the losses were still substantial. The presence of discs found in the bulk of the water after spreading did not appear to be affected by the nature of the spreading solvent. As mentioned earlier, both methanol and IPA were used as spreading solvents, in each case the alcohol was mixed with 50 % by weight with water and in addition to the type of spreading solvent, the effect of the concentration of the alcohol in water was also investigated, in each case, no convincing increase in the number of particles present after spreading was observed.

4. 3. 2. 3. Monolayers of AZ negative photoresist ovals

Compression and expansion isotherms were obtained for oval shaped AZ photoresist in order to determine how shape can affect the behavior of the monolayer undergoing compression at the air- water interface. Fig. 4. 21 shows isotherms recorded for the first compression- expansion cycle for photoresist ovals, together with the first compression- expansion cycle isotherm for photoresist discs. An important difference attributable to the oval shaped particles is the somewhat broader compression isotherm after the first knee in the isotherm. This demonstrates that the oval shaped particles are able to alleviate the stress induced by compression by reorientation of the particles, which cannot be achieved by the disc shaped particles. Like the disc shaped particles described earlier, the monolayer undergoes extensive

buckling after the second knee in the isotherm with a peak to peak wavelength of ~ 312 μm. During compression, when the monolayer became close packed, it was possible to observe a tendency for the ovals to stack together in small domains consisting of ~ 10 ovals making side to side contact (Fig. 4. 22). It is possible therefore that the ovals have responded to the large pressure increase by adopting a preferred orientation. Flipping was also observed for the AZ ovals after jamming of the monolayer had occurred; however although it is possible for flat oval shaped particles to flip around their long or short axes, it was found that the ovals preferred to flip such that their long axes were orientated perpendicular with the interface as shown in Fig. 4. 23 (a). The preferred orientation of the ovals during flipping is expected to result from the relative ease of rotating the ovals around their long axes as opposed to the opposite case, along the short axes, resulting in greater immersion of the ovals surface into the water. After compressing the monolayer beyond the second knee of the isotherm, extensive overlapping of ovals and particle ejection from the interface accompanying buckling of the monolayer was observed, as in the case of disc shaped particles as shown in Fig. 4. 23 (b) and once again, hysteresis between successive compression- expansion cycles was more prominent between the first and second cycles. During expansion of the monolayer the flipped particles settled back into the plane of the interface and the monolayer as a whole was more aggregated, as observed for the discs; some of the ovals however remained overlapped after expansion of the monolayer.

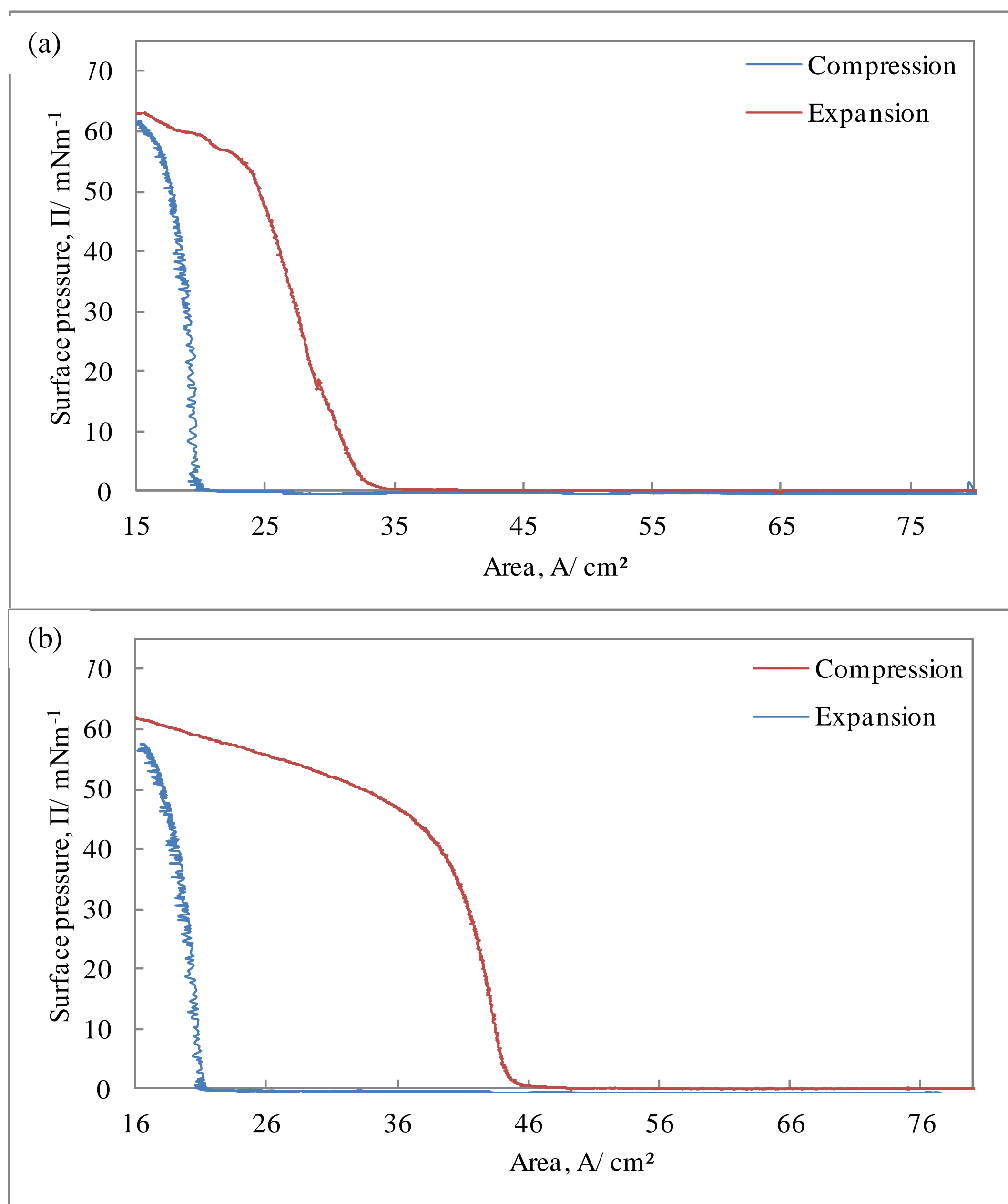

Fig. 4. 21. Isotherms recorded during compression and expansion of monolayers of flat photoresist ovals at the air- water interface in a Langmuir trough, showing the first compression and expansion cycle (a) and the first compression and expansion cycle for photoresist discs (b).

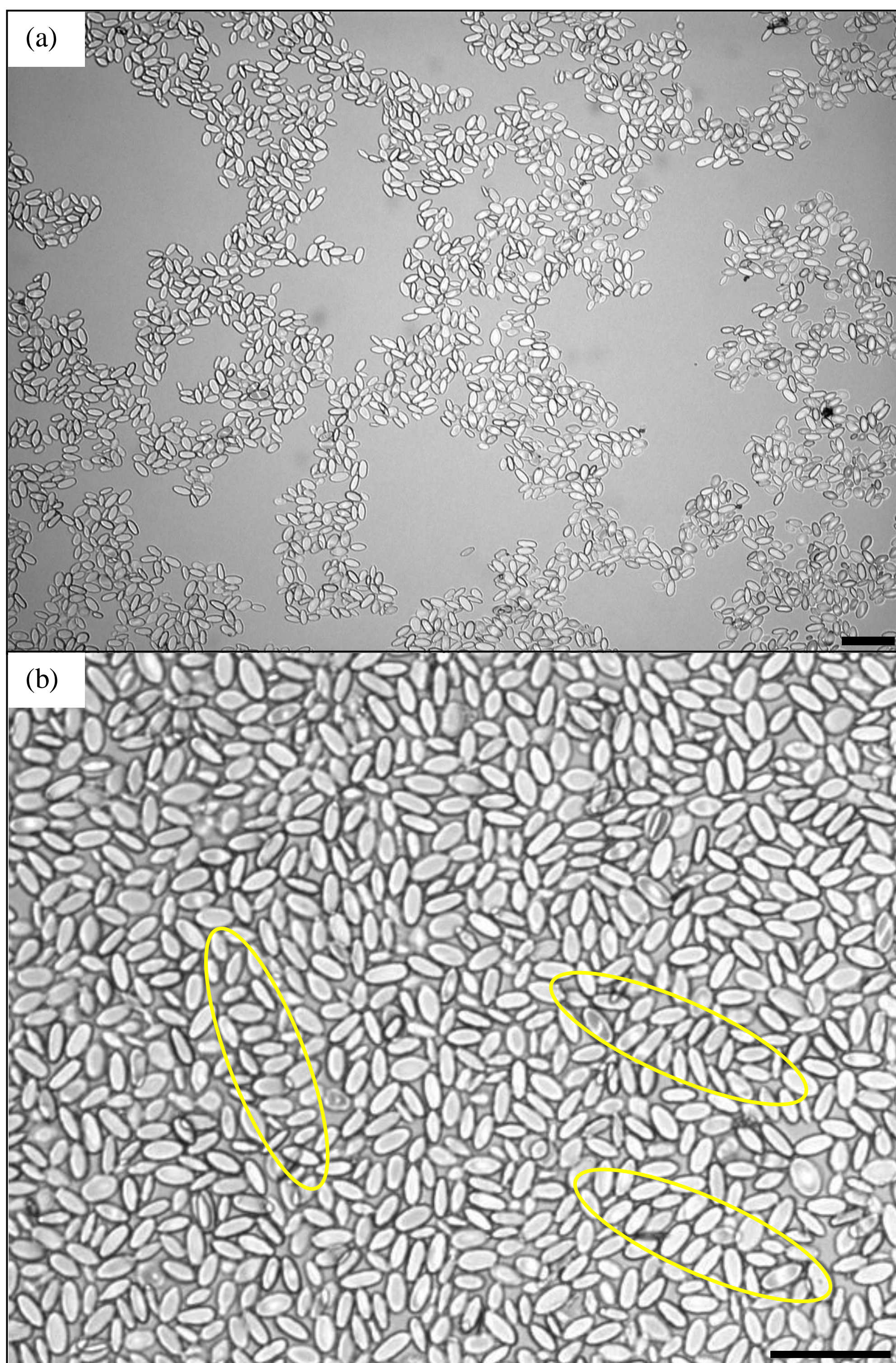

Fig. 4. 22. Optical microscopy image of flat oval shaped photoresist particles at an air- water interface in a Langmuir trough after spreading 1000 µl (a) and after monolayer jamming beyond the second knee in the isotherm (b). Ordered domains have been highlighted. Scale bars show 50 µm.

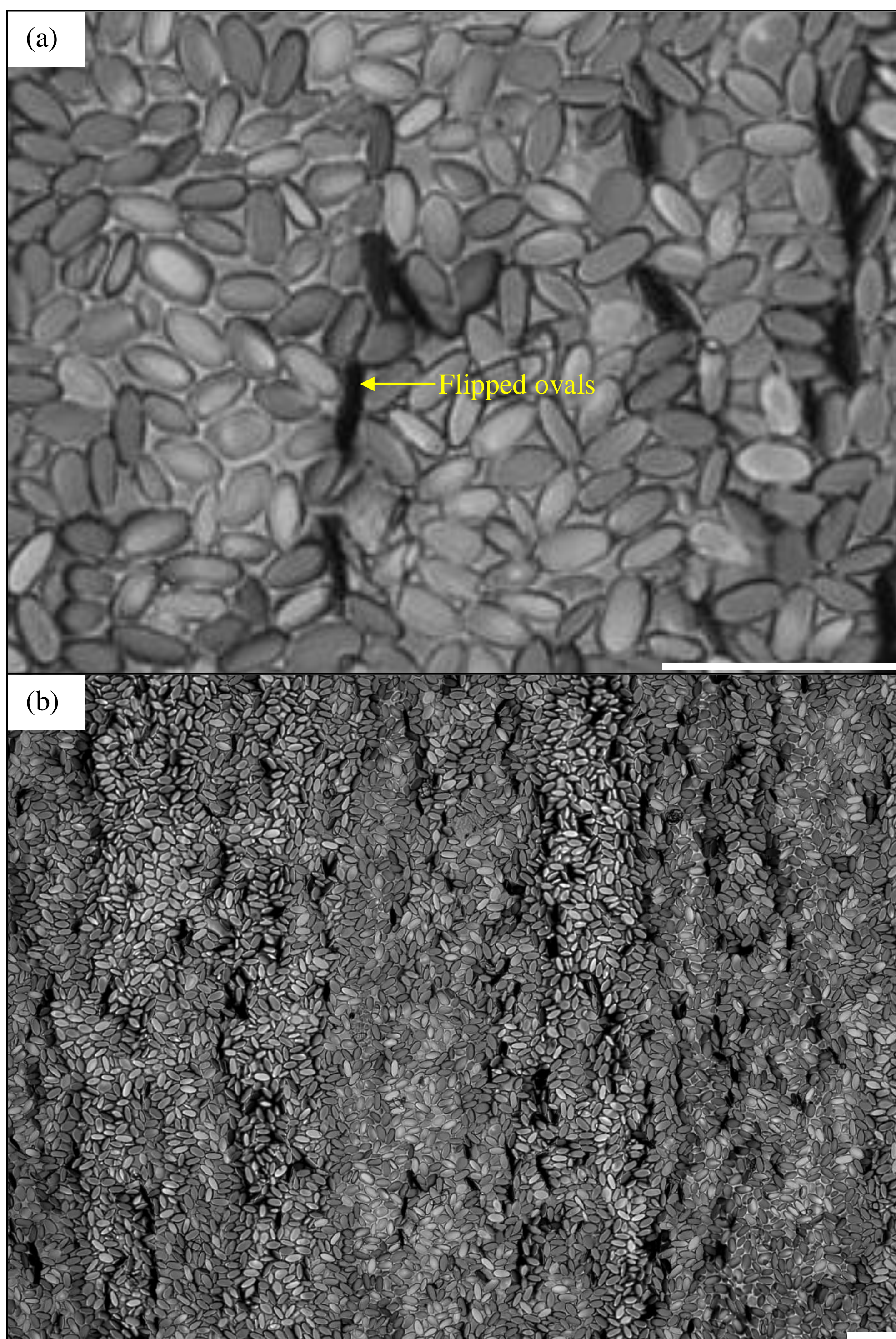

Fig. 4. 23. Flat oval shaped particles at the air- water interface during compression in a Langmuir trough. After monolayer jamming had occurred at the first knee in the isotherm, flipping and tilting of the ovals around their long axes was observed (a). After the second knee in the isotherm, the greater surface pressure caused buckling of the monolayer with the buckling accompanied by extensive flipping, overlapping and ejection of some of the particles from the interface (b). Scale bars show 50 μm.

As demonstrated in the previous section, there was a tendency for small domains of ordered ovals to occur after close packing of the monolayer. In order to determine if there was a tendency for the ovals to prefer a particular orientation over a larger area of the trough and to align in a particular direction during compression, it was decided to determine the orientation of the ovals during different stages of compression of the monolayer. This was achieved by measuring the angle between the long axes of the particles with respect to a horizontal line between the compressing barriers as illustrated in Fig. 4. 24. A macro was created using Image Pro Plus 5 software to allow the angle to be measured automatically by drawing straight lines along the long axes of the ovals. Approximately 500 ovals were measured at each area of the trough. It is intuitive to expect that the particles will preferentially orientate with their long axes parallel with the compressing barriers during confinement as the monolayer is compressed to smaller areas. As shown in Table. 4. 2, this was not the case. Although the average orientation of the particles was ~ 90 °, expected for a parallel alignment with the barriers, the standard deviation was very large (~ 53 °) suggesting a more random orientation, as images of the monolayer during compression indicate as shown in Fig. 4. 25 and Table. 4. 2. There was therefore no tendency for the ovals to adopt a particular orientation during compression of the monolayers at the air- water interface.

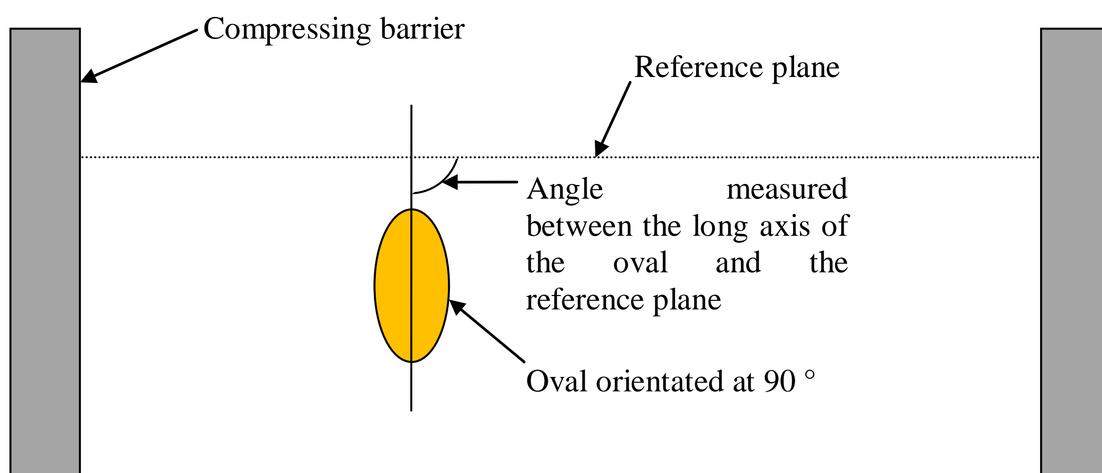

Fig. 4. 24. Scheme showing how the orientation of the oval shaped particles at the air- water interface was determined.

Table. 4. 2. Angles of orientation for oval shaped particles at different areas of the air- water interface during compression of the monolayer in a Langmuir trough. The data was obtained from ~ 500 particles per image.

Area/ cm^2	Average angle/ deg	Standard deviation/ deg
80	89	51
57	94	56
55	90	57
43	90	55
38	93	54

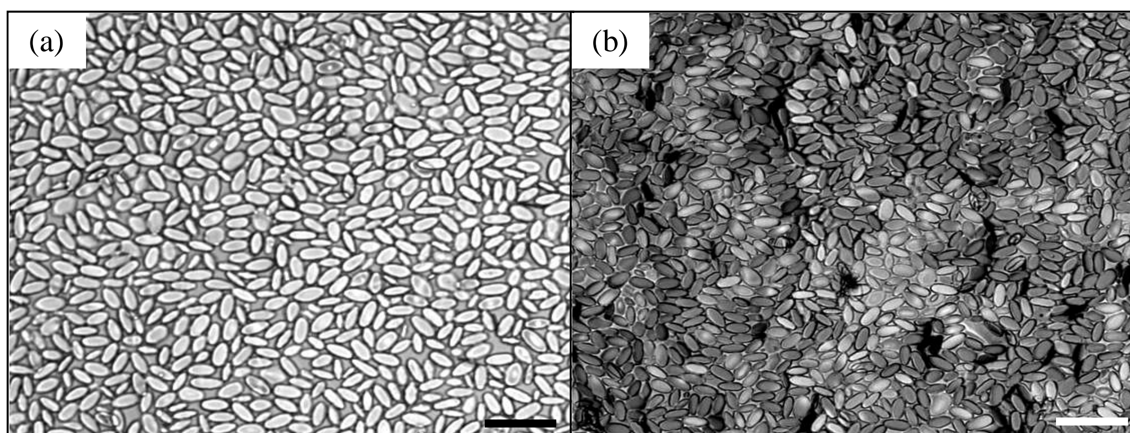

Fig. 4. 25. Optical microscopy images of oval shaped photoresist particles at the air-water interface during compression of the monolayer in a Langmuir trough at areas of 56. 6 cm^2 (a) and 43. 2 cm^2 (b). Scale bars show 50 μm.

4. 3. 2. 4. Monolayers of AZ negative photoresist rectangles

In order to demonstrate the tendency for non- spherical particles to adopt a particular orientation during compression of the monolayers and to establish how shape affects the behavior of the monolayers during compression, rounded rectangular particles composed of AZ photoresist were investigated. After spreading, the monolayer was compressed and expanded under the same conditions as described for the discs and ovals. During compression, the monolayer became denser but there was again no apparent tendency for the particles to assume a particular orientation: as shown in Table. 4. 3 the orientation of the rectangles was random, even at the smallest area of the trough. It is clear therefore that during compression, we observe the compression of an aggregated network; individual particles are not able to detach from the network to assume a preferred orientation. It was also clear that in the case of rectangle shaped particles; the isotherm became much more expanded than in the case of the lower aspect ratio discs and ovals as shown in Fig. 4. 27, where the compression and expansion isotherms for the three shapes are shown together. This stems from the ability of the rectangles to reorientate with more ease, as the rectangles can slide together along their long axes. Flipping of the rectangles around their long axes also occurred after the second knee in the isotherm; this behaviour accompanied buckling of the monolayer and particle ejection from the interface. Some images of the rectangles at different areas of the trough during compression are shown in Fig. 4. 26. Hysteresis was observed between the first compression and expansion cycle and also between subsequent compression and expansion cycles, and there was little variation in the appearance of the monolayer during expansion (Fig. 4. 26): the monolayer preserved its area after compression resulting in a vertical strip of particles surrounded by bare air- water interface. This finding (similar to the findings observed for the oval shaped particles, but to a greater extent) is explained by the entanglement of the particles within dense aggregates, similar findings are observed for discs; however in this case the monolayer fragments into large densely packed islands covering the whole area of the trough. If we consider also the expansion isotherm for the rectangles, it can be seen that as in the case of compression, the isotherm is broader (Fig. 4. 27). This evidence suggests that during expansion, the entangled rectangles are able to increase their area somewhat, allowing the reduction in surface pressure to become more gradual. At the bottom of

the isotherm there is a knee and subsequently a significantly slower drop in pressure, indicating an abrupt but small expansion of the monolayer as shown in Fig. 4. 27 (a). These observations suggest that monolayers composed of rectangular particles are more elastic than those observed with lower aspect ratio particles.

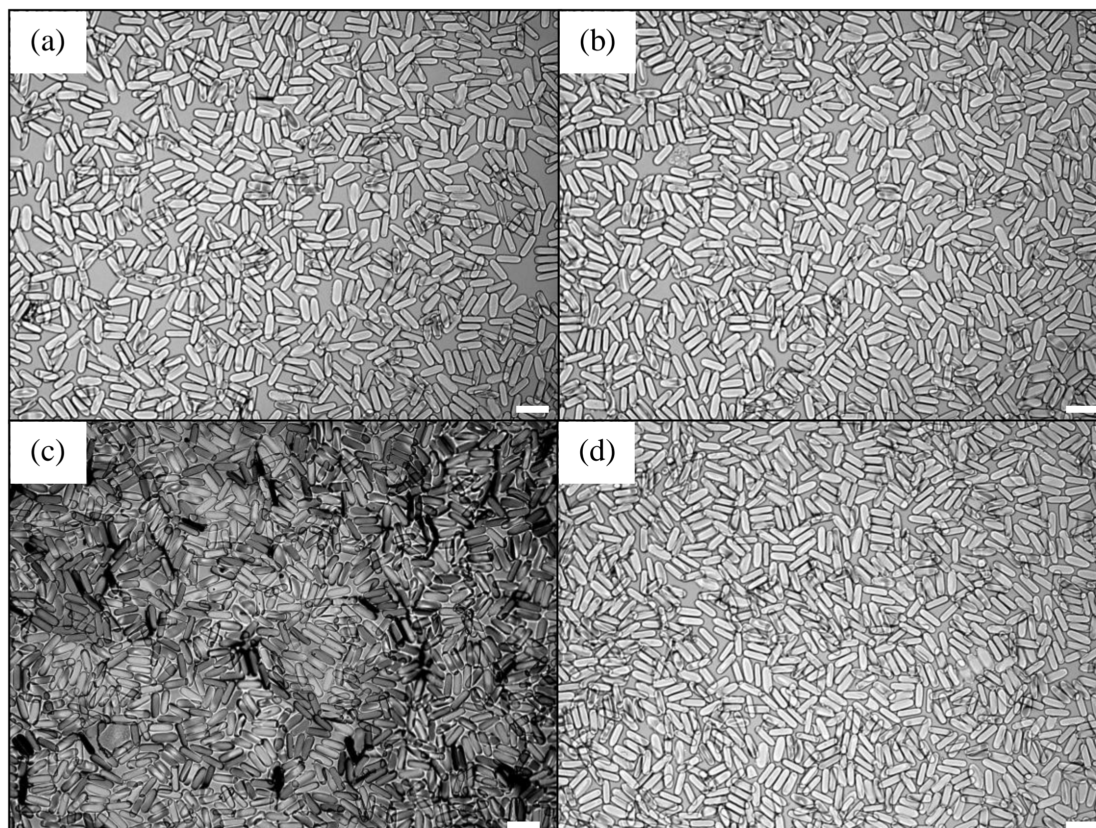

Fig. 4. 26. Optical microscopy images of flat rectangular photoresist particles during compression at the air- water interface in a Langmuir trough at areas of 60. 0 cm^2 (a), 53. 0 cm^2 (b) 33. 1 cm^2 (c), and after expansion of the monolayer to an area of 80. 0 cm^2 (d). The corresponding isotherm can be seen in Fig. 4. 27. Scale bars show 50 μm.

Table. 4. 3. Angles of orientation for rectangle shaped photoresist particles at different areas of the air- water interface during compression of the monolayer in a Langmuir trough. The data was obtained from ~ 500 particles per image.

Area/ cm^2	Average angle/ deg	Standard deviation/ deg
80	81	52
60	89	53
53	83	53
43	82	55
36	84	57
29	81	52

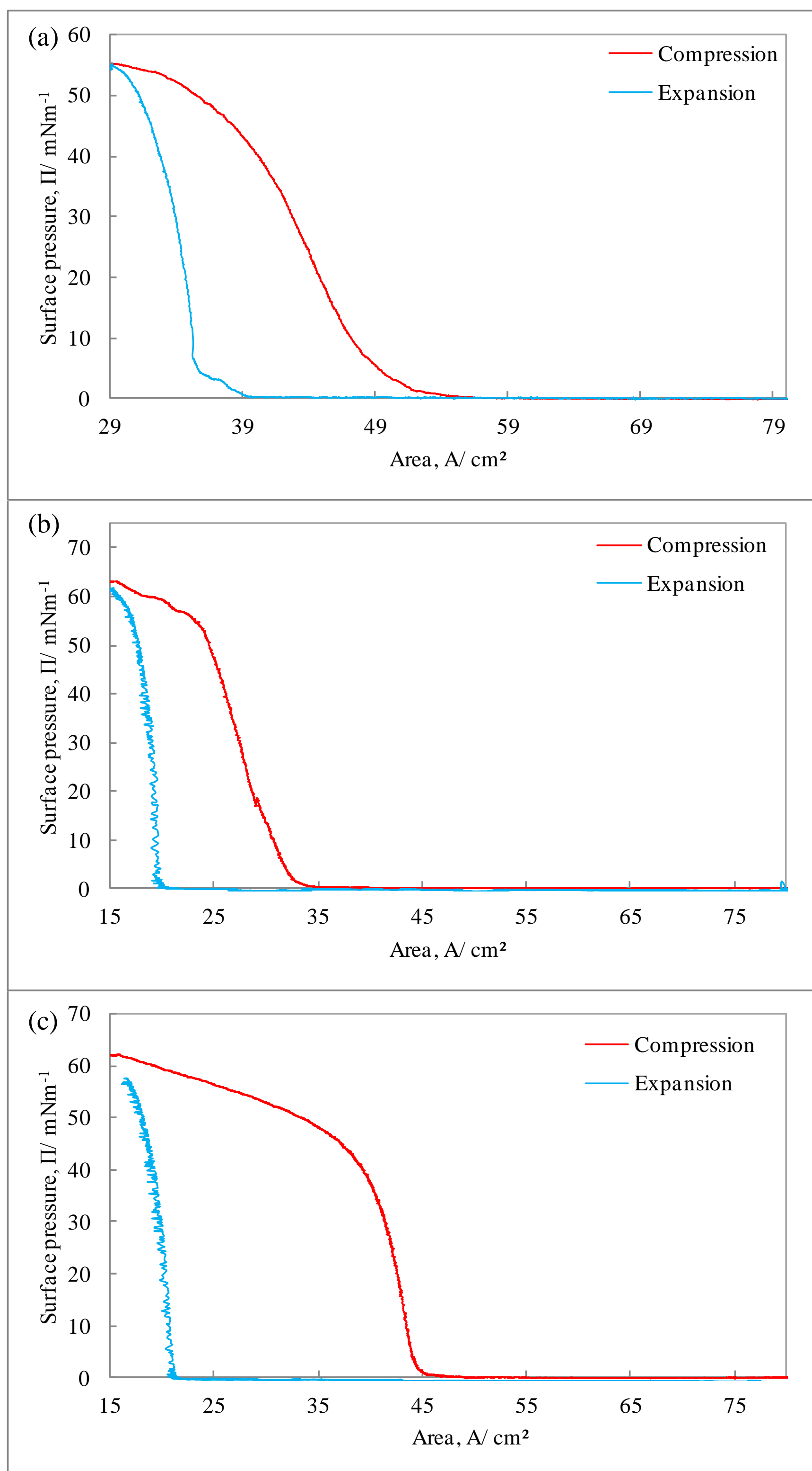

Fig. 4. 27. Pressure vs. area isotherms during compression and expansion of a monolayer of rectangular photoresist particles (a), oval shaped photoresist particles (b) and disc shaped photoresist particles (c) at the air- water interface in a Langmuir trough.

4. 3. 2. 5. Monolayers of AZ negative photoresist ovals at the oil- water interface

Experiments performed at the oil- water interface in the Langmuir trough for the oval shaped particles were performed under the same conditions as those at the air-water interface. The behavior of the monolayers and the isotherms obtained at the oil- water interface however were rather more interesting. First, the compression and expansion isotherms were somewhat more expanded in the oil- water case and abrupt changes in pressure resulting from monolayer jamming and buckling were more gradual. In addition, the hysteresis between the first compression and expansion of the monolayer was significantly reduced and also between subsequent compression-expansion cycles as shown in Fig. 4. 28. Observation of the monolayer during compression revealed that tilting and flipping of the ovals was observed beyond the first knee in the isotherm (Fig. 4. 29); however no particles were ejected from the interface into the water, even during buckling of the monolayer, and no monolayer material was found to accumulate on the compressing barriers as in the case of the air- water interface after compression. These findings demonstrate that the particles are anchored to the interface more strongly, resulting in a decrease in hysteresis. During expansion, the monolayer expanded until the entire area of the trough was populated by the particles and the monolayer resembled that seen before compression.

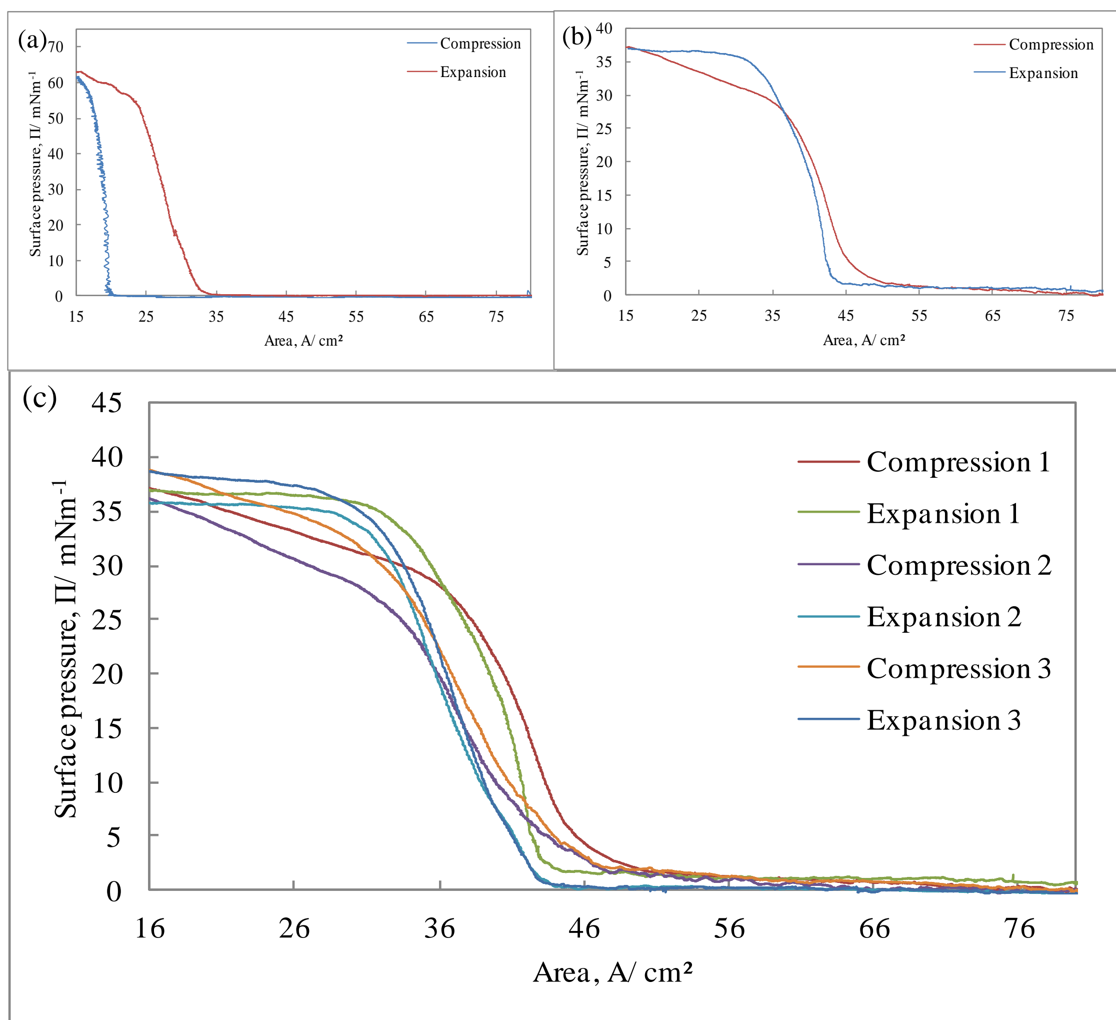

Fig. 4. 28. Isotherms obtained during compression and expansion of a monolayer of oval shaped photoresist particles at the air- water interface (a) and the tetradecane-water interface (b and c) in a Langmuir trough.

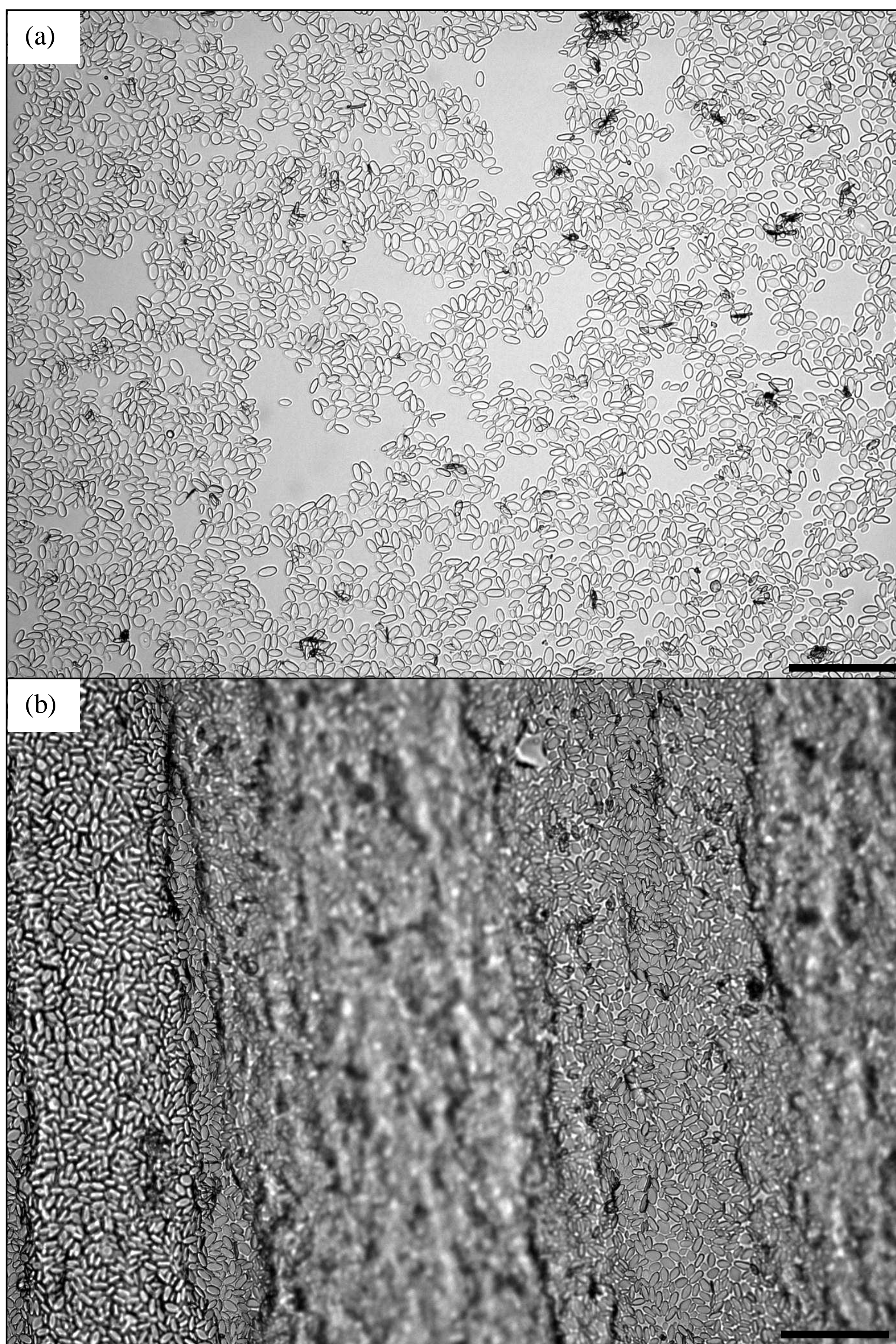

Fig. 4. 29. Optical microscopy images of a monolayer of oval shaped photoresist particles at the tetradecane- water interface during the first compression cycle in a Langmuir trough at areas of 48. 5 cm^2 (a) and 15. 4 cm^2 (b). Scale bars show 100 μm.

Fig. 4. 30 shows the number density of particles counted at the interface during compression and expansion of the monolayer. It can be seen that very few particles are lost from the interface during compression of the monolayer. There was no tendency for the ovals to adopt a particular orientation during compression at the oil-water interface as shown in Table. 4. 4, therefore as in the case of the air- water experiment, after the formation of an aggregated network formed after spreading the particles, compression of the monolayer resulted in the compression of the aggregate and therefore retention of the particle orientations.

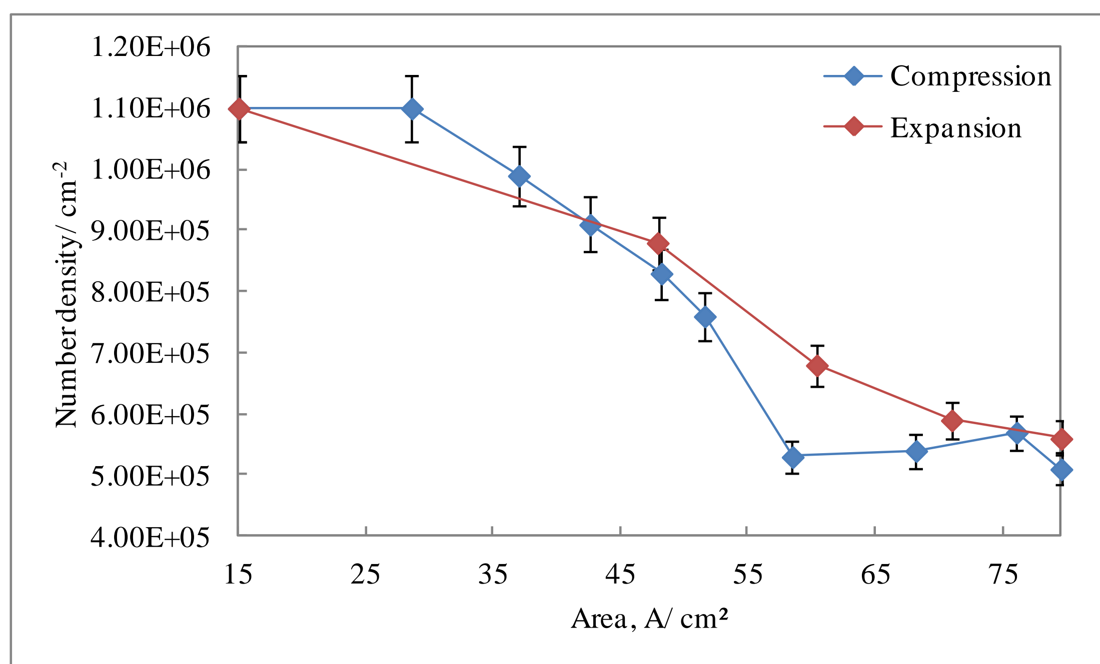

Fig. 4. 30. Number density of oval shaped photoresist particles counted at the tetradecane- water interface during compression and expansion of the monolayer in a Langmuir trough.

Table. 4. 4. Angles of orientation for oval shaped particles at different areas of the tetradecane- water interface during compression of the monolayer in a Langmuir trough.

Area/ cm^2	Average angle/ deg	Standard deviation/ deg
80	85	52
77	87	52
49	91	51
37	86	46
29	88	49
15	92	50

4. 3. 3. Comparison of plate- like and spherical microparticle behaviour in Langmuir trough experiments

PS- latex particles with diameters of 3 μm were also investigated at the air- water interface. The use of latex particle monolayers has been studied in some detail for many years. Here we highlight some of the important similarities and differences between the spherical and non- spherical particles were investigated. Monolayers of the spherical latex particles were prepared at the air- water interface in a Langmuir trough by spreading 200 μl of a 4 wt. vol. % suspension of the particles in a 50 wt. % water- methanol mixture. Before compressing the monolayer, it was noticed that the monolayer consisted of interconnected networks of particles with hexagonal ordering within the particle clusters (Fig. 4. 31), similar to the observations of Stamou *et al.*, and is attributed to long range capillary interactions due to interfacial deformations caused by asperities on the particle surface. [87] Initially after spreading, the monolayer consisted of single particles, dimers, trimers etc and small aggregates and within a few minutes, the aggregates became interconnected (Fig. 4. 31) as observed for the plate- like particles investigated in this chapter. The presence of the aggregates has not been attributed to contamination of the particles, as particles taken from the same batch exhibit perfect hexagonal ordering with particle centre to centre distances of several particle diameters at the oil- water interface- such behaviour is only observed under pristine conditions.

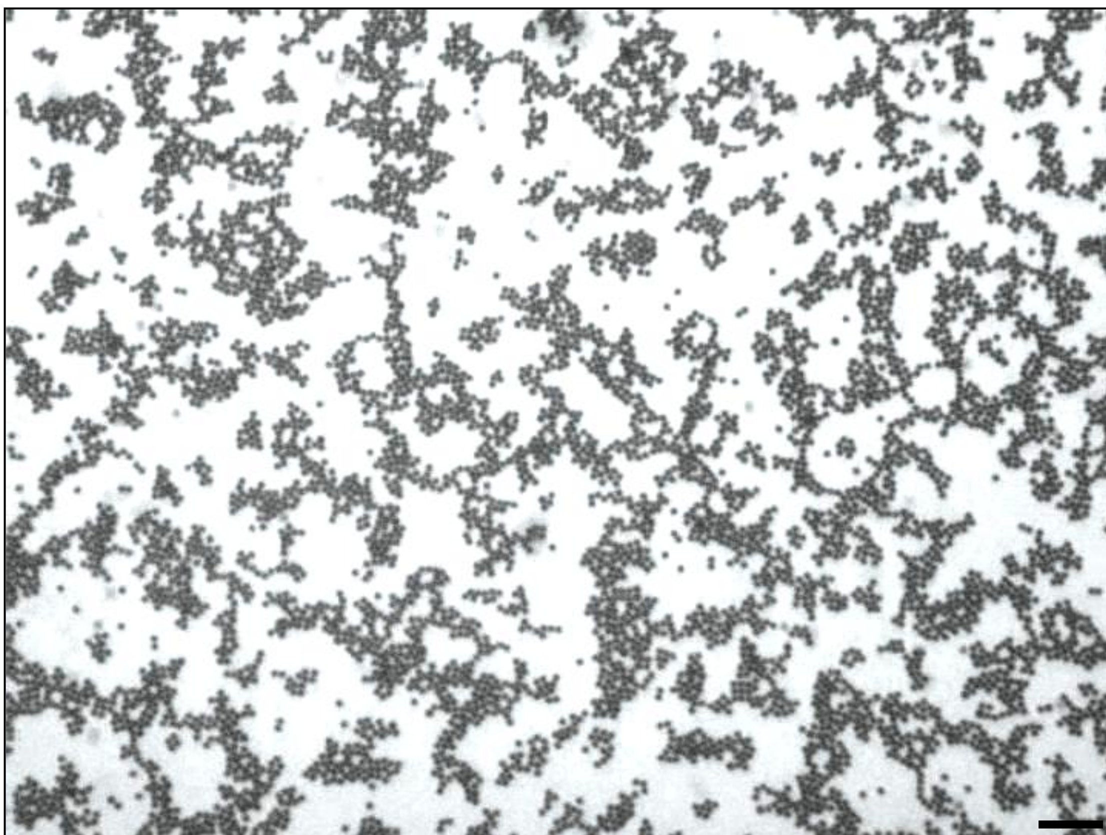

Fig. 4. 31. Optical microscopy image of a monolayer of 3 μm PS- latex particles at the air-water interface 5 min after spreading in a Langmuir trough. Scale bar shows 50 μm.

After 15 min had been allowed to elapse, the monolayer was compressed at a rate of 2 cm^2/ min from 79 cm^2 to 20 cm^2. At large areas, the surface pressure was practically unaffected by the presence of the monolayer as interactions between the particles were minimised by their large separation. At ~ 40 cm^2, the monolayer had jammed as a close packed monolayer was formed resulting in the first knee in the isotherm. Compression of the monolayer beyond this point resulted in a rapid rise in surface pressure (less gradual than that observed for plate- like particles) and what appeared to be creasing of the monolayer as shown by the dark lines running at angles of ~ 45 ° with respect to the compressing barriers as shown in Fig. 4. 33 (b). At the second knee, the creasing appeared to occur both diagonally and vertically, with a much greater magnitude than that observed at a lower pressure consistent with the early stages of buckling. At a surface pressure of 42 mN/ m, occurring just after the second knee in the isotherm, significant buckling of the monolayer occurred with the peaks running vertically. It was possible to measure a peak to peak wavelength

of ~ 200 μm. This wavelength was found to be consistent for all measurements made between surface pressures of 42 mN/ m and 62 mN/ m where the extent of buckling was even greater; demonstrating that only the amplitude of the buckles is increasing which is supported by the increasingly out of focus appearance of the buckles. Monolayer creasing during the rapid rise in pressure between the first and second knee in the isotherm can be said to be the initial stages of monolayer buckling. At the second knee in the isotherm, the pressure is relieved to some extent by an upward motion of the particles into air; this effectively reduces the number density of particles on the surface of the water. [82] After compression, the monolayer was expanded at the same rate immediately after compression. Further compression-expansion cycles were then carried out; in each case 15 min was allowed to elapse before compression. As shown in Fig. 4. 32, the compression and expansion isotherms do not coincide, especially for the first compression- expansion cycle. This demonstrates that there was significant hysteresis due to irreversible aggregation of the particles; such aggregation and hence hysteresis was not present when the monolayer was not compressed beyond the second knee in the isotherm, i. e., by assigning a target pressure below ~ 30 mN/ m as observed also for the ovals, discs and rectangles. During expansion of the monolayer, the aggregates eventually fragmented into large particle rafts, within which the particles were still hexagonally close packed. The area of the trough occupied by the particles was therefore reduced; hence the surface pressure fell rapidly at small areas as the monolayer fragmented. Because the particles already exist as aggregates, further compression simply resulted in the jamming of the aggregates and therefore occurs at much smaller areas with subsequent compression- expansion cycles following a similar path. In addition to particle aggregation, it is important to note that after the first compression, dense white regions of latex particles were observed in the vicinity of the trough barriers forming deposits on the stainless steel surface due to extensive folding of the monolayer, similar to the findings reported by Hunter *et al.* for esterified silica particles. [113]. This accumulation of latex particles persisted during expansion of the monolayer and simply fragmented at large areas with the fragments observed to be black in appearance due to the occurrence of multiple layers formed after folding, therefore in addition to the presence of hysteresis in the isotherms attributable to the formation of particle aggregates, the contribution of the folding of the monolayer at the trough barriers also contributed to the hysteresis as observed for

the plate- like photoresist particles at the air- water interface. During the initial stages of expansion, the surface pressure fell more slowly (over an area of ~ 2 cm^2) before falling sharply resulting in an almost vertical drop in pressure. The slower fall in pressure resulted from the relaxation of the buckled monolayer back into the plane of the interface and further expansion, where the pressure fell more sharply, resulted from the disengagement of the particle to particle contacts as the monolayer fragmented.

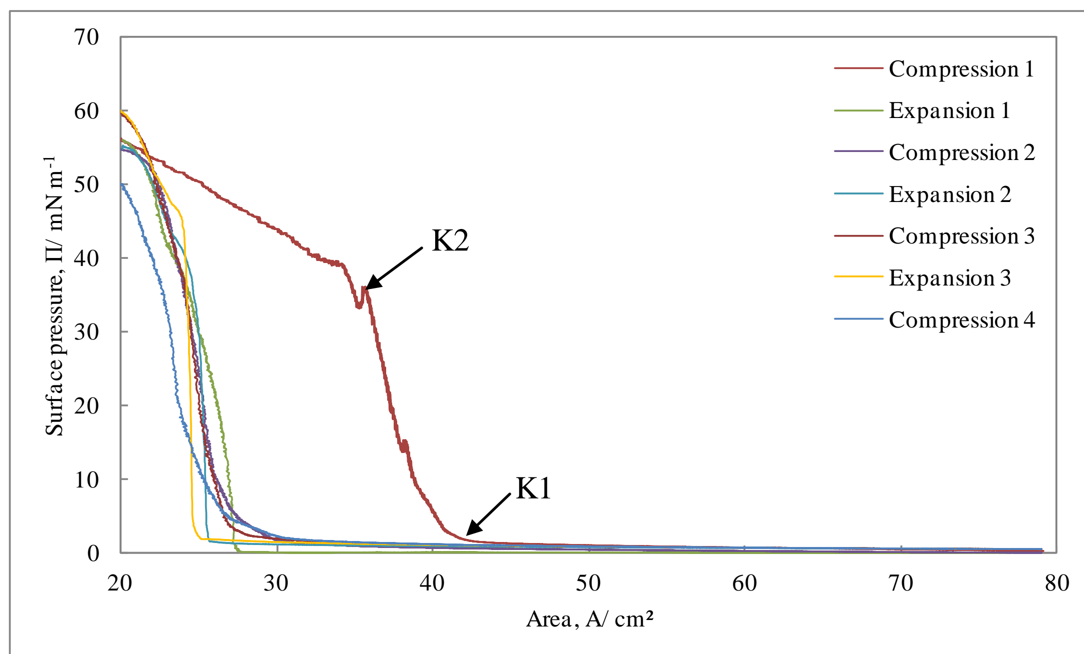

Fig. 4. 32. Isotherms resulting from repeated compression- expansion cycles of a monolayer of 3 μm PS- latex particles at the air-water interface. For clarity, further compression cycles are not shown- it is sufficient to mention that these isotherms fell within those already shown.

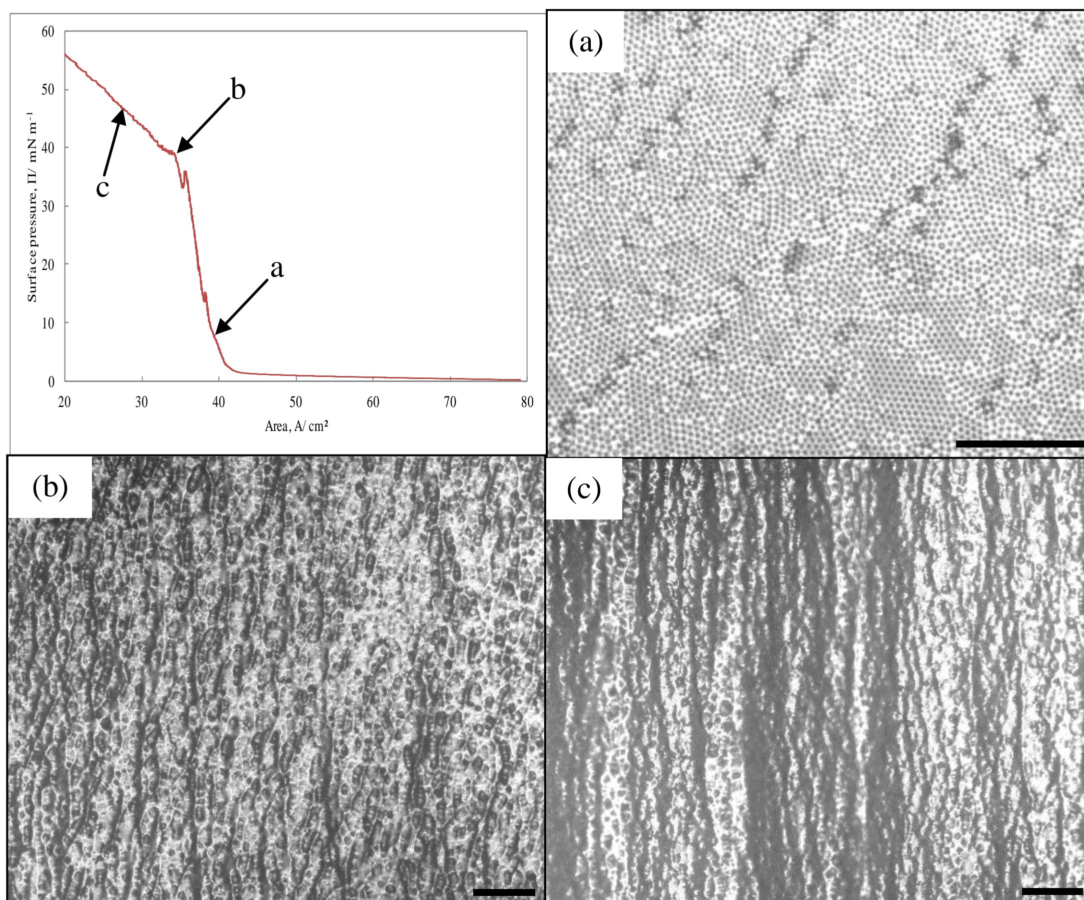

Fig. 4. 33. Optical microscopy images of a monolayer of 3 μm PS- latex particles at an air- water interface during compression in a Langmuir trough. The images labeled a, b and c were obtained at areas shown on the isotherm in the top left with the corresponding labels. Scale bars show 50 μm.

The spherical particles exhibited many similarities to the non- spherical particles studied so far; in all cases jamming of the monolayer occurred followed by a rapid rise in pressure- however this was more gradual for the plate- like particles. At the second knee in the isotherms, the monolayers underwent buckling; however in the case of the plate- like particles, creasing and buckling of the monolayers were accompanied by tilting and flipping of the particles followed by ejection of some of the particles from the interface. The plate- like particles were able to relieve some of the pressure during compression by tilting and flipping giving rise to a more expanded isotherm; in addition monolayers composed of oval and rectangular particles were able to reorientate during compression resulting in an even more expanded isotherm. Unlike the spherical particles at the air- water interface, oval and rectangular shaped particles exhibited a tendency to become entangled, thus locking the monolayer after compression which when expanded retains its area;

however the higher aspect ratio rectangles exhibited a tendency to expand elastically to some extent (Fig. 4. 27).

4. 4. Summary of the main findings

Monolayers of plate- like microparticles at the air- water interface rapidly formed aggregates of interconnected networks resulting from a strong capillary attraction between them. The origin of this capillary attraction is attributed to the roughness of the particle surface following development of the photoresist during the fabrication of the particles and also the shape of the particles. The particles consisted of both flat and rounded faces and were found to be orientated with either their flat or rounded face in the air or oil phase. Plate- like microparticles with oval or rectangular geometry exhibited a tendency to form ordered domains of tip to tip or side to side contacts. Side to side contacts were more favoured by the rectangular particles, as this allowed the particles to interact over a larger area, whereas the more rounded oval shaped particles tended to favour tip to tip contacts. Once the particles formed an interconnected network, they could no longer reorientate.

The disc shaped microparticles could stabilise emulsion droplets by forming dense layers on the droplet surface. Only transient foams could be generated due to stabilisation by electrostatic repulsion between the foam film surfaces rather than by the presence of particles. The particle contact angle was estimated to be ~ 90 ° and therefore the particles are not expected to stabilise foams effectively. Emulsion droplets of water in tetradecane could be stabilised more effectively with the surface of the emulsion drops densely populated by the discs.

The plate- like microparticles exhibited several similarities and differences to spherical latex particles undergoing compression and expansion in a Langmuir trough. For all of the particle shapes investigated, monolayers underwent jamming followed by a rapid rise in surface pressure until the monolayers underwent buckling at the second knee in the isotherm (the so called collapse pressure). The flat disc, oval and rectangular particles however were also able to tilt and flip at the interface during compression relieving some of the compressive stress. Oval and rectangular particles always flipped around their long axes in contrast to the ellipsoidal particles investigated by the group of Vermant where the ellipsoids were found to flip such that their long axes were submerged in the water. [93] The higher aspect ratio ovals

and rectangles resulted in broader isotherms than those obtained for spheres and discs. This results from a tendency for the higher aspect ratio particles to adjust their positions during compression in order to reduce the stresses resulting from compression. These higher aspect ratio particles did not adopt a particular direction during compression; instead the orientation of the particles was random due to compression of an interconnected network of aggregated particles formed after spreading. The broader isotherms resulting from the different shapes of particles used followed the order rectangles> ovals> discs> spheres, with the rectangles giving the most expanded (broader) isotherm. The higher aspect ratio rectangles and ovals displayed a tendency to become entangled after compression of the monolayers resulting in retention of the monolayer area during expansion. Monolayers of flat oval shaped particles exhibited important differences at the oil- water interface. Unlike the air- water interface, there was very little hysteresis between successive compression- expansion isotherms and the monolayer responded elastically during expansion of the monolayer; in addition unlike the air- water interface, no particles were ejected from the interface. Like those at the air- water interface, there was no tendency for the plate- like particles to adopt a particular orientation during compression at the oil- water interface. Thinner discs composed of SU- 8 photoresist did not exhibit a rapid rise in pressure during compression of their monolayers. Many of the particles were lost during spreading, and the monolayer resisted jamming by flipping- which was much more extensive than that observed for the thicker particles.

4. 5. Conclusions

Plate- like photoresist microparticles with different shape, aspect ratio and thickness were fabricated by photolithography and their behaviour at the air- water and oil- water interfaces was investigated. The effect of particle geometry on the structure of monolayers at the liquid interface was studied at rest or during compression/ expansion in a Langmuir trough by direct microscopy observations. The ability of discoid particles to stabilise foams and emulsions was also tested. The main conclusions from the obtained results are summarised below.

Plate- like particles made of photoresist by photolithography have significant surface roughness which impacts strongly on the particle behaviour and interactions at the

liquid interface. The roughness leads to a large contact angle hysteresis and prevents the particles from attaining their equilibrium configuration at the liquid interface. Particles lay flat at the interface with an apparent macroscopic contact angle of ~ 90 ^{o} and are almost equally immersed in both adjacent fluid phases.

Particle interactions at the liquid interface are dominated by the capillary attraction due to the undulated three phase contact line caused by the surface roughness. The capillary attraction prevails over electrostatic repulsion, leading to substantial aggregation of the plate- like particles at the air- water and even the oil- water interface. Particle shape and aspect ratio have pronounced effect on the structure of the aggregates. The fraction of non- spherical particles aggregating in a tip- to- tip configuration decreases with the increase of the aspect ratio. The opposite trend is observed for the fraction of particles aggregating in a side- to- side configuration. Side- to- side aggregation is preferred by non- spherical particles with aspect ratio larger than 2 due to stronger capillary attraction than that of tip- to- tip aggregation.

The shape and thickness of the plate- like microparticles has significant implications on the monolayers undergoing compression and expansion in a Langmuir trough. Particles with higher aspect ratios such as ovals and rectangles gave broader isotherms than those composed of discs or spheres, due to the tendency for the particles to reorientate during compression. Flat microparticles are able to undergo flipping and tilting at the interface during compression and higher aspect ratio particles flip exclusively such that their long axes are parallel with the interface. Thinner photoresist discs are easily removed from the interface by flipping during compression which is much more extensive than that observed for thicker particles. Compression of plate- like particle monolayers at the air- water interface leads to significant losses of interfacial particles due to their ejection into the water phase. This effect is more pronounced for thinner plate- like particles of SU- 8 photoresist. Particle ejection is not observed for monolayers at the oil-water interface.

The plate- like particles studied are not efficient in stabilising foams because their apparent macroscopic contact angle at the air- water interface is ~ 90 °; therefore the bubbles must be almost completely covered by particle mono- or multilayers to prevent coalescence. The observed release of the surface stresses in the monolayers during compression by particle flipping and ejection suggests that these particles

would not be very effective in preventing the bubble shrinking responsible for disproportionation (Ostwald ripening) in foams. The particles that were studied can stabilise emulsions with a dense coverage of the droplets by the particles.

CHAPTER 5 THE FABRICATION OF JANUS PLATE- LIKE MICROPARTICLES

5. 1. Introduction

It was demonstrated in Chapter 3, that microparticle arrays attached to a solid substrate via a sacrificial layer can be generated before the final stage of particle release. This gives an opportunity for asymmetric surface modification of the exposed half of the particle surface while the particles are still attached to the solid substrate. Subsequent release from the substrate should give Janus plate- like microparticles with two homogeneous but different faces. A summary of the approaches taken for Janus microplate preparation using photolithography is illustrated in Fig. 5. 1. Various approaches for the modification of one surface of the photoresist patterns are explored. These include application of various metal coatings, silanes, polyelectrolytes and colloidal particles, including magnetic particles. The photoresist surface is capable of binding silane groups such as DCDMS to render the surface more hydrophobic, and aminosilanes such as APTES to generate a surface rich in amino groups which are capable of undergoing further reactions. Certain metals possess excellent adhesion properties to the photoresist surface: these include chromium, aluminium and titanium. The surface of the cured photoresist can be exploited due to its negative charge arising from the presence of dissociated phenolic OH groups. [148] The AZ photoresist used in this work is expected to be weakly negatively charged with a zeta potential of ~ -30 mV at pH 6. 5 after exposure and development. [149] This value closely resembles SU- 8 photoresist, where the zeta potential was found to be -36 ± 0. 5 mV. [69, 150] It should be possible therefore to bind oppositely charged polyelectrolytes such as PAH and charged colloidal particles. The application of these approaches and the possibility of releasing the modified particles is investigated.

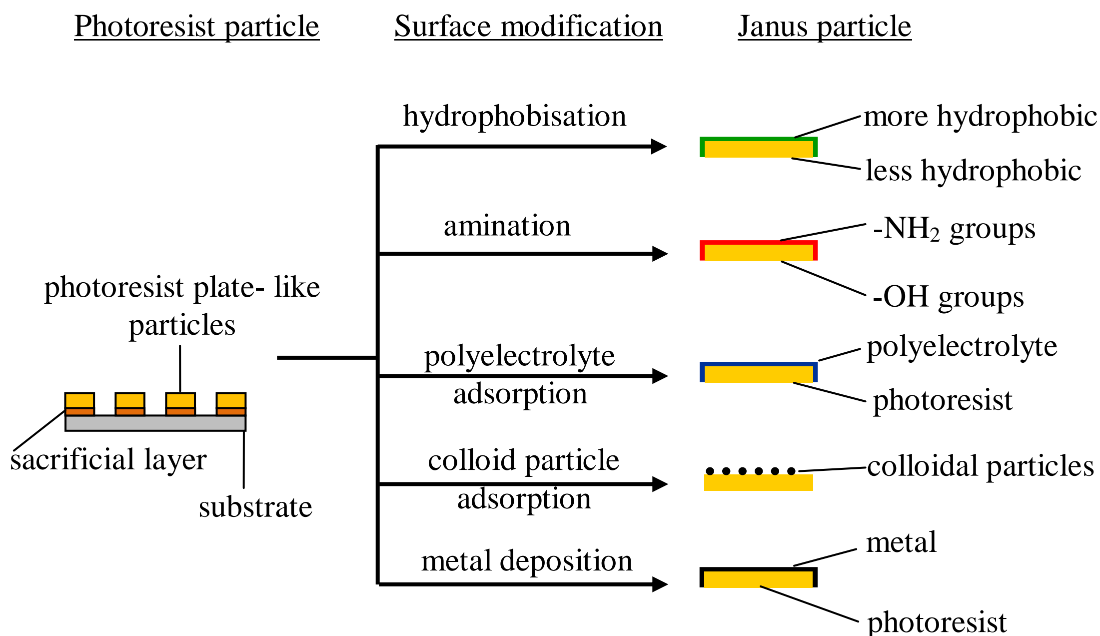

Fig. 5. 1. Schematic showing the Janus particle types generated by different surface modifications applied on a patterned photoresist surface.

The scheme for Janus microplate preparation shown in Fig. 5. 1 could be elaborated further for the fabrication of even more complex Janus particles (Fig. 5. 2). In this approach, the fabricated AZ negative photoresist microparticle pattern that is still attached to the substrate, is spin coated with AZ image reversal photoresist (acting as a positive photoresist) which is then exposed through a photomask that has been designed to permit a particular portion of the negative photoresist array to be coated with the positive photoresist after exposure and development of the latter. The positive photoresist then acts as a sacrificial mask that permits only particular portions of the negative photoresist particles to be modified. After removing the positive photoresist, the Janus microparticles are liberated from the substrate by dissolution of the sacrificial layer.

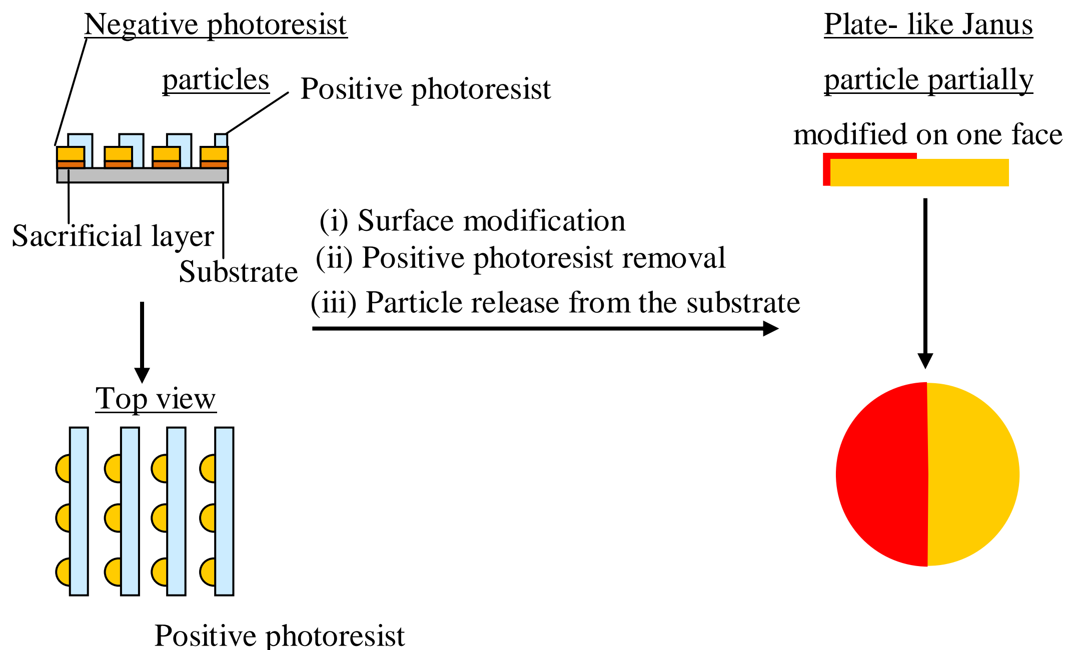

Fig. 5. 2. Schematic showing the generation of Janus particles by the modification of a portion of the top surface of negative photoresist particles. The surface of the microparticle array is partially coated with a positive photoresist mask and the entire surface is then modified (i), the positive photoresist is removed leaving behind a modified and unmodified negative photoresist surface (ii), the sacrificial layer is dissolved and the Janus microparticles are liberated from the substrate (iii).

One can conclude that photolithography could be used as a platform for the preparation of a huge variety of simple or complex Janus plate- like particles. This possibility still remains largely unexploited. Our aims are (i), to investigate the possibilities of photolithography for the fabrication of Janus microplates (a proof of principle) using the approaches illustrated in Figs. 5. 1 and 5. 2 and (ii), to study the behaviour of Janus plate- like microparticles if their fabrication in (i) has been successful.

5. 2. Preparation of Janus microplates with homogenous faces

5. 2. 1. Asymmetric functionalisation by chemical grafting

The chemical structure of the photoresist is shown in Fig. 5. 3. The composition of the microparticles fabricated from AZ type photoresists consists of a polymer resin formed by the polymerisation of phenol and formaldehyde. This gives a resin consisting of hydroxyl functional groups which are able to bind other chemical groups by means of a covalent bond. Usually silanes are used for this. An example is shown in Fig. 5. 4 with respect to DCDMS binding to the hydroxyl groups of the photoresist; in this case, the hydroxyl groups are replaced with methyl groups thus rendering the surface hydrophobic.

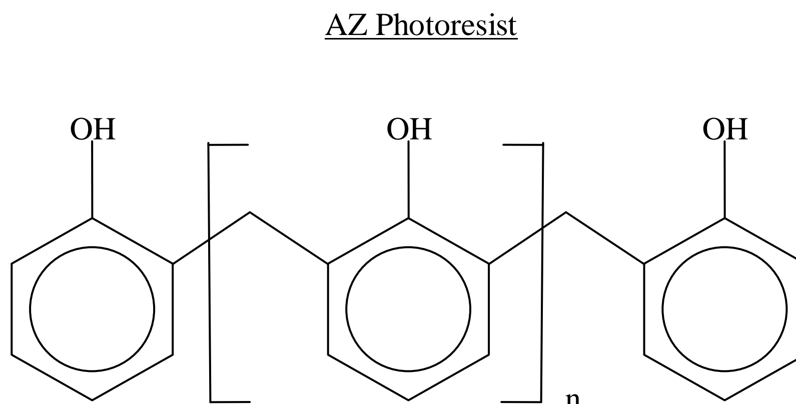

Fig. 5. 3. Chemical structure of the AZ photoresist resin remaining after exposure and development.

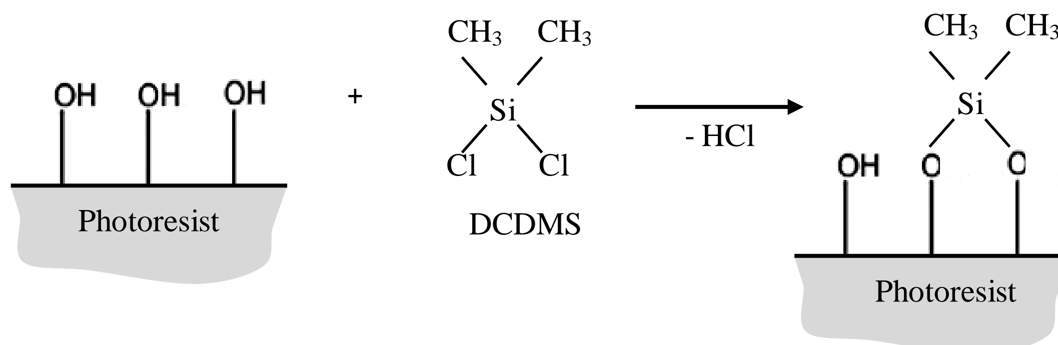

Fig. 5. 4. Schematic showing the binding of DCDMS to the surface hydroxyl groups of the AZ type photoresist.

The hydrophobisation of the top surface of the photoresist particles by application of DCDMS vapour is described in the materials and methods section of this thesis. In order to demonstrate the effectiveness of this approach, contact angles of sessile water drops on the hydrophobised surface in air were measured. For DCDMS treated photoresist, the advancing and receding contact angles were 104 ± 1 ° and 84 ± 1 ° respectively. The average contact angles for untreated photoresist and photoresist treated with DCDMS are 56 ± 38 ° and 94 ± 10 ° respectively; therefore the values for DCDMS treated photoresist are ~ 40 ° greater than the untreated photoresist. A significant reduction of the contact angle hysteresis on the hydrophobised photoresist surface was also observed.

Janus particles with oval shape were produced by rendering the top surface hydrophobic by DCDMS treatment, and their behaviour at the tetradecane- water interface was investigated. Despite the DCDMS treatment however, there was no tendency for the particles to behave differently in comparison to untreated ovals at the tetradecane- water interface; aggregates were formed with both tip- to- tip and side- to- side contacts and the rate of aggregation did not change.

5. 2. 2. Asymmetric functionalisation by polyelectrolyte adsorption

The approach used here involved treating the surface of pre- fabricated photoresist rectangles with polyelectrolytes (see Fig. 5. 1). Untreated photoresist is expected to be negatively charged due to the presence of ionised hydroxyl groups and therefore application of a positively charged polyelectrolyte such as PAH (polyallylamine hydrochloride) will reverse the surface charge following electrostatic adsorption, and permit the possibility of binding negatively charged particles such as silica to the treated photoresist surface. This approach therefore will allow the surface of the photoresist particles to undergo charge modification, or to introduce a second type of particle to the surface. In addition, a layer- by- layer assembly approach, for example, by applying a negative polyelectrolyte such as PSS (poly [sodium- 4-styrene sulfonate]) onto the PAH treated surface can be performed. The chemical structure of these polyelectrolytes is shown in Fig. 5. 5. By modifying the charge on the photoresist surface, it is anticipated that the surface can be further modified by a coating of smaller colloidal particles with the appropriate charge.

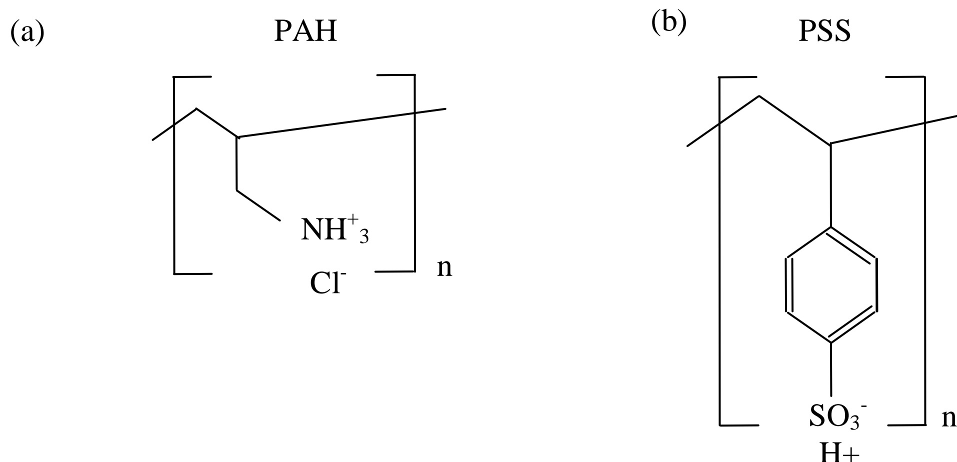

Fig. 5. 5. Chemical structure of the polyelectrolytes used. Polyallylamine hydrochloride (PAH) (a) and poly [sodium- 4- styrene sulfonate] (PSS) (b).

To test the efficiency of binding positively charged PAH to the photoresist surface, photoresist rectangles, after treatment with PAH, attached to a silicon substrate were immersed in a suspension of negatively charged silica particles. Photoresist that was not treated with PAH was very sparsely coated and the particles were not distributed uniformly over the surface (Fig. 5. 6). Aggregates of various sizes of silica particles on both the photoresist and silicon surface of the substrate were observed. After immersion of the photoresist coated substrate in the positively charged PAH polyelectrolyte, there was a significantly greater density of bound silica particles due to the electrostatic attraction between the oppositely charged groups (Fig. 5. 6). The number density of the bound silica was uniform over the entire surface. Application of PSS following PAH treatment of the photoresist surface resulted in a very significant decrease of the bound silica confirming (Fig. 5. 6 e and f) the reversal of the surface charge. It is expected that the the PSS is dissociated and therefore after binding, sodium ions are present in solution which can screen the electrostatic interactions between the polymer chains resulting in an increasing film thickness; however for the diluted solution used here, the ionised groups on the PSS polyelectrolyte are not expected to be screened significantly. [155]

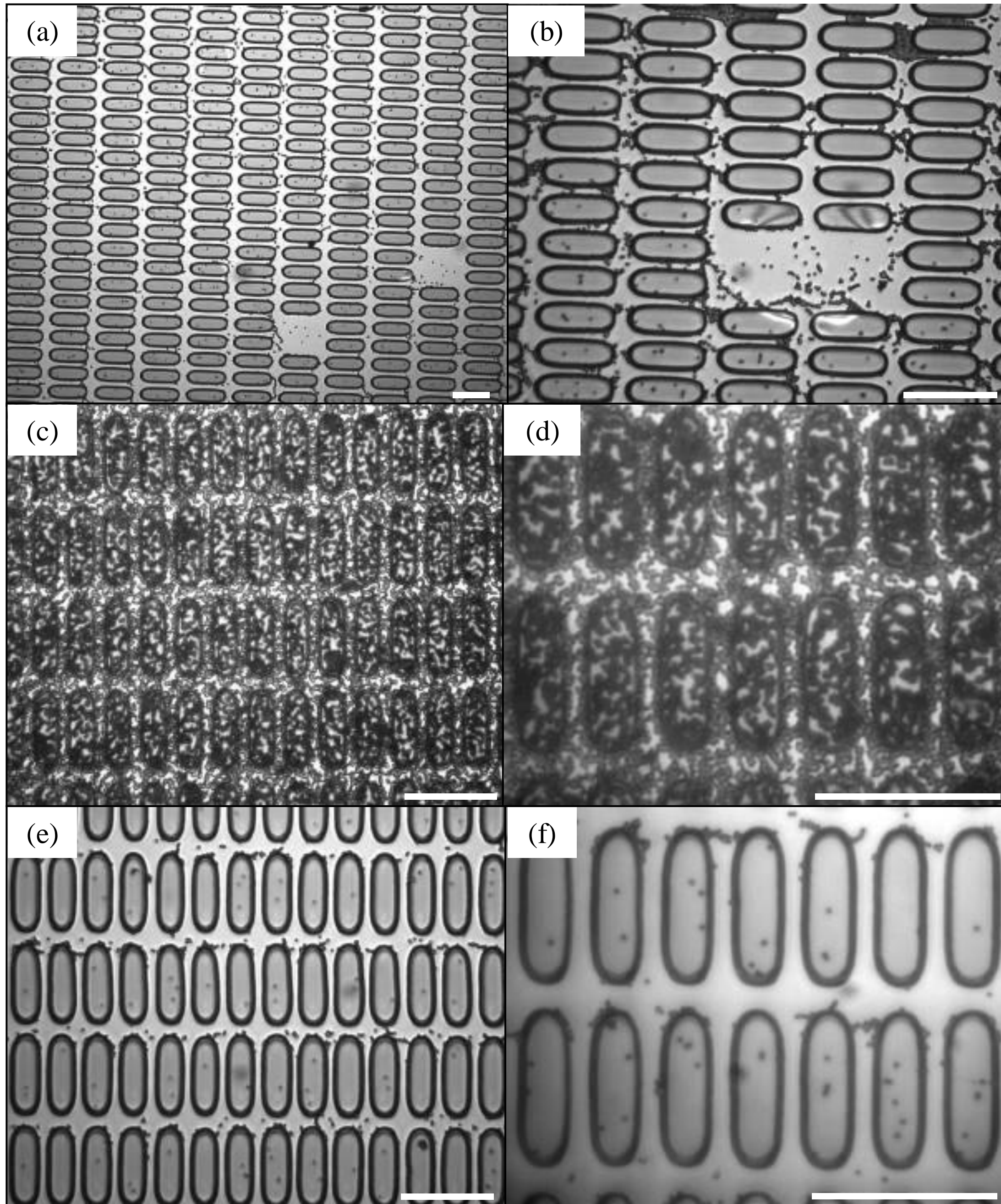

Fig. 5. 6. Optical microscopy images of untreated rectangle shaped photoresist attached to a silicon substrate via a sacrificial layer of LOR after immersion of the substrate in a silica particle suspension (a and b) and after treatment of the photoresist surface with PAH followed by immersion of the substrate in a silica suspension (c and d). The charge on the PAH treated surface was then reversed by application of PSS polyelectrolyte followed by immersion in a silica particle suspension (e and f). Scale bars show 50 µm.

The above experiments prove that PAH binds to the exposed photoresist surface, hence Janus microplates with one face covered with positively charged PAH and the other of unmodified photoresist could be produced.

Monolayers of the PAH treated photoresist rectangles at the decane- water interface were investigated. As shown in Fig. 5. 7, the rectangles had a strong tendency for side to side stacking. It was estimated from the images that ~ 55 % of Janus rectangles are in side- to- side (S- S) configuration and only ~ 5 % are in tip- to- tip (T- T) configuration. The aggregation of rounded rectangle particles with homogeneous surfaces (both faces the same) at the air-water interface were observed with ~ 27 % in S- S and ~ 9 % in T- T configuration (see Table. 4. 1). This suggests that Janus microplates may behave differently than homogeneous plate- like particles at liquid interfaces. More experiments are needed to quantify this, and reveal the reasons for the observed differences. This could be an interesting direction for future investigation.

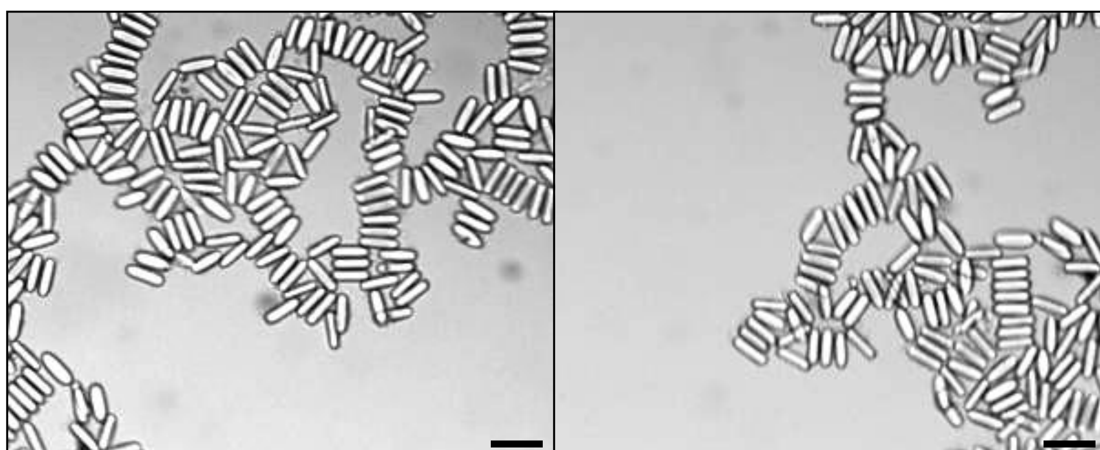

Fig. 5. 7. Optical microscopy images of Janus rectangle shaped photoresist particles (AZ nLOF 2070) treated on one face with PAH polyelectrolyte, after spreading at the decane- water interface. Scale bars show 50 μm.

5. 2. 3. Magnetic Janus plate- like microparticles

The ability to render the particles magnetic may allow the particles to be manipulated by an external magnetic field. Magnetic Janus particles could be realised by binding Fe_3O_4 particles to one face of the photoresist rectangles following treatment with suitable polyelectrolytes. Particles of this type are expected to be weakly positively charged with a zeta potential of 7 mV at a pH of 7 [152], therefore they should bind preferentially to the PSS treated photoresist surface. Janus particles

of this type may be manipulated with a magnetic field, allowing the monolayers of particles to align in the field. A suspension of the Fe_3O_4 particles with diameters of > 50 nm was prepared with a concentration of 1 mg/ cm^3 in pure water. After immersing the untreated photoresist in the suspension, the weakly negatively charged photoresist surface did not efficiently bind the iron oxide particles and the particles were easily washed away from the surface; however, the binding capacity of the photoresist surface was enhanced by application of PAH followed by the negatively charged PSS polyelectrolyte after adjusting the pH of the iron oxide suspension to 3 using HCl (Fig. 5. 8). At this pH, the zeta potential of the particles is ~ 25 mV. [152] It was found that when the surface of the photoresist was oxidised using 1M nitric acid by immersion for several days without the application of polyelectrolytes, the binding capacity of the particles to the photoresist surface was improved even further giving an estimated coverage of ~ 90 % as shown in Fig. 5. 8 (c and d). This alternative approach was motivated due to the fact that the polyelectrolyte treated photoresist particels were difficult to release from the substrate. After immersing the oxidised photoresist with the attached iron oxide particles in NMP to dissolve the sacrificial layer and release the photoresist particles, the release was rapid and efficient and the iron oxide coating was preserved. Fig. 5. 9 shows some of the rectangles with the Fe_3O_4 particles attached to the surface suspended in NMP and water. Some interesting behavior was observed by the rectangles, for example some were connected together by the tips to resemble a horseshoe configuration. This behavior was not observed before; however bending of suspended rectangles is a common feature for the photoresist with these dimensions. The suspended rectangles were found to be very responsive to a magnetic field: when a neodymium magnet with a diameter of ~ 1cm was applied outside of the suspension contained within a Teflon tube, with the magnet in contact with the surface of the tube, the particles rapidly migrated towards the magnet.

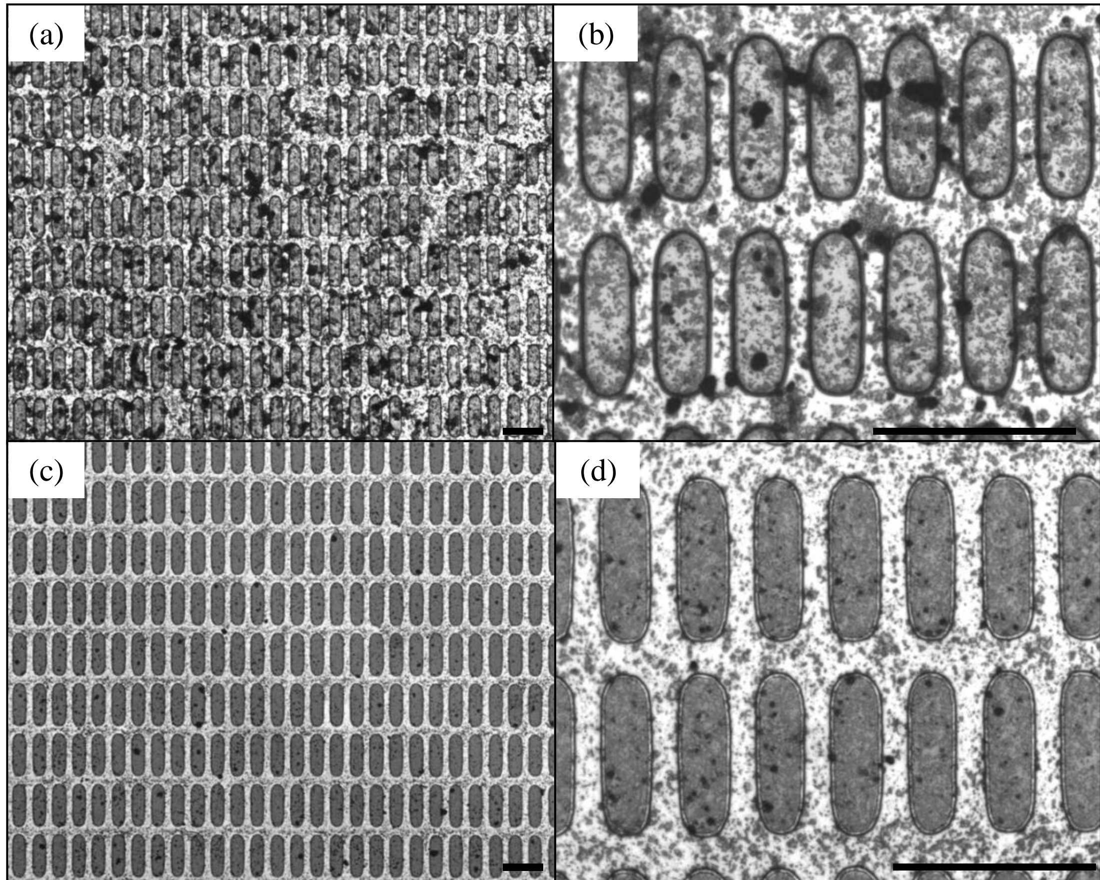

Fig. 5. 8. Optical microscopy images of rectangle shaped photoresist (AZ nLOF 2070) attached to a silicon substrate via a sacrificial layer of LOR after treatment with PAH/ PSS followed by immersion in a Fe_3O_4 particle suspension at pH 3 (a and b) and after immersion of photoresist (without polyelectrolyte), that had been oxidised with 1M HNO_3 for several days, in the same Fe_3O_4 particle suspension (c and d). Scale bars show 50 µm.

Fig. 5. 9. Optical microscopy images of rectangle shaped photoresist particles with Fe_3O_4 particles attached to one of the surfaces in NMP and water. Scale bars show 50 μm.

5. 3. Preparation of Janus microplates with one patterned face

It was demonstrated in the previous sections that photolithography can be used for the preparation of Janus microplates with homogeneous but different faces. It was found that the behaviour of such type of Janus particles at the water- fluid interface, however, was not significantly different to that of homogeneous plate- like microparticles. This could be attributed to the lack of preferential orientation of the Janus microplate faces with respect to the adjacent fluid phases. For example hydrophilic/ hydrophobic Janus plate- like particles attach to the liquid interface with the hydrophilic face immersed in water or in the non- polar phase indiscriminately. In addition, the electrostatic interactions between the PAH treated photoresist surface (hydrophilic) of the particles is expected to occur mainly between the side surfaces of the plate- like particles (the rim); therefore the influence on the capillary attraction due to the undulated three phase contact line is not strong. This situation could change significantly if only part of the plate- like face has been made hydrophobic or

hydrophilic (Fig. 5. 2). A Janus microplate with such a structure should generate significant deformations of the liquid interface due to different wetting properties in different regions of the same surface.

This part of our study is focussed on the preparation of Janus microplates with one partially patterned face using the photolithographic technique. This could be achieved by partial masking of negative photoresist microparticle arrays with positive photoresist patterns, followed by chemical modification of unmasked particle surface, removal of the positive photoresist and release of the Janus particles from the substrate as shown in Fig. 5. 10.

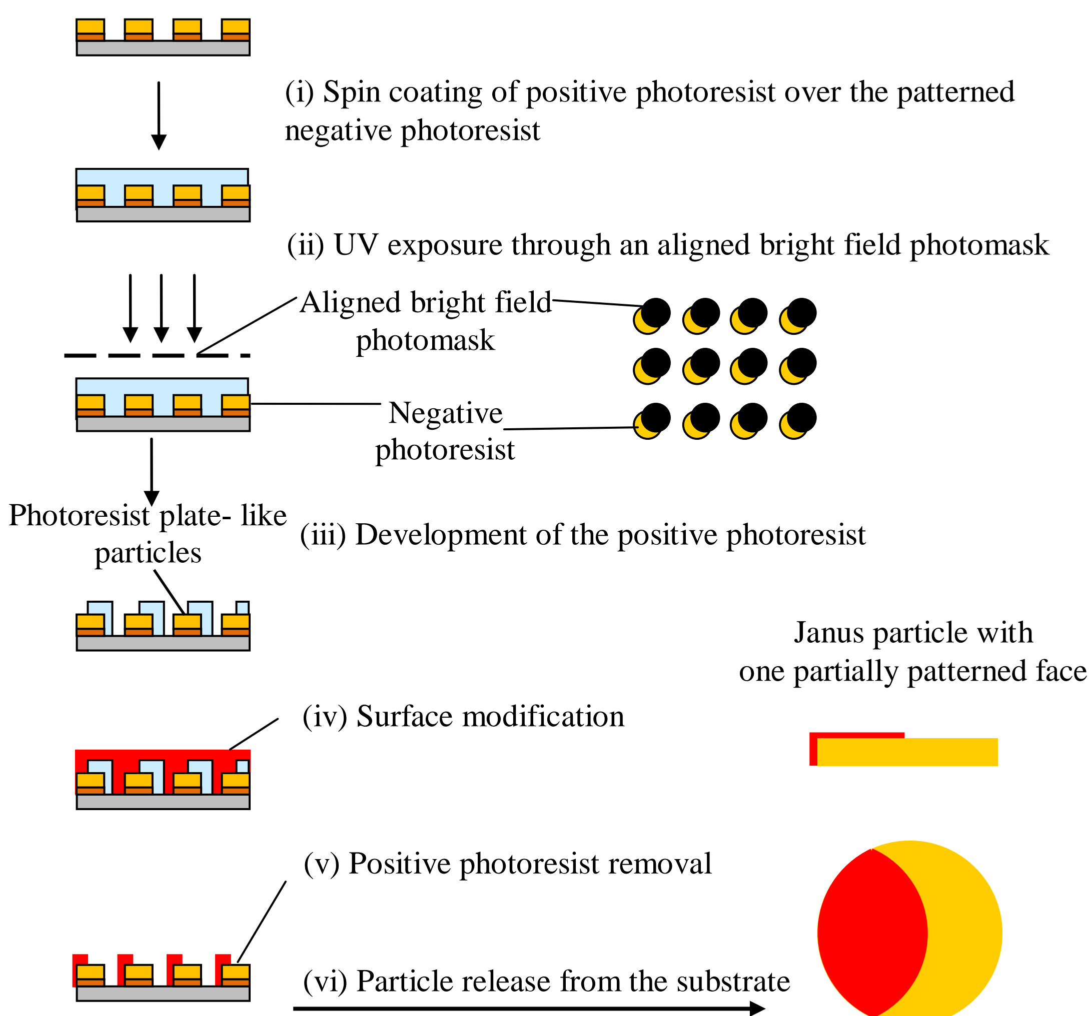

Fig. 5. 10. Schematic representation of the photolithographic process for the partial masking of a negative photoresist pattern with positive photoresist followed by modification of the surface to generate Janus particles with partial modification on one face only.

5. 3. 1. Partial masking of negative photoresist microparticle arrays with positive photoresist patterns

5. 3. 1. 1. Coating of negative photoresist disc arrays with positive photoresist

The first step was to determine if it was possible to apply a layer of positive photoresist onto an existing negative photoresist pattern. The negative photoresist discs were fabricated onto a small silicon substrate by patterning through a darkfield photomask consisting of a square array of UV transparent circles with diameters of 25 μm and 20 μm pitch. The diameter of the negative photoresist discs after fabrication was found to be 33. 0 μm ± 0. 5 μm, due to overexposure; however this was not critical for the outcome of this experiment. Before application of the photoresist, a sacrificial layer of LOR was spin coated onto the substrate, and after patterning the negative photoresist discs and hard baking (Fig. 5. 11 a), a layer of positive photoresist was applied to the top surface as shown in Fig. 5. 11 b. The positive photoresist was found to coat the negative photoresist pattern successfully, without any indication of dewetting or the presence of defects. The spin coating parameters chosen for the positive photoresist were the same as those applied to the negative photoresist.

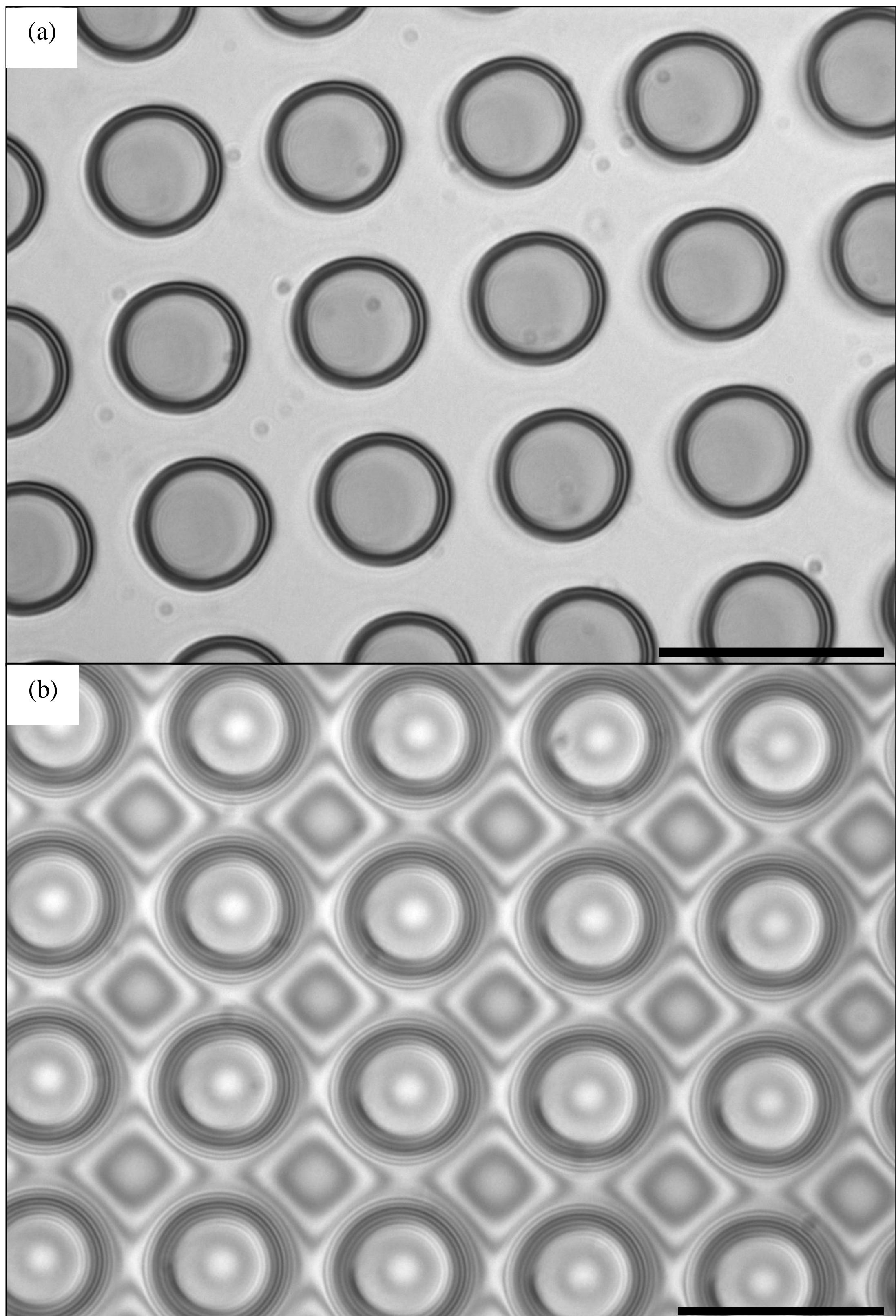

Fig. 5. 11. Optical microscopy images of negative photoresist discs attached to a silicon substrate via a sacrificial layer of LOR (a), and after coating the pattern with positive photoresist (b). Scale bars show 50 μm.

5. 3. 1. 2. Photomask alignment and pattern transfer onto the positive photoresist

The next step was to align the photomask as described in chapter 2 (Fig. 2. 5). In this method, the photomask was placed loosely over the substrate and adjusted by hand until satisfactory alignment was achieved. The positive photoresist was then exposed through the photomask. The substrate and photomask were secured to a glass backing plate. An example showing the aligned photomask on the surface of negative photoresist discs is shown in Fig. 5. 12. The focus of this approach was on demonstrating the technique of transferring an image onto the existing negative photoresist discs, rather than precise control of the photomask alignment process. As described in the next section, in order to transfer the pattern onto the positive photoresist, it was necessary to optimise the development time carefully.

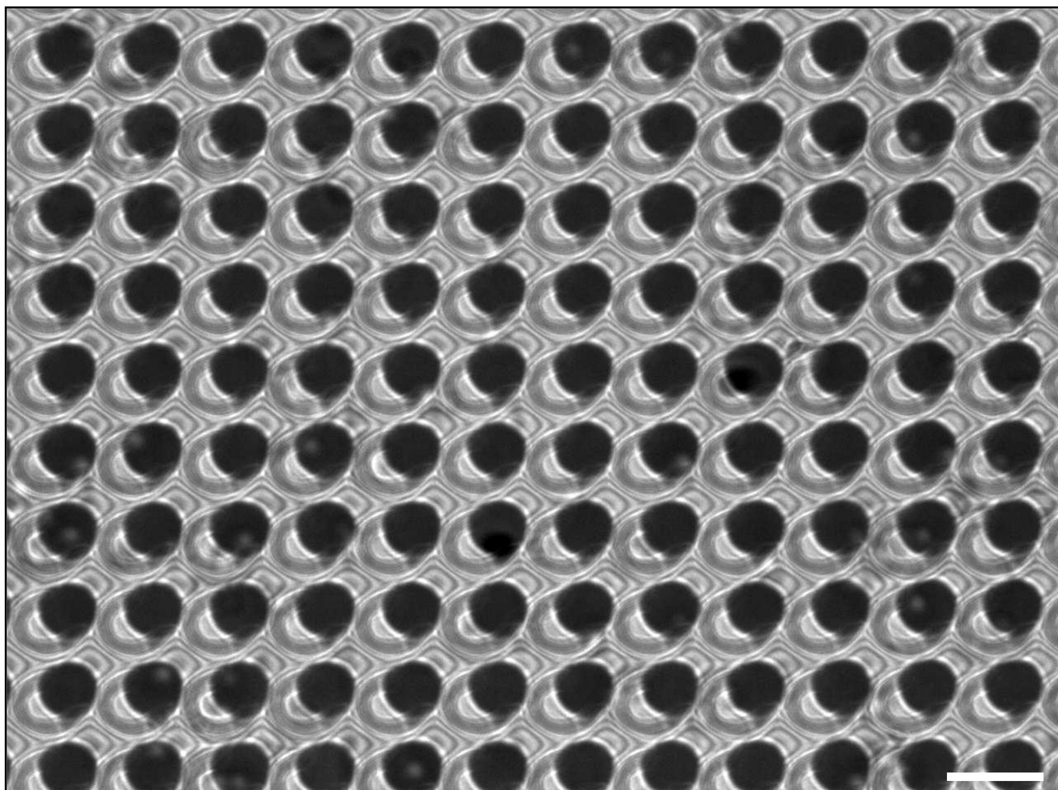

Fig. 5. 12. Optical microscopy image showing a clearfield photomask consisting of 25 μm diameter UV opaque circles on a positive photoresist layer coated over negative photoresist discs. Scale bar shows 50 μm.

This approach was found to be unsuccessful for the transfer of a uniform positive photoresist pattern on the existing negative photoresist pattern; therefore, a new photomask set up was applied by incorporating a flexible backing sheet for the substrate and minimizing deformations of the flexible photomask. This approach

significantly improved the results. Although the positive photoresist discs were successfully transferred onto the negative photoresist discs; the development time was insufficient for complete development after 60 s as shown in Fig. 5. 13. By increasing the development time, further development of the positive photoresist discs had occurred (Fig. 5. 14); however the extent of development varied at different locations of the substrate as some of the positive photoresist discs were almost completely etched away. It was also possible to observe regions of the positive photoresist that were masked and unmasked during exposure (Fig. 5. 14). The masked region clearly shows the positive photoresist discs partially covering the negative photoresist discs. Further development for a total time of 160 s resulted in complete dissolution of the positive photoresist in some regions due to the variation in development rate at different locations on the patterned surface; therefore it was decided not to develop the photoresist further in order to prevent complete loss of the photoresist pattern. Fig. 5. 15 shows a portion of the surface of the patterned photoresist after 160 s development; as can be seen, much of the exposed and developed photoresist was developed as far as the silicon surface.

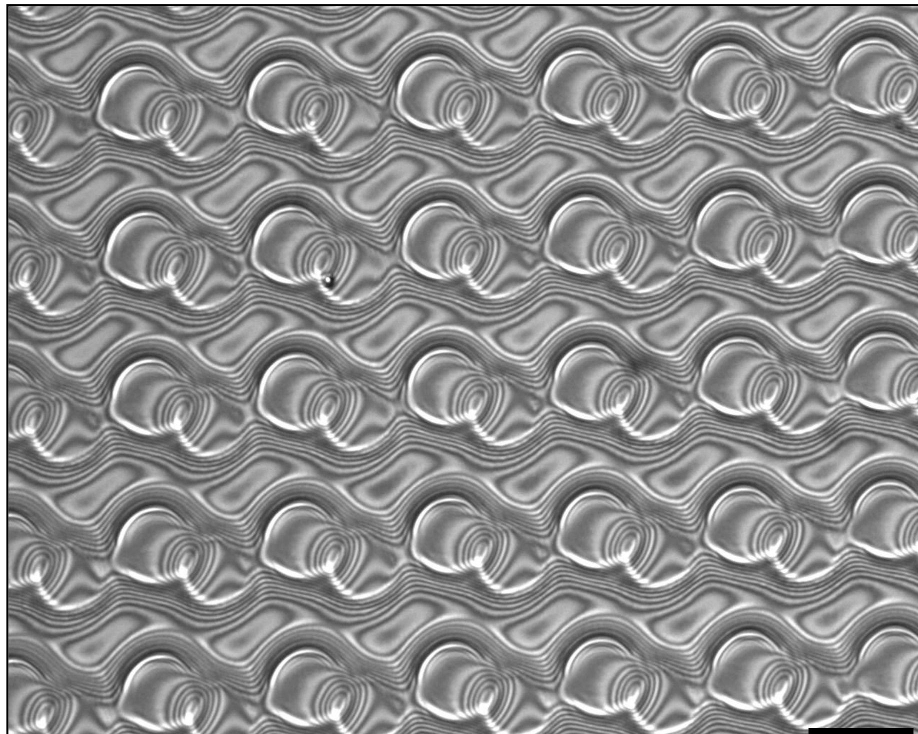

Fig. 5. 13. Optical microscopy image of negative photoresist discs coated with partially developed positive photoresist after exposure of the positive photoresist through a clearfield photomask consisting of 25 µm circles and development for 60 s. Scale bar shows 50 µm.

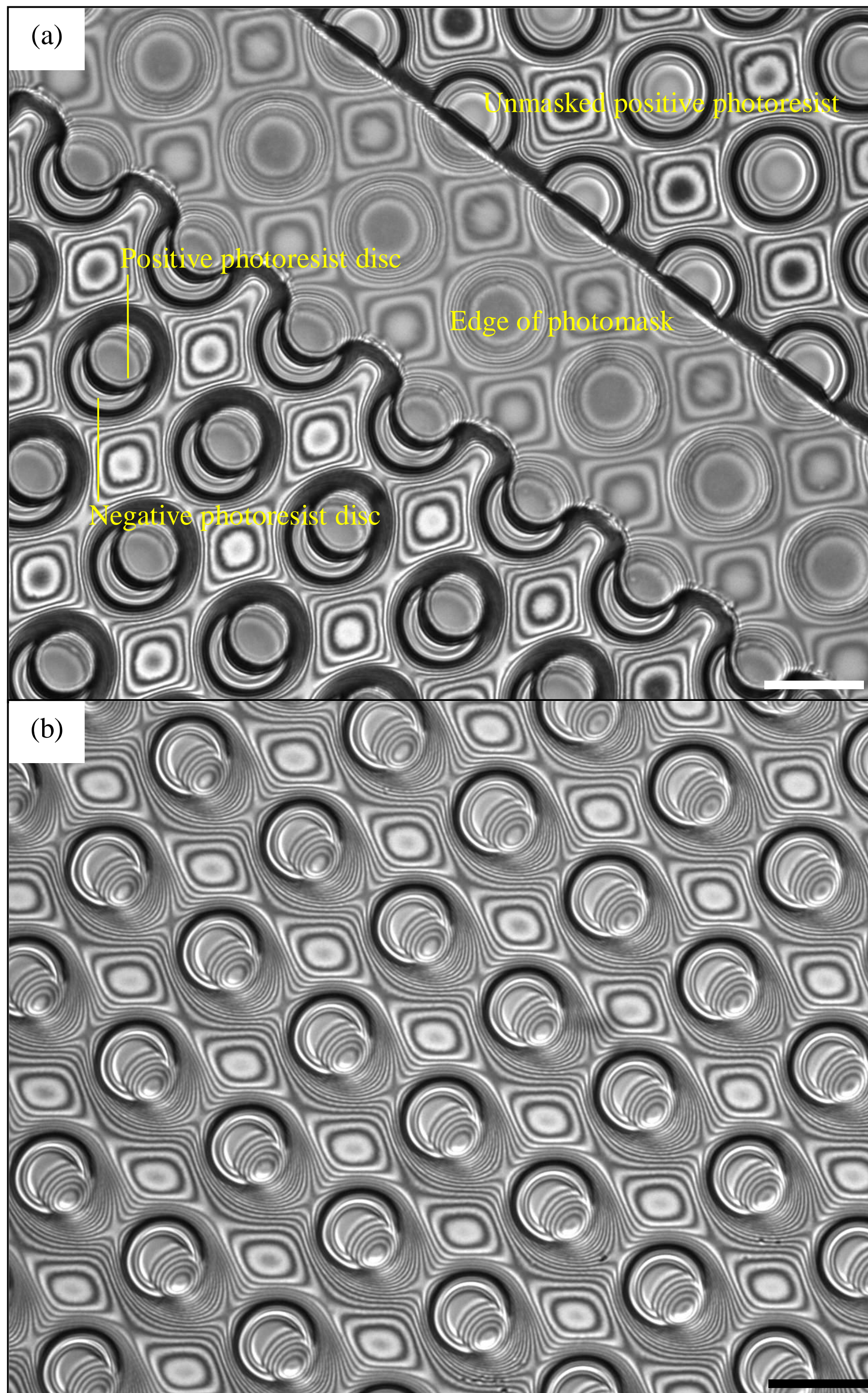

Fig. 5. 14. Optical microscopy images of negative photoresist discs coated with positive photoresist discs after exposure of the positive photoresist through a clearfield photomask consisting of 25 µm circles and development for 110 s. Substrate edge (a) and substrate centre (b). Scale bars show 50 µm.

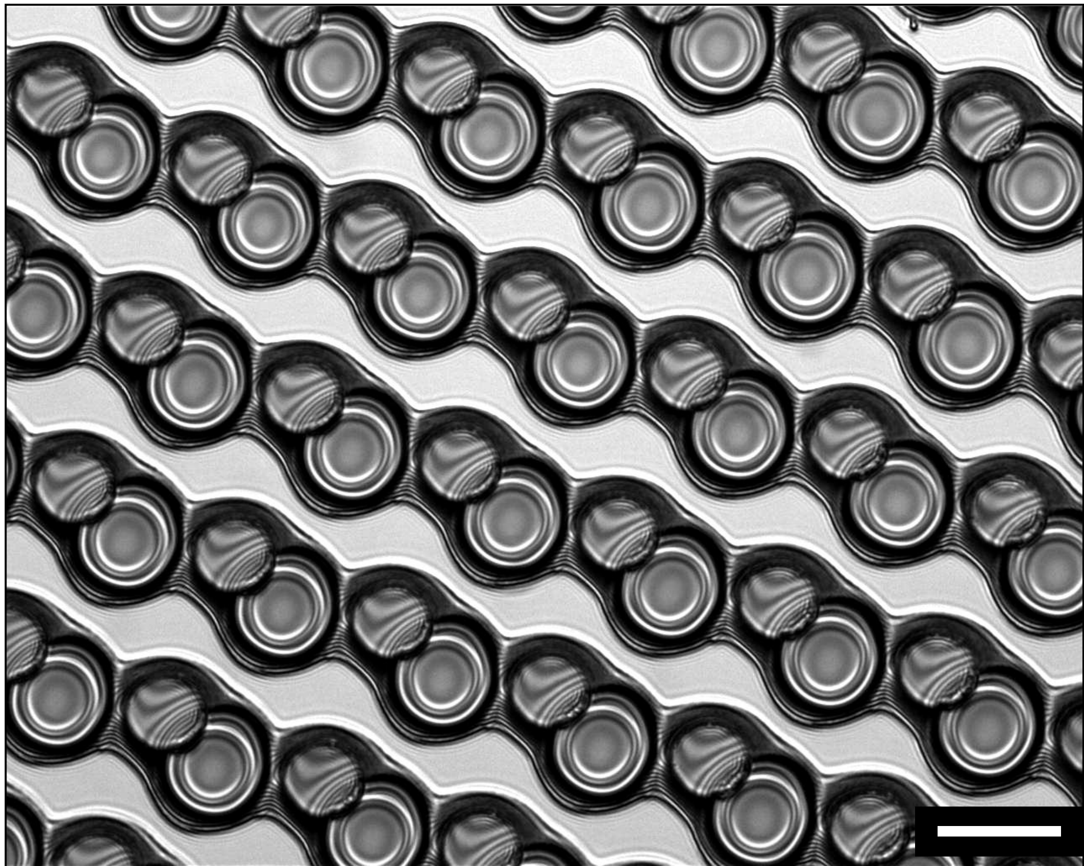

Fig. 5. 15. Optical microscopy image of negative photoresist discs coated with positive photoresist discs after exposure of the positive photoresist through a clearfield photomask consisting of 25 µm circles and development for 160 s. Scale bar shows 50 µm.

5. 3. 2. Procedures for removal of positive photoresist patterns from partially masked negative photoresist microparticle arrays

Before proceeding further with the chemical modification of partially masked negative photoresist microparticle arrays, procedures for removal of positive photoresist patterns had to be developed in order to demonstrate if partial modification of the negative photoresist surface has been successful. A simple way for removal of positive AZ photoresist recommended in the literature is by using acetone, [72] therefore this solvent was investigated first. To improve the contrast between unmasked and masked regions by the positive photoresist surface, we have treated the negative photoresist microparticle array with APTES to covalently attach amine groups to the surface as shown in Fig. 5. 16. Then we used the fluorescent dye rhodamine 6G, that strongly binds to the amine groups of APTES, before observing the patterns with a fluorescent microscope.

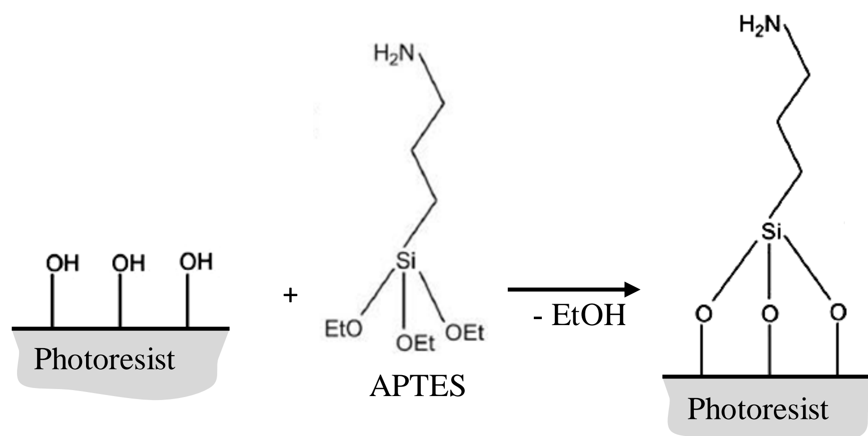

Fig. 5. 16. Schematic showing the covalent attachment of APTES to the hydroxyl groups of the photoresist surface.

It emerged that rhodamine 6G binds even stronger to the surface of the positive photoresist after treatment with APTES (Fig. 5. 17) and provided very good contrast between the patterned and bare negative photoresist surface.

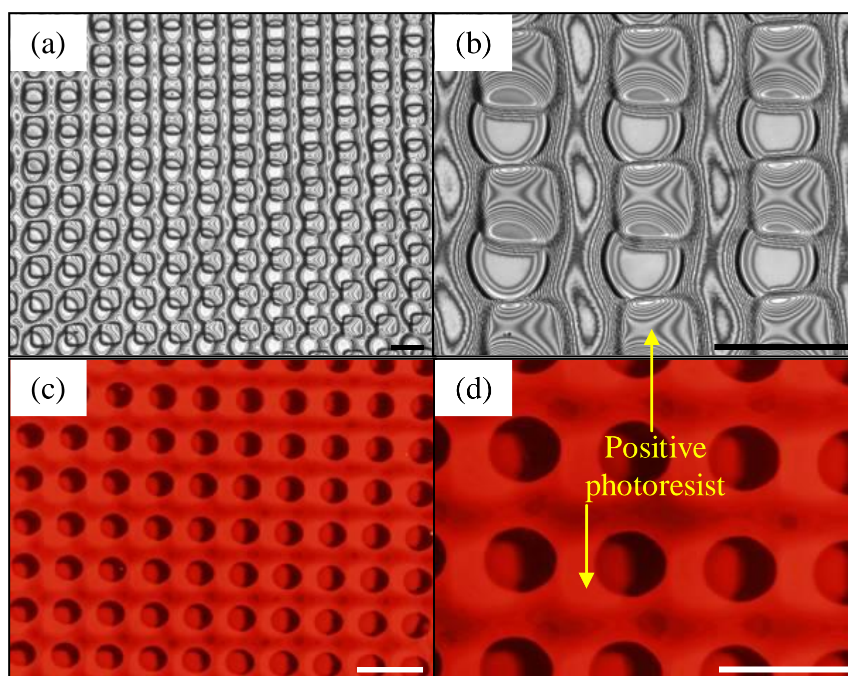

Fig. 5. 17. Optical microscopy images of negative photoresist discs attached to a silicon substrate via a sacrificial layer of LOR after coating and patterning with positive photoresist squares (a and b). Fluorescence microscopy images of the same surface after immersion in APTES and rhodamine 6G (c and d). Scale bars show 50 μm. It can be seen that the positive photoresist squares appear brighter in fluorescent light.

The immersion of the patterned negative photoresist particle array in acetone completely removed the positive photoresist; however the negative photoresist discs were damaged as a result of crack formation on their surface (Fig. 5. 18). Some of the discs had detached from the substrate leaving behind a ring of the LOR sacrificial layer. The diameters of the detached discs was ~ 2 μm smaller than the negative photoresist discs observed on the LOR surface as seen from above using an optical microscope, therefore before the discs had detached, those that remained on the substrate are observed in the presence of LOR around the periphery of the discs, which accounts for the larger than expected diameter. The cracking of the photoresist therefore, rather than dissolution of the LOR, had caused the photoresist to detach. Clearly, acetone is not a suitable media for the removal of the positive photoresist if the patterned features of the negative photoresist are to remain intact.

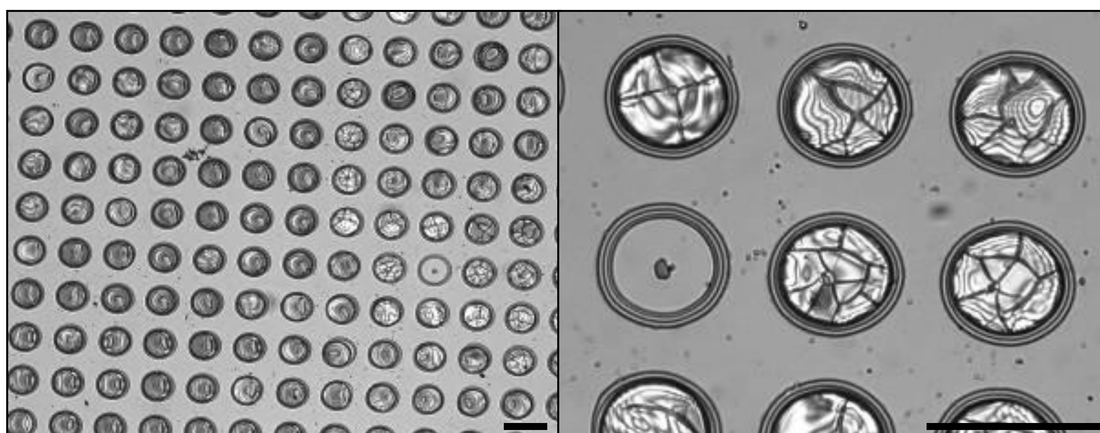

Fig. 5. 18. Optical microscopy images of negative photoresist discs after immersion in acetone for 60 min to remove the top surface of positive photoresist squares. Scale bars show 50 μm.

Our previous findings showed that positive AZ photoresist is soluble in IPA, while the negative resist is stable in this solvent (see Chapter 3); therefore it was decided to use IPA as a solvent for the removal of the patterned positive photoresist. After repeating the fabrication procedure and treating the patterned photoresist with APTES and rhodamine, the substrate was immersed in IPA. After 15 min immersion, no positive photoresist was observed on top of the negative photoresist discs (Fig. 5. 19); however it was suspected that some residual positive photoresist was present on the surface of the silicon that could not be removed after several hours of immersion. Fluorescence microscopy images (Fig. 5. 19) revealed that it was very difficult to differentiate between the masked and unmasked positive

photoresist, possibly indicating that not all of the positive photoresist was completely removed. IPA was therefore found to be unsuitable for the effective removal of the positive photoresist.

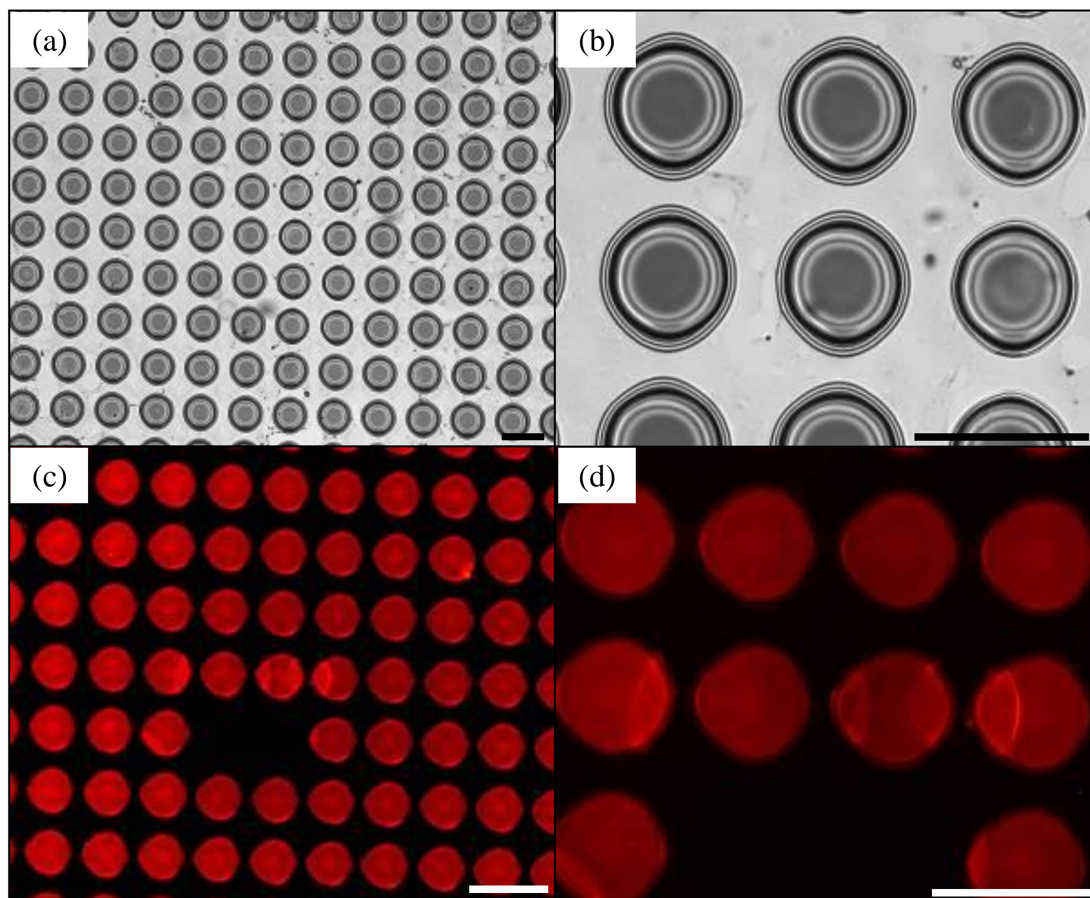

Fig. 5. 19. Optical microscopy images of negative photoresist discs attached to a silicon substrate via a sacrificial layer of LOR after removal of the top surface of patterned positive photoresist by immersion in IPA for 15 min (a and b). Fluorescence microscopy images of the same surface (c and d), indicate that some residual positive photoresist was still present. Scale bars show 50 µm.

Efficient removal of the positive photoresist may be achieved when the substrate is immersed in NMP to dissolve the sacrificial layer and remove the negative photoresist particles from the substrate, and may ensure that any residual positive photoresist is completely removed. In this experiment, it was decided to fabricate rectangular shaped photoresist particles on a 150 mm diameter silicon substrate and then to release the particles by dissolution of the sacrificial layer of LOR with simultaneous dissolution of the patterned positive photoresist using NMP. The particles that were released are shown suspended in NMP together with images of

the same particles in fluorescent light (Fig. 5. 20). It can be seen that fluorescence occurred over the entire area of the particle surface, with very little contrast between treated and untreated areas. It has been reported by other researchers that a very similar photoresist with the same components undergoes fluorescence, without addition of a fluorescent dye, after exposure to a wavelength of 568 nm (green light) due to photoactivation of the DNQ group. The fluorescence diminishes in regions that are exposed to UV light due to degradation of the DNQ component of the photoresist. [151]As shown in Fig. 5. 20, regions of the particles that were previously masked by the positive photoresist, and therefore were not exposed directly to the rhodamine, possessed greater fluorescence intensity. This may indicate that the positive photoresist was not completely removed; however it is not expected that any positive photoresist remains after immersion of the photoresist in hot NMP followed by sonication and centrifugation several times. A more plausible explanation could be due to the difference in fluorescence intensity due to the exposure of the negative photoresist to UV. Regions of the negative photoresist that were previously masked with the positive photoresist were only exposed to UV once, and the remaining regions were exposed to UV twice; degrading any remaining DNQ even further causing the fluorescence intensity to diminish in these areas. In addition, where the APTES and rhodamine was expected to bind to the negative photoresist (the unmasked regions), the fluorescence intensity had decreased, which may indicate that either the APTES or the rhodamine did not successfully bind to the surface: if bound to the surface, the rhodamine would be expected to fluoresce with greater intensity than the residual DNQ component of the photoresist.

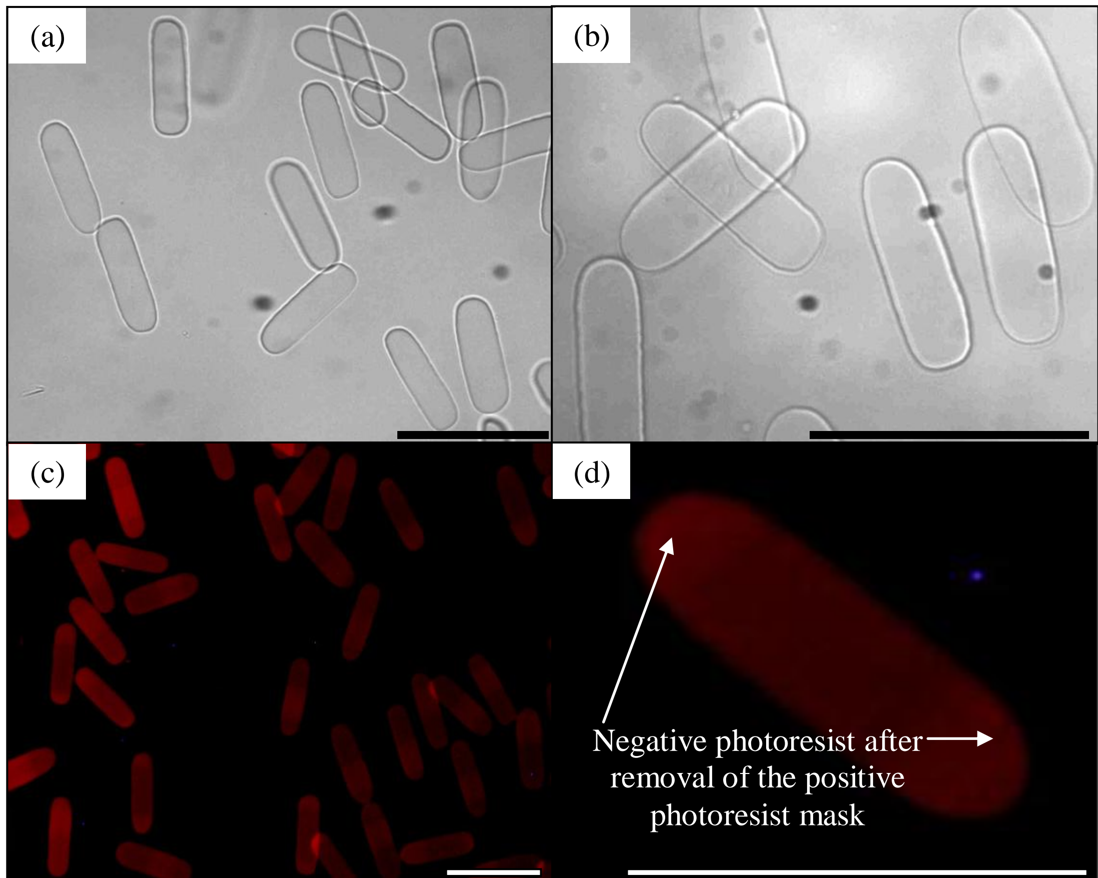

Fig. 5. 20. Optical microscopy images of rectangle shaped photoresist particles suspended in NMP after release from a silicon substrate by dissolution of the sacrificial layer of LOR (a and b)- the masking positive photoresist was expected to be removed in the NMP. Fluorescence microscopy images of the same particles in NMP after APTES and rhodamine treatment(c and d). The photoresist contains a DNQ photoactive component that is expected to fluoresce at the same wavelength as rhodamine, therefore making differentiation between treated and untreated portions difficult. The APTES and rhodamine treated portion of the particles was located either at their tips or the centre of the long axes of the rectangles. Scale bars show 50 µm.

5. 3. 3. Preparation of Janus microplates patterned with grafted amine groups by APTES treatment

Introducing amine groups to the photoresist surface permits further modification of the surface by chemically reacting isothiocyanates, sulfonyl chlorides[152] or PEG polymer chains. In order to demonstrate that the particle surface has been patterned with the APTES successfully, FITC fluorescent dye was used. Because fluorescein can bind only to the surface of the APTES, and binds very strongly due to the formation of covalent bonds, it is expected that if the APTES has bound successfully to the photoresist, a strong green fluorescence will be observed. To verify that the photoresist does not exhibit significant fluorescence at the wavelength of fluorescein emission (450- 480 nm); the untreated photoresist was observed in fluorescent light with a blue light filter. On this occasion, it was found that very little fluorescence at this wavelength was observed as shown in Fig. 5. 21.

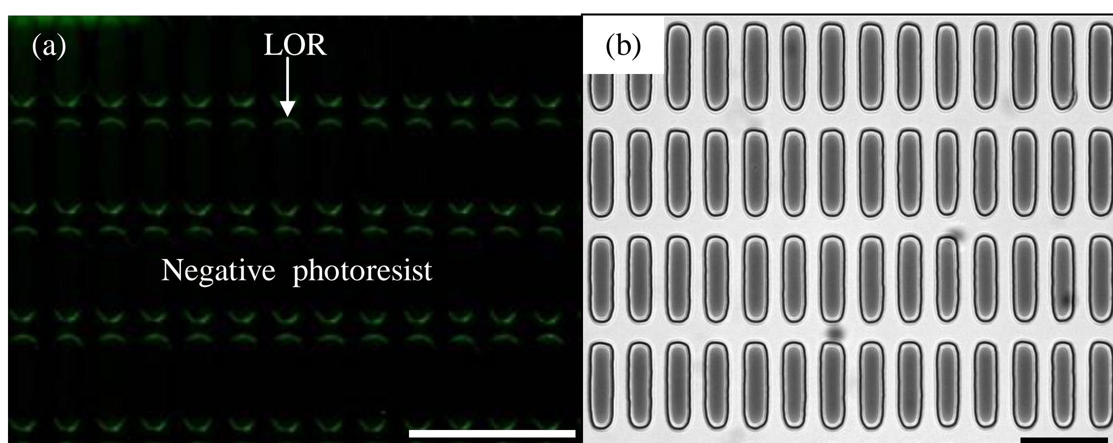

Fig. 5. 21. Fluorescence microscopy image, obtained through a fluorescein filter, of rectangle shaped negative photoresist attached to a silicon substrate via a sacrificial layer of LOR (a) and a non- fluorescent optical microscopy image of photoresist rectangles (b). Scale bars show 50 µm.

In order to demonstrate if the presence of the fluorescein can be observed and therefore, if the APTES has bound successfully to the photoresist, it was decided to apply APTES and fluorescein to the surface of the photoresist rectangles after masking with a positive photoresist in order to demonstrate if the fluorescence can be confined to a particular portion of the surface. Photoresist rectangles on a silicon substrate were patterned with positive photoresist in lines perpendicular to the long axes of the rectangles. The patterned photoresist was then immersed in an APTES

solution in water for 4 hrs and after rinsing, and without removing the positive photoresist, the substrate was placed in a 5. 5 mM solution of FITC in absolute ethanol for 17 hrs in a refrigerator, which is expected to remove any remaining positive photoresist. The fluorescence microscopy images (Fig. 5. 22) reveal that there was strong fluorescence around the periphery of the rectangles, where the LOR was expected to be present; however there was also some fluorescence where the positive photoresist was present before removal (where the APTES and dye should not be after dissolution of the positive photoresist). This may indicate that the positive photoresist was not entirely removed; however no visible evidence of the presence of the positive photoresist after fluorescene treatment was observed. In order to determine if fluorescence occurred on the top surface of the rectangles in the regions that were unmasked, line profiles showing the variation in light intensity were acquired from a microscopy image (Fig. 5. 23). From the plots and the corresponding image it can be seen that the fluorescence intensity on the surface of the rectangles is greater at the edges of the rectangles. The anticipated variation in intensity between the regions of the rectangles that were coated and uncoated with the positive photoresist was not observed and may mean that the positive photoresist was not completely removed, or the APTES did not cover the surface sufficiently. In order to see the situation more clearly, the rectangles were then removed from the substrate by dissolution of the sacrificial layer of LOR in NMP. In this way any residual positive photoresist would be completely removed. Images of the rectangles suspended in a mixture of NMP and water are shown in Fig. 5. 24. Surprisingly, the particles exhibited some fluorescence over the entire surface. In some cases it was possible to differentiate between regions that were coated and uncoated with positive photoresist; however the contrast was very poor. This suggests that most of FITC on the particle surface was not covalently bound to a sufficient number of amine groups and the positive photoresist was not completely removed as suspected.

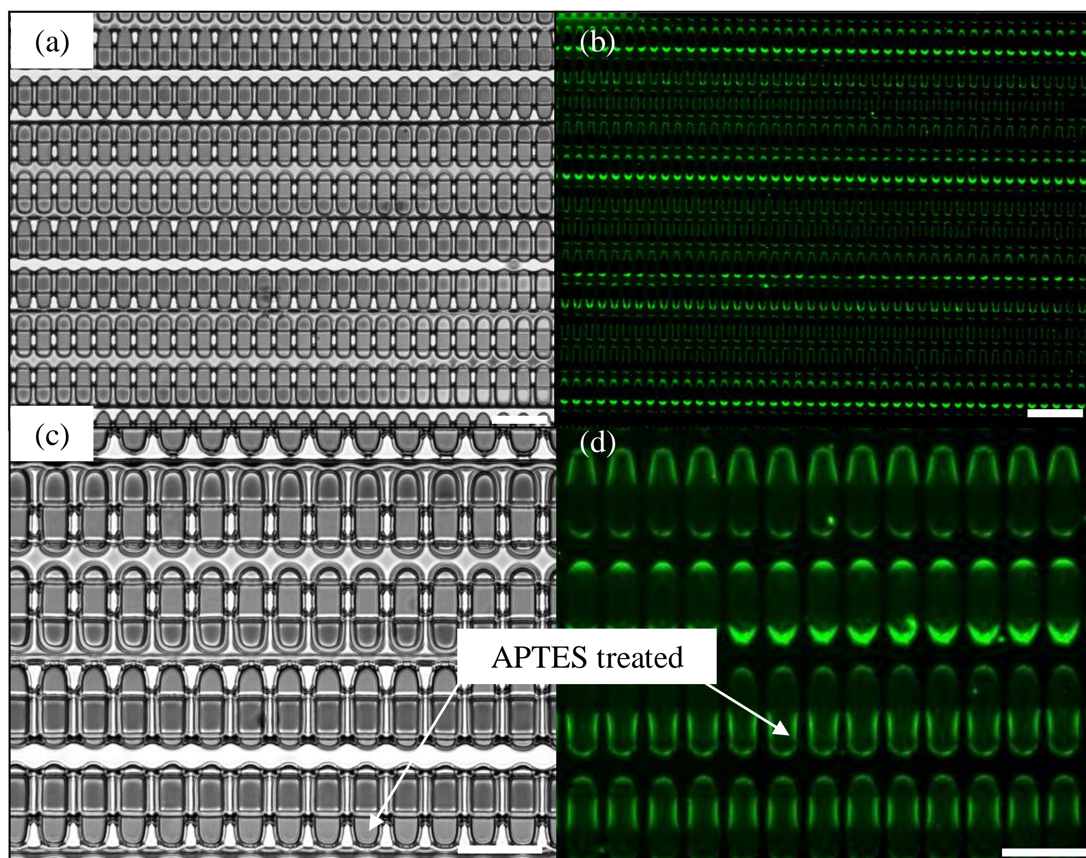

Fig. 5. 22. Optical microscopy images of the surface of negative photoresist (AZ nLOF 2070) rectangles partially coated with positive photoresist lines on a silicon substrate via a sacrificial layer of LOR (a and c), and fluorescence microscopy images after treatment of the surface of the rectangles with APTES and FITC followed by dissolution of the positive photoresist (b and d). Scale bars show 50 μm.

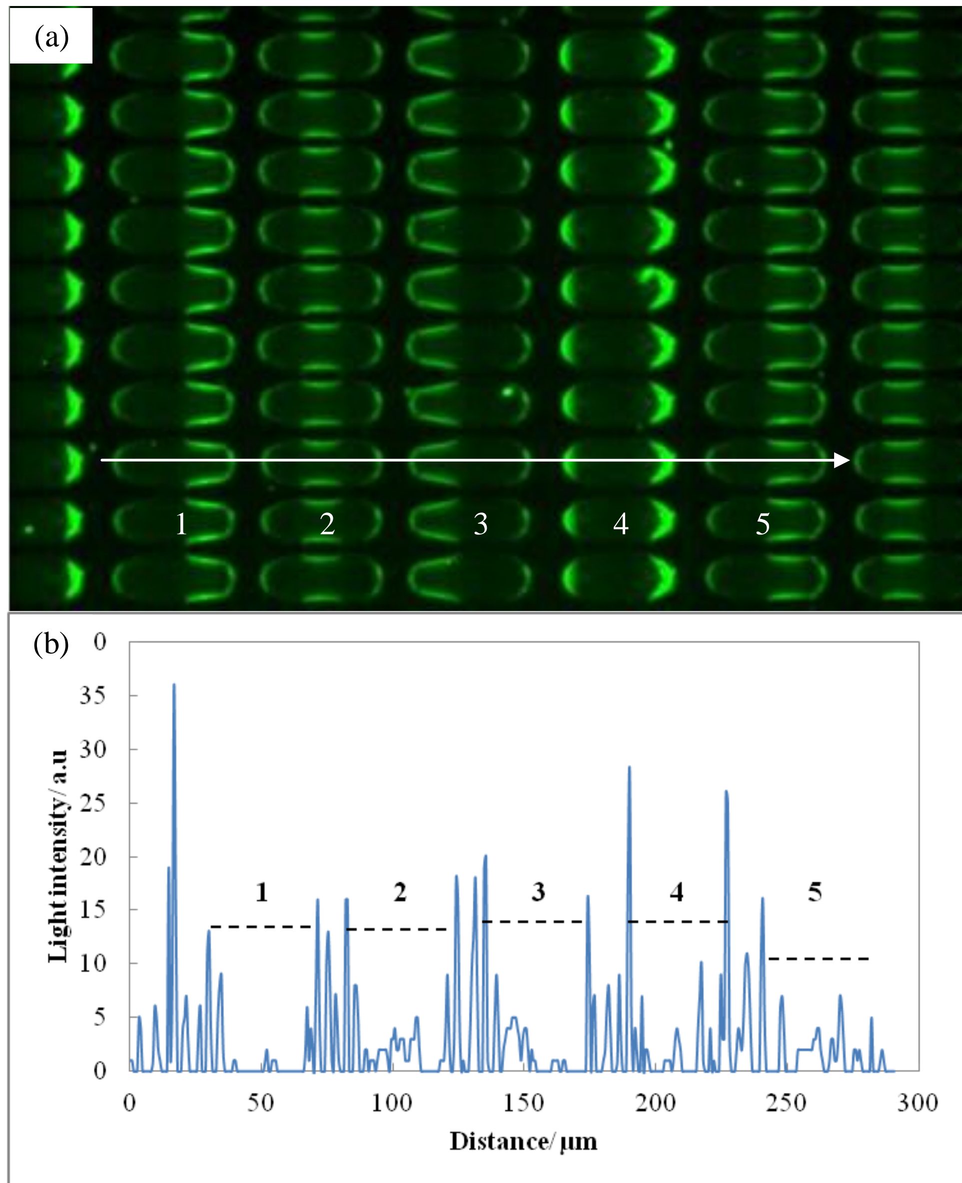

Fig. 5. 23. (a) Fluorescent microscopy image of negative photoresist (AZ nLOF 2070) rectangles (after removal of the mask of positive photoresist lines) on a silicon substrate via a sacrificial layer of LOR after APTES and fluorescein treatment (a) and (b) shows a plot of light intensity vs. distance along the arrow depicted on the microscopy image in (a). The major peaks correspond to the bright regions at the top and bottom of the rectangles.

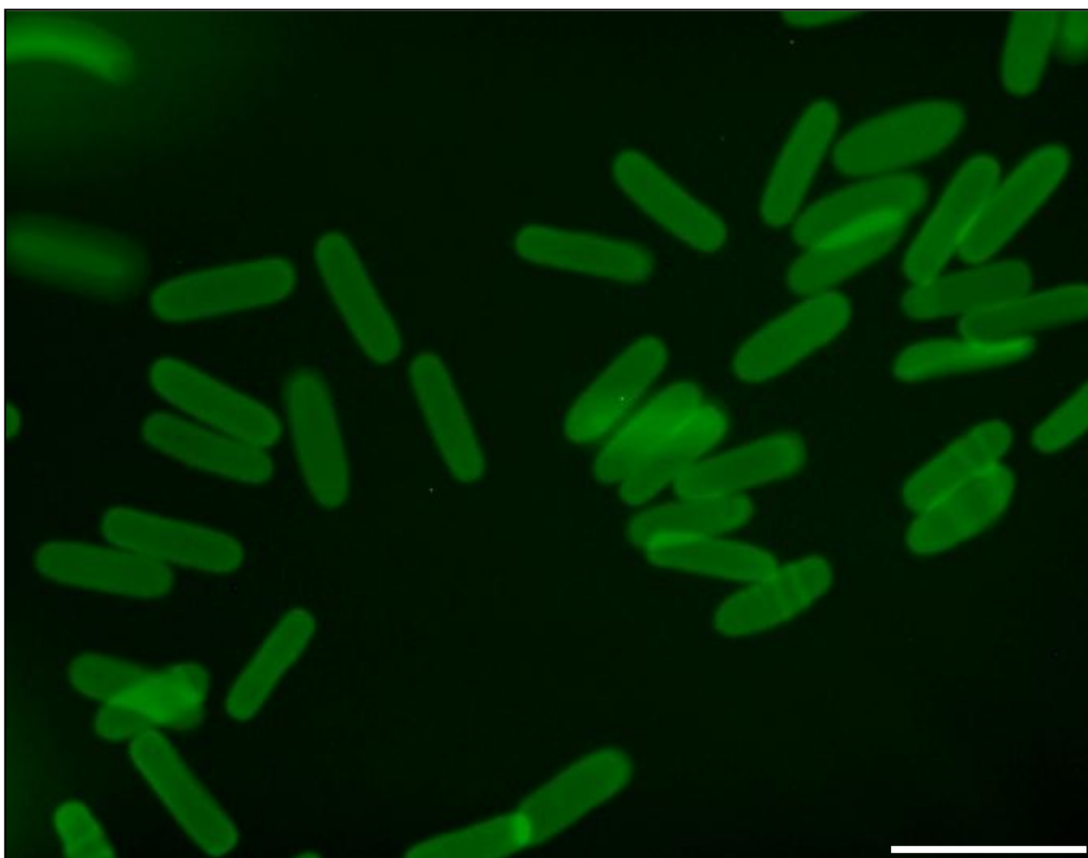

Fig. 5. 24. Fluorescence microscopy image of APTES and FITC treated photoresist rectangles in NMP and water. The APTES and FITC treated portion of the particles was located either at the tips or the centre of the particles as lines with heights of several micrometres perpendicular to the long axes of the particles. Scale bar shows 50 µm.

In order to confirm the presence of APTES on AZ nLOF 2070 photoresist surfaces, it was decided to analyse the surface after APTES treatment using infrared spectroscopy. For the primary amine present in the APTES molecule, two absorption peaks are expected to be seen in the spectra between 3500 cm^{-1} and 3300 cm^{-1}. Spectra were obtained after various immersion times in APTES as shown in Fig. 5. 25. It was found that the presence of the primary amine was barely detected, even after 24 hrs immersion in the APTES and the presence of a second peak was difficult to observe. The presence of the phenolic- OH groups however were easily observed which suggests that very few of the OH groups (2395 cm^{-1}) have been replaced with the APTES amino groups. The primary amine of analine, which has a very similar structure to that proposed by the replacement of the OH groups on the phenol group of the resin by the amine groups of the APTES, shows that the two

peaks of the IR spectra due to the presence of the amine are very distinctive- which was not observed on the photoresist. Application of APTES in anhydrous toluene is the procedure recommended by Aldrich, UK; however this solvent is not suitable in the presence of the positive photoresist.

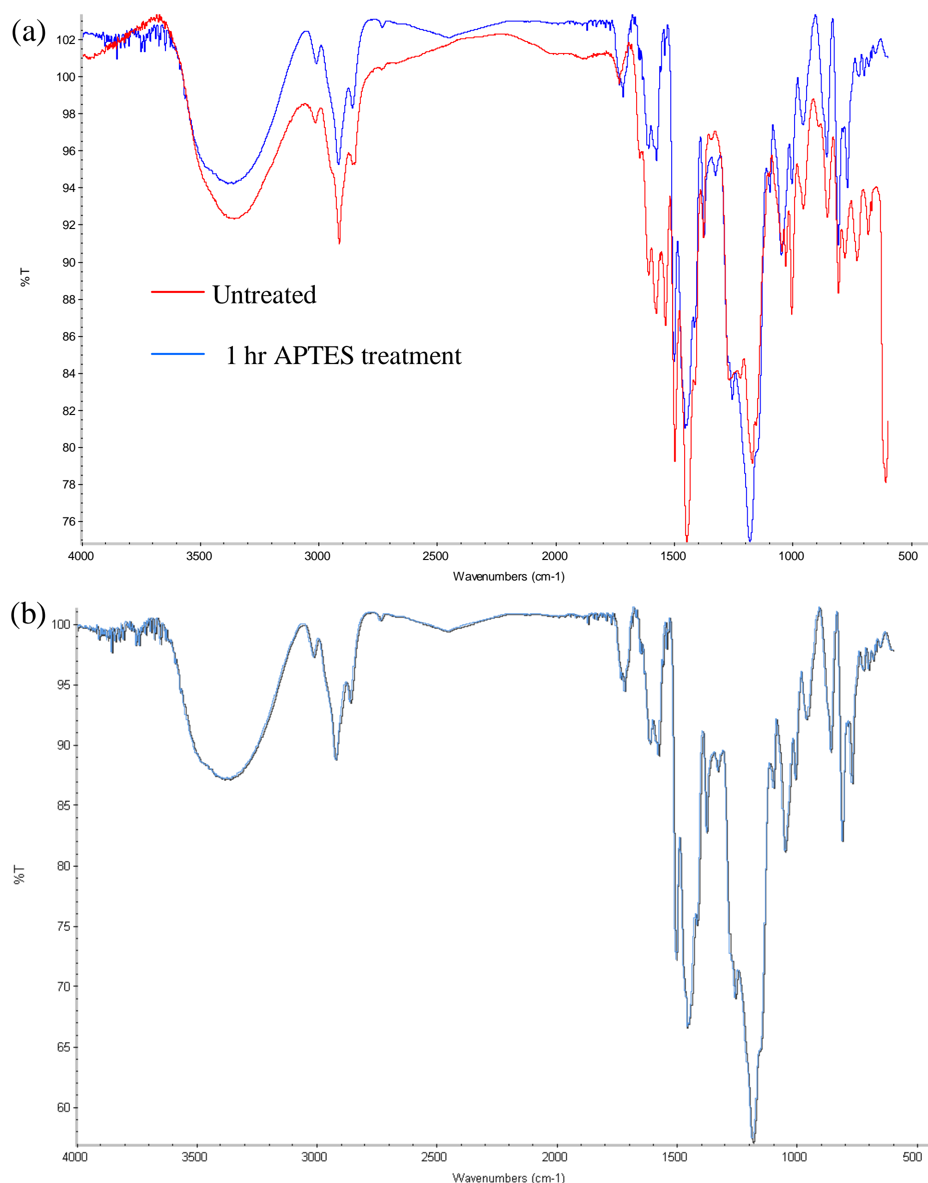

Fig. 5. 25. FT- IR spectra of phenolic photoresist resin without APTES treatment and after 1 hour treatment with APTES (a) and after 24 hrs APTES treatment (b).

In summary, application of FITC dye to APTES treated photoresist surfaces indicated that the dye does not bind uniformly on the surface. It was found to be very difficult to differentiate between the treated and untreated regions of the photoresist surface for particles that were suspended in solution. FT- IR analysis of the dry photoresist resin before and after APTES treatment showed that very little

APTES binds to the phenolic OH groups of the resin; therefore, amination by APTES treatment of the photoresist surface proved to be ineffective. Perhaps a better approach for the application of APTES would be to oxidise the surface of the photoresist with nitric acid in order to improve the binding efficiency of the APTES. This approach may be suitable for future work.

5. 3. 4. Preparation of patterned Janus plate- like particles by metal deposition

Another possible route for adding functionality to photoresist particles is by depositing a metal coating first, followed by chemical grafting on the metal covered surface. It is known that this approach works very well on gold or silver coated surfaces using thiol derivatives (R-SH), because thiols bind strongly to gold/ silver via a sulphur-metal bond. [153] Here we focus on the first step of metal deposition and the possibility of selective coverage of the photoresist surface with the metal. The aim is to develop protocols for depositing metal patterns on one face of the plate-like microparticles only. For a proof of principle, chromium was used in most of experiments as it was more readily available than gold. Two approaches for metal decorated microparticles illustrated in Fig. 5. 26 were investigated. In the first approach, the metal was applied by evaporation onto the patterned photoresist surface, masked with positive photoresist, followed by removal of the positive photoresist and liberation of the particles by dissolution of the sacrificial layer (Fig. 5. 26). In the second approach, the metal was evaporated onto the negative photoresist pattern before application of a positive photoresist mask, and then the uncoated metal was etched away in chromium etchant (Fig. 5. 26 b).

(a) Metal deposition on partially masked microparticle arrays

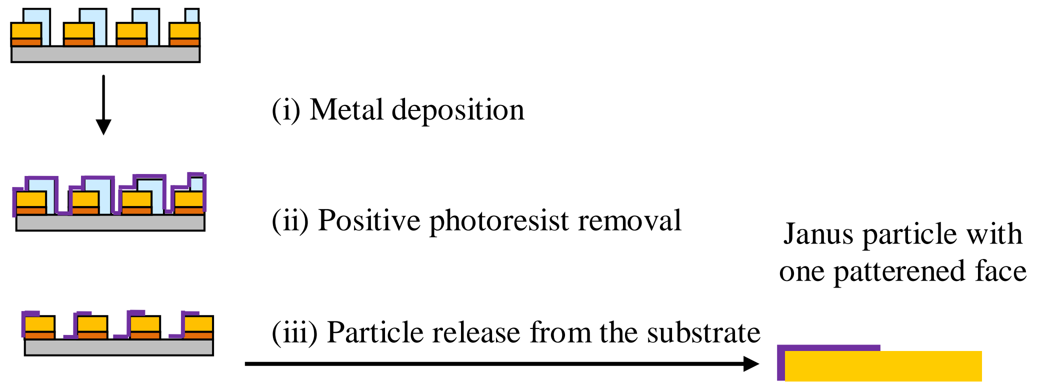

(b) Metal etching of partially masked metal coated microparticle arrays

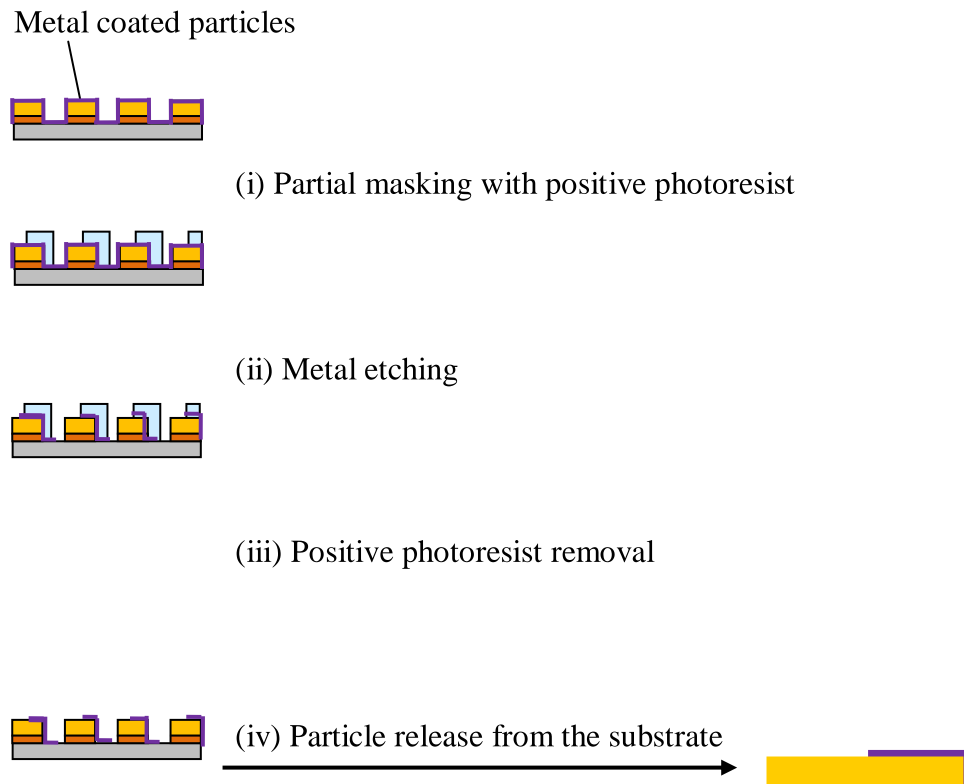

Fig. 5. 26. Schematic representation of the photolithographic process for the partial coating of a negative photoresist pattern with a metal.

5. 3. 4. 1. Experiments using metal deposition on partially masked microparticle arrays

Using the procedure shown in Fig. 5. 26 (a), positive photoresist was applied to the surface of negative photoresist rectangles attached to a silicon substrate. After alignment of the photomask, followed by exposure and development of the positive photoresist, it was demonstrated that the aligned pattern was successfully transferred to the existing negative photoresist rectangles (Fig. 5. 27) and the pattern was consistent at different locations on the substrate. It was easier to observe the positive photoresist lines in regions were some of the negative photoresist rectangles had detached from the substrate (Fig. 5. 27 b and d). After patterning the surface of the rectangles with positive photoresist, a layer of chromium was applied by metal evaporation as shown in Fig. 5. 28. Photomask alignment onto photoresist discs using a clearfield photomask consisting of lines with 10 µm thickness and 10 µm spacing was less successful due to the difficulty of observing the photomask and discs simultaneously during alignment.

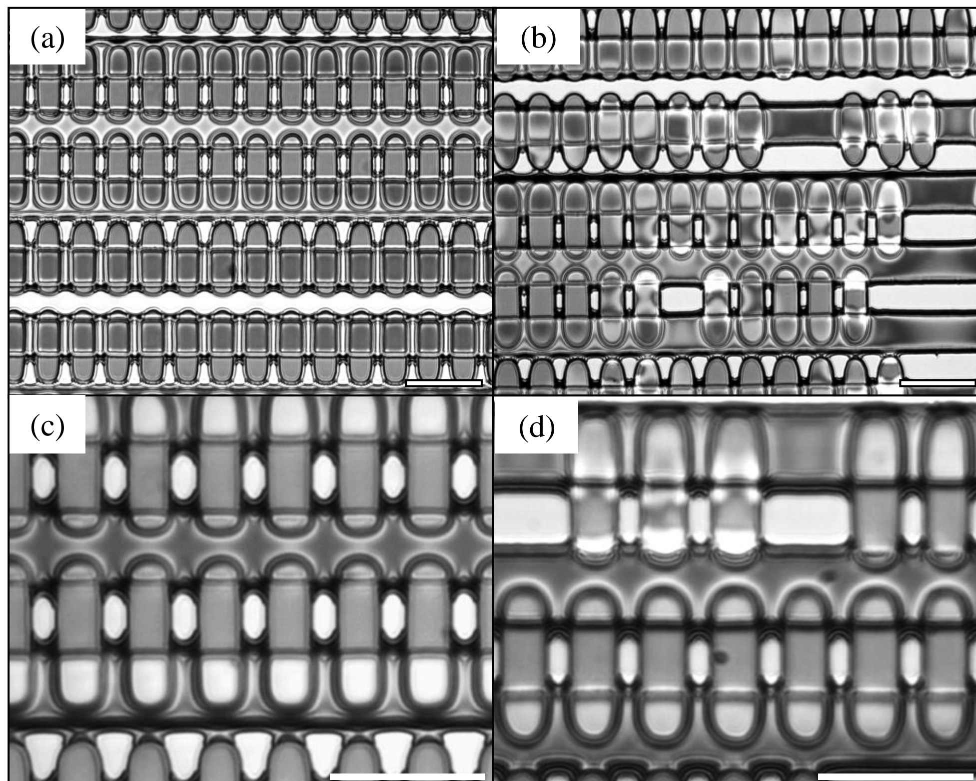

Fig. 5. 27. Optical microscopy images of negative photoresist rectangles coated with positive photoresist lines patterned using a photomask consisting of lines with a width of 20 µm, at 20 x magnification (a and b) and 40 x magnification (c and d). Scale bars show 50 µm.

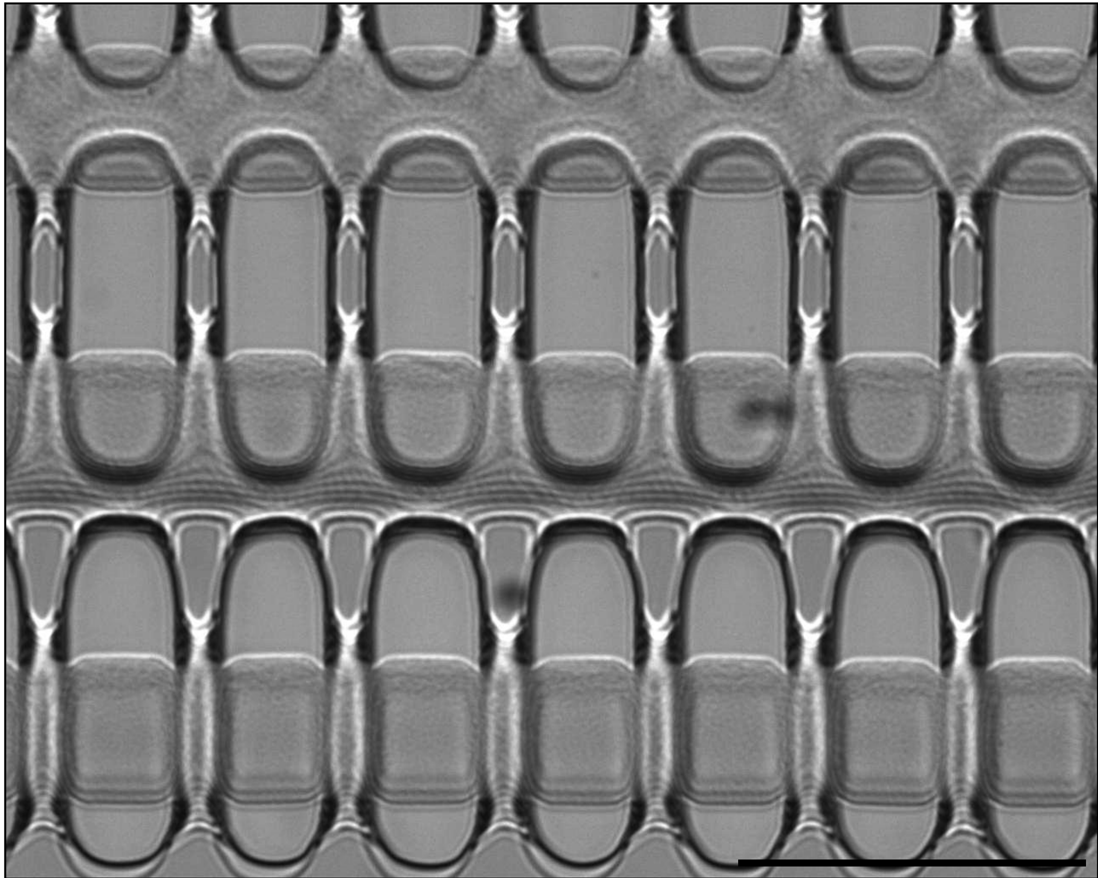

Fig. 5. 28. Optical microscopy image of negative photoresist rectangles coated with positive photoresist lines followed by evaporation of a 30 nm layer of chromium. Scale bar shows 50 µm.

It was then attempted to release the metal patterned photoresist rectangles by immersion of the substrate in developer solution to dissolve the sacrificial layer: NMP was not used on this occasion in order to reduce the possibility of damage to the metal layer. After immersion of the substrate in the developer solution, no evidence of particle detachment from the substrate was observed after 30 min immersion, and less than 10 % of the particles were released into the developer after several hours of immersion. This indicates that the developer solution does not have sufficient access to the sacrificial layer. If the sacrificial layer is not undercut beneath the photoresist, the sacrificial layer will also be coated with the metal, providing a barrier to its dissolution. In order to address this, a method to undercut the sacrificial layer before metal application was investigated, by carefully increasing the development time of the photoresist in order remove a sufficient amount of the sacrificial layer so that the layer is undercut beneath the particles. As

shown in Fig. 5. 29, this approach resulted in successful undercutting of the photoresist rectangles; however it was found that undercutting did not resolve the problem associated with the difficulty of releasing the particles. As shown in Fig. 5. 29, many of the rectangles appeared to be bent, where they were not supported by an under layer of LOR, and consequently in some cases the rectangles were in intimate contact with the silicon. The implication of this was that the metal was not lifted from the substrate as anticipated due to the intimate contact between the rectangles and substrate, and therefore although the sacrificial layer dissolved in the developer, the metal had pinned the rectangles to the substrate, preventing their release.

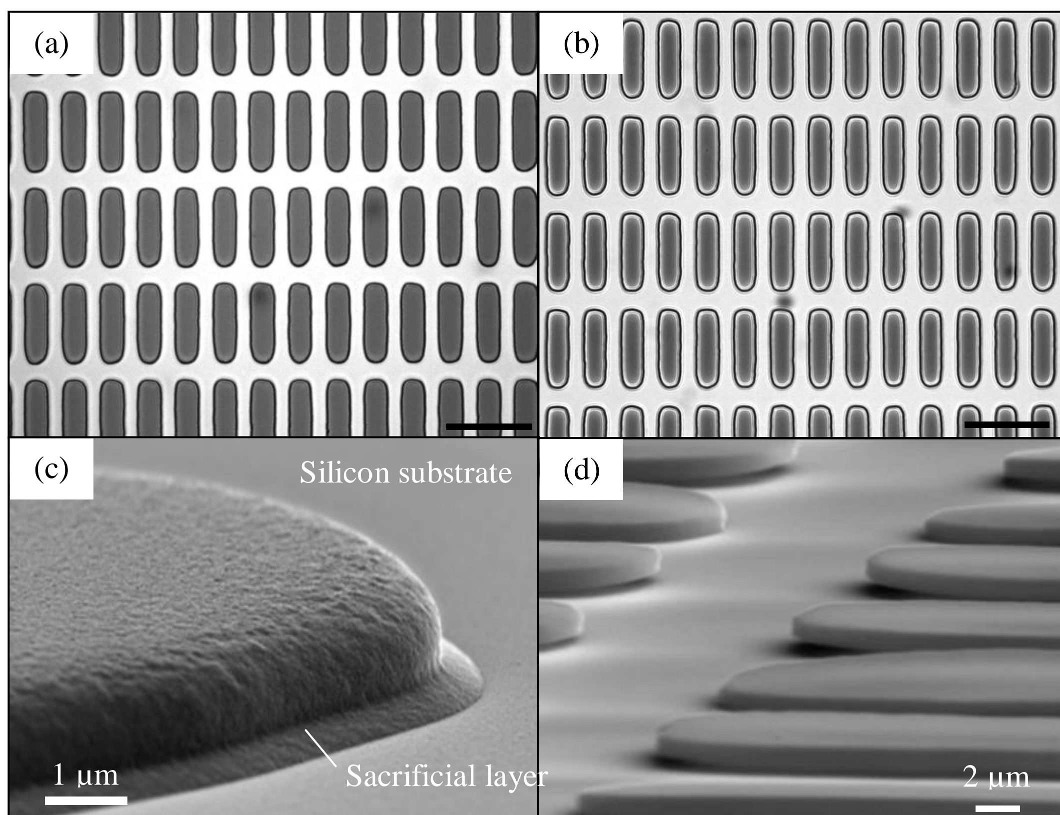

Fig. 5. 29. Optical microscopy images of negative photoresist rectangles attached to a silicon substrate via a sacrificial layer of LOR before further development of the LOR to undercut the sacrificial layer (a, c) and after further development of the LOR to undercut the sacrificial layer (b, d). Scale bars show 50 µm. SEM images of negative photoresist rectangles attached to a silicon substrate via a sacrificial layer of LOR before (c) and after (d) undercutting the sacrificial layer.

5. 3. 4. 2. Experiments using metal etching of partially masked metal coated particle arrays

In the previous experiments, approaches to fabricate metal coated Janus particles using photolithography resulted in the inability to release the particles due to difficulties associated with optimising the profile of the sacrificial layer. In this experiment, as outlined in Fig. 5. 26 (b), photoresist rectangles will be partially coated with chromium by etching through the metal aroung the positive photoresist mask. The metal pattern will be defined by fabricating positive photoresist rectangles by application of two successive exposures of the positive photoresist through photomasks consisting of lines, with the second photomask aligned 90 ° with respect to the first. This approach proved to be difficult as the photomasks were very difficult to align and in addition, the positive photoresist was easily overdeveloped giving rise to smaller and more rounded features. Despite these technical difficulties, it was decided to proceed with the experiments in order to prove if it is possible to generate Janus particles as outlined in Fig. 5. 26. In order to ensure that the chromium was completely etched after patterning the positive photoressit rectangles, the etching rate was monitored by immersing transparent glass slides coated with the same thickness of chromium in the chromium etchant. It was found that the chromium was completely removed within 60 s for the chromium coated glass slides. After etching the chromium onto the patterned positive photoresist for 37 s in the chromium etchant, the chromium was no longer present and the positive photoresist was not affected by the etching process (Fig. 5. 30) - it is worth noting that some particles had detached from the substrate, which could not occur if the particles were covered with a layer of chromium. Some of the attached rectangles revealed that a part of the chromium surface had rolled up and was not removed by etching, possibly due to the presence of undeveloped positive photoresist. Such features were not observed before applying the positive photoresist and therefore occurred after evaporation of the chromium. Further etching for a total time of 133 s (Fig. 5. 30) did not produce any noticeable changes. In many cases, it was found that residual chromium was present, which was presumably masked with residual photoresist before etching; therefore some of the rectangles were bridged together by the chromium (Fig. 5. 30).

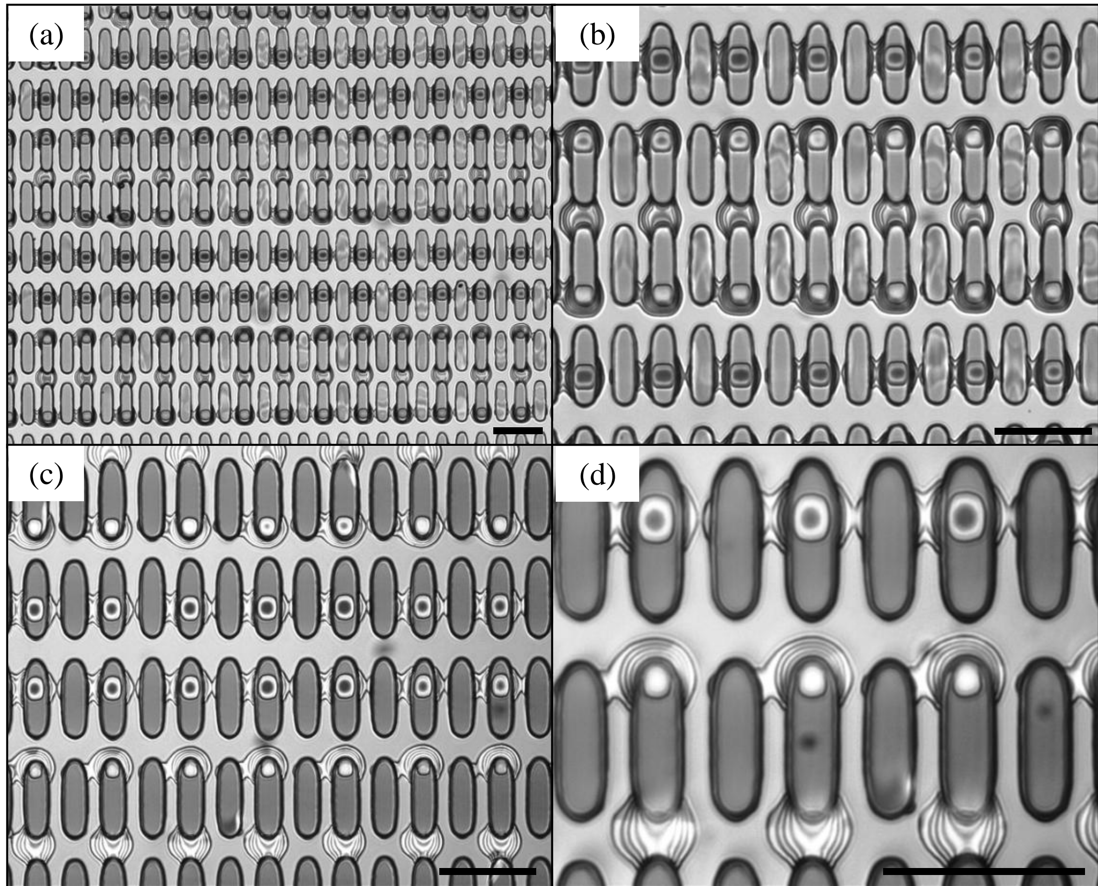

Fig. 5. 30. Optical microscopy images of negative photoresist rectangles partially coated with positive photoresist rectangles followed by evaporation of a 10 nm layer of chromium. The surface is shown before etching of the chromium (a and b) and after etching the surface for 37 s (c and d). Scale bars show 50 μm.

It is expected that the photoresist rectangles that are partially coated with the chromium can be detached from the substrate by dissolution of the sacrificial layer using developer solution, assuming that the chromium is sufficiently etched. This will also remove any remaing positive photoresist. After immersing the substrate in developer, it became apparent that the positive photoresist had been completely etched and removed in the developer, leaving behind only the chromium pattern; however as shown in Fig. 5. 31, much of the chromium was preserved by residual positive photoresist and therefore remains in undesired regions. After further immersion in the developer to completely remove the sacrificial layer and liberate the particles, most of the particles remained attached to the substrate, even after immersion for a total time of 65. It became apparent at this stage that access to the sacrificial layer was hampered due to the residual chromium mentioned above, which pinned the particles to the substrate. The chromium on those particles that

had detached was preserved intact (Fig. 5. 31). When the substrate was immersed in NMP for 30 min, the chromium was found to peel off the particles.

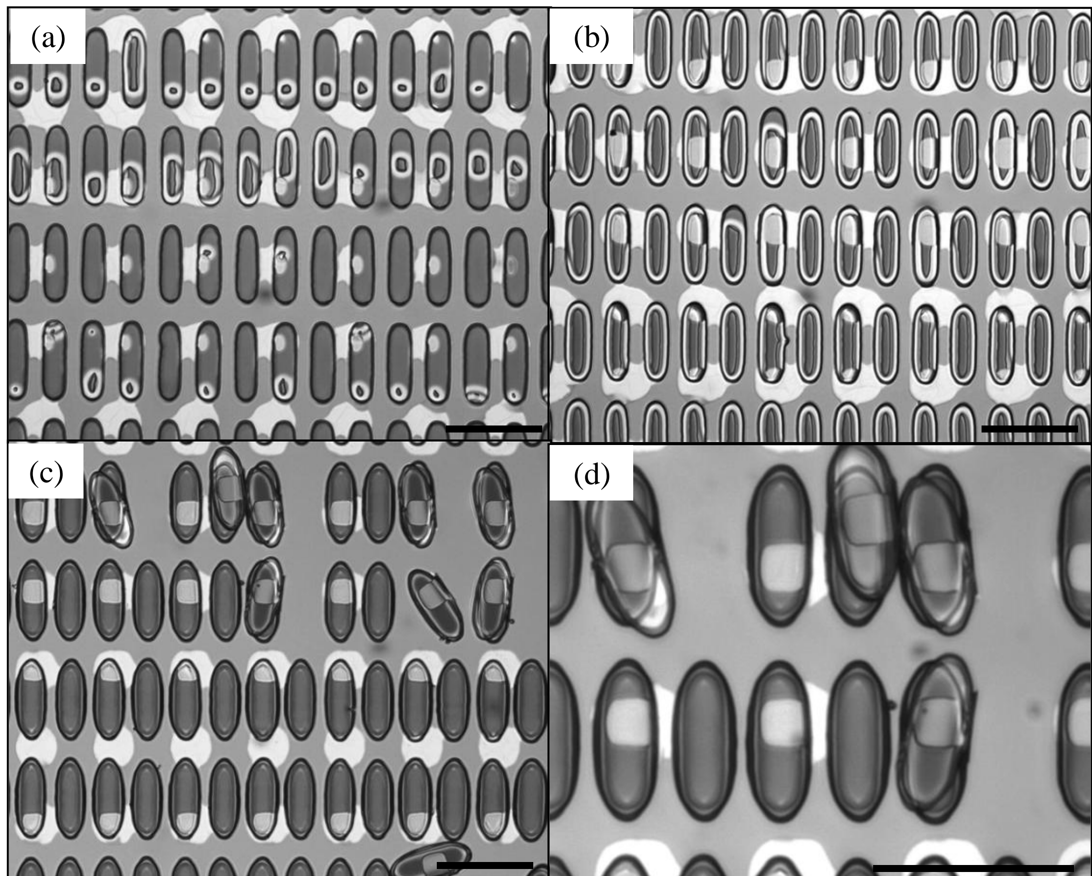

Fig. 5. 31. Optical microscopy images of negative photoresist rectangles partially coated with chromium after immersing the substrate in developer solution for ~ 4. 5 min to dissolve the sacrificial layer of LOR. The images are shown at show 20 x magnification (a and b) and show 40 x magnification (c and d). Scale bars show 50 μm.

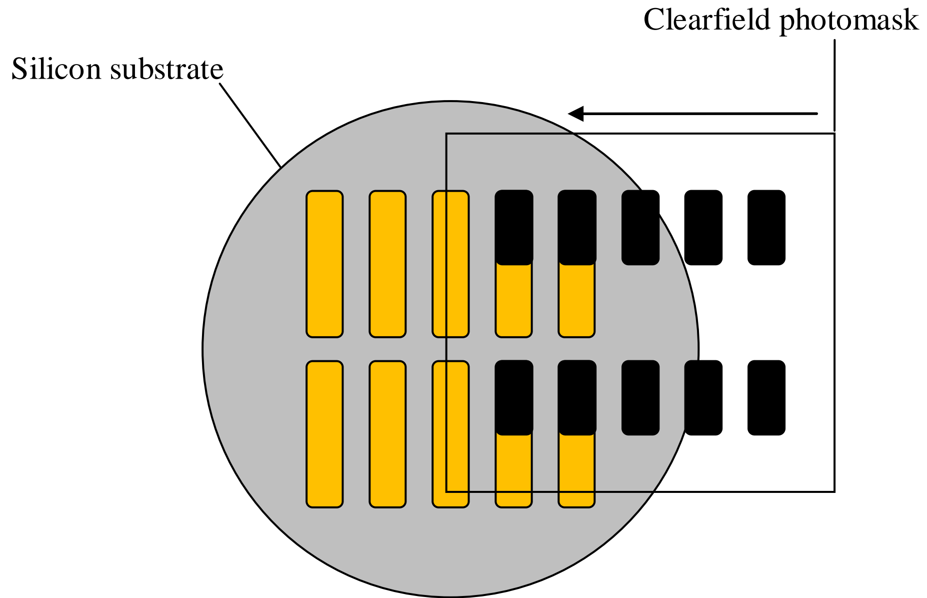

Fig. 5. 32. Schematic representation of a clearfield photomask consisting of an array of rectangles (10 × 20 µm) overlaid on a periodic array of AZ negative photoresist rectangles (10 × 40 µm) coated with a layer of positive photoresist

By using specially designed photomasks, it is intended that only the top half of the fabricated negative photoresist rectangles will be coated with positive photoresist without casuing residual photoresist to be present which was found to hamper removal of the patterned rectangles as observed previously. The use of a single photomask consisting of UV opaque with dimensions that will fit exactly over the negative photoresist rectangles such that half of their surface is covered with the pattern will permit pattern transfer from a single exposure and eliminate difficulties that may arise from application of a second exposure. In this case, the positive photoresist pattern was created using clearfield photomasks consisting of UV opaque rectangles with dimensions of 10 × 20 µm with a pitch designed such that the rectangles will cover the top half of the negative photoresist rectangles as shown in Fig. 5. 32. The patterned negative photoresist rectangles were first coated with a 10 nm layer of chromium by evaporation from directly above. The underlying chromium was then etched and removed from the etchant after 60 s. After rinsing, the substrate was then immersed in undiluted developer solution. After 10 min immersion, only the positive photoresist was removed with the sacrificial layer; however the particles remained mostly attached to the substrate, again due to pinning by residual chromium (Fig. 5. 33). Both approaches for pattern formation of the positive photoresist mask therefore proved to be ineffective for the efficient removal

of the metal patterned photoresist rectangles from the substrate. A few drops of the developer solution were deposited on a microscope slide and observed under an optical microscope. Although very few particles were found suspended in the solution, it was clear that the chromium coating was always preserved intact as shown in Fig. 5. 33.

In summary, the application of a metal onto photoresist rectangles on particular portions of one surface to generate Janus particles was found to be successful; however the presence of residual positive photoresist was difficult to avoid and the residual metal that resulted from this prevented the liberation of the particles from the substrate. This technique was limited by the difficulty of processing the positive photoresist effectively under these conditions.

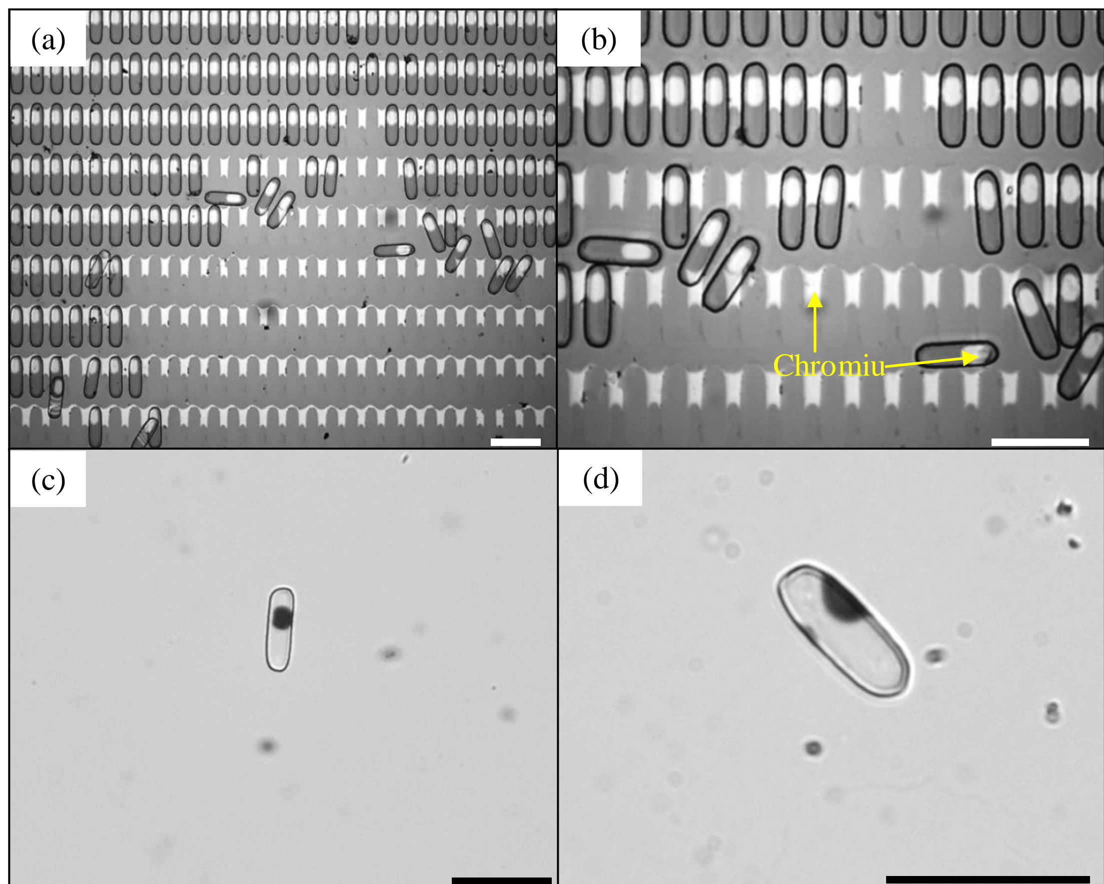

Fig. 5. 33. Optical microscopy images of negative photoresist rectangles partially coated with chromium after immersing the silicon substrate in developer solution for ~ 50 min to dissolve the sacrificial layer of LOR (a and b). Particles that were released from the substrate and suspended in the same developer solution shown in transmitted light (c and d). Scale bars show 50 µm.

5. 4. Summary of the main findings

In these experiments, various methods for the fabrication of Janus particles by modifying one surface of non- spherical photoresist particles have been investigated. The main findings are summarised below.

It has been demonstrated that PAH polyelectrolyte binds to the photoresist surface successfully and hence Janus microplates with one face covered with positively charged PAH and the other of unmodified photoresist were produced. Further application of PSS polyelectrolyte to the PAH treated surface allowed the efficient binding of magnetic Fe_3O_4 particles to the PSS treated surface. Surface oxidation of the photoresist using HNO_3 imparts even greater binding efficiency for the magnetic particles without the need for polyelectrolyte. The rectangular photoresist particles with one surface coated with magnetic Fe_3O_4 particles could be removed successfully from the substrate by dissolution of the sacrificial layer of LOR in NMP, without causing detachment of the Fe_3O_4 particles and the resulting Janus particles in suspension responded to the application of a magnetic field.

The plate- like microparticles could be patterned in predesignated portions of the top face of the particles with a positive photoresist, permitting the possibility of selectively patterning the photoresist top surface with other groups such as APTES. FT- IR analysis of dry photoresist resin before and after APTES treatment however showed that very little APTES binds to the phenolic OH groups of the resin. Application of FITC dye to the APTES treated photoresist surfaces indicated that the dye does not bind uniformly on the surface due to the poor binding of the APTES. This could be a result of the low density of OH groups on the photoresist surface available for binding.

Chromium metal was applied successfully to the photoresist surface by metal evaporation, and the sacrificial layer could be undercut to ensure effective coating on only the top surface of the photoresist; however the metal coated particles could not be released from the substrate as anticipated due to intimate contact between the rectangles and substrate caused by bending of the rectangles, which resulted in the metal layer pinning the particles to the substrate. A metal etching technique demonstrated that the metal could be etched in the presence of a positive photoresist

mask without damaging the photoresist, but this requires that the positive photoresist pattern is very well resolved and defect free.

5. 5. Conclusions

In conclusion, various experimental approaches for the modification of one face of photoresist microparticles were investigated for the fabrication of plate- like Janus particles including polyelectrolytes followed by colloidal particles, APTES followed by fluorescent dyes and metal coatings. It was found that when processed under normal laboratory conditions, the patterned photoresist surface could be modified successfully using polyelectrolytes which could then effectively bind magnetic Fe_3O_4 particles to one face of the photoresist microparticles; the binding efficiency of the latter could be enhanced in the absence of polyelectrolyte by oxidation of the photoresist surface using nitric acid. This presents opportunities for further investigations of magnetic plate- like particles at the liquid- fluid interface. Partial masking of the negative photoresist particles using positive photoresist was less successful due to the processing difficulties involved for defect- free positive photoresist patterns on an existing negative photoresist pattern. The amination of AZ negative photoresist surface by using APTES proved to be ineffective under these conditions.

CHAPTER 6
SUMMARY OF MAIN FINDINGS, CONCLUSIONS AND FUTURE WORK

The aims of this thesis are to develop protocols for fabricating homogeneous and Janus plate- like microparticles with a range of different shapes and aspect ratios and investigate the behavior of such particles at the air- water and oil- water interface. The interfacial behaviour of plate- like microparticles with controlled geometry and wetting properties has not been investigated before.

The technique of photolithography is utilised for the fabrication of a range of particles with different geometries under normal laboratory conditions without using expensive facilities and equipment (chapter 3). The effect of particle geometry on the structure of monolayers at the liquid interface is studied at rest or during compression/ expansion in a Langmuir trough by direct microscopy observations and results are presented in chapter 4. The ability of the plate- like particles to stabilise foams and emulsions is also investigated (chapter 4). The possibilities of photolithography for the fabrication of Janus plate- like microparticles with a simple or more complex patterned structure is explored and the interfacial behaviour of Janus microplates with homogeneous but different faces is described (chapter 5). The main findings of our investigation and conclusions are summarised below.

6. 1. Main findings and conclusions

Various experimental factors in the photolithographic process for the fabrication of non- spherical particles with controlled shape and aspect ratio, with different types of photoresist on glass and silicon substrates have been investigated and the results are described in chapter 3. It has been demonstrated that particles with a range of different shapes and controlled thickness could be achieved using this technique with an AZ photoresist that has not been studied in this way previously. The approach taken introduces a means of applying the technique in a relatively inexpensive and simple way, making the technique more accessible without the use of clean rooms and expensive equipment such as mask aligners. This merely affects the quality of the features fabricated yet still allows important parameters such as particle thickness, shape and aspect ratio to be realised. A range of different factors including photoresist type, substrate type, photomask type and processing conditions

were investigated. Plate- like particles consisting of discs, ovals and rectangles with a thickness of ~ 1. 1 μm have been successfully fabricated and their geometric characteristics are summarised in Fig. 3. 28 and Table. 3. 1 of chapter 3.

Protocols for the application of photolithography for the fabrication of non- spherical particles with well controlled geometry have been established; these include the appropriate selection of photoresists, substrates and equipment and optimisation of: substrate preparation, photoresist dispensing conditions and spin coating parameters, pre and post baking conditions, exposure and development of the photoresist and release of the photoresist particles from the substrates. It was found to be necessary to optimise each step carefully and this depended crucially on the quality of the spin coated photoresist film. The best quality films were obtained on large circular silicon substrates. Next, the baking of the photoresist films, exposure, development and release of the particles was carefully optimised to give reproducible results. Under normal laboratory conditions (without the use of clean rooms) the particles that were generated using this technique were reasonably monodisperse and chemically stable so that they could be modified by attaching other chemical groups to the surface. The best results were obtained for AZ type photoresist consisting of a phenolic resin; however SU- 8 type photoresist was not suitable for precise processing under these conditions.

In chapter 4, the behaviour of monolayers of particles prepared using the technique of photolithography with a range of aspect ratios and thicknesses have been investigated at the liquid interface. It is found that the plate- like particles made of photoresist by photolithography have significant surface roughness which impacts strongly on the particle behaviour and interactions at the liquid interface. The roughness leads to a large contact angle hysteresis and prevents the particles from attaining their equilibrium configuration at the liquid interface. Particles lay flat at the interface with an apparent macroscopic contact angle of ~ 90 ^{o}, almost equally immersed in both adjacent fluid phases. Particle interactions at the liquid interface are dominated by the capillary attraction due to an undulated three phase contact line caused by the surface roughness. The capillary attraction prevails over electrostatic repulsion leading to substantial aggregation of the plate- like particles at the air-water and oil-water interface. Particle shape and aspect ratio have pronounced effect on the structure of aggregates. The fraction of non- spherical particles aggregating in

a tip- to- tip configuration decreases with the increase of the aspect ratio. The opposite trend is observed for the fraction of particles aggregating in a side- to- side configuration. Side- to- side aggregation is preferred by non- spherical particles with aspect ratio larger than 2 due to stronger capillary attraction than that of tip- to- tip aggregation.

The shape and thickness of the plate- like microparticles has significant implications on the monolayers undergoing compression and expansion in a Langmuir trough. Particles with higher aspect ratios such as ovals and rectangles give broader isotherms than those composed of discs or spheres due to the tendency for the particles to reorient during compression. Flat microparticles are able to undergo flipping and tilting at the interface during compression; higher aspect ratio particles flip exclusively such that their long axes are perpendicular with the interface. There is no tendency for the particles to align preferentially by confinement during compression due to the strong contacts and jamming between particles at the liquid interface. Compression of the particle monolayers at the air- water interface leads to significant losses of interfacial particles due to their ejection into the water phase. This effect is more pronounced for thinner plate- like particles. Such ejection is not observed for monolayers at the oil- water interface.

During compression and expansion of the monolayers at the air- water interface, it is found that there are similarities and differences between spherical latex particles and the photoresist particle discs investigated in this work. For both types of particles, the particles undergo aggregation following spreading, and the monolayers buckle during compression with isotherms shifted to smaller areas after repeated compression- expansion cycles. In contrast to the spherical latex particles, the photoresist discs are observed to flip during compression and detach to some extent from the interface after the buckling of the monolayer. The more expanded isotherms observed for the plate- like particle are attributed to these findings. By fixing the photoresist thickness, oval and rectangular particles have also been investigated. The change in aspect ratio of the particles has a significant effect on the shape of the pressure vs. area isotherms; oval and rectangular particles, like the discs, could flip at the interface preferentially around the long axes of the particles. In addition the isotherms become broader to an extent which followed the order, rectangles> ovals> discs> spheres. The rectangles therefore give the broadest

isotherm and this is attributed to the ability of the rectangles to rearrange more efficiently than the lower aspect ratio particles during compression.

Thinner disc shaped particles composed of SU- 8 photoresist at the air- water interface during compression of the monolayer in a Langmuir trough revealed a tendency to flip more easily, flipping was even observed before compression of the monolayer when the number of particles present at the interface was large; in addition there was an increasing tendency for the discs to overlap each other during compression. The number of particles lost into the water sub- phase during spreading and compression of the monolayer was substantial. The number of particles at different areas of the trough were counted for particles that lay flat on the surface of the water, overlapped particles and flipped particles. A decrease in the number of particles lying flat on the surface of the water corresponded to an increase in the number of flipped particles. A large degree of particle loss resulted during the initial spreading process. It was found that the number of particles remaining at the interface was only ~ 9 % of the total number expected in the spreading suspension. Monolayer jamming and a resulting rapid rise in surface pressure was not observed during compression of the monolayer consistent with an insufficient number of particles present at the interface due to the loss of particles from the interface.

Monolayers of oval shaped particles composed of AZ photoresist at the oil- water interface behave differently to those at the air- water interface. In contrast to the findings reported for the air- water interface, the compression- expansion isotherms were reversible with no indication of hysteresis present. The isotherms were broader than those observed for the air- water interface and may result from an enhanced repulsion between the particles through the oil; however as mentioned, the particles aggregated rapidly after spreading which indicates that the charges on the particle surfaces are insufficient to offset the capillary attraction. In addition, the particles were not ejected from the interface on this occasion after buckling of the monolayer, due to the greater energy of attachment of the particles at the oil- water interface. After expansion, the monolayer recovered its original state as before compression; in the case of the air- water interface the monolayer fragmented into islands during expansion.

The plate- like particles studied are not efficient in stabilising foams because their apparent macroscopic contact angle at the air- water interface is almost 90 ^{o}. Therefore the bubbles must be almost completely covered by particle mono- or multilayers to prevent coalescence. The observed release of the surface stresses in the monolayers during compression by particle flipping and ejection suggests that these particles would not be very effective in preventing bubble shrinking responsible for the disproportionation (Ostwald ripening) in foams. The particles can stabilise emulsions more effectively.

In chapter 5, various experimental approaches for the modification of one face of photoresist microparticles have been investigated for the fabrication of plate- like Janus particles including hydrophobisation by using DCDMS, amination by treatment with APTES, polyelectrolyte adsorption, with or without subsequent attachment of colloidal particles, direct attachment of magnetic nanoparticles to the oxidised microplate surface and metal coatings.

Janus particles with homogeneous but different faces have been successfully fabricated by hydrophobisation, adsorption of positive polyelectrolyte (PAH) and magnetite nanoparticles. The amination of AZ negative photoresist surface by using APTES is found to be ineffective under the experimental conditions applied.

It is found that monolayers of the PAH treated photoresist Janus microparticles with rounded rectangle shape at the decane- water interface behave differently than common homogeneous plate- like particles with the same geometry. The Janus microrectangles have shown significantly stronger tendency for side- to- side stacking (~ 55 % of all particles) than the homogeneous ones (~ 27 %). More experiments are needed to quantify and reveal the reasons for the observed differences and this could be an interesting direction for future investigation.

Magnetic Janus microrectangles have been successfully fabricated by binding magnetic Fe_3O_4 particles to one of the microparticle faces. It has been found that these plate- like particles responded to an external magnetic field in the bulk and at the liquid interface. This presents opportunities for further investigations of such stimuli- responsive magnetic plate- like particles at the liquid- fluid interface.

Partial masking of the negative photoresist particles using positive photoresist was found to be less successful due to the processing difficulties involved for defect- free positive photoresist patterns on an existing negative photoresist pattern. Nevertheless the feasibility of this approach has been demonstrated by making Janus microrectangles with one face patterned by metal deposion.

6. 2. Future work

The technique of photolithography is an effective means of fabricating chemically stable polymeric colloidal particles with a very large range of shapes and thicknesses ranging from several hundred micrometres to sub- micrometer thickness. Such a technique permit a means of closely linking particle shape with physical interactions both at interfaces and in the bulk; therefore it is possible to investigate particles with more complex shapes than those presented here, for example the particles could be star shaped, diamond or triangular shaped as demonstrated by the group of Stroock. [68] It is important to realise that the shape of the particles is not limited, and the desired shape can be drawn using software such as CAD and converted into a photomask for transferring the pattern onto the photoresist. It is difficult to fabricate a sufficient number of particles for the routine investigation of emulsions or foams and the technique would benefit from a more automated procedure; incorporating mask aligners and reduction steppers to would improve yields.

The technique of photolithography is also a very attractive for the fabrication of Janus particles with controlled size and shape, as this can be performed with the particles still attached to the substrate and therefore it is not necessary to trap the particles in a matrix or confine the particles in any way. Dissolution of a positive photoresist mask to reveal a surface that is partially coated with other chemical groups is also possible but difficult using the techniques applied in this thesis. It is necessary to ensure that the positive photoresist pattern does not contain any defects that can compromise further treatment of the surface and hamper dissolution of the photoresist at a later stage. This will necessitate the use of a clean room and ideally a mask aligner. If successful, it may be possible to release the particles and then modify the other surface of the photoresist with suitable groups.

Further insights into the interactions of monolayers of non- spherical particles fabricated by photolithography at different stages of compression could be realised

by rheological testing. For example, application of a stress rheometer with cone or rod geometry could be used to perform oscillatory shear measurements in order to gain information on the elastic modulus of the monolayer which may reflect the rigidity of the monolayer with respect to particle interactions as demonstrated by Vermant *et al.* [92] In addition, the photoresist film could be characterised in terms of the photoresist charge by using streaming zeta potential measurements and will provide further insight into their interactions at the interface. It is also possible to prepare suspensions consisting of particles with two or more different shapes or sizes and therefore provides an attractive means of imparting some control on the rheology of the monolayers.

Further work could be performed on rectangular photoresist particles coated on one surface with magnetic Fe_3O_4 particles. Preliminary experiments to investigate the particle monolayers at the air- water interface have been performed in a Petri dish; however application of a magnetic field from a simple hand held magnet orientated perpendicularly to the interface caused rapid and irreversible aggregation of the particles into a particle raft in which the individual particles were orientated randomly. Clearly such an approach will require very careful application of the magnetic field in order to determine if it is possible to align the particles in a particular direction.

References

1. G. Y. Onoda, *Phys. Rev. Lett,* 1985, **55**, 226- 229.
2. F. Ghezzi and J. C. Earnshaw, *J. Phys. Condens. Mat,* 1997, **9**, L517.
3. G. Y. Tolnai, F. Csempesz, M. Kabai-Faix, E. Kálmán, Z. S. Keresztes, A. L. Kovács, J. J. Ramsden and Z. Hórvölgyi, *Langmuir,* 2001, **17 (9)**, 2683- 2687.
4. E. Wolert, S. M. Setz, R. S. Underhill and R. S Duran, *Langmuir,* 2001, **17**, 5671- 5677.
5. H. Schwartz, Y. Harel and S. Efrima, *Langmuir,* 2001, **17**, 3884- 3892.
6. P. H. Hansen, S. Rödner and L. Bergström, *Langmuir* 2001, **17 (16)**, 4867- 4875.
7. M. Szekeres, O. Kamalin, R. A. Schoonheydt, K. Wostyn, K. Clays, A. Persoons and I. J. Dékány, *Mat. Chem, 2002*, **12 (11)**, 3268- 3274.
8. A. J. Armstrong, R. C. Mocklet and W. J. O' Sullivan, *J. Phys. A. Gen*, 1986, **19**, 123- 129.
9. A. J. Hurd and D. W. Schaefer, *Phys. Rev. Lett*, 1985, **54**, 1043- 1046.
10. W. Ramsden, *Proc. R. Soc*, 1903, **72**, 156- 164.
11. S. U. Pickering, *J. Chem. Soc*, 1907, **91**, 2001-2021.
12. R. G. Alargova, D. S. Warhadponde, V. N. Paunov and O. D. Velev, *Langmuir*, 2004, **20**, 10371- 10374.
13. R. G. Alargova, K. H. Bhatt, V. N. Paunov and O. D. Velev, *Adv. Mat*, 2004, **16**, 1653- 1657.
14. W. Zhou, J. Cao, W. Lin and S. Stoyanov, Angew. *Chem. Int. Ed*, 2009, **48**, 378- 381.
15. P. G. De Gennes, *Rev. Mod. Phys*. 1992, **64**, 645- 648.
16. R. Aveyard and D. A. Haydon, *An Introduction to the Principles of Surface Chemistry*, Cambridge University Press (Cambridge), 1973, p. 88.
17. P. W. Atkins, *Physical Chemistry*: Fifth Edition, Oxford University Press (Oxford), 1994, p. 962.
18. B. P. Binks. and T. S Horozov, *Colloidal Particles at Liquid Interfaces,* eds, Cambridge University Press (Cambridge), 2006, p. 1- 15.
19. Irving Langmuir, *J. Am. Chem. Soc*, 1917, **39**, 1848.
20. V. M. Kaganer, H. Möhwald and P. Dutta, *Rev. Mod. Phys*, 1999, **71 (3)**, 779- 818.

21. H. Schuller, *Kolloid. Z. Z. Polymer,* 1967, **380**, 216-217.

22. E. Sheppard, and N. Tcheurekdjian, *J. Coll. Int. Sci,* 1968, ***28***, 481- 486.

23. A. Doroszkowski and R. Lambourne, *J. Poly. Sci. Part C,* 1971, **34**, 253-264.

24. M. J. Garvey, D. Mitchell and A. L. Smith, *Coll. Poly. Sci.* 1979, **257**, 70-74.

25. J. H. Clint and S. E. Taylor, *Coll. Surf,* 1992, **65**, 61- 67.

26. S. C. Olugebefola, S. Y. Park, P. Banerjee and A. M. Mayes, *Langmuir,* 2002, **18**, 1098- 1103.

27. Z. Horvolgyi, M. Mate and M. Zrinyi, *Coll. Surf. A,* 1994, **84***,* 207- 216.

28. J. Stankiewicz, M. A. C. Vilchez and R. H. Alvarez, *Phys. Rev. E,* 1993, **47 (4)**, 2663- 2668.

29. D. J. Robinson and J. C. Earnshaw, *Phys. Rev. A,* 1992*,* **46***,* 2045- 2054.

30. D. J. Robinson and J. C. Earnshaw, *Langmuir,* 1993, **9**, 1436- 1438.

31. D. F. Williams and J. C. J. Berg, *Coll. Int. Sci*, 1992, **152**, 218- 229.

32. N. A. Kotov, F. C. Meldrum, C. Wu and J. H. J. Fendler, *Phys. Chem*, 1994, ***98***, 2735- 2738.

33. J. H. Fendler and F. C. Meldrum, *Adv. Mat*, 1995, **7**, 607- 632.

34. M. Achermann, M. A. Petruska, S. A. Crooker and V. I. Klimov, *J. Phys. Chem. B,* 2003, **107 (50)**, 13782- 13787.

35. M. Szekeres, O. Kamalin, P. G. Grobet, R. A. Schoonheydt, K. Wostyn, K. Clays, A. Persoons, I. Dékány, *Coll. Surf. A, Physicochem. Eng. Asp,* 2003, **227**, 77- 83.

36. S. Reculusa, P. Massé, S. Ravaine, *J. Coll. Int. Sci,* 2004, **279**, 471- 478.

37. S. Reculusa and S. Ravaine, *Appl. Surf. Sci,* 2005, **246**, 409- 414.

38. A. Deák, I. Székely, E. Kálmán, Z. S. Keresztes, A. L. Kovács and Z. Hórvölgyi, *Thin Solid Films,* 2005, **484**, 310- 317.

39. K. M. Keville, E. I. Franses and J. M. Caruthers, *J. Coll. Int. Sci*, 1991, **144**, 103- 126.

40. C. C. Ho, A. Keller, J. A. Odell and R. H. Ottewill, *Coll. Poly. Sci*, **271**, 469- 479, 1993.

41. M. G. Basavaraj, G. G. Fuller, J. Fransaer and J. Vermant, *Langmuir*, 2006, **22**, 6605- 6612.

42. B. Madivala, J. Fransaer and J. Vermant, *Langmuir*, 2009, **25**, 2718- 2728.

43. B. Madivala, S. Vandebril, J. Fransaer and J. Vermant, *Soft. Mat*, 2009, **5**, 1717- 1727.

44. A. Mohraz and J. Solomon, *Langmuir,* 2005, **21**, 5298- 5306.

45. P. P. Lele and E. M. Furst, *Langmuir*, 2009, **25 (16)**, 8875- 8878.

46. Z. Zhang, P. Pfleiderer, A. B. Schofield, C. Clasen and J. Vermant, *J. Am. Chem. Soc*, 2011, **133 (3)**, 392- 395.

47. P. P. Lele and E. M. Furst, *Langmuir*, 2009, **25 (16)**, 8875- 8878.

48. C. Xu, Q. Wang, H. Xu, S. Xie and Z. Yang, *Coll. Poly. Sci*, 2007, **285**, 1471- 1478.

49. A. Courbaron, O. J. Cayre and V. N. Paunov, *Chem. Comm*, 2007, 628- 630.

50. O. D. Velev, A. M. Lenhoff, E. W. Kaler, *Science*, 2000, **287**, 2240- 2243.

51. S. H. Lee, S. J. Gerbode, B. S. John, A. K. Wolfgang, F. A. Escobedo, I. Cohen and C. M. Liddell, *J. Mat. Chem*, 2008, **18**, 4912- 4916.

52. P. M. Johnson, C. M. Van Kats and A. Van Blaaderen, *Langmuir*, **21 (24)**, 11510- 11517.

53. A. F. Demirörs, P. M. Johnson, C. M. Van Kats, A. Van Blaaderen and A. Imhof, *Langmuir*, 2010, **26 (18)**, 14466- 14471.

54. D. M. E. Thies- Weesie, A. P. Philipse and S. G. J. M. Kluijtmans, *J. Coll. Int. Sci*, 1995, **174**, 211- 223.

55. A. F. Mejia, P. He, M. Netemeyer, D. Luo, M. Marquez and Z. Cheng, *Soft. Mat*, 2010, **6**, 4885- 4894.

56. D. Hwang, D. Dendukuri and P. S. Doyle, *Lab. Chip*, 2008, **8**, 1640- 1647.

57. L. Liu, M. Ren and W. Yang, *Langmuir*, 2009, **25 (18)**, 11048- 11053.

58. S. Kim, J. Sim, J. Lim and S. Yang, *Angew. Chem*, 2010, **122**, 3874- 3878.

59. L. Zhang, F. Zhang, W. Dong, J. Song, Q. Huo and H. Sun, *Chem. Comm*, 2011, **47**, 1225- 1227.

60. K. D. Anderson, M. Luo, R. Jakubiak, R. R. Naik, T. J. Bunning and V. V. Tsukruk, *Chem. Mat*, 2010, **22**, 3259- 3264.

61. A. Synytska, R. Khanum, L. Ionov, C. Cherif and C. Bellmann, *ACS App. Mat. Int*, 2011, **3**, 1216- 1220.

62. L. Hong, S. Jiang and S. Granick, *Langmuir*, 2006, **22**, 9495- 9499.

63. S. Jiang, M. J. Schultz, Q. Chen, J. S. Moore and S. Granick, *Langmuir*, 2008, **24**, 10073- 10077.

64. S. Ye and R. L. Carroll, *ACS App. Mat. Int*, 2010, **2 (3)**, 616- 620.

65. M. D. McConnell, M. J. Kraeutler, S. Yang and R. J. Composto, *Nano. Lett*, 2010, **10**, 603- 609.

66. K. Fujimoto, K. Nakahama, M. Shidara and H. Kawaguchi, *Langmuir*, 1999, **15**, 4630- 4635.

67. J. M. G. Cowie, *Polymers: Chemistry and Physics of Modern Materials* (Second Edition), CRC Press, New York, 1991.

68. S. Badaire, C. Bizonne, J. W. Woody, A. Yang, and A. D. Stroock, *J. Am. Chem. Soc*, 2007, **129**, 40-41.

69. S. Badaire, C. Bizonne and A. D. Stroock, *Langmuir*, 2008, **24**, 11451-11463.

70. C. J. Hernandez and T. G. Mason, *J. Phys. Chem. C*, 2007, **111**, 4477-4480.

71. K. Zhao and T. G. Mason, *Phys. Rev. Lett*, 2007, **99**, 268301- 268304.

72. A. B. D. Brown, C. G. Smith and A. R. Rennie, *Phys. Rev. E*, 2000, **62**, 951-960.

73. E. Sheppard and *N.* Tcheurekdjian, *Kolloid Z. Z. Poly,* 1968, **225**, 162- 163.

74. P. Pieranski, *Phys. Rev. Lett*, 1980, **45**, 569- 572.

75. G. Tolnai, A. Agod, M. Kabai- Faix, A. L. Kovács, J. J. Ramsden and Z. Hórvölgyi, *J. Phys. Chem. B*, 2003, **107**, 11109- 11116.

76. D. F. Williams and J. C. Berg, *J. Coll. Int. Sci*, 1992, **152 (1)**, 218- 229.

77. R. Aveyard, J. H. Clint, D. Nees and V. N. Paunov, *Langmuir*, 2000, **16**, 1969- 1979.

78. R. Aveyard, J. H. Clint, D. Nees and N. Quirke, *Langmuir*, 2000, **16**, 8820-8828.

79. F. Reincke, S. G. Hickey, W. K. Kegel and D. Vanmaekelbergh, *Angew. Chem. Int. Ed*, 2004, **43**, 458- 462.

80. T. S. Horozov, R. Aveyard, J. H. Clint and B. P. Binks, *Langmuir*, 2003, **19**, 2822- 2829.

81. T. S. Horozov, R. Aveyard, B. P. Binks and J. H. Clint, *Langmuir*, 2005, **21**, 7405- 7412.

82. Z. Hórvölgyi, S. Németh and J. H. Fendler, *Langmuir*, 1996, **12**, 997- 1004.

83. M. Máte, J. H. Fendler, J. J. Ramsden, J. Szalma and Z. Hórvölgyi, *Langmuir*, 1998, **14**, 6501- 6504.

84. D. Y. C. Chan, J. D. Henry and L. R. White, *J. Coll. Int. Sci*, 1980, **79 (2)**, 410- 418.

85. M. G. Nikolaides, A. R. Bausch, M. F. Hsu, A. D. Dinsmore, M. P. Brenner, C. Gay and D. A. Weitz, *Nature*, 2002, **420**, 299- 301.

86. B. J. Park and E. M. Furst, *Soft. Matt*, 2011, **7**, 7676- 7682.

87. D. Stamou, C. Duschl and D. Johannsmann, *Phys. Rev. E*, 2000, **62 (4)**, 5263- 5272.

88. F. Ghezzi, J. C. Earnshaw, M. Finnis, and M. McCluney, *J. Coll. Int. Sci*, 2001, **238**, 433- 446.

89. J. Ruiz-García and B. I. Ivlev, *Mol. Phys*, 1998, **95 (2)**, 371- 375.

90. J. Ruiz-García, R. Gámez-Corrales, and B. I. Ivlev, *Phys. Rev. E*, 1998, **58**, 660- 663.

91. H. Lehle, E. Noruzifar and M. Oettel, *Eur. Phys. J. E*, 2008, **26**, 151- 160.

92. B. Madivala, J. Fransaer and J. Vermant, *Langmuir*, 2009, **25**, 2718- 2728.

93. M. G. Basavaraj, G. G. Fuller, J. Fransaer and J. Vermant, *Langmuir*, 2006, **22**, 6605- 6612.

94. J. N. Isrealachvili, *Intermolecular and Surface Forces*, Academic, London, 1992, 22nd Ed.

95. J. C. Loudet, A. G. Yodh and G. Pouligny, *Phys. Rev. Lett,* 2006, **97**, 018304- 18308.

96. J. C. Loudet, A. M. Alsayed, J. Zhang and A. G. Yodh, *Phys. Rev. Lett*, 2005, **94**, 018301- 018304.

97. E. P. Lewandowski, J. A. Bernate, P. C. Searson and K. J. Stebe, *Langmuir*, 2008, **24**, 9302- 9307.

98. M. Cavallero, L. Botto, E. P. Lewandowski, M. Wang and K. J. Stebe, *PNAS,* 2011, **108 (52)**, 20923- 20928.

99. E. P. Lewandowski, M. Cavallaro. Jr, L. Botto, J. C. Bernate, V. Garbin and K. J. Stebe, *Langmuir*, 2010, **26 (19)**, 15142- 15154.

100. B. P. Binks and P. D. I. Fletcher, Langmuir, 2001, **17**, 4708- 4710.

101. H. Yu, M. Chen, P. M. Rice, S. X. Wang, R. L. White and S. H. Sun, *Nano. Lett*, 2005, **5**, 379- 382.

102. N. Glaser, D. J. Adams, A. Böker and G. Krausch, *Langmuir*, 2006, **22**, 5227- 5229.

103. K. Isenbügel, Y. Gehrke and H. Ritter, *Macromol. Rap. Comm*, 2012, **33**, 41- 46.

104. B. J. Park, T. Brugarolas and D. Lee, *Soft. Mat*, 2011, **7**, 6413- 6417.

105. S. Gangwal, A. Pawar, I. Kretzschmar and O. D. Velev, *Soft. Mat*, 2010, **6**, 1413- 1418.

106. S. Gangwal, O. J. Cayre and O. D. Velev, *Langmuir*, 2008, **24**, 13312-13320.

107. L. Zhang and Y. Zhu, *App. Phys. Lett*, 2010, **96**, 141902.

108. B. J. Park and D. Lee, *ACS Nano*, 2012, **6 (1)**, 782- 790.

109. J. N. Isrealachvili, Intermolecular and Surface forces: Second Edition, Academic Press, (London), 1991.

110. K. D. Danov and P. A. Kralchevsky, Adv. Coll. Int. Sci, 2010, **154,** 91–103.

111. 1. V. N. Paunov, *Langmuir*, 2003, **19,** 7970- 7976.

112. B. P. Binks and J. A. Rodriguez, *Langmuir,* 2003, **19 (12)**, 4905- 4912

113. T. N. Hunter, E. J. Wanless and G. J. Jameson, *Coll. Surf A: Physicochem. Eng. Asp*, 2009, **334**, 183.

114. J. Kang, K. Cho, J. Kim, C. Park, S. Uhm and B. Khatua, *J. Adh. Sci. Tech*, 2004, **18**, 1815- 1831.

115. B. Lev, *Quan. Inf. Comp*, 2003, **3 (5)**, 450- 464.

116. http://www. microchemicals. eu/technical_information/TroubleShooter_EN. pdf. 25. 05. 12.

117. A. Campo and C. Greiner, *J. Micromech. Microeng*, 2007, **17**, R81-R95.

118. K. E. Herold and A. Rasooly, *Lab on a Chip Technology: Fabrication and microfluidics, Volume 1*, Horizon Scientific Press, 2009.

119. L. Mashev and S. Tonchev, *App. Phys*, 1981, **26**, 143- 149.

120. http://www. microchem. com/pdf/SU-82000DataSheet2025thru2075Ver4. pdf. 25. 05. 2012.

121. C. Lin, G. Lee, B. Chang and G. Chang, *J. Micromech. Microeng,* 2002, **12 (5)**, 590.

122. H. Miyajima and M. Mehregany, *J. Micromech. Microeng,* 1995, **4 (4)**, 220-229.

123. M. Wu and G. M. Whitesides, *J. Micromech. Microeng*, 2002, **12**, 747–758.

124. W. J. Venstra, J. W. Spronck, P. M. Sarro and J. V. Eijk, *J. Micromech. Microeng*, 2009, **19,** 1- 6.

125. P. M. Dentinger, W. M. Clift and S. H. Goods, *Microelec. Eng*, 2002, **61-62**, 993- 1000.

126. S. Jiguet, A. Bertsch, H. Hofmann and P. Renaud, *Adv. Func. Mat*, 2005, **15 (9)**, 1511- 1516.

127. www. microchemicals. eu/technical-information, 19. 07. 2010.

128. M. W. Toepke and P. J. A. Kenis, *J. Am. Chem. Soc.* , 2005, **127**, 7674-7 675.

129. W. J. Venstra, J. W. Spronck, P. M. Sarro and J. V. Eijk, *J. Micromech. Microeng*, 2009, **19,** 1- 6.

130. Y. Chen, K. Peng and Z. Cui, *Microelec. Eng*, 2004, **73- 74**, 248- 281.

131. V. S. Rao, V. Kripesh, S. W. Yoon and A. A. O. Tay, *J. Micromech. Microeng*, 2006, **16**, 1841.

132. R. Yang and W. Wang, *Sens. Act. B*, 2005, **110**, 279- 288.

133. Y. J. Chuang, F. G. Tseng and W. K. Lin, *Microsys. Tech*, 2002, **8**, 308-313.

134. X. Tiang, G. Liu, Y. Tiang, P. Zhang and X. Zhang, *Microsys. Tech,* 2005, **11**, 265- 270.

135. W. J. Kang, E. Rabe, S. Kopetz and A. Neyer, *J. Micromech. Microeng,* 2006, **16**, 821- 831.

136. F. J. Blanco, M. Agirregabiria, J. Garcia, J. Berganzo, M. Tijero, M. T. Arroyo, J. M. Ruano, I. Aramburu and K. Mayora, *J. Micromech. Microeng,* 2004, **14**, 1047.

137. R. Yang and W. Wang, *Sens. Act. B. Chem*, 2005, **110 (2)**, 279- 288.

138. R. M. Diebold and D. R. Clarke, *Lab. Chip*, 2011, **11**, 1694- 1697.

139. L. W. Flanagin, V. K. Singh and C. G. Willson, *J. Vac. Sci. Technol. B*, 1999, **17**, 1371-1379.

140. S. L. Ahn. J. H. Kim. W. C. Zin, *J. App. Pol. Sci*, 2007, **104**, 2361-2365.

141. K. Yun and E. Yoon, *Lab. Chip*, 2008, **8**, 245–250.

142. M. Chan-Park. J. Zhang. Y. Yan and C. Y. Yui, *Sensors and actuators B*. 2004, **101**, 175-182.

143. I. I. Smolyoninov, D. L. Mazzoni and C. C. Davis, *Appl. Phys. Lett*. 1995, **67 (26)**, 3859- 3861.

144. J. Liang, F. Kohsaka, T. Matsuo, X. Li and T. Ueda, *J. Micromech. Microeng*, 2008, **85**, 1000-1003.

145. X. Xia, H. Yang, Y. Sun, Z. Wang, L. Wang, Z. Cui and C. Gu, *Microelect. Eng*, 2008, **85**, 1433- 1436.

146. Y. Wei and R. L. Brainard, *Advanced Processes for 193-Nm Immersion Lithography,* SPIE Press, 2009, p. 26.

147. N. A. Kalkon, S. Aksoy, E. A. Aksoy and N. Hasirci, *J. App. Poly. Sci*, 2012, **123**, 711.

148. http://www. cnf. cornell. edu/cnf_process_photo_photoresists. html. 05. 01. 12.

149. Y. K. Lee, D. J. Kim, H. J. Kim, T. S. Hwang, M. Rafailovich and J. Sokolov, *J. App. Poly. Sci*, 2003, **89**, 2589- 2596.

150. A. Iqbal, Dissertation: *Electrokinetic characteristics of particulate/ liquid interfaces and their importance in contamination from semiconductor process liquids*, University of Arizona, 1990.

151. L. Bogunovic, D. Anselmetti and J. Regtmeier, *J. Micromech. Microeng*, 2011, **21**, 027003.

152. S. Flink, F. J. C. M. Van Veggel and D. N. Reinhoudt, *J. Phys. Org. Chem*, 2001, **14**, 409.

153. A. Ulman, *Chem. Rev*. 1996**, 96**, 1533-1554.

154. T. S. Horozov, *Curr. Opin. Colloid Interface Sci.* 2008, **13**, 134– 140.

155. A. V. Dobrynin and M. Rubentein, *Prog. Poly. Sci*, 2005, **30**, 1053.